The role of MRPL45 and OXA1L in human mitochondrial protein synthesis

Nicole Mai

Supervisors:

Professor Zofia Chrzanowska-Lightowlers
Professor Robert Lightowlers

A thesis submitted for the degree of
Doctor of Philosophy

Institute of Neuroscience
Wellcome Trust Centre for Mitochondrial Research

October 2016

Abstract

Mitochondria produce 90% of the adenosine triphosphate (ATP) used by eukaryotic cells as a source of energy. ATP synthesis is carried out by the oxidative phosphorylation (OXPHOS) system whose components are partially-encoded by mitochondrial DNA and translated by mitoribosomes found in the organelle itself. The interaction between mitoribosomes and the inner mitochondrial membrane (IMM) has been claimed to be important for efficient protein synthesis in these organelles, but how this association occurs is still unclear.

The aim of this study was to investigate the association between mitoribosomes and IMM in human mitochondria. My attention focused on MRPL45, a component of the mitoribosome that might be a key player of this interaction due to its proximity to the polypeptide exit tunnel and its structural similarity to the IMM-interacting proteins TIM44 and Mba1. During the course of this study, in order to further investigate the interaction, interest in the IMM protein OXA1L arose. The yeast homologue of this protein has been reported to interact with the mitoribosome, offering an interacting point between the IMM and the translation machinery.

I performed depletion studies that confirmed the importance of MRPL45 for the stability of the mitoribosomal large subunit (mt-LSU) and mitochondrial translation. With the development of a protocol to investigate membrane-interaction, I demonstrated that MRPL45 is able to interact directly with the IMM. The addition of a FLAG-tag at the C-terminal of MRPL45 did not affect the ability of the protein to interact with the membrane and did not have effects on the homeostasis of the cells. Therefore, immunoprecipitation of MRPL45FLAG was performed in the absence of assembled mitoribosomal subunits to identify potential IMM binding partners. No obvious candidates, however, were detected from mass spectrometry analysis of the immunoprecipitated sample. Modifications of MRPL45 based on structural similarities with TIM44 and Mba1 were performed to identify the membrane-associating domain of the protein. Mutation of charged amino acids on a protruding α-helix of MRPL45 were performed. The resultant protein was completely integrated into the mt-LSU in the absence of the endogenous counterpart, partially rescuing the phenotype observed upon depletion of MRPL45. Membrane-interaction studies showed that the modifications did not affect the ability of this mutant to interact directly with the membrane. Another attempt to disrupt the interaction between MRPL45 and the membrane was performed by expressing a mutant protein lacking 117 amino acids at the N-terminal, which is predicted to correspond to the putative membrane-interacting domain of TIM44. Only a minor proportion of this protein was integrated in the mt-LSU in absence of the endogenous MRPL45, although the mutant protein retained the ability to interact directly with the membrane.

The role of another mitochondrial protein, OXA1L, in mitochondrial translation was also investigated in this work. This was motivated by the discovery of a paediatric patient with mutations in the gene encoding OXA1L. Since the published studies showing OXA1L to interact with the mitoribosome were attempted *in vitro,* I performed immunoprecipitation studies which

confirmed the ability of OXA1L to associate with the mitoribosome in intact human cells. In order to characterise the role of OXA1L in mitochondrial translation, depletion studies were performed. These suggested that OXA1L was important for the stability of both the large and, unexpectedly, the small mitoribosomal subunit. Due to this surprising result, extensive studies were performed to confirm its robustness, which confirmed the reduction of the steady-state level of the mitoribosomal subunits and of OXPHOS components upon depletion of OXA1L.

To conclude, my studies showed the importance of the mitoribosomal protein MRPL45 for the stability and the assembly of the large subunit of the mitochondrial translation machinery, as well as its ability to interact directly with the IMM. Although it was not possible to identify the domain of MRPL45 involved in membrane interaction, insights on the importance of the N-terminal domain for its integration in the mt-LSU were identified. The ability of OXA1L to interact with the mitoribosome *in vivo* was determined and a role of this protein in the stability and assembly of the mitoribosome was demonstrated.

Acknowledgments

First of all I want to thank my supervisors, Bob and Zosia, for the constant support and the guidance during this project. Thank you for giving me the chance to do this PhD and grow professionally.

A special thanks to the Barbour Foundation for supporting my PhD studies as well as helping many other students. Thank you for to Prof Jeremy Lakey and Prof Rita Horvath for their contribution and support during the year reviews. Another thank goes to Prof Taylor, for involving me in his work and for putting me in touch with Dr. Rosalba Carrozzo, who I also thank. Thanks to (almost Dr.) Charlotte for all the help with the sequencing. Thanks to Dr Aurelio Reyes for sharing is mitochondrial fractionation protocol which helped the optimisation of the membrane-soluble fraction protocol presented in this work. Thank you to Dr Achim Treumann for the help with the mass spectrometry analysis.

Thank you to all the members of the Mitochondrial Research Group for their help and for always be up for a chat. A special thanks goes to Amy, for being a special friend, and to Ewen and Hannah. Thank you for sharing this adventure with me. Thank you Pav for being always there for me.

A massive thanks goes to Monika, Rawaa, Christie, Kyle, Agata, Fei, Marysia and Francesco and whoever else has been in the Lightowler's lab for the past 3 years. You had to deal with my roller-coaster of emotion throughout this PhD. Thank you for the kindness, for all the support and suggestions and for making me feel so welcome. This experience wouldn't be the same without you. I wish you all the best for your future!

Thank you to all my friends here in Newcastle. Being so far away from home can be very hard, and you made this a lot easier! How not to thank also my friends back home, which are still there despite the distance. The support of all of you has been immeasurable.

A gigantic thank you to Matt. Thank you for dealing with me on a daily basis. I know that is not easy! Your love and support have been an unlimited source of energy that made me power through all the difficulties I had. The past year, which we both spent writing up, made us stronger. I am so happy that I've found you (with a little help from Pav and Stacey!). I wouldn't have made it without you.

Il grazie piu' grosso e'dedicato ai miei miei genitori che hanno dovuto sopportare la lontananza cosi' tanto a lungo. Grazie per il vostro sostegno continuo e illimitato che mi avete dato durante tutta la mia vita, e che ancora mi darete in future. Senza il vostro aiuto, oggi non sarei dove sono.

Table of Contents

List of figures

List of tables

Abbreviations

ADP: adenosine diphosphate
AFG3L2: AFG3-like matrix AAA peptidase subunit 2
AGO2: Protein argonaute 2
AIF: apoptosis inducing factor
APS: ammonium persulfate
ATP: adenosine triphosphate
ATPn: subunit of complex V (n= number and/or letter)
Bax: Bcl2-associated X protein
Bcl2: B-cell lymphoma 2
BGH: bovine growth hormone
Bp: base pair
BSA: bovine serum albumin
cDNA: complementary DNA
CH_3COONa: sodium acetate
CLPP: Caseinolytic Peptidase
CM: cristae membranes
CMV: cytomegalovirus
CO_2: carbon dioxide
COX: subunit of complex IV
Ct: Cycle threshold
CyB: Cytochrome B
DAP3: death associated protein 3
DDX28: DEAD-box helicase 28
dH_2O: distilled water
DIABLO: Direct IAP-binding protein with low PI
DMEM: Dulbecco's modified eagle medium
DNA: deoxyribonucleic acid
dNTP: Deoxynucleotide
Drp1: dynamin related protein 1
DTT: dithiothreitol
DW: distilled water
EDTA: ethylene diamine tetraacetic acid
EGTA: ethylene glycol tetraacetic acid
eIF4e: eukaryotic translation initiationn factor 4E
ELAC2: elaC homologue 2
EM: electron microscopy
ERAL1: Era-like 12S mitochondrial rRNA chaperone 1)
EtBr: ethidium bromide
FAD: flavin adenine dinucleotide
FASTK: Fas Activated Serine/Threonine Kinase

FCS: foetal calf serum
Fe/S: Iron-sulphur
FMN: flavin mononucleotide
GDH: glutamate dehydrogenase
GDP: guanosine diphosphate
GRSF1: G-rich RNA sequence binding factor 1
GTP: guanosine triphosphate
GW182: Glycine-tryptophan protein of 182 kDa
HEK: human embryonic kidney
HeLa: Henrietta Lacks
hmtPAP: human mitochondrial poly(A) polymerase
H^+: hydrogen
HSP: heavy strand promoter
Hsp60: heat shock protein 60
IAP: IAPs (inhibition of apoptosis protein
IBM: inner boundary membranes
ICT1: Immature colon carcinoma transcript 1
IMM: inner mitochondrial membrane
IMS: inter membrane space
IP: immunoprecipitation
KCl: potassium chloride
kDa: kilodalton
LACTB2: Lactamase beta 2
LB: Luria Bertani
LetM1: Leucine zipper-EF-hand containing transmembrane protein 1
LONP: Lon Peptidase 1
LRPPRC: Leucine rich pentatricopeptide repeat containing
LSP: light strand promoter
MALSU1: Mitochondrial assembly of ribosomal large subunit 1
MERF: myoclonic epilepsy and ragged red fibres
MELAS: mitochondrial encephalopathy, lactic acidosis, stroke-like episodes
$MgCl_2$: magnesium chloride
MIB: mitochondrial intermembrane space bridging
MICOS: mitochondrial contact site and cristae organizing system
Min: minute
miRNA; microRNA
MITRAC: MItochondrial translation regulation assembly intermediate of cytochrome c oxidase
Mnf: mitofusin
MPV17L2: MPV17 mitochondrial inner membrane protein like 2)
MRM: mitochondrial methyl transferase
mRNA: messenger RNA
MRP: mitoribosomal protein
mtDNA: mitochondrial DNA

mtEF-G: mitochondrial elongation factor G
mtEF-Tu: mitochondrial elongation factor thermo unstable
mtEF-Ts: mitochondrial elongation factor thermo stable
mTERF: mitochondrial transcription terminator factor
mt-Hsp70: mitochondrial heat shock protein 70
mtIF2: mitochondrial initiation factor 2
mtIF3: mitochondrial initiation factor 3
mt-LSU: large subunit of the mitoribosome
mt-NAPs: nucleoid associated proteins
mtRRF: ribosomal recycling factor
mt-SSB: mitochondrial single stranded DNA-binding
mt-SSU: small subunit of the mitoribosome
NADH: nicotinamide adenine dinucleotide
NaCl: sodium chloride
NH_4Cl: ammonium chloride
NaOH: sodium hydroxide
ND: subunit of complex I
NDUFA9: NADH:Ubiquinone oxidoreductase Subunit A9
NDUFB8: NADH:Ubiquinone oxidoreductase Subunit B8
NH_4OH: ammonium hydroxide
NP-40: nonyl phenoxypolyethoxylethanol
NSUN4: NOP2/Sun RNA Methyltransferase Family Member 4
NT-siRNA: non targeting silencing RNA
OL: origin of replication of L-strand
OH: origin of replication of H-strand
Omi/HtrA2: HtrA serine peptidase 2
OMM: outer mitochondrial membrane
O/N: over night
Opa1: optic atrophy 1
ORF: Open reading frame
OXA1L: oxidase (cytochrome c) assembly 1-like
OXPHOS: oxidative phosphorylation
PAGE: polyacrylamide gel electrophoresis
PAM: presequence translocase-associated motor
PCR: polymerase chain reaction
PEO: progressive external ophthalmoplegia
PES: polypeptide exit site
PMSF: phenylmethylsulfonyl fluoride
PNPase: Polynucleotide Phosphorylase
POLG: DNA polymerase γ
POLRMT: mitochondrial DNA-directed RNA polymerase
PTC: peptidyl transferase centre
qPCR: real-time PCR

REXO2: RNA exonuclease 2
RITOLS: RNA incorporation through-out the lagging strand
RNA: ribonucleic acid
ROS: reactive oxygen species
Rpm: rounds per minute
rRNA: ribosomal RNA
S: Svedberg
SAM: sorting and assembly
SDH70: Succinate dehydrogenase 70 kDa
SDS: sodium dodecyl sulphate
Sec: seconds
siRNA: small interfering RNA
SLIRP: Stem-loop interacting RNA binding protein
Smac; Second mitochondria-derived activator of caspases
SMP: submitochondria particle
SOC: super optimal broth with catabolite repression
SPG7: paraplegin
ssDNA: single-stranded DNA
SUPV3L1: Suv3-like RNA helicase
TACO1: transcriptional activator of complex I
TCA: tricarboxylic acid
TEFM: mitochondrial transcription elongation factor
TFAM: mitochondrial transcription factor A
TFB2M: mitochondrial transcription factor B2
TIM44: translocase of inner mitochondrial membrane 44
TOM20: translocase of outer mitochondrial membrane 20
tRNA: transfer RNA
T-TBS: tween 20%- Tris Buffered Saline
U: unit
U2OS: human osteosarcoma cell line
UTR: untranslated region
V: volt

Chapter 1: Introduction

1.1. Mitochondria

Mitochondria are a distinctive feature of eukaryotic cells. These double-membraned organelles are thought to be derived from the phagocytosis of an α-proteobacteria, retained by the pre-eukaryotic cell for selective advantage (Gray MW, 1999). Mammalian mitochondria contain their own small DNA molecule (mtDNA) of approximately 17,000 bases, derived from the reduction of the genome of the prokaryotic ancestor. On contrary, plants contain a wider mitochondrial genome, which can be composed of up to 2,500,000 bases (Galtier N, 2011). The mammalian mtDNA encodes for 13 polypeptides, 2 rRNA and 22 tRNA (Anderson S et al., 1981). All the remaining proteins found in mitochondria are encoded by the nuclear genome and imported into the organelle (Mokranjac D et al., 2005).

One of the key functions of mitochondria is ATP production, which is the main source of energy used by eukaryotic cells. This is synthesised by the oxidative phosphorylation (OXPHOS) system found in the inner mitochondrial membrane (IMM) and accounts for approximately the 90% of the energy required by cells. However, it is important to remember that these organelles perform several other important functions. These include regulation of apoptosis (Wang C et al., 2009), involvement in calcium homeostasis (Rizzuto R et al., 2012) and formation of iron-sulphur clusters (Lill R et al., 2005). The β-oxidation of fatty acids also takes place in the mitochondria (Kunau WH et al., 1995) and so do crucial stages of the biosynthesis of heme (Ponka P, 1999) and pyrimidine (Jones ME, 1980).

The involvement of mitochondria in several crucial processes highlights their importance for the homeostasis of cells. Mutations that change the sequence of mitochondrial proteins are linked to a vast and heterogeneous group of pathologies named mitochondrial diseases (reviewed in (Lightowlers RN et al., 2015)). These can arise in early childhood or in adulthood and present a variety of symptoms that can affect different tissues, from skeletal muscle and heart, to the nervous system. Because of the severity and heterogeneity of these pathologies, a complete understanding of the mitochondrial biological processes is essential to provide useful information to understand the mechanism involved in diseases and help in the development of therapies.

1.2. The origin and evolution of mitochondria

According to the endosymbiotic theory, mitochondria originate from the phagocytosis of α-proteobacteria by ancestral eukaryotic cells (Falkenberg M et al., 2007; Gray MW, 1999). The concept of symbiosis (Latin 'living together') was developed by the Swiss botanist Simon Schwendener in 1867 after discovering that lichens consisted of a fungus and a photosynthesiser (Schwendener S, 1867). In the following years, the German botanist Heinrich Anton de Bary defined this coexistence of 2 organisms that can result in the formation of a new organism as symbiosis (De Bary A, 1878).

The phagocytosis of α-proteobacteria is thought to have occurred approximately 1.5 billion years ago (Brocks JJ et al., 1999) and resulted in the formation of different mitochondria-like organelles. These can be classified as classical mitochondria, mitosomes and hydrogenosomes (Embley TM et al., 2003; van der Giezen M et al., 2005). While mitochondria synthesise ATP aerobically, hydrogenosomes are anaerobic, do not have respiratory complexes and synthesise ATP through fermentation of pyruvate to acetate, CO_2 and H_2, carried out by pyruvate:ferredoxin oxidoreductase. In addition, mitochondria contain their own genome, which is absent in most of the hydrogenosomes. DNA is also absent in mitosomes, which are organelles that are not able to synthesise ATP but that are important for the assembly of iron-sulphur clusters used as cofactors by several enzymes.

Because most of the nucleated eukaryotic cells contain mitochondria, it is likely that the α-proteobacteria was retained because it offered a selective advantage in the environmental conditions present at the time of the phagocytosis. This advantage might be related to the presence of a high concentration of oxygen, rather than the need for an additional source of energy. The ATP/ADP translocases that shuffle ATP and ADP across the membrane appear to be acquired by eukaryotic cells throughout evolution and were, therefore, not present in the α-proteobacteria. As a consequence, at the time of the phagocytosis, the ATP could not be transported from the 'parasite' to the host (Karlberg O et al., 2000). Instead, the reduction of the oxygen tension due to the retained α-proteobacteria (Kurland CG et al., 2000) could have helped cells resist the high oxygen levels present in the atmosphere at the time of the phagocytosis (Des Marais DJ, 1998).

Several mitochondrial proteins are related to bacterial forms, further supporting the hypothesis of the prokaryotic origin of these organelles. The human mitochondrial proteome is composed of over 1,000 proteins (Lotz C et al., 2014), but the human mtDNA encodes for only 13 of these. Therefore, during evolution, many genes have been either lost or have migrated to the nuclear genome.

The presence of mtDNA in modern mitochondria forces the cells to synthesise the thousand proteins necessary for mitochondrial gene expression within the cytosol and then import these into the organelles. Although this process appears counter-productive, its potential advantages have been explained by 2 theories. The 'hydrophobic theory', (von Heijne G, 1986) arose from the observation that all the mt-encoded proteins are highly hydrophobic components of the OXPHOS system. According to this theory, these proteins will be difficult to import into mitochondria, and therefore their genes have been retained to be transcribed and translated within the organelles. A second theory, known as the 'colocalisation for redox regulation theory', hypothesised that the genes have been retained to allow their expression to be controlled by the redox state of the organelle (Allen JF et al., 1996).

1.3. Mitochondrial structure

Mitochondria are composed of an inner matrix, surrounded by a double layer of membranes, named inner and outer mitochondrial membranes (OMM and IMM, respectively). Due to its multiple invaginations (cristae), the IMM presents a large surface area and is the site of the ATP production. Between the IMM and the OMM is found a compartment named inter membrane space (IMS) (Fig. 1.1).

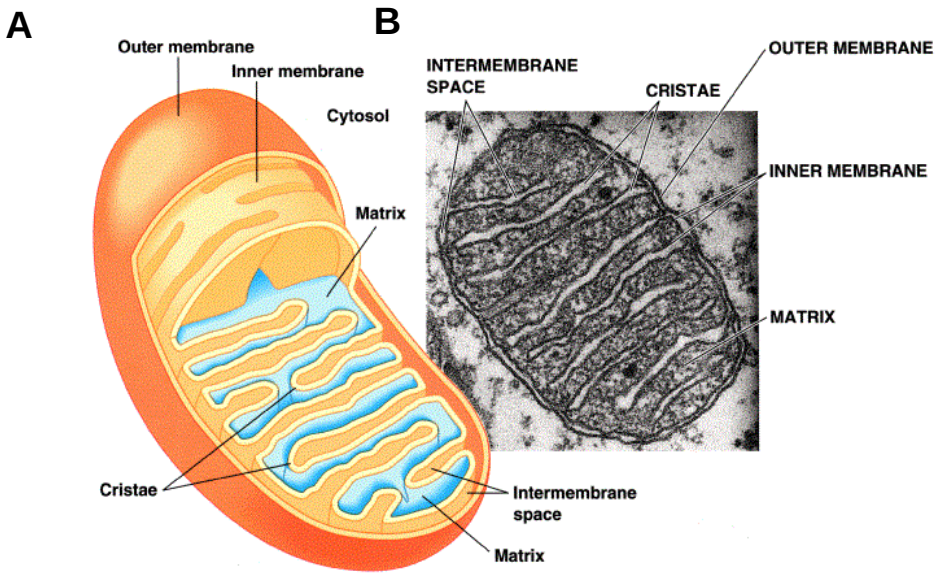

Figure 1.1 Structure of the mitochondrion.

A) Schematic representation of mitochondria: outer mitochondrial membrane (orange), inner mitochondrial membrane (yellow), matrix (light blue). **B)** Electron-micrograph of a mitochondria.

Figure from Mathews and val Holde: Biochemistry 2/e

The mitochondrial matrix contains a high number of proteins and molecules. Amongst these are found the components involved in mitochondrial gene expression, as well as β-oxidation of fatty acids and the citric acid cycle.

The OMM is relatively permeable due to the presence of porins that allow small molecules (up to approximately 5,000 Da) to pass through it (Benz R, 1994; Mannella CA, 1992). The permeability of the IMM, by contrast, is more selective as this membrane is only freely permeable for water, carbon dioxide and oxygen. This characteristic is important to maintain the membrane potential, essential to harness the H+ gradient generated by the OXPHOS complexes to synthesise ATP.

In addition to this difference in permeability, the OMM and IMM present a different protein content, as well as a different phospholipid composition (Horvath SE et al., 2013). The IMM is more protein rich with a protein:lipid ratio of 3:1, compared to the 1:1 of the OMM (Gohil VM et al., 2009). Several of the phospholipids present in the mitochondrial membranes are common to other cellular membranes (phosphatidylcholine, phosphatidylethanolamine, phosphatidylinositol, phosphatidylserine, and phosphatidic acid), while phosphatidylglycerol and cardiolipin, are exclusively components of mitochondrial membranes (Colbeau A et al., 1971). A greater amount

of cardiolipin is found in the IMM, when compared to the OMM. Studies reported the importance of this phospholipid not only for the structure of the membrane, but also for other functions, such as fission and fusion (Frohman MA, 2015; Ortiz A et al., 1999), or the assembly and stability of several IMM proteins (reviewed in (Paradies G et al., 2014)). These membranes also exhibit a low content of sphingolipids and cholesterols, which are widely represented in the plasma membrane.

More recently, the IMM has been suggested to be divided into cristae membranes (CM) and inner boundary membranes (IBM), which is found parallel to the OMM. The former contains the OXPHOS complexes, while the latter harbours the protein import machinery and the proteins required for the processes of fission/ fusion (Vogel F et al., 2006). CM and IBM are connected by cristae junctions, pore-like structures whose formation depends on a complex named MICOS ('mitochondrial contact site and cristae organizing system') (Kozjak-Pavlovic V, 2016). This complex associates with the SAM ('sorting and assembly') machinery, creating the 'mitochondrial intermembrane space bridging' (MIB) complex, which creates the cristae junctions by joining the IMM with the OMM (Fig. 1.2). This organisation of the IMM defines a new compartment within the IMS, named intracristal space. Due to the presence of the cristae junctions, which limit the diffusion of molecules, the composition of the intracristal space is different from the one observed in the remaining IMS. An example of the importance of these junctions with respect to the concentration of cytochrome *c* (Scorrano L et al., 2002). This protein is involved in the apoptosis cascade (Jiang X et al., 2004) and is able to pass through the OMM when its permeability is increased (Gogvadze V et al., 2006). The containment of this protein within the intracristal space limits its diffusion in the IMS and its permeation through the OMS, controlling apoptosis.

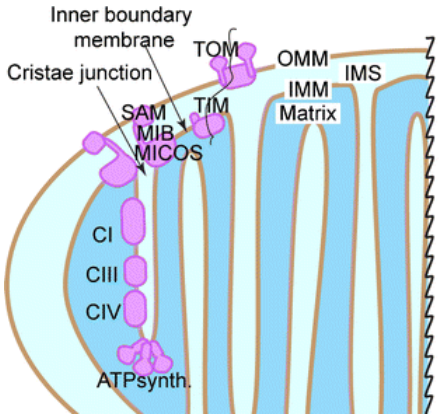

Figure 1.2 Organisation of the mitochondrial inner membrane.

Representation of the inner mitochondrial membrane (IMM) of mitochondria and its division into inner boundary membrane and cristae membrane. The former contains proteins from the membrane import machinery (TOM, translocase of the outer mitochondrial membrane; TIM, translocase of the inner mitochondrial membrane), while the latter contains the OXPHOS system (complexes I, III, IV, V. Complex II was absent in the original figure). The MICOS (mitochondrial contact site and cristae organizing system) and SAM (sorting and assembly machinery) associate to create the MIB (mitochondrial intermembrane space bridging) complex, responsible of the formation of the cristae junctions. OMM= outer mitochondrial membrane, IMS= intermembrane space.

Figure from Kozjak-Pavlovic V (2016), Licence number 3924681399708.

Mitochondria are highly dynamic organelles that move in the cytoplasm along microtubule tracks (Morris RL et al., 1995). While moving, mitochondria can encounter and undergo fission and fusion (Fig. 1.3), creating the dynamic tubular network characteristic of mitochondria (reviewed in (Chan DC, 2006)). In mammals, the fusion machinery is composed of mitofusin 1 and 2 (Mfn1, Mfn2), which mediate the fusion of the OMM, and optic atrophy 1 (Opa1), whose role is to fuse the IMM. Fusion can be either transient, if only soluble proteins are exchanged, or complete if the membrane proteins can combine and the mtDNA is mixed between the organelles (Liu X et al., 2009). When division of the mitochondrial mass is needed, mitochondria undergo fission, mediated by dynamin related protein 1 (Drp1) (Labrousse AM et al., 1999; Shin HW et al., 1997). This cytosolic protein is recruited to the fission site and creates a spiral around the mitochondrial mass, dividing it to create 2 organelles (Smirnova E et al., 2001).

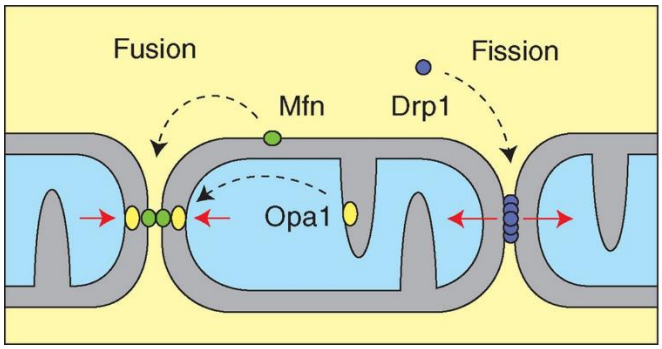

Figure 1.3 Mitochondrial fission and fusion.

Schematic representation of the processes of fission and fusion. Mfn (mitofusin) on the outer mitochondrial membrane and Opa1 (optic atrophy 1) on the inner mitochondrial membrane mediate the fusion of 2 individual mitochondria. The division of mitochondrial mass is, instead, performed by Drp1 (dynamin related protein 1).

Figure from van der Bliek AM et al. (2013), © Cold Spring Harbor Laboratory Press

1.3.1. Nucleoids and RNA granules

The existence of 2 new compartments within the matrix, named nucleoids and RNA granules, has been suggested.

RNA granules are ribonucleoparticles known to exist within the nucleus and cytoplasm of somatic cells, neurons and germ cells. These are not delimited by a membrane and are used to compartmentalise certain processes, such as RNA splicing and mRNA degradation (Anderson P et al., 2006). RNA granules have also been described within organelles including chloroplasts (Uniacke J et al., 2008) and mitochondria (Antonicka H et al., 2013; Jourdain AA et al., 2013). These compartments are used in mitochondria to organise the processing of the polycistronic RNA transcripts derived by mitochondrial transcription (qv 1.6.2. and 1.8.1.). Several factors for RNA modification and processing have been localised within the mitochondrial RNA granules (reviewed in (Jourdain AA et al., 2016)). The first proteins identified in these granules were GRSF1 and mt-RNaseP, involved in mitochondrial RNA processing and translation (Antonicka H et al., 2013; Jourdain AA et al., 2013). Other proteins present in the RNA granules are

members of the FASTK family (important for RNA processing and mitoribosome assembly), the mitochondria poly(A) polymerase (qv 1.8.1.), RNA helicases, methyltransferases. The complex hSuv3-PNPase, involved in degradation of RNA (qv 1.8.4.), was also localised in this compartment, together with the 12S and 16S mt-rRNA. Because of the presence of the rRNA, it was proposed that, together with RNA processing, this compartment was also involved in the assembly of the mitoribosome.

In close proximity to the RNA granules, are other compartments named nucleoids (reviewed in (Hensen F et al., 2014)). Their main functions are to protect the mtDNA from damage and to provide a compartment for its replication and transcription. The confirmation of the colocalisation of proteins and mtDNA came in 2001, when Twinkle, a mtDNA helicase, was shown to colocalise with the mitochondrial genome (Spelbrink JN et al., 2001). Since then, several proteins have been reported to associate with the nucleoids (Bogenhagen DF, 2012). Due to the use of different isolation methods, combined with mass spectrometry analysis, debate is still present in the field and a unique list of proteins localised in the nucleoids is not available (Hensen F et al., 2014; Kukat C et al., 2015). It is also possible that the factors involved in different steps of mtDNA metabolism can be either permanently or transiently associated with the nucleoids, suggesting that they should be referred to as nucleoid associated proteins (mt-NAPs). Of the proteins most frequently found to be associated with the nucleoids is the transcription factor TFAM, the DNA binding proteins mt-SSB and RNA polymerase, POLRMT (Kukat C et al., 2015).

1.4. Functions of mitochondria

Despite mitochondria being commonly associated with their ability to efficiently synthesise ATP (qv 1.4.1.), these organelles perform several other essential functions, which will be briefly described in this section.

Iron-sulphur (Fe/S) clusters are important for the functions of several proteins, which use them as cofactors able to accept and donate electrons. In eukaryotic cells these clusters are found in mitochondria, cytosol and nucleus but synthesised in mitochondria before being used as cofactors by proteins involved in the tricarboxylic acid cycle (aconitase), electron transport in the OXPHOS chain (complexes I, II, III), β-oxidation of fatty acids (ETF-ubiquinone oxidoreductase) and for lipoate and biotin biosynthesis (lipoate and biotin synthases) (Rawat S et al., 2011) as well as DNA polymerases. Due to the central role of these cofactors in several processes within mitochondria, numerous diseases have been connected with defects in their biogenesis (Rouault TA, 2012).

Production of NADH and $FADH_2$ in mitochondrial is essential to donate electrons that will contribute to ATP synthesis performed by the OXPHOS system (Berg JM et al., 2002). Pyruvate in mitochondria is metabolised to acetyl-CoA, which is used in the tricarboxylic acid (TCA) cycle to generate NADH and $FADH_2$ (3 and 1 molecules for every acetyl-CoA oxidised, respectively) (Berg JM et al., 2002).

Mitochondria also play a central role in apoptosis. The Bcl2 family members Bax and Bac regulate the release from the IMS towards the OMM of proteins that, once in the cytosol, can initiate apoptosis (Cory S et al., 2002; Hockenbery D et al., 1990). One of the proteins released is cytochrome *c* (Xuesong L et al., 1996) usually confined within the intercristal space. This protein reaches the cytosol where it activates the caspase cascade that will initiate apoptosis. Omi/HtrA2 (Suzuki Y et al., 2001) and Smac/DIABLO (Rehm M et al., 2003) are also released from mitochondria to induce apoptosis. Both lead to the activation of caspases by removing their inhibition performed by components of the IAPs (inhibition of apoptosis protein) family, although by a different mechanism. While Omi/HtrA2 mediates the irreversible degradation of IAPs (Yang QH et al., 2003), Smac/DIABLO function as an antagonist of these inhibitors (Srinivasula SM et al., 2000). Together with caspases activation, apoptosis can also be promoted by degradation of nuclear chromatin DNA. The mitochondrial proteins AIF (apoptosis inducing factor) (Susin SA et al., 1996) and endonuclease G (Li LY et al., 2001) can activate apoptosis via this second pathway. AIF is an IMM protein that can be truncated and migrate to the nucleus. Endonuclease G is located in the IMS, but how its release is mediated is still unclear.

Mitochondria are also the major source of reactive oxygen species (ROS), which are generated in the matrix and play an important role in cell signalling (Ray PD et al., 2012).

In addition to these functions, mitochondria are also involved in calcium handling (Rizzuto R et al., 2012), thermogenesis (Ricquier D et al., 2000), β-oxidation of fatty acids (Kunau WH et al., 1995), and heme (Ponka P, 1999) and pyrimidine (Jones ME, 1980) biosynthesis.

1.4.1. Oxidative phosphorylation

The production of ATP is carried out by respiratory chain and ATP synthase through a process called oxidative phosphorylation. The first step involves 4 complexes whose purpose is to create a proton gradient that is used by ATP synthase to phosphorylate ADP (Fig. 1.4).

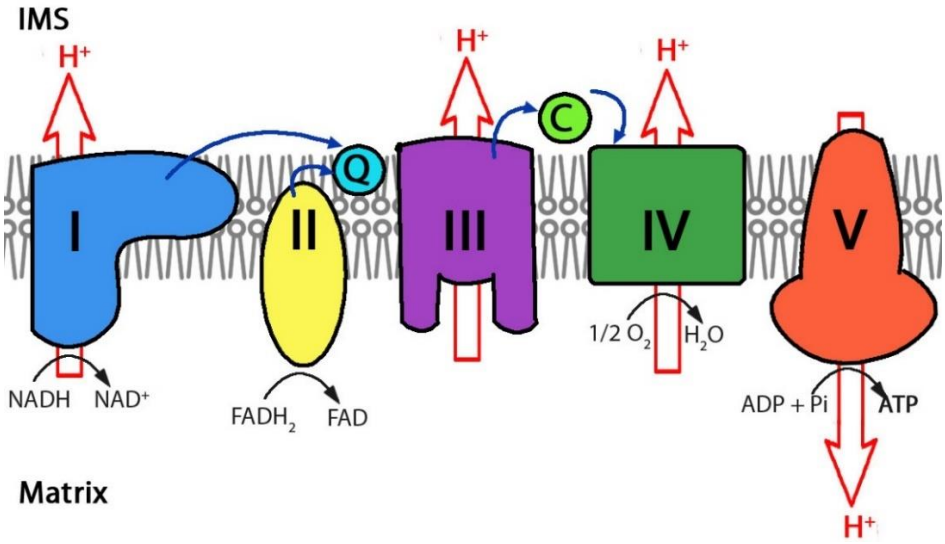

Figure 1.4 OXPHOS system.

Representation of the main components of the oxidative phosphorylation system found in the IMM. Complex I (blue), complex II (yellow), complex III (violet), complex IV (dark green), complex V (red). The movement of protons (H+) and electrons are indicated by white and blue arrows, respectively. The electron acceptors ubiquinone (cyan) and cytochrome c (green) are also depicted. Reactions occurring in the matrix side at the complexes are also reported.

The formation of the OXPHOS system is dependent both on mitochondrial and nuclear DNA (Table 1.1). Therefore mutation in either of these genomes can lead to an alteration of these complexes and cause severe diseases (Smeitink J et al., 2001).

Table 1.1 Composition of the complex of oxidative phosphorylation.

Complex	n-DNA encoded subunits	mtDNA encoded subunits
I	38	7 (ND1, ND2, ND3, ND4, ND5, ND6, ND4L)
II	4	0
III	10	1 (CyB)
IV	10	3 (COXI, COXII, COXIII)
V	14	2 (ATP6, ATP8)

The first complex (NADH:ubiquinone oxidoreductase) is composed of 45 subunits, of which 7 are mtDNA encoded. The subunits associate into an L-shape with the hydrophobic part integrated into the membrane and the hydrophilic portion directed into the matrix. In order to perform its biological activity, this large complex relies on prosthetic groups (1 flavin mononucleotide and 8 Fe-S clusters). These cofactors allow the transfer 2 electrons from NADH

(nicotinamide adenine dinucleotide) to ubiquinone, creating ubiquinol that can diffuse in the membrane. This process also results in the net transfer of 4 protons from the matrix to the intermembrane space (Efremov RG et al., 2010).

Succinate:ubiquinone oxidoreductase is the second complex of the respiratory chain and it is the only one completely encoded by the nuclear genome. It is composed of 4 subunits and contains a FAD (flavin adenine dinucleotide) group, 3 Fe-S clusters and a heme group. Two of the subunits project into the matrix and the other 2 anchor the complex to the membrane. This complex converts succinate to fumarate by transferring 2 electrons from the former to FAD. The electrons are then conveyed through the Fe-S clusters to ubiquinone, which is reduced to ubiquinol. Unlike the complex I, this complex does not act as a proton pump.

Complex III (ubiquinol:cytochrome *c* oxidoreductase) is a dimer composed of two 11 polypeptides monomer. Each monomer contains 4 prosthetic groups: 2 *b*-type cytochrome (mt-encoded), a cytochrome *c* and a Rieske protein (Fe-S cluster). In this stage, ubiquinol is oxidised to ubiquinone and protons are pumped into the interspace space increasing the proton gradient.

Cytochrome *c* oxidase (complex IV) is the terminal electron acceptor of the respiratory chain. It is composed of 13 subunits, of which 3 encoded by mtDNA, and it contains 2 non-covalently bound cytochrome and 2 copper centres (Tsukihara T et al., 1996). It reduces oxygen to 2 molecules of water, resulting in the pumping of 4 protons into the intermembrane space. The reduction of oxygen can lead to the formation of ROS that can cause damage to protein or DNA.

The proton gradient that is built by the complexes of the respiratory chain is then used by ATP synthase to produce ATP. This integral membrane complex is composed of 2 mitochondrial encoded subunits and 14 nuclear encoded subunits and is divided into 2 structural domains: F_0, a proton channel located in the IMM, and F_1, which is found in the matrix and that synthesises ATP from ADP and phosphate (Jonckheere AI et al., 2012).

1.5. Mitochondrial diseases

Due to the involvement of mitochondria in several cellular functions, a wide range of pathologies can be related to dysfunction of these organelles. Patients can be affected from the early childhood, or be asymptomatic until adulthood. These diseases are characterised by a variety of symptoms, which can have a different grade of severity and involve single or multiple organs. These usually involve tissue with high energy demands, such as the nervous system, skeletal muscle and cardiac muscle. A comprehensive summary of the genes involved in mitochondrial diseases has been recently published (Lightowlers RN et al., 2015).

Because functional mitochondria rely on both nuclear and mitochondrial DNA, these diseases can arise from mutations of either of these genomes. Mitochondrial DNA has a higher mutation rate (Schneider S et al., 1999) when compared to nuclear DNA, partially due to the presence or ROS within mitochondria and to the reduced mechanisms available for DNA repair (Dianov GL et al., 2001; Souza-Pinto N et al., 2009). Although most of the mutations are neutral, to date over

250 mutations of mtDNA have been identified. The majority of the point mutations are located in genes encoding for mt-tRNA, while the majority of the deletions are found in areas for the control of mtDNA replication and transcription (Tuppen HA et al., 2010). Few factors are involved in characterising the onset and the severity of mitochondrial diseases related to mtDNA mutations. Since mitochondria contain several molecules of mtDNA, it is possible that a mixture of wild-type and mutated mtDNA is present within the organelles (heteroplasmy). Biochemial dysfunction, which can lead to the development of clinical symphtomps, can arise when the level of mutated mtDNA reaches a threshold (Rossignol R et al., 2003). This scenario is further complicated by the random segregation of mitochondria that occurs during mitosis and can lead to a different level of dysfunctional mitochondria in the daughter cells (Matthews PM et al., 1995). Pathologies due to mtDNA mutations include progressive external ophthalmoplegia (PEO) (Dodson RF et al., 1976), MELAS (mitochondrial encephalopathy, lactic acidosis, stroke-like episodes) (Pavlakis SG et al., 1984) or MEERF (myoclonic epilepsy and ragged red fibres).

Since the majority of the mitochondrial proteome is nuclear encoded, nuclear-DNA mutations can also lead to mitochondrial diseases. These mutations will follow the classical Mendelian rules and their identification is rapidly increasing thanks to the use of next generation sequencing. Several mitochondrial diseases have been related to the mutation of nuclear-encoded genes, for example, Alpers syndrome is due to mutation of the mitochondrial DNA polymerase (Davidzon G et al., 2005), while Leigh syndrome can arise from mutations of SURF1, a gene important for the biogenesis of complex IV (Péquignot MO et al., 2001). Mitochondrial myophaty can also be due to mutations of nuclear-encoded genes encoding for the mitochondrial thymidine kinase (Saada A et al., 2001). Defects in the assembly of complex III due to mutation of BCS1L gene have been reported to lead to GRACILE syndrome (Growth Retardation, Aminoaciduria, Cholestasis, Iron overload, Lactacidosis, Early death) (Visapaa I et al., 2002).

In addition, mitochondrial dysfunction has also been suggested to play a role in other pathologies such as Parkinson disease (Schapira AH et al., 1989), Alzheimer disease (Swerdlow RH et al., 2010) and cancer (Warburg O, 1956).

Due to their complexity and variability, few options are currently available to treat mitochondrial diseases. It is, therefore, important to fully understand the different functions carried out by mitochondria to provide useful information for the diagnosis and development of treatments.

1.6. Mitochondrial DNA

The presence of double-stranded circular DNA within mitochondria was discovered in 1963 by Nass (Nass MK et al., 1963). The human mitochondrial genome is a 16,569 bases molecule encoding 13 polypeptides, 22 tRNAs and 2 rRNAs (Fig. 1.3). The polypeptides encoded by the mtDNA are all components of the OXPHOS machinery, the mt-rRNA (12S and 16S) are a part of the translation machinery and the mt-tRNAs (1 for each amino acid and 2 each for leucine and serine) are involved in translation or in the case of mt-tRNA^{Val} it is also a component of the

ribosome (Brown A et al., 2014). All the other proteins found in mitochondria are encoded by the nuclear genome and are imported into mitochondria (Mokranjac D & Neupert W, 2005) (qv 1.7.) after being synthesised by cytosolic ribosomes.

The human mitochondrial genome is very different from the nuclear counterpart. Not only is mtDNA is smaller than the nuclear one, but it is also circular, has no introns and contains only one non-coding region (displacement-loop or D-loop, Fig. 1.5), which contains important elements that regulate replication and transcription. The mitochondrial genome is organised on 2 strands: the heavy strand that contains the majority of the coding material (12 open reading frames, both the rRNAs and 14 tRNAs), and the light strand that contains just 1 open reading frame (ORF) and 8 tRNAs. The genes encoded by mtDNA are usually separated by a few bases, but in two cases they overlap (ATPase8-ATPase6 and ND4L-ND4). In the D-loop there is one promoter for the transcription for the light strand (LSP) and two for the heavy strand (HSP1 and HSP2). The presence of two HSPs has been debated in the literature. Replication of mtDNA starts from a site named O_H, which is located in this fragment too (Gustafsson CM et al., 2016)

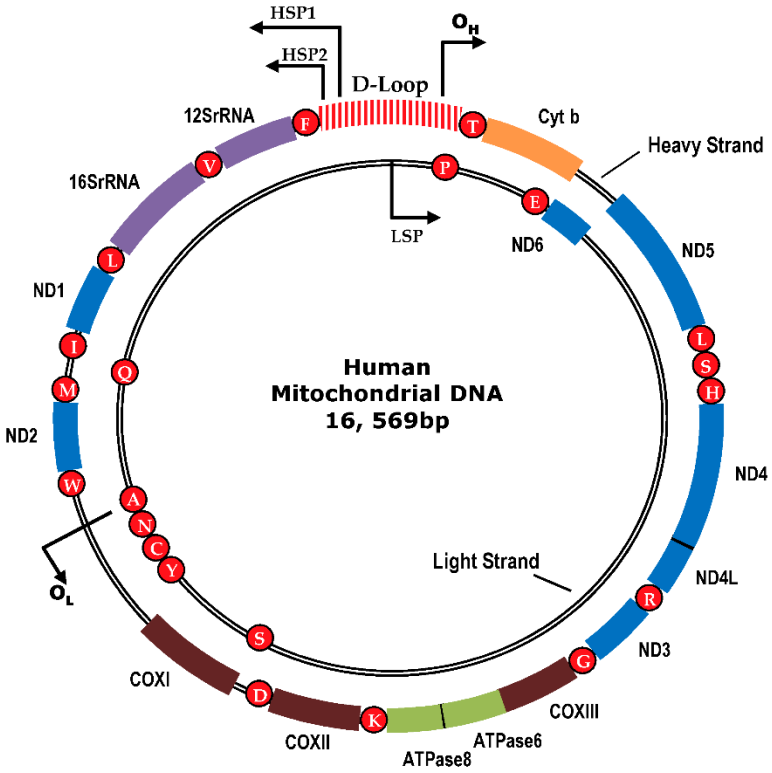

Figure 1.5 Structure of human mitochondrial genome.

The tRNA genes are indicated by red circles and their respective single letter code. The rRNA are in violet. The 13 ORF are labelled and colour-coded according to the complex of the OXPHOS that they belong to (complex I= blue, complex III= orange, complex IV= brown, complex V= green). The non-coding region (D-loop) of the heavy strand is coloured with white and red stripes. The origins of replication (O_H and O_L) as well as the origins of transcription (HSP1, HSP2, LSP) are also visualised.

The mitochondrial genome is constantly replicated (qv 1.6.1.) and this process is independent from the cell cycle (Bogenhagen D et al., 1977). As a consequence, whilst there are only 2 copies of the nuclear genome for each cell, there can be thousands of copies of mtDNA. The copy number has been reported to change dramatically between different cell lines, ranging in human from 600 in skin fibroblasts to 1,500,000 in oocytes (Greggains GD et al., 2014). The copies share the same sequence (homoplasmy), although the coexistence of molecules with different sequence due to polymorphisms or under disease conditions is also possible (heteroplasmy). During cell division, the mtDNA molecules are segregated randomly giving rise to mitochondria with different mtDNA populations. If the number of pathogenically mutated mtDNA molecules passes a threshold level, a respiratory chain deficiency can develop (Smeitink J et al., 2001).

Another difference between the nuclear and mitochondrial human genomes is found in their inheritance pattern. While the nuclear DNA contains information coming from the 2 parents, the mitochondrial genome is exclusively maternally inherited. Although documented cases of paternally-inherited mitochondria have been reported (Schwartz M et al., 2002), the organelles derived from the sperm cell are usually degraded just after fertilisation (Al Rawi S et al., 2011).

Mitochondrial DNA is not packed into chromosomes, but is instead found in structures called nucleoids (qv 1.3.1.) that groups mtDNA together with several proteins required for replication and transcription, such as DNA polymerase, DNA binding proteins (mtSSB), DNA helicase (twinkle), transcription factors (TFAM), chaperones and proteases (Bogenhagen DF, 2012). These structures are also useful to preserve the genome from a high exposure to ROS produced by oxidative phosphorylation.

1.6.1. Replication

Unlike nuclear DNA, the replication of the mitochondrial genome is independent of the cell cycle. Replication can be divided in initiation, elongation and termination (Holt IJ et al., 2012) and is performed by a specific machinery encoded in the nucleus. It is composed of DNA polymerase γ (POLG), Twinkle (DNA helicase, that unwinds the DNA), topoisomerases (that remove supercoils from the DNA molecule) and mtSSB (mitochondrial single strand DNA binding protein). While the machinery has been well defined, the process of mtDNA replication is still under debate. Although POLG and Twinkle are sufficient to synthesise ssDNA up to 2 kb *in vitro*, mtSSB are necessary to synthesise up to 16 kb (Korhonen JA et al., 2004).

Initiation begins after the mitochondrial RNA polymerase (POLRMT) synthesises the RNA primer necessary for POLG to start the replication. Once the replication machinery is assembled then elongation takes place. A number of theories have been proposed for this phase: the strand-displacement model (proposed by Clayton (Clayton DA, 1982) and revisited by Holt et al. (Holt IJ et al., 2000)), the strand-coupled bidirectional model (Bowmaker M et al., 2003) and the RITOLS (RNA Incorporation Through-Out the Lagging Strand) model (Yasukawa T et al., 2006).

According to the strand-displacement model, the H-strand is replicated from O_H found within the D-loop, using the L-strand as template. The displaced strand is covered by mtSSB, in order to protect it from damage, and it is copied only after O_L is reached. The L-strand is then synthesised in the opposite direction. The strand-coupled bidirectional model, instead, suggests that the replication of both strands happened simultaneously, starting from a common origin and proceeding bidirectionally. Evidence has been presented for both the models and it is possible that both the processes are adopted *in vivo* (Holt IJ et al., 2000).

The most recent and controversial theory is the RITOLS (or bootlace) model. According to this model, the replication follows the strand-displacement model, but the displaced strand is covered with RNA to protect the DNA from damage until the O_L is reached and its synthesis can begin.

Once elongation is completed, mtDNA replication is concluded by ligation of the ends (Ligase III) and the introduction of supercoils, which allow DNA to compact. Details regarding this stage are very sparse.

1.6.2. Transcription

The first step of gene expression is transcription, which is the synthesis of RNA molecules reading from the genome as template. In mitochondria, this process leads to the formation of 3 polycistronic species that are then processed to obtain rRNA, tRNA and open reading frames (ORFs). Transcription is performed by POLRMT, a monomeric enzyme whose C-terminal part resembles the bacteriophage T7 counterpart. The enzyme catalyses the formation of a phosphodiester bond between 2 nucleotides, coordinating their phosphate groups with 2 magnesium cations. In addition to its role in transcription of RNA required for translation, this enzyme is also responsible for the synthesis of the RNA fragment necessary to start the mtDNA replication (qv 1.6.1.). POLRMT is unable to bind and interact with the promoter sequence on the DNA by itself and it needs the help of mitochondrial transcription factor A (TFAM) that bends the promoter region and stimulates the recruitment of RNA polymerase and of TFB2M. The latter is the mitochondrial transcription factor B2 and its role is to assist the enzyme during the melting of mtDNA (Arnold JJ et al., 2012). The RNA polymerase activity has also been reported to be modulated by other components, such as mitochondrial transcription elongation factor (TEFM) (Minczuk M et al., 2011), mitochondrial transcription termination factors (mTERFs) and mitochondrial ribosomal protein L12 (MRPL12) (Wang Z et al., 2007).

The light strand is transcribed from its only promoter (LSP) and the derived polycistronic species contains the ORF for *MTND6* and 8 mt-tRNA species. Transcription of the heavy strand, instead, is 'debatably' controlled by 2 different promoters and, as a consequence, leads to the production of 2 different polycistronic species (Montoya J et al., 1982). The smaller product is composed mainly of the 2 rRNAs and it is produced from the promoter HSP1, situated 16 bp before $tRNA^{Phe}$. The larger product corresponds to the entire H-strand and it is created when

transcription starts at HSP2, situated slightly before the beginning of the gene encoding for the 12S rRNA (Fig. 1.6). Transcription of the species containing the 2 rRNA has been reported to be performed 50-100 times more than the one of the larger transcript (Gelfand R et al., 1981).

Among the 3 promoters identified, only one of them (HSP1) has a corresponding termination site and factor named mTERF1 (Fernandez-Silva P et al., 1997), which terminate at the $tRNA^{Leu}$ (Asin-Cayuela J et al., 2005). This factor has also been suggested to be involved in the initiation at HSP1 and HSP2, facilitating the recycling of the transcription machinery (Martin M et al., 2005). The termination site for LSP promoter has still not be identified, while the one for HSP2 has been located beyond the non-coding region although the binding factors are still unknown (Camasamudram V et al., 2003).

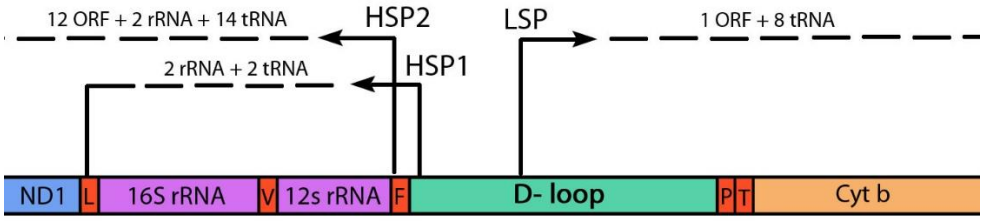

Figure 1.6 Initiation sites of mitochondrial transcription.

Representation of the initiation sites of transcription HSP1, HSP2 and LSP. These are contained in the D-loop (green). Genes encoding for tRNA are depicted in red and reported with the letter corresponding to the amino acid. The rRNA 12S and 16S are in violet. Cytochrome b (Cyt b) is in orange, while ND1 is in blue. The content of the transcript produced from every initiation site is also reported (ORF= open reading frame).

The polycistronic RNA species created during transcription need to be processed to lead to individual RNA species and then matured to produce functional mRNA, tRNA and rRNA. It is important to remember that 2 bicistronic transcript are also present, with overlapping sequences (*ND4L/ND4* and *ATP8/ATP6*). The current theory for the cleavage of transcripts is the 'tRNA punctuation model' (Ojala D et al., 1981). In the human mtDNA, the 22 tRNA genes are interspaced between the majority of genes encoding for the 13 polypeptides and the 2 rRNAs (Fig. 1.5). This model suggest that the individual RNA fragments are generated by cleavage at the 5' and 3' ends of tRNA, respectively by RNase P (Doersen CJ et al., 1985) and RNase Z (ELAC2) (Brzezniak LK et al., 2011). However, this process does not explain how the transcripts corresponding to ATP6 and COXIII are divided because no gene encoding for a tRNA species is present between the genes *MTATP6* and *MTCO3.* The transcript cannot be processed via the same mechanism, but how this is processed is still unclear.

1.7. Protein import in mitochondria

Because over 99% of the mitochondrial proteins are encoded by the nuclear, mitochondria developed a system to import several components of its proteome from the cytosol.

In order to be targeted to mitochondria, nuclear-encoded proteins need to present either a cleavable N-terminal presequence or an internal targeting signal. The cleavable presequence usually forms an amphipathic α-helix of 10-30 amino acids and is adopted by proteins destined to the matrix as well as by few IMM proteins. The internal signal, instead, is usually used by proteins of the OMM, IMS and by some IMM proteins. By interaction with different protein complexes, the mitochondrial proteins reach their destination (Fig. 1.7). All the proteins will interact with the translocase of the outer mitochondrial membrane (TOM complex). After that, OMM proteins will interact with the sorting and assembly machinery (SAM complex), while the presequence translocase (TIM23 complex) and its associated import motor (PAM complex) will take care of matrix proteins. Finally, proteins destined to the IMM will be inserted in the membrane with the help of the carrier translocase (TIM22 complex).

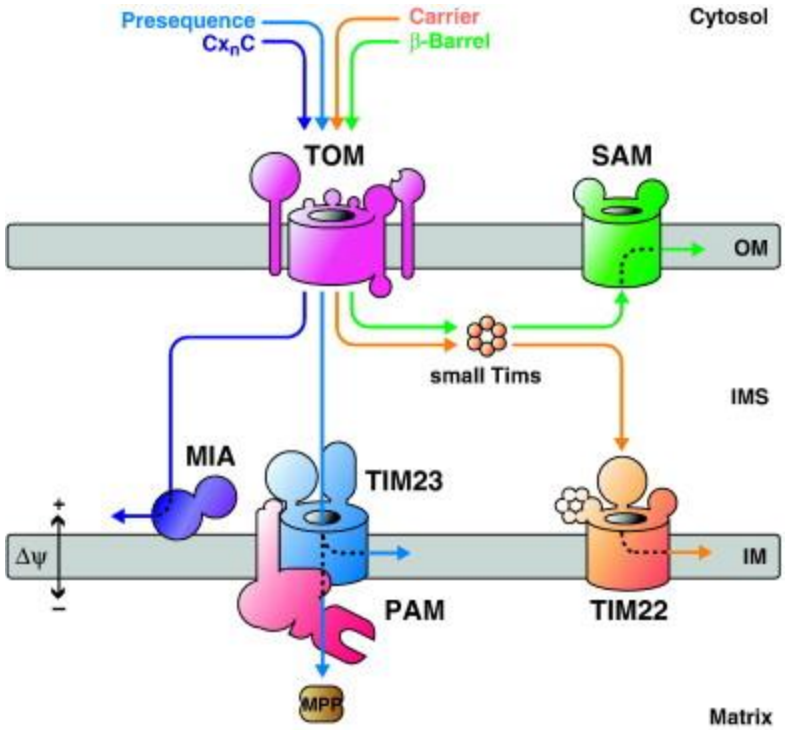

Figure 1.7 Pathways of protein import in mitochondria.

The figure (Dudek J et al., 2013) summarised the pathways of import followed by proteins of the OMM, IMM, IMS and matrix. Full description is given in the text.

Licence number: 4003280468275.

As previously mentioned, the TOM complex (Fig. 1.7, in magenta) is the first gate used by nuclear-encoded mitochondrial proteins to enter the OMM. This is composed of 7 subunits, of which 4 are receptors (Tom5, Tom20, Tom22, Tom70), 1 forms a channel (Tom40) and the other 2 are required for the stability of the complex (Tom6, Tom7). After recognition of the targeting sequence by Tom20 and Tom22 (Abe Y et al., 2000; Brix J et al., 1997), the preprotein is transferred, with the help of Tom5, to the Tom40 translocation channel. The activity and the assembly of the TOM complex have been reported to depend on cytosolic protein kinases (Schmidt O et al., 2011). In particular phosphorylation of Tom70 by protein kinase A affected its

role as a receptor. Another kinase (casein kinase 2) phosphorylate Tom22 and the import protein Mim1 (necessary for the assembly of TOM20) (Waizenegger T et al., 2005), promoting the assembling of the TOM complex. The OMM proteins with simple topology are inserted in the membrane directly by the TOM complex, while more complex proteins (such as Porin, Tom40, Sam50 and Mdm10) require the help of the SAM complex to be successfully inserted within the OMM. Carrier proteins destined to the IMM (such as ADP/ATP or phosphate carriers) are led to the receptor of the TOM complex Tom70 (Brix J et al., 1997) by the molecular chaperones Hsp90 and Hsp70 (Young JC et al., 2003) and then translocated through Tom40 to the complex Tim9-Tim10 found in the IMS (Vial S et al., 2002). These IMM proteins are then inserted in the inner membrane via the TIM22 complex (Fig. 1.7, in orange). This complex present a pore composed of Tim22, and other 3 proteins (Tim12, Tim18, Tim54). In order to insert the preprotein in the pore and to laterally release it in the IMM, membrane potential is essential. As previously mentioned, some IMM proteins also contain N-terminal presequence. These contain a hydrophobic stop signal and their translocation is arrested within the IMM, to allow their lateral movement and insertion in the lipid layer of the IMM (Glick BS et al., 1992). This fate is also followed by proteins destined to the IMS that contain an N-cleavable presequence, which are released in the IMS by cleavage of the IMM portion. IMS proteins containing cysteine residues, instead, rely for their import and assembly on the MIA machinery, also found in the IMS. The core of this machinery is Mia40, a protein which forms a disulfide bridge with the IMS protein, resulting in oxidation of the latter which will then undergo folding in the IMS (Banci L et al., 2010; Banci L et al., 2009; Hofmann S et al., 2005).

After interaction with the TOM complex, matrix proteins reach their destination by interacting with the TIM23 complex (Fig. 1.7, in light blue), which is composed of 3 integral membrane proteins (Tim50, Tim23, Tim17). After translocation through Tom40 of the TOM complex preproteins interact with Tim50, which leads them to the TIM23 complex. As with the translocation carried out by TIM22 complex, membrane potential is essential for the process and drives the positively-charged presequence towards the matrix side (Martin J et al., 1991). This process is also aided by the PAM complex (Fig. 1.7, in pink) that is localised in the matrix. The PAM complex is composed of the membrane-interacting protein Tim44 (which binds to the chaperone mtHsp70 and to the TIM23 complex) and 3 proteins that assist the process (Pam18, Pam16, and Mge1). The order of the events involved in this final step of the translocation in the matrix is not yet fully understood.

Once the N-terminal cleavable presequence is no longer needed, it is cleaved by mitochondrial processing metalloendopeptidases (Taylor AB et al., 2001). The imported mitochondrial matrix proteins are finally assisted by mitochondrial chaperones to complete their folding (Bukau B et al., 1998; Hartl FU et al., 2002).

1.8. Mitochondrial protein synthesis

1.8.1. Pre-Translation Events

The assembly of the mitoribosome, as well as the modifications and stabilisation of mRNA and tRNA are important aspects of mitochondrial translation, which are necessary prior to the beginning of the process and of which several aspects remains uncharacterised. In the following paragraphs, an overview on modifications of mRNA and tRNA, as well as on the assembly of the mitoribosome to date will be discussed.

- **mt-mRNA processing and stabilisation**

In human mitochondria, oligo/polyadenylation is necessary for the maturation of mt-mRNA transcripts, with the exception of *MTND6* (Slomovic S et al., 2005; Tomecki R et al., 2004). This process is carried out by a mitochondrial poly(A) polymerase (mtPAP), which introduces a poly- or oligo-(A) extension needed to complete the UAA stop codon in 7 transcripts (Ojala D et al., 1981). While polyadenylation is generally used in bacteria to promote the degradation of the transcripts (Xu F et al., 1995) and in the cytosol of mammalian cells to increase their stability ,(Bernstein P et al., 1989), its role on the stability of mammalian mitochondrial transcripts is still unclear (Bratic A et al., 2016; Nagaike T et al., 2005; Tomecki R et al., 2004; Wilson WC et al., 2014).

The association of mt-mRNA with mRNA-specific proteins has an influence on their stability. The degradation of transcripts encoded by the mtDNA heavy strand is prevented by the complex LRPPRC/SLIRP (Sasarman F et al., 2010), whereas *MTCO1, MTCO2, MTCO3, MTATP6/8, MTCYB* and *MTND3* are stabilised by FASTKD4 (Wolf AR et al., 2014). The only protein coding transcript derived from the light strand, *MTND6*, interacts with the binding protein FASTDK (Jourdain AA et al., 2015) and GRSF1, which is reported to affect its stability (Antonicka H et al., 2013; Jourdain AA et al., 2013).

- **Maturation of mt-tRNAs**

Several modifications are needed to promote function and stability of mt-tRNA. A comprehensive description of these modifications have been described by Suzuki (Suzuki T, 2014) and Salinas-Giege et al (Salinas-Giege T et al., 2015). After the mt-tRNAs have been modified and the CCA is added to the 3' terminus (Nagaike T et al., 2001), the transcripts are ligated to the appropriate amino acid by the relevant mitochondrial aminoacyl-tRNA synthetase (Diodato D et al., 2014). The mt-tRNAs are then competent to participate in mitochondrial translation.

- Assembly of the mitoribosome

The mitochondrial translation machinery is, like other ribosomes, composed of 2 subunits. Several key players are needed to correctly assemble the rRNA and the ribosomal proteins into complete and functional subunits but while this process is well understood for the bacterial ribosome (Hage AE et al., 2004), the steps of the biogenesis of the mammalian mitoribosome are mainly unknown.

After transcription, the rRNA molecules are cleaved from the polycistronic transcript and are likely to be stabilised and modified prior to its assembly in the subunits. The rRNAs are subjected to pseudouridylation, base methylation and 2'-O-ribose methylation at conserved sites that are important during translation. The extent of the modification was originally assessed on mammalian mitochondria from hamster cells, where 9 modifications were detected (Dubin DT et al., 1978). Five were base methylations of 12S mt-rRNA, of which 3 are performed by TFB1M (adenine) (Metodiev MD et al., 2009; Seidel-Rogol BL et al., 2002) and NSUN4 (cytosine) (Metodiev MD et al., 2014). Three 2'-O-ribose methylation were detected on 16S mt-rRNA, performed by methyltransferases (MRM1, MRM2, MRM3) (Lee KW et al., 2014 ; Rorbach J et al., 2014). The 16S mt-rRNA is also supposed to be pseudouridylated (Ofengand J et al., 1997), although this modification was not detected in the study performed on hamster. Recently, some mitoribosomal protein have been identified in association with unprocessed RNA, suggesting that mitoribosomal assembly proceeds co-transcriptionally (Rackham O et al., 2016).

GTPases and ATP-dependent RNA helicases are required for the formation of ribonucleoprotein particles. However, few of these enzymes have been identified in mammalian mitochondria (De Silva D et al., 2015). To date, 2 mitochondrial GTPases (Mtg1, Mtg2) have been reported to interact with the incomplete mt-LSU (Kotani T et al., 2013), and 1 (C4orf14, or NOA1) appears to play a role in the assembly of the mt-SSU (He J et al., 2012). Different hypotheses have been suggested for the role of GTPases in this process. It is possible that the hydrolysis of GTP regulates the association or dissociation of proteins, or that this promotes conformational changes. It has also been suggested that these proteins might act as place holders for other proteins prior their recruitment in the biogenesis process. Finally, the GTPases might act as sensors for GTP/GDP ratio, reducing the assembly of new mitoribosomal subunits in conditions of starvation (lower GTP/GDP ratio). ERAL1 is an RNA-binding GTPase that has been reported to stabilise 12S mt-rRNA (Dennerlein S et al., 2010; Uchiumi T et al., 2010).

ATP-dependent RNA helicases are enzymes that bind and remodel RNA and ribonucleoprotein particles. Their roles can involve unwinding RNA (important to initiate ribonucleoprotein assembly) or protein displacement from RNA (Linder P et al., 2011). At present few have been identified in human mitochondria. DDX28 (Tu YT et al., 2015) and DHX30 are both involved in mitoribosome assembly (Antonicka H et al., 2015). In addition,

another helicase, SUPV3L1, has been reported to play a role in mt-RNA metabolism (Borowski LS et al., 2013).

Together with GTPases and helicases, only a few other factors involved in the assembly of mammalian mitoribosomes have been reported. mTERF3, involved in mitochondrial transcription, appears to be able to associate to 16S mt-rRNA and play a role in the biogenesis of the mt-LSU (Wredenberg A et al., 2013). FASTKD2 (Fas-activated Serine Threonine Kinase) and the helicase DDX28 are also shown to be required for mt-LSU (Antonicka H & Shoubridge EA, 2015; Popow J et al., 2015; Tu YT & Barrientos A, 2015). In yeast the maturation of MRPL32 is required for its insertion in pre-ribosomal particles and is supported by the components of the mAAA-protease system (Nolden M et al., 2005). Another protein, C7orf30 (MALSU1), has been reported to interact with MRPL14 and might be involved in the assembly of the mt-LSU (Fung S et al., 2013; Rorbach J et al., 2012). Depletion of the IMM-interacting protein MPV17L2, also known to interact with the mt-LSU, showed a reduction of both subunits, suggesting a possible role in their assembly (Dalla Rosa I et al., 2014). Finally, mt-SSU assembly has been suggested to be aided by GRSF1 as its depletion leads to accumulation of incomplete subunit (Antonicka H et al., 2013; Jourdain AA et al., 2013).

Concerning the localisation of mitoribosomal assembly, 2 submitochondrial compartments have been suggested, the RNA granules and the nucleoids (qv 1.3.1.). Briefly, RNA granules are the centre of posttranscriptional RNA processing and maturation, while nucleoids are the site for mtDNA maintenance, replication and transcription. Proteins involved in mitoribosomal biogenesis have been detected in both nuceloids and RNA granules compartments, together with several mitoribosomal proteins (Antonicka H & Shoubridge EA, 2015; Bogenhagen DF et al., 2014), suggesting that mitoribosome assembly might begin in the nucleoids and continue in the RNA granules. More studies are needed to identify the involvement of these compartments in this process, as well as all the steps that lead to fully assembled mitoribosomal subunits.

1.8.2. Molecular Mechanisms of Mitochondrial Translation

Transcription of human mtDNA leads to the formation of 9 monocistronic and 2 dicistronic mRNA species that are translated by the mitoribosome in a process that can be divided in initiation, elongation and termination (reviewed in (Christian BE et al., 2012; Mai N et al., 2016; Ott M et al., 2016)). While the process does not differ significantly from the one described for the other ribosomes, it is important to remember that mitochondrial coding system varies in different organism. In mammalian mitochondria, the canonical stop codon UGA is recognised as tryptophan, while AUA encodes for methionine, and AGA and AGG are codons not recognised by any mt-tRNA or protein (Chrzanowska-Lightowlers ZM et al., 2011; Suzuki T et al., 2011).

The first step in protein synthesis is initiation (Fig. 1.8). At the beginning of this phase, the mt-SSU is bound to the initiation factor mtIF3, which inhibits the early formation of the monosome. The complex is joined by the initiation factor mtIF2:GTP and, subsequently, the mRNA enters the mRNA tunnel. The recruitment of mRNA has been suggested to be helped by a mitoribosomal protein found at the entrance of the mt-mRNA channel of the mitoribosome, named MRPS39 (Amunts A et al., 2015; Greber BJ et al., 2015). AUG, AUA, AUU are recognised as start codons by a formylated methionyl-tRNA (Tucker EJ et al., 2011), which is also recruited by mtIF2:GTP to the mitoribosome. In the case of a positive codon:anticodon interaction, a stable complex is created and the interaction with the mt-LSU follows. The formation of the monosome causes the hydrolysis of the mtIF2-bound GTP to GDP and the release of mtIF2 and mtIF3 from the complex. If the start codon is not present in the P-site or f-Met-tRNAMet is not available, the inspection fails and the mRNA is released.

A peculiar feature of human mt-mRNAs is the absence of a 5' untranslated sequence, used by prokaryotes to position the start codon in the ribosome. Of the monocistronic transcripts, only 3 mt-mRNA present a few nucleotides prior the start codon, while the others have the AUG immediately at the 5' end (Christian BE et al., 2010). The 2 bicistronic transcripts, *RNA7* (*MTND4/MTND4L*) and *RNA14* (*MTATP8/MTATP6*), present an upstream sequence ahead of the second ORF, which corresponds to the upstream sequence. How these start codons are correctly localised within the mitoribosome is still unclear.

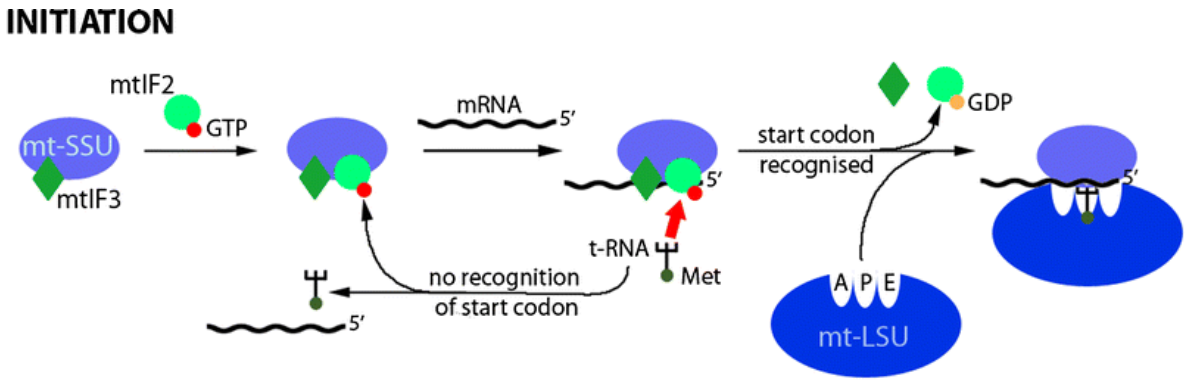

Figure 1.8 Initiation of mitochondrial translation.

Diagram of the stages and the key players of mitochondrial translation initiation. A complete description of the process can be found in the text.
mt-SSU: small mitoribosomal subunit; mt-LSU: mitoribosomal large subunit; mtIF2, mtIF3: mitochondrial initiation factor 2 and 3; Met: methionine; GTP: guanosine triphosphate; GDP: guanosine diphosphate.

Figure from Mai N et al. (2016).

After the monosome is formed, the elongation of the nascent chain can start (Fig. 1.9). The mitochondrial elongation factor mtEF-Tu, GTP and a charged mt-tRNA form a complex, which can enter the A-site, where the codon:anticodon interaction takes place. In the case of a positive interaction, the mitoribosome stimulates the hydrolysis of GTP and the subsequent release of GDP:mtEF-Tu. The interaction of mtEF-Tu with the nucleotide exchange factor mtEF-Ts

restores the GTP:mtEF-Tu complex (Cai YC et al., 2000). After the release of mtEF-Tu, the peptidyl transferase centre (PTC) in the mt-LSU catalyses the formation of the peptide bond. As a result, a polypeptidyl-tRNA is found in the A-site, while the P-site of the mitoribosome is occupied by a deacylated mt-tRNA. The release of the mt-tRNA from the P-site and the movement of the peptidyl-tRNA to the same site are mediated by the alteration of the structural conformation of the mitoribosome triggered by the elongation factor mtEF-G1 with the mitoribosome. The recent publication of the porcine and human structures (Amunts A et al., 2015; Greber BJ et al., 2015) confirmed the presence of an E-site in mammalian mitoribosome where the deacylated mt-tRNA moves to before exiting the monosome. This process is then repeated until a stop codon is presented in the A-site.

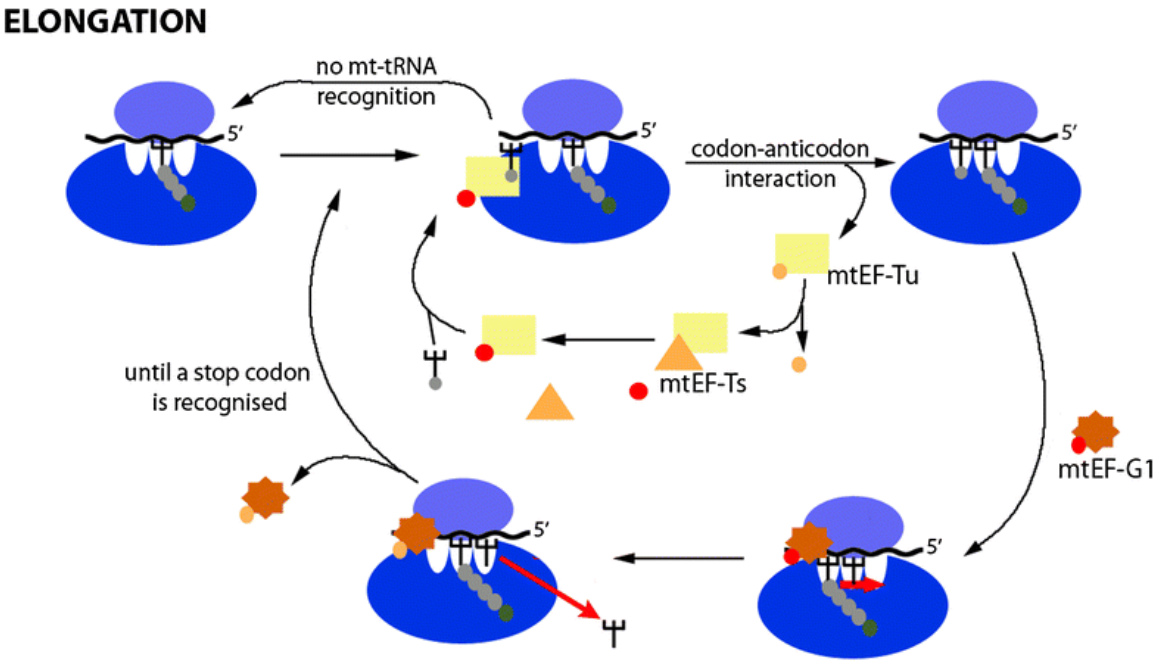

Figure 1.9 Elongation process in mitochondrial translation.

Schematic representation of the elongation of the nascent polypeptide chain during mitochondrial translation. The description of all the stages and components involved can be found in the main text. The mt-SSU is depicted in light blue, while the mt-LSU is in dark blue. The red dot represents GTP, while the orange one GDP.
mt-SSU: small mitoribosomal subunit; mt-LSU: mitoribosomal large subunit; mtEF-Tu, mtEF-Ts, mtEF-G1: mitochondrial elongation factor Tu, Ts and G1; GTP: guanosine triphosphate; GDP: guanosine diphosphate

Figure from Mai N et al. (2016).

The termination of protein synthesis takes place once a stop codon enters the A-site (Fig. 1.10). In human mitochondria, this codon is recognised by mtRF1a (mitochondrial release factor 1a), which is believed to be sufficient to terminate the synthesis of all the 13 mt-encoded polypeptides (Soleimanpour-Lichaei HR et al., 2007). This factor belongs to class I release factors that, unlike class II, is able to recognise specific sequences of the mRNA and has two functions. The first is the recognition of a stop codon on the A-site and mediated by its sequence recognition domains. The second function, which is dependent on the first, is performed by a

conserved GGQ domain that promotes the catalysis of the hydrolysis of the ester bond between terminal mt-tRNA in the P-site and the nascent polypeptide (Frolova LY et al., 1999). In the presence of GTP, mtRF1a promotes the release of the polypeptide from the mt-LSU (Schmeing TM et al., 2005).

UAA and UAG are used as stop codons in human mitochondria to terminate 9 and 2 ORFs respectively. The coding sequence for the remaining 2 ORFs, *MTCO1* and *MTND6*, terminates in AGA and AGG respectively. Because no corresponding tRNA was present in the mitochondrial genome, these triplets were originally suggested as alternative stop codons (Anderson S et al., 1981). Recent studies, however, showed that a classical UAG codon was also used by these two species to terminate translation (Temperley R et al., 2010). This was explained by the occurrence of a -1 frameshift, which might be due to structured RNA found downstream of the termination codons. This mechanism, reasonable for humans, does not lead to the creation of a stop codon in all other vertebrates. More recently, ICT1 has been proposed to act as a mitochondrial translation release factor and may be involved in the termination of the synthesis of COXI and ND6. This protein has an indiscriminate peptidyl-tRNA hydrolase activity (Richter R et al., 2010) and might enter the A-site to promote the release of the polypeptide chain (Akabane S et al., 2014), as performed by its bacterial homologue ArfB (Gagnon MG et al., 2012). In contrast with this hypothesis, ICT1 has been identified as a constitutive component of mt-LSU where it is not located in proximity of the A-site (Brown A et al., 2014; Greber BJ et al., 2014), having therefore limited access to this site. Despite this, it has been proposed that a limited free pool of ICT1 might perform the hydrolase activity. Recent studies on isolated ICT1 confirmed its ability to hydrolyse peptidyl-tRNA on stalled ribosomes but, intriguingly, not when the RNA template extended more than 14 nucleotides past the A-site (Feaga HA et al., 2016). As *MTCO1* and *MTND6* mt-mRNA have 3' extensions longer than 14 nucleotides, it is unlikely that ICT1 might act as a natural translation terminator in vivo.

Finally, the dissociation of the mitoribosomal subunits is promoted by 2 ribosomal recycling factors, mtRRF1 and mtEF-G2, leading to the release of mt-mRNA and deacylated mt-tRNA (Rorbach J et al., 2008; Tsuboi M et al., 2009). After the release of the 2 recycling factors the translation cycle can reinitiate.

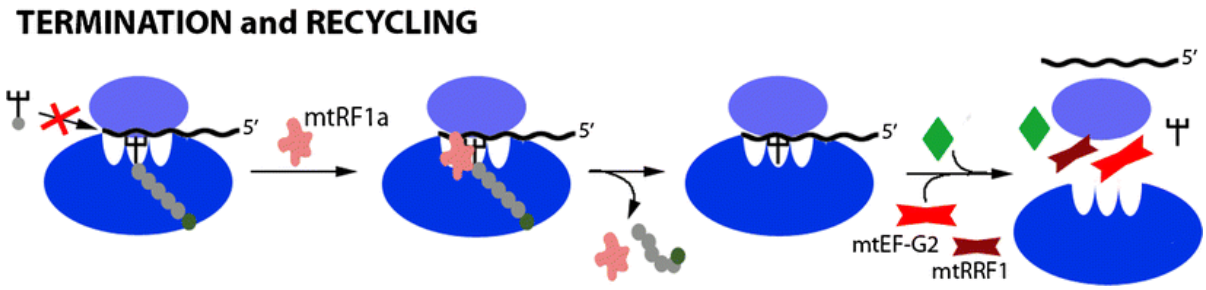

Figure 1.10 Termination of mitochondrial protein synthesis and recycling of the mitoribosomal subunits.

The last stages of mitochondrial translation are summed up in this figure. A complete description is present in the text. The mt-SSU and mt-LSU are depicted in lighter and darker blue, respectively.
mt-SSU: small mitoribosomal subunit; mt-LSU: mitoribosomal large subunit; mtRF1a: mitochondrial release factor 1a; mtRRF1: mitochondrial ribosomal recycling factor 1; mtEF-G2: mitochondrial elongating factor G2.

Figure from Mai N et al. (2016).

1.8.3. Regulation of mitochondrial translation

The efficient assembly of the OXPHOS complexes relies on the coordination of cytosolic and mitochondrial translation. In yeast, translation can be activated by several proteins, which associate with the untranslated regions (mainly 5') of all yeast mt-mRNA species (reviewed in (Herrmann JM et al., 2013)). Published data suggested the involvement of these proteins in feedback loops, regulating mitochondrial translation depending on the availability of nuclear-encoded components of the OXPHOS that leads to a successful assembly of the complex.

The absence of untranslated regions in the majority of human mt-mRNA transcripts indicates that any translational activators would have to act via a different mechanism. At present, only 1 translational activator has been identified in human mitochondria. This was named TACO1 and its absence in patients presenting mutations in the encoding gene resulted in the selective loss of translation of *MTCO1* (COXI of complex IV) (Weraarpachai W et al., 2009). Translational activators bind in most cases to the 5'-UTR of transcripts. Since this is absent in *MTCO1,* it has been suggested that TACO1 might have an effect on the translation of this mRNA by stabilising the nascent polypeptide or by promoting the recognition of the start codon. Another hypothesis suggests a role of TACO1 in the release of the complete COXI, via interaction with the translation termination factor (Weraarpachai W et al., 2009).

Recent studies suggested that the assembly of the OXPHOS complexes can regulate mitochondria translation, helping to maintain the balance with nuclear translation. Studies on complex IV assembly identified a complex named MITRAC (MItochondrial TRanslation Regulation Assembly intermediate of cytochrome c oxidase (Mick DU et al. 2012)). Two of its components, C12orf62 and MITRAC12, appeared to regulate COXI synthesis, as their loss affected this process (2012; Weraarpachai W et al., 2012). Recent studies showed that the translation of COXI was stalled in absence of the nuclear encoded COXIV, futher suggesting an

effect of the assembly of complex IV on mitochondrial translation (Richter-Dennerlein R et al., 2016). Similarly, defects in the assembly of complex III were reported to decrease the translation of cytochrome *b* (Tucker EJ et al., 2013).

As a result of the mitochondrial levels of ATP, acetyl-CoA and NADH, mitoribosomal proteins can be phosphorylated (Miller JL et al., 2009) or acetylated, affecting the interaction between the 2 subunits of the machinery. For example, a role in the formation of the monosome might be played by the mt-specific protein DAP3 (also known as MRPS29). This protein presents phosphorylation sites on its intersubunit face (Miller JL et al., 2008), which might have an impact on the formation of the monosome (Miller JL et al., 2009). In addition, DAP3 is bound to GDP in the mammalian 55S structures (Amunts A et al., 2015; Greber BJ et al., 2015), and it is possible that the hydrolysis of GTP to GDP might play a role in ribosome assembly (Amunts A et al., 2015). Modifications of other mitoribosomal proteins have been identified at the subunits interface or in domains crucial for translation (mRNA channel, the PTC or the PES) and are also likely to have a role in regulating the assembly of the monosome (Miller JL et al., 2009). This process is also promoted by mTERF4-NSUN4, an mt-SSU-interacting complex that supports the recruitment of the mt-LSU (Cámara Y et al., 2011; Metodiev MD et al., 2014). Studies on the pentatricopeptide repeat (PPR) domain protein MRPS27 suggested a potential role of this protein in regulating mitochondrial translation, although the mechanism is still unknown (Davies SM et al., 2012). Recently, the protease CLPP was suggested to regulate translation by removing ERAL1 from the 12S rRNA (Szczepanowska K et al., 2016).

Finally, mitochondrial translation was also reported to be affected by the cellular environment. In the cytosol, the interaction of microRNAs with the proteins AGO2 and GW182 creates a complex capable of reducing translation of cytosolic mRNAs (Czech B et al., 2011). A complex between microRNAs and AGO2 was also observed in mitochondria, where it increased the translation of certain transcripts during muscle differentiation (Zhang X et al., 2014). However, the presence of miRNAs in mitochondria is still unclear (Mercer TR et al., 2011).

1.8.4. Post-Translation events

While the mitoribosomal subunits are recycled at the end of mitochondrial protein synthesis, the fate of mt-mRNA is still unclear. The mt-mRNAs species might be protected and translated again, thanks to the interaction with RNA chaperones (like LRPPRC/SLIRP, FASTKD2, FASTKD4), but it is also possible that these species are degraded. The helicase responsible for RNA metabolism has been identified as SUPV3L1 (Minczuk M et al., 2002). It was found to interact with the human polynucleotide phosphorylase (PNPase) (Borowski LS et al., 2010), which was shown to be important for mitochondrial RNA degradation (Chujo T et al., 2012). However, the localisation of this protein within the mitochondrial intermembrane space (Wang G et al., 2010) makes unlikely its involvement in RNA degradation in the matrix. An exonuclease, named REXO2 was identified both in the cytosol and in mitochondria and might play a role in the degradation of RNA species in mitochondria (Bruni F et al., 2013). In addition to REXO2,

recent studies identified an endoribonuclease, LACTB2, with mitochondrial localisation. The physiological role of this protein is still unclear (Levy S et al., 2016).

1.9. The mitoribosome

The existence of a mitochondrial machinery for protein synthesis was discovered in 1958 by John R. McLean in rat liver (McLean J et al., 1958) and this was then isolated from the same organ in 1967 by Thomas W. O'Brien (O'Brien TW et al., 1967). Like the other ribosomes, mitochondrial ribosomes are composed by 2 subunits, large and small, that associate together to form a fully functional monosome. Because it has been proposed that mitochondria derive from the endosymbiosis of an α-proteobacteria, it was originally thought that their ribosome would resemble the bacterial counterpart more than the cytosolic one. However, several differences are present between bacterial and mitochondrial ribosomes and, further, differences can be highlighted between mammalian and yeast mitoribosomes, suggesting a parallel evolution of these 2 machineries from the common bacterial ancestor. The most striking difference between these 3 regards the amount of RNA and protein. While the bacterial ribosome and yeast mitoribosome are mainly composed of RNA (approximately 70% of its total weight), the RNA:protein ratio is reversed to 30:70 in the mammalian mitoribosome, as a consequence of the shortening of the rRNA molecules and the presence of additional protein mass (Fig. 1.11), already identified in proteomics studies carried out in 2001 (Koc EC et al., 2001; Koc EC et al., 2001). The different RNA:protein ratio observed for the mammalian mitoribosome also results in a different composition of intersubunit bridges. In bacteria, the two ribosomal subunits interact mainly via RNA:RNA bridges (Liu Q et al., 2016), whereas in the mammalian 55S particle there is a higher proportion of protein-protein and RNA:protein connections (Amunts A et al., 2015; Greber BJ et al., 2015). As opposed to mammalian mitoribosomes, the yeast mt-rRNAs acquired new domains (Foury F et al., 1998). Despite this, the yeast mitoribosome present several mitochondrial-specific (mt-specific) proteins absent in the bacterial counterpart.

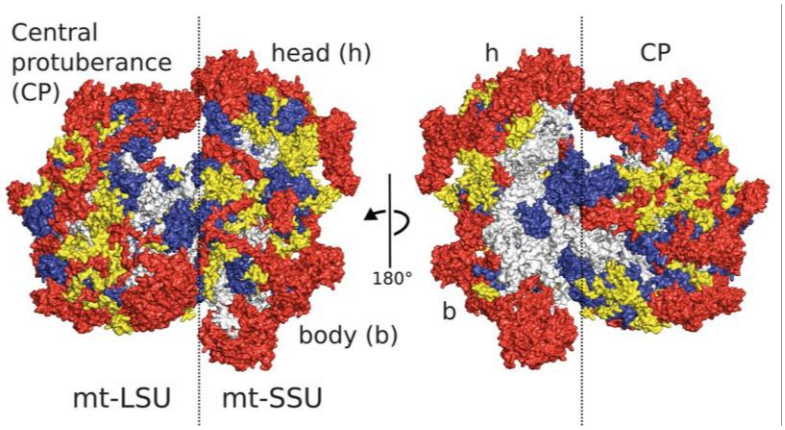

Figure 1.11 Distribution of conserved and mitochondrial specific proteins in the human mitoribosome.

Representation of the human mitoribosome. Proteins conserved with bacteria are depicted in blue, extensions of homologous proteins in yellow, and mitochondria-specific proteins in red. rRNA is shown in grey.

Figure from Amunts A et al. (2015), License number 3930190789240

The increase of protein content observed for mitochondrial ribosomes is a result of both the extension of homologous proteins and the acquisition of mt-specific proteins. In mammalian mitoribosomes, a small proportion of the new protein mass is filling the void due to the shortening of rRNAs. The majority of this new mass is, instead, found peripherally (Brown A et al., 2014) and has been suggested to protect the mt-rRNA from potential damages due to the presence of high ROS levels within the organelle (Lightowlers RN et al., 2014). In addition to ROS protection, some of the mt-specific proteins also present a second function. For instance, several DAP3 (Kissil JL et al., 1999), MRPL37 (Levshenkova EV et al., 2004), MRPL41 (Yoo YA et al., 2005) and MRPL65 (previously named MRPS30) (Sun L et al., 1998) have been linked to apoptosis. Another protein, MRPL12, seems to play a role in POLRMT function and stability (Nouws J et al., 2016; Surovtseva YV et al., 2011). The cryo-EM studies performed on human and porcine samples also confirmed the presence of, ICT1, a ribosome-dependent peptidyl-tRNA hydrolase (Richter R et al., 2010) has been confirmed as a structural component of the mt-LSU but might also play a role in translation as mentioned in the previous paragraph (Akabane S et al., 2014; Feaga HA et al., 2016).

Despite all of the differences, the functional core of the mitoribosome is mainly conserved, suggesting that the mechanism of protein translation does not differ considerably from the bacterial counterpart. This is composed of the mt-mRNA recognition site on the mt-SSU and peptidyl transferase centre in the mt-LSU.

In the last few years, a new nomenclature has been adopted for mitoribosomal proteins, according to the presence of homologues of these proteins in bacteria (Ban N et al., 2014). However, in this study, the old nomenclature will be reported. If needed, a table reporting new and old nomenclature can be found at Appendix 1.

1.9.1. Structure of the mammalian mitoribosome

While the first low resolution cryo-EM structure of the bovine monosome was released in 2003 (Sharma MR et al., 2003), the structure of the human (Amunts A et al., 2015; Brown A et al., 2014) became available after the beginning of this study, together with the high-resolution structure of the porcine counterpart (Greber BJ et al., 2015; Greber BJ et al., 2014).

As previously mentioned, the functional core of the mitoribosome has been conserved throughout evolution and, as in most ribosomes, the A, P and E sites can be identified (Wettstein FO et al., 1965). The residues of the mt-SSU important for the decoding at the A-site are present, and the ability of mt-tRNA to interact with the mt-LSU has also been conserved. Due to the shortening of the rRNA, no A-site finger was detected on porcine mitoribosomes. This structure might not be necessary as mammalian mt-tRNAs do not show the typical cloverleaf structure observed in their bacterial counterparts (Suzuki T et al., 2011). The P-site is well preserved, although the presence of a P-site finger introduces a stronger interaction with the T-loop of mt-tRNAs than those seen in bacteria (Schuwirth BS et al., 2005). This structure might be necessary to keep mt-tRNAs in position, because their T-loop is smaller than those of bacterial tRNA. Finally, despite most of the contact points between the bacterial ribosome and tRNA on the E-site seemed absent on the mammalian mitoribosome until the recent cryo-EM studies confirmed its modified presence (Greber BJ et al., 2014).

- **Mitoribosomal small subunit**

The mammalian mt-SSU is composed of 30 proteins (14 mt-specific in human) and a 12S mt-rRNA (Amunts A et al., 2015; Greber BJ et al., 2015). Due to the presence of the mt-specific proteins, the shape of the subunit differs from the bacterial counterpart and appears more elongated.

The mt-mRNA entrance channel is one of the most divergent areas of the mt-SSU. RPS4 and the C-terminus of RPS3 (uS3) define the entrance of this channel in the bacterial ribosome but are absent in the mt-SSU (Fig. 1.12A). The ring-shaped entrance is, instead, defined by a mt-specific extension of MRPS5 (Fig. 1.12B). Another mt-specific protein, MRPS39 (PTCD3) is found in close proximity to the entrance site for mRNA. Because this protein belongs to the pentatricopeptide repeat containing (PPR) protein family that are able to bind RNA (Filipovska A et al., 2013; Lightowlers RN et al., 2013), it is possible that this protein could be involved in recruiting the mt-mRNA to the mt-SSU.

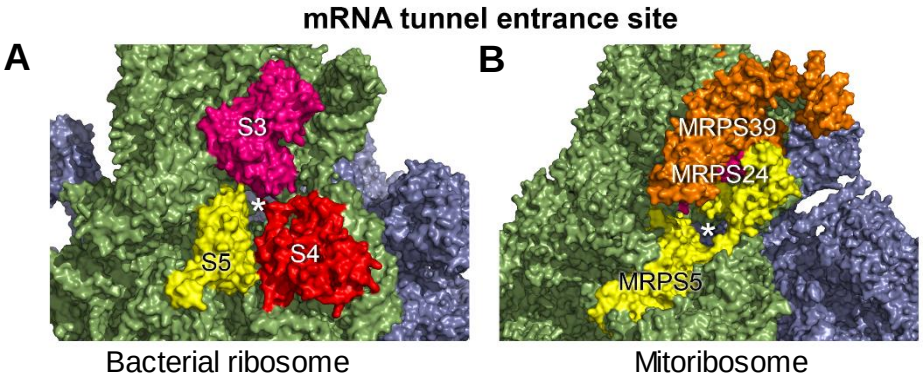

Figure 1.12 mRNA entrance site for the human mitochondrial and bacterial ribosomes.

Representation of the proteins defining the entrance site of the mRNA tunnel of human mitochondria ribosomes (**B**, PDB 3J9M (Amunts A et al., 2015)) and the bacterial counterpart (**A**, PDB 4YBB (Noeske J et al., 2015)). The small subunit is in green, whereas the large is in blue. The entrance of the tunnel is indicated by an asterisk. Homologues protein are depicted in the same colours. Magenta corresponds to S3 in the bacterial ribosome, which is the homologue of MRPS24 of the human counterpart.

Figure modified from Mai N et al. (2016).

Bacterial ribosomes present an anti Shine-Dalgarno sequence on the rRNA, close to the exit of the mRNA exit site. This domain is absent in the 12S mt-rRNA and reflects the absence on mt-mRNAs of the corresponding 5'-untranslated region (Montoya J et al., 1981). The space generated by the lack of this rRNA domain is now occupied by the mitochondrial-specific protein mS37 that takes on the interaction with the 12S mt-rRNA. In contrast to these structural modifications, the central portion of the mRNA channel that is directly involved in the translation process, is mostly conserved (Greber BJ et al., 2014).

- Mitoribosomal large subunit

The mammalian mt-LSU is composed of 16S mt-rRNA and 52 proteins (53 in humans), of which 22 are mt-specific (Brown A et al., 2014; Greber BJ et al., 2014). An additional rRNA molecule (5S) is found in the central protuberance of bacterial LSU (Ban N et al., 2000). No additional rRNA is encoded by the mitochondrial genome but, in 2014 a cryo-EM structure of the mammalian mitoribosome revealed the presence of an unidentifiable RNA density similar to a domain of bacterial 5S rRNA (Greber BJ et al., 2014). The recent higher-resolution cryo-EM studies on mt-LSU confirmed the presence of an additional RNA species, identifying a mt-tRNA^{Phe} for the porcine mitoribosome (Greber BJ et al., 2014) and mt-tRNA^{Val} for the human counterpart (Brown A et al., 2014).

One of the most altered domain of the mitoribosome is the polypeptide exit site (PES) (Fig. 1.13). In mammals, a second layer of mt-specific proeins (MRPL39, MRPL44 and MRPL45) are found on top of a conserved ring of proteins (MRPL22, MRPL23, MRPL24, MRPL29) that define the exit site itself. Because the mitoribosome is specialised in the synthesis of highly

hydrophobic proteins, it is possible that the recruitment of these additional proteins might aid their synthesis and couple it with their insertion in the IMM.

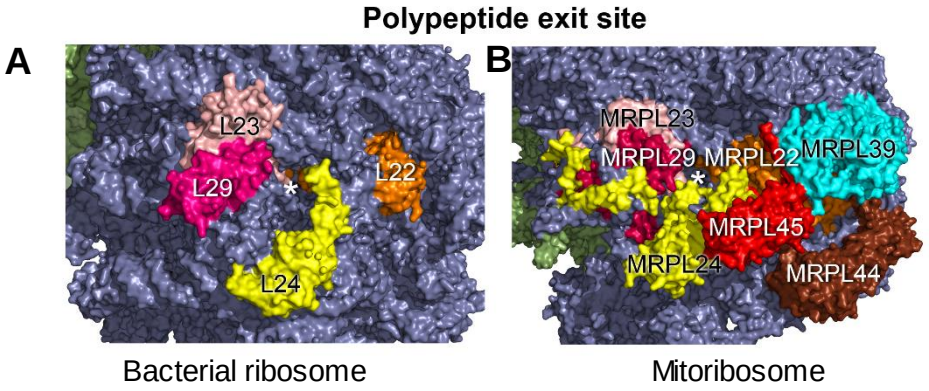

Figure 1.13 Polypeptide exit site of bacterial and human mitochondrial ribosomes.

The polypeptide exit site of bacterial (**A**, PDB 4YBB (Noeske J et al., 2015)) and human mitochondrial (**B**, PDB 3J9M (Amunts A et al., 2015)) ribosomes were visualised in Pymol. The SSU are depicted in green, while the LSU in green. The exit site is indicated by an asterisk and homologous proteins are reported in the same colour.

Figure modified from Mai N et al. (2016).

1.9.2. Interaction of the mitoribosome with the inner mitochondrial membrane

Mitochondrial ribosomes are specialised in the synthesis of highly hydrophobic polypeptides, which are all components of the OXPHOS system. In order to avoid their aggregation and precipitation in the matrix, their translation is likely to be coupled with their insertion within the IMM. This will be aided by the anchoring of the mitoribosome to the membrane so that the polypeptide exit site can be aligned with the insertion machinery.

Studies in yeast identified the IMM-interacting protein Mba1 (Ott M et al., 2006; Pfeffer S et al., 2015), the IMM protein Mdm38 (Lupo D et al., 2011) and Oxa1 (Jia L et al., 2003) as able to interact with the mitoribosome. Recently, this important interaction was confirmed in yeast by cryo-EM tomography (Pfeffer S et al., 2015). This study was able to show mitoribosomes anchored to the IMM and to identify Mba1 and rRNA as interacting points.

These important interactions are still mainly unexplored in mammalian mitoribosomes. Studies on the bovine system reported that approximately 50% of mitoribosomes interact with the IMM (Liu M et al., 2000). The authors suggested that the interaction might be mediated by both electrostatic interactions of the mitoribosome with the membrane, and direct interaction between the mitoribosome and IMM proteins. Amongst the IMM proteins, OXA1L (homologue of yeast Oxa1) has been cross-linked to components of the mt-LSU, suggesting its involvement in the interaction (Haque ME et al., 2010). LetM1, another IMM protein, is the homologue of yeast ribosome-interacting protein Mdm38 and has also been reported to interact with the mitoribosome (Piao L et al., 2009). Finally, MPV17L2 is a protein that has been recently reported

to interact with both the IMM and the mt-LSU, suggesting that it might be involved in anchoring the subunit to the IMM (Dalla Rosa I et al., 2014).

Amongst the mitoribosomal proteins, MRPL45 is a mt-specific protein found in close proximity to the polypeptide exit site, an ideal position for membrane-interaction, a hypothesis also suggested by Greber et al. shortly after this study began (Greber BJ et al., 2014). The potential involvement of MRPL45 in the interaction with the IMM is also supported by its homology with the membrane-interacting yeast protein Mba1 (Ott M et al., 2006; Pfeffer S et al., 2015) and by its structural homology with another IMM-interacting protein, Tim44 (Handa N et al., 2007).

As the role of the proteins involved in the interaction between mitoribosome and IMM is the theme of my thesis, these aspects will be more extensively discussed in the introductions of the results chapters.

1.10. Aims

Several aspects of mitochondrial translation still need to be explored. In this study, I decided to focus my attention on the interaction between the mitoribosome and the IMM. As stated in the introduction, this interaction is important for coupling the synthesis of 13 highly hydrophobic components of the OXPHOS system with their insertion into the membrane. Defects in this process can lead to problems in the assembly of the OXPHOS complexes, which can lead to a reduction of available ATP as source of energy to the cell.

As discussed earlier, MRPL45 might be one of the mediators of this important interaction, because of its similarity with other membrane-interacting proteins and its ideal location. The main focus of my project was assessing the involvement of MRPL45 in the interaction with the IMM and its role in the stability of the mitoribosome. During the project, interest for OXA1L, another candidate player in this important interaction, arose. While the yeast homologue of this protein has been widely characterised in yeast, more work is needed on the human homologue to understand its role in mitochondrial translation and in the interaction with the mitoribosome. Therefore, I decided to also investigate this protein in this study. A patient cell lines with mutations in the gene encoding for OXA1L was identified during the course of my project and was therefore also characterised in this study. In the Appendix 17, a brief discussion and characterisation of another IMM protein, named LetM1, suggested to play a role in the interaction with the mitoribosome will be discussed.

In detail, the aims of my project were:

- Understand the importance of MRPL45 for the stability of the mitoribosome by using siRNA technology to deplete levels in human cell lines
- Develop a protocol to investigate the interaction of proteins with the membrane
- Study the interaction of the mitoribosome with the IMM and the ability of MRPL45 to directly interact with the IMM with the developed protocol
- Assess the involvement of candidate domains for membrane interaction of MRPL45 by generation of site directed mutants
- Identify the putative binding partners of MRPL45 in the IMM via immunoprecipitation experiments
- Investigate the involvement of the IMM protein OXA1L in the interaction with the mitoribosome
- Characterise the role of OXA1L in mitochondrial translation via siRNA depletion studies
- Characterise the biochemical and molecular phenotype of patients carrying mutation in OXA1L.

Chapter 2: Material and methods

2.1. Tissue culture

2.1.1. Cell maintenance and propagation

Different human cell lines were used in this study:

- HEK293 Flp-In™ T-Rex™ *(Invitrogen).* This cell line derived from human embryonic kidney cells (HEK293). The cells are engineered with the Flp-In™ System, which has both the integration into a specific cassette and tetracycline-inducible expression of a gene of interest.
- HeLa. Human cervical cancer carcinoma cells from Henrietta Lacks.
- U2OS. Human osteosarcoma cell line.
- U2OS Flp-In™ T-Rex™. Human osteosarcoma cell line engineered with the Flp-In™ System.
- 143B. Human osteosarcoma cells.
- 143B ρ^0. Human osteosarcoma cells lacking of mitochondrial DNA. Maintained in 1mM sodium pyruvate, 50 µg/mL of uridine and 200 ng/mL of ethidium bromide.
- Primary fibroblast. Isolated from patient or control.

  Patient: LetM1 (M2129-21, courtesy of Dr. Carrozzo Rosalba, Ospedale Bambino Gesù, Rome)

  Control: M0456-11, M0528-12
- Immortalised fibroblast. Derived from primary fibroblast.

  Patient: OXA1L (M0686-13)

  Control: M1171-13, M0528-12
- Tetracycline inducible cell lines.

  HEK293-MRPS27FLAG (Prepared by M. Wydro)

  HEK293-LuciferaseFLAG (Prepared by M. Wydro)

  HEK293-MRPL45
  HEK293-MRPL45FLAG
  HEK293-MRPL45FLsil
  HEK293-MRPL45FLala
  HEK293-MRPL45FLΔ
  U2OS-OXA1L

  } Prepared during the project

HEK293 Flp-In, HeLa, U2OS, U2OS Flp-In and 143B cells were grown in Dulbecco's Modified Eagle's medium (DMEM) containing 4500 mg/L glucose and 1 mM pyruvate

(*Sigma*, cat no D6429) supplemented with 10% foetal calf serum (FCS, *Gibco,* cat no 10270), 1x of non-essential amino acids (*Sigma*, cat no M7145) and 50 µg/mL of uridine (*Sigma*, cat no U3003). 143B ρ^0 cells were cultured in the same medium supplemented with 200 ng/mL of filter-sterilised ethidium bromide (*Sigma*, cat no E1510). Transfected HEK293 Flp-In™ and U2OS Flp-In™ were maintained in media with addition of 10 µg/mL Blasticidin^S (*Melford*, cat no B1105) every third feed.

Cells were grown at 37°C with 5% CO_2 in a humidified atmosphere. At 70-80% confluence, the media was removed and the cells were harvested with PBS (*Sigma*, cat no P4417) containing 1 mM EDTA (*Sigma*, cat no E5134). Primary and immortalised fibroblast were detached after incubation for 2 minutes at 37°C with 1x Trypsin (*Sigma*, cat no 59427C) in PBS. The cells were centrifuged for 4 minutes at 280g, resuspended in fresh media and seeded at a density of 1 in 3 for fibroblast and 1 in 5 for HEK293, HeLa and U2OS cells.

All the flasks used were manufactured by Greiner bio-one, whereas the plates were manufactured by Corning.

2.1.2. Cell storage

Cell lines were stored for later use. For every sample, a confluent 75 cm^2 flask was harvested and the cell pellet was resuspended in FCS supplemented with 10% dimethyl sulfoxide (DMSO, *Sigma,* cat no D5879) in cryostorage vials. After 24 hours at -80°C in a cryo-box, the vial was transferred to the liquid nitrogen dewar for long term storage.

2.1.3. Cell counting

When needed, cells were counted with a haemocytometer (depth 0.1 mm, surface 1/400 mm^2). To exclude dead cells from the count, an aliquot of cells (10 µL) was diluted 1:1 with trypan blue (*Sigma*, cat no T8154), which dead cells are unable to pump out, turning them dark. The number of live cells per mL was obtained multiplying the number of counted cells for $2 \cdot 10^4$.

2.1.4. Ethidium bromide treatment

Depletion of mt-DNA was obtained by growing cells in supplemented media (qv 2.1.1) in presence of 250 ng/mL of ethidium bromide for 10 days.

2.1.5. siRNA transfection

Cells were transfected with siRNA in 6 well plates (*Corning*) for 3 days (reverse transfection) or 6 days (reverse transfection for 3 days, followed by forward transfection for other 3 days).

- **Reverse transfection**

After pre-warming medium and *Opti-MEM I + GlutaMAX-I* (*Gibco*, cat no 51985), a mixture composed of 250 µL of Optimem, 2.5 µL of 20 µM siRNA and 2 µL of *Lipofectamine™ RNAiMAX* (*Invitrogen*, cat no 13778030) was prepared for each well from a 6-well plate that needs to be treated. The final siRNA concentration was 33 nM, unless differently stated. The mixture was incubated for 25 minutes at room temperature, then added to the wells and incubated for further 10 minutes. In the meantime, cells were harvested, counted and diluted so that 1.25 mL contained the desired amount of cells per well. In particular, 200,000 cells were seeded for every single well of a 6-well plate for a 3 days transfection, whereas the number was lowered for a 6 days transfection to 100,000 cells. The plate was then placed at 37°C with 5% CO_2 for 3 days. After that, the media was removed and the cells were collected for further analysis or transfected again.

- **Forward transfection**

This procedure was used on adherent cells to extend the transfection for further 3 days. In an Eppendorf, 2 µL of *Lipofectamine™ RNAiMAX* were mixed with 15 µL of Optimem (for each well of a 6-well plate), and in another Eppendorf, 2.5 µL of 20 µM siRNA were mixed with 125 µL of Optimem *I* (for each well of a 6-well plate). Both the solutions were left to incubate for 10 minutes and then were mixed and left to incubate for another 25 minutes. During this time, the old medium present in the wells was removed and 1.353 mL of new warm medium was added to each well. The cells were not detached. After the incubation, the solution of siRNA and lipofectamine was added to the well (144.5 µL each). The final siRNA concentration was 33 nM. Everything was mixed by rocking the plate and then the cells were grown for other 3 days at 37°C with humidified 5% CO_2. At the end the cells were harvested to perform further analysis.

2.1.6. Stable transfection

Genes of interest were inserted into engineered cells via the Flp-In™ system. Cells were plated in a 6-wells plate at approximately 30% confluence. On the following day, when the confluence of the cells will be approximately 60%, every well was incubated with 500 µL of DMEM lacking supplements (FCS, non-essential amino acids and uridine), but containing 0.8 µg of pcDNA™5/FRT/TO (carrying the gene of interest) and 1.2 µg of pOG44 premixed with 10 µL of *Superfect* (*Qiagen*, cat no 301305), as per manufacturer's instructions. As a control for the following antibiotic selection, one well was left untreated and incubated with media. After 1 hour of incubation at 37°C with 5% CO_2, the mixture of plasmids and Superfect was replaced with supplemented growth media and the cells were then grown for one day. After that 100 µg/mL Hygromycin^B (*Sigma*, cat no. H9773) and 10 µg/mL Blasticidin^S were added to supplemented growth media to every well, in order to select the successfully transfected clones. Once no cells

were left in the control well, individual clones were picked and expanded in a new well. Protein overexpression was induced by adding to the media 1 µg/mL tetracycline (*Sigma*, cat no T7660) and then verified via western blot analysis.

When *Viafect* (*Promega*, cat no E4983) was used instead of *Superfect* to carry out the transfection, the cells were left in the mixture containing the two plasmids and the transfecting reagent for 24 hours. After that, the media containing the selective antibiotics was added to carry out the selection.

The clones were cultured in supplemented media with addition of 10 µg/mL Blasticidin^S every third feed.

2.2. Bacteria culture

2.2.1. Propagation and storage

Chemically competent cells (α-select *Bioline*, cat no BIO-85025) were used in cloning experiments. The cells had the following genotype:

F- deoR endA1 recA1 relA1 gyrA96 hsdR17(rk-,mk+) supE44 thi-1 phoA Δ(lacZYA-argF)U169 Φ80lacZΔM15 λ-).

Cells were grown at 37°C in liquid LB media containing the appropriate antibiotic and prepared as follows. The pH of the solution was brought 7.5 and then autoclaved before use. For plates 3% agar (*BD*, cat no 214010) was added to the liquid LB media (LB-agar) prior autoclaving.

Table 2.1 LB media components.

Reagents	Final concentration
Bacto-tryptone (*BD*, cat no 211705)	1% w/v
Yeast extract (*BD,* cat no 212750)	0.5% w/v
NaCl (*Sigma*, cat no S7653)	1% w/v
NaOH (*Sigma*, cat no S5881)	Until pH 7.5

Transformed strains were stored in glycerol stocks. When needed, a small amount of frozen glycerol stock was scraped, plated on LB-agar and let grow overnight at 37°C.

Glycerol stocks were prepared resuspending the cells in LB media supplemented with 18% glycerol and then stored at -80°C for future use.

2.2.2. Transformation

Heat shock was used to transform chemically competent cells (*Bioline*, cat no BIO-85025) with the desired plasmid. Aliquots of competent cells (40 µL) were thawed on ice and then

incubated on ice with 4 µL of ligation mixture (qv 2.3.9.) or 10 ng of plasmid DNA for 30 minutes. The suspension was then placed at 42°C for 45 seconds and placed on ice for the following 2 minutes. After the heat-shock, 900 µL of SOC media (Table 2.2A) were added and the cells were incubated at 37°C for 1 hour with shaking. At the end of the incubation, the suspension was centrifuged at 15,700 g for 1 minute. The pellet of cells was resuspended in 100 µL of fresh SOC media, plated on LB agar with the appropriate antibiotic (Table 2.2B) and incubated inverted overnight at 37°C.

Table 2.2 Composition of SOC media used during transformation (A) and concentration of antibiotics used during the selection (B).

A

Reagents	Final concentration
Bacto tryptone	2% w/v
Yeast extract	0.5% w/v
NaCl	0.05% w/v
KCl (*VWR*, cat no 26764.260)	2.5 mM
$MgCl_2$ (*Sigma*, cat no M8266)	10 mM
Glucose (*BDH*, cat no 10117)	20 mM
NaOH	Until pH 7.0

B

Antibiotic	Final concentration
Ampicillin	100 µg/mL
Kanamycin	50 µg/mL

2.2.3. Isolation of plasmid DNA

The cells containing the plasmid were plated on LB agar (Table 2.1) with the appropriate antibiotic and grown at 37ºC overnight. The following day, single colonies were picked and expanded overnight at 37ºC in 5 mL of LB media (Table 2.1) supplemented with the appropriate antibiotic. Cells were pelleted and the plasmid was extracted following the protocol of the *GeneJET™ Plasmid Miniprep kit* (*Thermo Scientific*).

2.3. DNA manipulations

2.3.1. DNA isolation from human cells

Cells were harvested and resuspended in 400 µL of 10 mM Tris (*Sigma*, cat no T1503) pH 7.4 supplemented with 1 mM EDTA. SDS (*Sigma*, cat no L3771) and proteinase K (*Roche*, cat no 25530) were added at a final concentration of 1% and 20 mg/mL respectively. The sample was then incubated overnight at 37ºC. DNA was extracted via phenol extraction and then precipitated with ethanol (qv 2.3.5.).

2.3.2. DNA electrophoresis

Gel electrophoresis was used throughout the cloning procedure to analyse the quality of samples or the success of reactions. Usually, gels were prepared at 1.2% of agarose (*Bioline*, cat no BIO41025), in 1xTAE buffer (Table 2.3A). The solution was warmed until the agarose was completely melted and, after the addition of 0.05 µL/mL of ethidium bromide, the gel was poured and left to solidify.

Table 2.3 Composition of 1xTAE buffer (A) and 6x DNA Loading dye (B).

A

Reagents	Final concentration
Tris base	40 mM
Glacial acetic acid (*VWR*, cat no 20104.367)	0.114% v/v
EDTA	0.1 mM

B

Reagents	Final concentration
Glycerol (*Sigma*, cat no G5516)	50%
Bromophenol blue (*Sigma*, cat no B5525)	0.125%
Xylene cyanol (*Sigma*, cat no X4126)	0.125%

The DNA samples to analyse were mixed with loading dye (Table 2.3B, 1x final concentration) and then loaded on the agarose gel, together with 3 µL of 1 kb marker (*Invitrogen*, cat no 15615). The gel was then electrophoresed at 55-60 V (for a 30 mL gel) or 70-80 V (for a 50 mL gel) for approximately 1 hour, or until the samples were separated as required. After that, the bands were visualized using the *Chemi Doc™ MP* Imaging System (*Bio-Rad*®).

2.3.3. DNA amplification via polymerase chain reaction

Defined DNA regions were amplified using PCR. The technique was mainly used to prepare inserts for cloning of genes of interest within plasmids. A complete list of the primers used is reported in Appendix 5. The cDNA obtained for reverse transcription from RNA extracted from HEK293 WT cells (qv 2.4.2.) was used as a template for the PCRs. The reactions were carried out in the *PTC200 PCR Thermal Cycler* (*MJ Research*), using 500 µL thin-wall tubes with the proof-reading *KOD Hotstart DNA Polymerase* (*Merk Millipore,* cat no 71086) in the mixture reported in Table 2.4.

Table 2.4 PCR reaction mixture.

Reagents	Final concentration	Volume for 1 tube
dH_2O	/	32 µL
10x KOD Hotstart Buffer	1x	5 µL
25 mM $MgSO_4$	1 mM	5 µL
2 mM dNTPs	0.2 mM	5 µL
50 µM Sense Primer	1 µM	1 µL
50 µM Anti-sense Primer	1 µM	1 µL
1 U/µL KOD Hotstart DNA polymerase	1U	1 µL
cDNA	/	2 µL
		50 µL total

The conditions used for the PCR reactions are reported in the following table. The annealing temperature used for every reaction took into consideration the melting temperature of the primers (reported in Appendix 5). Extension times were dependent upon the length of the product. The sequence of denaturation-annealing-extension cycle was repeated 30 times.

Table 2.5 PCR reaction conditions used for KED Hotstart DNA polymerase on *PTC200 PCR Thermal Cycler.*

Reaction	Temperature	Time	
Initial denaturation	95ºC	3 min	
Denaturation	95ºC	1 min	**X 30**
Annealing	variable *	1 min	
Extension	70ºC	1 min	
Final extension	72ºC	5 min	

The PCR reaction was resolved on a 1.2% agarose gel (qv 2.3.2.) to confirm the success of the reaction. The desired product was isolated by excision of the band and the DNA was extracted with the *QIAquick® Gel Extraction Kit* (*Qiagen*, cat no 28704) as per manufacturer's instructions.

2.3.4. Real-time PCR

The RNA content of cell samples was estimated with real-time PCR. RNA was reverse transcribed to cDNA (qv 2.4.2.) and every real-time PCR was prepared as shown in the following table. Triplicates for every pair of primers used were prepared. To exclude DNA contaminations, a reaction without DNA was also performed.

Table 2.6 Real time reaction mixture.

Components	Volume per reaction
2x FastStart SYBR Green Master (*Roche*, cat no 04673484001)	10 µL
Nuclease-free water	6 µL
10 µM Forward primer	1 µL
10 µM Reverse primer	1 µL
DNA from reverse transcription or from 5 µg/µL stock	2 µL

The list of primers used is reported in the Appendix 5. All the primers used were validated personally or in the laboratory. The reactions were sun on the *LightCycler® Nano* (*Roche*), using the following program (set up by Christie Waddington):

Table 2.7 Conditions of real time reaction.

Temperature	Time	Ramp	
95ºC	10 min	5	
95ºC	10 sec	5	**X 45**
60ºC	10 sec	4	
72ºC	15 sec	5	
65ºC	50 sec	4	
95ºC	15 sec	0.1	

The program will elaborate the data and calculate the C_t (Cycle threshold) value of every sample. This number is equivalent to the cycles needed for the fluorescent signal to cross the background fluorescence level and correlates to the amount of targeted DNA in the sample. The $\Delta\Delta C_t$ method was used to analyse the results obtained for RNA species. This method allows the upregulation or the downregulation of a species of interest to be evaluated. As a consequence, when testing any condition (e.g. overexpression, siRNA knockdown, etc), a control condition (e.g. uninduced cells, transfection with NT-siRNA) is needed. For every condition, the amount of the ribosomal RNA 18S ('reference') was quantified and used to normalise the level of the RNA of interest ('target'). The average of every triplicate was calculated and then used in the following calculations:

ΔC_t (Condition) = ΔC_t (ConditionTarget) – ΔC_t (ConditionReference)

ΔC_t (Control) = ΔC_t (ControlTarget) - ΔC_t (ControlReference)

$\Delta\Delta C_t$ = ΔC_t (Condition) - ΔC_t (Control)

Difference in fold for the target between the condition tested and the control= $2^{-\Delta\Delta Ct}$

The calculations were repeated for every target RNA measured. The values obtained in the last calculation were used in a bar graph to represent the data acquired.

2.3.5. Phenol extraction and ethanol precipitation of DNA

PCR products, plasmids and whole cell DNA were purified following this protocol. Each sample was diluted up to 50 µL with nuclease-free water and an equal volume (50 µL) of buffer equilibrated phenol (*Sigma*, cat no P4557) was added. The sample was vortexed and then centrifuged at 15,700 g for 2 minutes at room temperature. The upper aqueous layer was retained and mixed with 25 µL of phenol and 25 µL of chloroform (*Sigma*, cat no C2432). After vortexing and centrifugation as in the previous step, the upper aqueous layer was saved. Following the addition of 50 µL of chloroform, the sample was vortexed and centrifuged one more time. Finally, the resulting upper aqueous layer was diluted with 2 volumes of cold ethanol (*Fisher Chemicals*, cat no BP2818) and 0.1 volumes 3M CH_3COONa (*BDH,* cat no 102355P) at pH 5. The sample was frozen at -80°C for 2 hours, and the DNA precipitated was centrifuged for 10 minutes at 15,700g. The pellet was air dried and resuspended in 20 µL of nuclease free water.

2.3.6. DNA purification

In order to buffer-exchange the DNA sample after the gel or phenol-chloroform extraction, this was dialysed against a solidified solution composed of 1% agarose and 100 mM glucose in water for 90 minutes on ice.

2.3.7. DNA digestion

The plasmid (≈ 3 µg) and the insert (≈ 1 µg) were digested with the appropriate restriction enzyme and reaction buffer (Table 2.8). The reaction was incubated at 37ºC for 90 minutes. When the plasmid was digested, 1 µL of the solution was analysed on a 1.2% agarose gel to verify the success of the digestion.

Table 2.8 Restriction enzymes relative buffers used to digest DNA samples.

Restriction enzyme	10x Buffer
AflII (*NEB*, cat no R0520)	NEB4
BamHI (*Roche*, cat no BAMHI-RO)	Roche M
BssHII (*NEB*, cat no R0199)	NEB3
HindIII (*Roche*, HINDIII-RO)	Roche M
KpnI (*Roche*, cat no KPNI-RO)	Roche L
NotI (*NEB*, cat no R0189)	NEB3

2.3.8. DNA dephosphorylation

In order to avoid the self-religation of the plasmid, its 5'-ends were dephosphorylated. A volume of digested plasmid (20 µL) was mixed with 1 µL of 10% SDS, 3.5 µL of 1 M Tris pH 9

and 1 µL of alkaline phosphatase (*Sigma,* cat no APMB-RO). The reaction was incubated at 37°C for 30 minutes and then at 50°C for further 30 minutes.

2.3.9. Ligation

The insert was ligated into digested and dephosphorylated vector using *the Rapid DNA Ligation Kit* (*Thermo Scientific*, cat no K1422). The following equation was used to calculate the amount of insert to use in the ligation reaction:

$$\frac{(\text{ng of vector} \times \text{kb size of insert})}{(\text{kb size of vector})} \times 3 = \text{ng of insert}$$

The ligation mixture was prepared as in Table 2.9 and incubated at room temperature for 30 minutes. At the end of the reaction, the mixture was transformed into competent cells (qv 2.2.2.) or frozen for future use.

Table 2.9 Ligation mixture (Rapid DNA Ligation Kit, *Thermo scientific*).

Ligation mixture
50 ng vector
x ng insert
4 µL 5X ligation buffer
1 µL DNA ligase
dH_2O up to 20 µL

2.3.10. Colony screening and DNA sequencing

It is possible that during the ligation step the plasmid will recircularise on itself, without integrating the insert. After transformation of competent cells (qv 2.2.2.) it was, therefore, fundamental to identify colonies successfully transformed with the plasmid containing the insert.

For a quick screening of colonies, the cracking-gel technique was used. Individual colonies obtained from the transformation were expanded of fresh LB-agar plates overnight at 37°C. Half of each colony was then transferred to an Eppendorf and cells were disrupted in 20 µL of cracking buffer (Table 2.10).

Table 2.10 Cracking buffer composition.

Reagents	Final concentration
NaOH	50 mM
SDS	0.5%
EDTA	5 mM

The samples were incubated at 55°C for 30 minutes and then vortexed for 1 minute. The samples were then mixed with loading dye and analysed via DNA electrophoresis (qv 2.3.2.). The gel was then visualised at the *ChemiDoc* to assess the migration of the plasmid contained in each colony.

As an alternative, the presence of the insert was verified via PCR. Individual colonies were spread on LB agar plates and grown overnight at 37°C. After that, half of each colony was harvested, dissociated with 40 µL of 10% Triton X-100 (*Sigma,* cat no T8787) and frozen at -20°C for 30 minutes. The cells were then thawed and centrifuged at 15,700 g for 1 minute. The resulting supernatant was used as template for a PCR reaction to assess the presence of the insert. The plasmid pcDNA5/FRT/TO was used for all the cloning reactions presented in this work. To detect the presence of the insert, the multiple cloning site was amplified using primers for CMV and BGH sequences, which flank at either side of this site. The reaction was performed with *DreamTaq™ Polymerase* (*Thermo Scientific*, cat no EP0701*)* with the following conditions:

Table 2.11 Components (A) and conditions (B) for the amplification of the multiple cloning site of pcDNA5/FRT/TO, to identify the presence of the insert.

A

Reagents	Final concentration	Volume for each reaction
Nuclease-free water	/	19.575 µL
10x DreamTaq™ Buffer	1x	2.5 µL
10 mM dNTPs	0.2 mM	0.5 µL
50 µM CMV primer	1 µL	0.5 µL
50 µM BGH primer	1 µL	0.5 µL
5 U/µL DreamTaq Polymerase	1U	0.125 µL
DNA	/	1.3 µL
		25 µL tot.

B

Reaction	Degrees	Time	
Initial denaturation	95ºC	3 min	
Denaturation	95ºC	1 min	**X 34**
Annealing	52ºC	1 min	
Extension	72ºC	1 min	
Final extension	72ºC	8 min	

The presence of the insert was verified by loading 5 µL of each reaction on a 1.2% agarose gel. In presence of the insert, a higher molecular weight band will be detected.

If a single restriction enzyme was used to prepare a fragment to insert within the plasmid, the orientation of the insert post ligation needed to be checked. For this purpose, a diagnostic digestion was performed. This technique consists of the digestion of the construct with a

restriction enzyme that cuts both the insert and the plasmid once only. Through the analysis of the size of the fragments obtained by this digestion, it was possible to verify the orientation of the fragment. As a control, the plasmid was also linearized by digestion with a restriction enzyme that performs a single cut in the construct. The products of the digestion were analysed on a 1.2% agarose gel. Details for the diagnostic digestion performed in this study can be found in the results sections.

Once the orientation of the insert was confirmed, the multiple cloning site of the plasmid was sequenced to exclude the presence of undesired mutations and to further confirm the identity of the insert. For this purpose, the *BigDye Terminator v3.1 Cycle Sequencing Kit* (*Life Technologies,* cat no 4337455) was used. Two reactions, each containing 450 ng of plasmid, were set up. One reaction contained the CMV forward primer, whereas the other contained the BGH reverse primer. The reactions and the condition used are reported in the following tables:

Table 2.12 DNA sequencing reaction (A) and conditions (B) with *BigDye Terminator v3.1 Cycle Sequencing* Kit.

A

Sequencing reaction mixture
450 ng plasmid
3 µL 5X sequencing buffer
3 µL Big Dyes v3.1
dH2O to 15 µL

B

Reaction	Degrees	Time	
Initial denaturation	95ºC	5 min	
Denaturation	95ºC	30 sec	**X 30**
Annealing	50ºC	10 sec	
Extension	60ºC	4 min	

At the end of the reaction, the sample was stored at -20°C or sequenced with *3130xl Genetic Analyzer* (*Applied Biosystems*).

The sequence resulting from the analysis was then aligned with the target sequence using the online alignment tool BLAST® (http://blast.ncbi.nlm.nih.gov/Blast.cgi) and translated using ExPASy (http://web.expasy.org/translate/).

2.3.11. Preparation of the insert using PCR-script

When problems in obtaining positive colonies were present, the *PCR-script Amp Cloning* Kit (*Stratagene*, cat no 211188) was used to prepare the insert.

The PCR product (insert) was ligated in the pPCRscript Amp SK(+) plasmid incubating the mixture in Table 2.13 at room temperature for 1 hour.

Table 2.13 Reaction mixture for insert ligation in pPCR-script cloning vector.

Reagents	Final concentration	Volume for 1 tube
10 ng/µL pPCR-script cloning vector	10 ng	1 µL
10x PCR-script reaction Buffer	1x	1 µL
10 mM rATP	1 mM	0.5 µL
Insert	/	2-4 µL
5 U/µL Sfr I restriction enzyme	5 U	1 µL
4 U/µL T4 DNA ligase	4 U	1 µL
dH_20	/	Up to 10 µL

The solution was heated for 10 minutes at 65°C and the mixture was then used to transform competent cells (qv 2.2.2.). The colonies obtained were spread on new LB plates containing 100 µg/mL of ampicillin and screened on a cracking gel (qv 2.3.10.). The positive colonies were grown O/N at 37°C in 5 mL of LB media (containing 100 µg/mL of ampicillin). The corresponding plasmids were extracted with *GeneJET™ Plasmid Miniprep* kit and then digested with the appropriate restriction enzyme. The product of the digestion was loaded on an agarose gel and the bands corresponding to the insert were then excised for DNA extraction. The product obtained was purified (qv 2.3.6.) and then ligated into the vector of interest (qv 2.3.9.).

2.4. RNA manipulations

To reduce the risk of degradation, all the solution used in RNA manipulation were prepared with water treated with 0.1% DEPC (*Sigma*, cat no D5758) and then autoclaved.

2.4.1. RNA extraction

Cells were harvested and washed in 1.5 mL of cold PBS. The pellet obtained after 5 minutes of centrifugation at 400 g at 4ºC was resuspended with 200 µL of TRIzol® reagent (*Thermo Scientific*, cat no 15596) and incubated at room temperature for 5 minutes. Chloroform (40 µL) was added to the sample that was then vortexed for 15 seconds and incubated at room temperature for 3 minutes. After that, the sample was centrifuged at 12,000 g for 15 minutes at 4ºC. The clear top layer contained the RNA and was carefully moved to a clean Eppendorf, avoiding contamination of TRIzol® and of the white DNA layer. Isopropanol (100 µL) was added to the solution and, after 10 minutes of incubation at room temperature, the sample was centrifuged at 12,000 g for 10 minutes at 4ºC. The centrifugation pelleted the RNA that was then rinsed in 1 mL of cold 75% ethanol. The ethanol was discarded and the pellet was let to air-dry for 10 minutes. The RNA was resuspended in DEPC water. The samples were stored at -80ºC.

When the RNA to be extracted was from a liquid sample, *TRIzol® LS reagent* (*Thermo Scientific*, cat no 10296) was used, following the same protocol stated above.

When the amount of RNA to extract was very small, this was co-precipitated with 1 µL of Glycoblue® (*Invitrogen*, cat no AM9516) or 10% glycogen (*Ambion*, cat no AM9510). This was added to the clear top layer obtained from the first centrifugation step, prior addition of isopropanol.

2.4.2. Reverse transcription

The cDNA was obtained by reverse transcription from RNA. The reaction was carried out with *Superscript®III Reverse Transcriptase kit* (*Life Technologies*). Annealing reaction and master mix were prepared as follows:

Table 2.14 Annealing reaction and Master mix reaction for reverse transcription.

Annealing reaction	Master mix
5 µg RNA	2 µL 10x RT buffer
50 pmol random hexamers (*Gibco* BRL, cat no 51709)	2 µL 25 mM $MgCl_2$
	2 µL 0.1 mM DTT (*Sigma*, cat no D0632)
DEPC H_2O up to 12 µL	1 µL 10 mM dNTP mix (*Bioline*, cat no BIO-39044)

The annealing reaction was heated at 70ºC for 10 minutes, and then mixed with the master mix. After addition of 1 µL of enzyme, the solution obtained was incubated at 42ºC for 50 minutes. Finally, the temperature was raised to 70ºC for 15 minutes, to denature the enzyme. The samples obtained were used to prepare inserts for cloning or analysed via qPCR.

2.5. Protein manipulations

2.5.1. Preparation of cell lysate

Lysis buffer (15 µL, Table 2.15) was added to each sample for every 5-10 mg of wet weight cells to resuspend the sample. The suspension was then vortexed for 30 seconds and centrifuged at 4ºC for 4 minutes at 800g. The supernatant was transferred in a clean Eppendorf and after determination of protein concentration, was used for western blot analysis.

Table 2.15 Cell lysis buffer composition

Reagents	Final concentration
Tris pH 7.5	50 mM
NaCl	130 mM
$MgCl_2$	2 mM
PMSF (*AppliChem*, cat no A0999)	1 mM
NP-40 (*Sigma*, cat no N6507)	1% (v/v)
EDTA-free protease inhibitor (*Pierce*, cat no 88666)	1 tablet for 10 mL

In rare cases, the lysate was viscous, because of the presence of genomic DNA. To solve this issue, benzonase, a DNase/RNase (*Millipore*, cat no 70746) was added after protein quantification (qv 2.5.2.). The enzyme was diluted 1/10 and 1 µL was added to the sample and the reaction was incubated at 37°C for 20 minutes.

2.5.2. Protein quantification

The protein content of samples was assessed using the Bradford assay. A standard curve obtained with bovine serum albumin (BSA - *Sigma*, cat no A2153) was used as a reference and was prepared as shown in the following table:

Table 2.16 Standard curve with BSA for Bradford assay.

BSA (1 µg/µL)	**Water**	**Bradford reagent** (*Biorad*, cat no 500-0006)
0 µL	800 µL	200 µL
2 µL	798 µL	200 µL
5 µL	795 µL	200 µL
10 µL	790 µL	200 µL
15 µL	785 µL	200 µL
20 µL	780 µL	200 µL

A specific volume of sample (usually 1 or 2 µL) was diluted with water up to 800 µL and then mixed with 200 µL of Bradford reagent. Every point of the standard curve and every sample were prepared in duplicate. Aliquots of 200 µL of each sample were loaded on a 96-well plate that was analysed at 595 nm using *SpectraMax M5* (*Molecular devices*) to determine the absorbance of the samples, from which the concentration was inferred.

2.5.3. TCA protein precipitation

When more concentrated samples were needed, proteins were precipitated by addition of an equal volume of 20% trichloroacetic acid (TCA) (*Sigma,* cat no T9159). After 30 minutes of incubation on ice, the samples were centrifuged for 15 minutes at 15,700 g and the pellets obtained were washed 3 times with 200 µL of cold acetone. The final pellets were resuspended in the appropriate buffer and the solubilisation of the sample was aided with the addition of 1% SDS, and heating up the solution at 50°C for 30 minutes.

2.5.4. SDS-PAGE

Proteins were separated according to their molecular weight on denaturing 12% acrylamide resolving gel. Resolving and stacking gels were prepared prior to the analyses as reported in Table 2.17 B and C. The resolving gel was poured in between the 2 glass plates. Once this was

polymerised, the stacking gel was poured on top and the comb was inserted to create the wells for loading the samples. Samples were prepared adding Laemmli sample buffer (Table 2.17A) and were denaturated at 95°C for 3 minutes.

Table 2.17 Composition of 5x Laemmli sample buffer (A), Resolving gel (B) and Stacking gel (C) for SDS-page analysis.

A

Reagent	Final concentration
Tris pH	312.5 mM
6.8	50%
Glycerol (*Sigma*, cat no G3516)	10%
SDS	0.05%
Bromophenol blue (*Sigma*, cat no B5525)	
DTT	Added fresh, 100 mM final in the sample

B

Reagent	Final concentration
Tris pH 8.5	380 mM
30% acrylamide-bisacrylamide 29:1 (*NBS Bio Logical*, cat no NBS2600-05)	12%
SDS	0.1%
APS (*Sigma*, cat no A3678)	0.1%
Temed (*Sigma*, cat no T22500)	0.1%

C

Reagent	Final concentration
Tris pH 6.8	125 mM
30% acrylamide-bisacrylamide 29:1	3.75%
SDS	0.1%
APS	0.1%
Temed	0.1%

The system for the SDS-PAGE was built and 1x running buffer (Table 2.18) was added to the tank until the correct level was reached. The samples were carefully loaded on the gel and, together with them, 4 µL of *Spectra™ Multicolour Broad Range Ladder* (*Thermo Scientific*, cat no 26634) or 1.5 µL of *BLUE Wide Range recombinant protein marker* (*Clever Scientific*, cat no CSL-BBL) were also loaded and used as size markers.

The gel was run initially at 100V, until the samples reached the resolving gel. After that, the voltage was incremented to 150V for approximately 1 hour in 1x running in the *Mini-PROTEAN® Tetra Cell* (*Biorad*).

Table 2.18 Running buffer (1x) composition.

Reagent	Final concentration
Tris base	25 mM
Glycine (*Sigma*, cat no G7126)	192 mM
SDS	0.1%

2.5.5. Western blotting

After the SDS-PAGE analysis, the proteins were transferred from the acrylamide gel to the *Immobilon®-P* PVDF membrane (*Millipore*, cat no IPVH00010) using the *Mini-PROTEAN® Tetra Cell* system (*Biorad*). The membrane was activated in methanol, rinsed in water and 1x transfer buffer (Table 2.19A). The transfer unit, containing membrane and gel, was assembled, immersed in 1x transfer buffer and exposed to 100V for 1 hour. At the end of the process, the membrane was incubated with 20 mL of 5% non-fat dried milk in T-TBS (Table 2.19B) for 1 hour (blocking) and then incubated overnight at 4°C with the primary antibody (in 5% milk T-TBS). The list of the primary antibodies used is reported in the Appendix 2.

Table 2.19 Composition of 1x transfer buffer (A) and T-TBS (B).

A

Reagent	Final concentration
Tris base	25 mM
Glycine	192 mM
SDS	0.02%
Methanol (*Fisher Chemicals*, cat no A412)	15%

B

Reagent	Final concentration
Tris base	20 mM
NaCl	150 mM
Tween® 20 (*Sigma*, cat no P2287)	0.1%
	pH 7.4

Following ~16 hours incubation, the membrane was washed 3 times in T-TBS for 5 minutes and then incubated with the appropriate secondary antibody (Appendix 2) for 1 hour at room temperature.

The membrane was washed 3 times in T-TBS for 5 minutes and then detected with *Chemi Doc™ MP* system after 5 minutes of incubation with *ECL prime* (*GE healthcare biosciences*, cat no RPN2232) or *ECL+* (*Thermo Scientific*, cat no 32106). If necessary, after an extended wash, the membrane was probed again with a different primary antibody, following the same protocol just described. The data were collected were analysed with the software *Imagelab (Biorad)*.

The molecular weight of the signal detected by every antibody was compared to the protein ladder to confirm the identity its correspondence to the molecular weight of the targeted protein. The protein ladder will be omitted in the figures presented in this thesis.

When needed, the quantification of the bands was performed. For every protein detected, a box was drawn around the band using the rectangle tool from the 'Volume tools' menu. Another box of the same size was drawn in an empty part of the blot to subtract the background. The values ('volume') calculated by the program for every box was found in the 'Analysis table' option. The final value of the band was obtained by difference of the protein signal with the background. Once these values were calculated for a housekeeping gene (β-Actin, Porin, SDH70, TOM20, etc.), the values obtained for other proteins were normalised according to the quality of the loading. The results were shown as percentages of the control condition using bar graphs.

2.5.6. Silver staining

Protein samples can be visualised with a high sensitivity by silver staining. After the samples were resolved via SDS-PAGE (qv 2.5.4.), the polyacrylamide gel was washed for 1 hour in 50% methanol. Meanwhile, the staining solution was prepared by adding drops of 0.2 g/mL silver nitrate solution (*Sigma*, cat no S6506) to a conical flask containing water, 0.075% NaOH and 1.4% NH_4OH, until the solution lost its transparency. The gel was incubated with the staining solution for 15 minutes at room temperature and then washed with water 3 times for 5 minutes. The developer solution (Table 2.20A) was added to the gel until the desired intensity was achieved. The solution was then discarded and replaced with the stop solution (Table 2.20B). The gel was finally rinsed in water and imaged at the *ChemiDoc* system.

Table 2.20 Composition of developer solution (A) and stop solution (B) for silver staining.

A

Reagents	Final concentration
Citric acid (*Sigma*, cat no C2404)	0.005%
Formaldehyde	0.05%

B

Reagents	Final concentration
Methanol	45%
Acetic acid	10%

2.6. Isolation of mitochondria

Cells were harvested and resuspended in 1.4 mL of homogenisation buffer (Table 2.21) supplemented with 0.1% of BSA and 1 mM PMSF. All the steps were performed on ice, using pre-chilled tubes and centrifuging the samples at 4°C.

Table 2.21 Homogenisation buffer composition.

Reagents	Final concentration
Tris pH 7.4	10 mM
Mannitol (*Sigma*, cat no M4125)	0.6 M
EGTA (*Sigma*, cat no E4378)	1 mM

In order to obtain a mitochondria-enriched fraction, the cells were homogenised and then centrifuged at 400 g for 10 minutes. This step was performed 3 times on the same pellet, saving the supernatant obtained for every homogenisation. The supernatants were then centrifuged at 400 g for 5 minutes, in order to remove contamination from the previous pellet. The centrifugation of the resulting supernatant at 11,000 g for 10 minutes led to a pellet that represented a fraction enriched in mitochondria, and a supernatant contained the cytosolic proteins (which was often saved for Western blot analysis).

The mitochondria-enriched fraction was washed twice with homogenization buffer containing 1 mM PMSF (but without BSA), and then resuspended in the 100 µL of the same buffer.

2.7. Mitochondrial sub-fractionation

Mitochondria were extracted (qv 2.6.) and the protein content was quantified (qv 2.5.2.). A sample of 600 µg of proteins was diluted up to 300 µL with homogenization buffer (Table 2.21). A volume of this solution (12.5 µL) was used to prepare a sample for western blot analysis, while the rest was diluted by adding 2.5 mL of 10 mM Tris/1 mM EDTA. The solution obtained was centrifuged at 11,000 g for 10 minutes at 4ºC and then the pellet was resuspended in the same volume of the previous Tris buffer. The sample was halved and 1.44 µg of proteinase K was added to one half of the suspension. Both halves of the sample were left on ice for 30 minutes.

After the incubation, 1 mM of PMSF was added and the samples were centrifuged at 11,000 g for 10 minutes at 4ºC. The pellets were washed twice with 1 mL of 10 mM Tris/1 mM EDTA and then resuspended with 137.4 µL of homogenization buffer. A volume of 12.5 µL for each sample was saved for a western blot analysis. The sample obtained in absence of proteinase K represented mitoplasts, while the one incubated with this enzyme represented the shaved mitoplasts.

The sample digested with proteinase K was washed with 1.262 mL of homogenization buffer. The pellet obtained after centrifugation at 12,000 g for 10 minutes at 4ºC was resuspended with 2.6 mL of 100 mM Na_2CO_3 (*Sigma*, cat no S7795) and incubated for 30 minutes on ice. Subsequently, the sample was centrifuged in the *Optima™ TLX Ultracentrifuge* (*Beckman*) (rotor TLA120.2) for 15 minutes at 53,000 rpm (122,000 g) and 4ºC. The supernatant was discarded, whereas the pellet was resuspended in 80 µL of homogenization buffer. Finally, 12.5 µL of the sample were saved for a western blot analysis.

2.8. Isokinetic sucrose gradient

This technique was used to separate cellular components in different layers according to their density and dimension. The experiment was carried out in an ultracentrifuge tube (*Beckman Coulter*, cat no 343778) containing a gradient with an increasing concentration of sucrose from the top to the bottom of the tube. The gradient was prepared mixing the sucrose gradient buffer (Table 2.22) with sucrose to obtain a 10% and a 30% sucrose solutions. A syringe was used to add first 0.5 mL of 10% sucrose solution at the bottom of the ultracentrifuge tube and then to add 0.5 mL of 30% sucrose solution at the bottom of the first layer. The gradient was created with the *107 Gradient Master Ip* (*BioComp*) using the built-in setting 'TLS55, short sucrose 10%-30%, 55 seconds' and then placed in the cold room for 45-60 minutes.

Table 2.22 Sucrose gradient buffer.

Reagents	Final concentration
Tris pH 7.2	50 mM
MgAcetate (*Sigma*, cat no M5661)	10 mM
NH_4Cl (*Sigma*, cat no A9434)	40 mM
KCl	100 mM
PMSF	1 mM
Chloramphenicol (*Duchefa Bioch*, cat no C0113.0025)	50 µg/mL

Cell lysate (100 µL at 7-8 µg/µL) was carefully added at the top of the gradient and the tube was centrifuged in the *Optima™ TLX Ultracentrifuge* (rotor TLS 55) at 39,000 rpm (100,000 g) for 2 hours and 15 minutes at 4°C. At the end of the process, 100 µL fractions were collected from the top of the gradient and stored at -20°C for further analysis. Generally, 10 µL from each fraction were used for Western blot analysis.

2.9. Immunoprecipitation

Cells were harvested, mitochondria were extracted (qv 2.6.) and lysed in 500 µL of the following buffer for 30 minutes at 4°C on a rotating wheel.

Table 2.23 Immunoprecipitation lysis buffer composition.

Reagents	Final concentration
Tris pH 7.4	50 mM
NaCl	150 mM
EDTA	1 mM
Triton X-100	1%
EDTA-free protease inhibitor	1x
PMSF	1 mM
$MgCl_2$	10 mM
RiboSafe (Bioline, cat no BIO-65028)	1.5 µL

In the case where a FLAG-tagged protein was immunoprecipitated, the *FLAG® Immunoprecipitation kit* (*Sigma*, cat no FLAGIPT1-1KT) was used. Packed beads (20 µL) were washed 3 times with 500 µL of wash buffer (Table 2.24), pelleting the beads by centrifugation at 6,000 g for 30 seconds at 4°C, and being careful to not discard the beads.

Table 2.24 Immunoprecipitation wash buffer.

Reagents	Final concentration
Tris pH 7.4	50 mM
NaCl	130 mM
Protease inhibitor	1x
PMSF	1 mM
$MgCl_2$	10 mM
RiboSafe	2.5 µL

When the lysis was complete, the suspension was centrifuged at 12,000 g for 10 minutes at 4°C to eliminate unbroken mitochondria. The protein concentration was checked by Bradford assay (qv 2.5.2.). A sample of 15 µg of mitochondria lysate was saved for western blot analysis. Up to 3 mg of protein were added to the beads in a final volume of 500 µL. The sample was then incubated on the rotating wheel for 2 hours at 4°C. At the end of the incubation, the sample was centrifuged at 6,000 g for 30 seconds at 4°C. The supernatant represents the unbound proteins and was saved for further analysis.

Finally, the beads were washed 3 times as previously performed. The bound proteins were eluted either with incubation with 110 µL of wash buffer with 250 µg/mL of 3x FLAG peptide (*Sigma*, cat no F4799) for 45 minutes at 4°C with shaking, or incubating the sample with 1x sample buffer (Table 2.17A) at 95°C for 3 minutes.

In case the protein to precipitate did not have a FLAG-tag, the magnetic beads *Dynabeads® Protein G* (*Thermo Scientific,* cat no 10004D) were used. A volume of 20 µL (≈ 0.6 mg) of beads were washed 3 times with 200 µL of IP lysis buffer (Table 2.23). As these beads are magnetic, instead of centrifugation, a magnetic stand was used to separate them from supernatant. After being washed, the beads were coated with the antibody of interest (between 0.6-6 mg of antibody for every mg of beads) and incubated at 4°C with shaking for 45 minutes. After that the beads were washed again 3 times with 200 µL of IP lysis buffer and then incubated 300 µL of mitolysate at 4°C with shaking up to 2 hours. At the end of the incubation, the beads were washed with IP lysis buffer and then the proteins were eluted at 95°C for 3 minutes in 25 µL of IP lysis buffer containing 1x sample buffer (Table 2.17A).

2.10. Bioinformatic analyses tools

The bioinformatic tools that were used in this study are listed in the following Table:

Table 2.25 Bioinformatic tools.

Name	Use
BLAST http://blast.ncbi.nlm.nih.gov/Blast.cgi	Nucleotide or protein alignments for 2 sequences
JalView	Sequence alignments within different organisms
NEBcutter http://nc2.neb.com/NEBcutter2/	Restriction enzyme digestion sites
PyMol (Open source)	Visualisation and analysis of protein structures from PDB files
Phyre2 http://www.sbg.bio.ic.ac.uk/phyre2/html/page.cgi?id=index	Secondary and tertiary structure predictions from protein sequences
Reverse Complement http://www.bioinformatics.org/sms/rev_comp.html	Transformation of DNA sequences into the reverse complement
SeqScanner	Analysis of data obtained from sequencing

Chapter 3: MRPL45 in human mitochondria

3.1. Introduction

Amongst the 80 proteins that compose the human mitoribosome, my attention focused on a protein named MRPL45. This protein is one of the mitochondria-specific mitoribosomal components that lacks a bacterial orthologue. It contains a TIM44-like domain, the importance of which is that TIM44, as a component of the translocase inner membrane (IMM) machinery found in the matrix, is reported to interact with membranes (Marom M et al., 2009) and so mediate the interaction between the core of the translocase machinery and matrix proteins (Voos W et al., 1996). Due to this similarity of TIM44-like domain, one hypothesis is that MRPL45 is involved in the interaction between the mitoribosome and IMM. As discussed in the introduction, this interaction is essential for an efficient protein synthesis because all the products of mitochondrial translation are highly hydrophobic polypeptides that need to be immediately integrated in the IMM.

A few months after the beginning of this project, the first high resolution structure of the large mitoribosomal subunit was released (Greber BJ et al., 2014). This structural data on the porcine subunit, confirmed that MRPL45 is a component of the mitoribosome and that it is localised in close proximity to the polypeptide exit site. This location is consistent with an interaction with the IMM and supports the hypothesis of MRPL45 playing a role in this interaction, as was postulated by the authors.

Shortly after, the high resolution structure of the human mt-LSU was released (Brown A et al., 2014) and confirmed the localisation of MRPL45 observed in the porcine counterpart. This structure gave further insight into the structure of the protein, which differs from the porcine orthologue. The structure of MRPL45 and its similarity to orthologous proteins will be discussed in the following chapter.

Human MRPL45 is encoded by chromosome 17 and is composed of 306 amino acids, giving a predicted molecular weight of 36 kDa. Data presented in chapter 6 of this thesis suggested that MRPL45 is targeted to mitochondria by a presequence which is cleaved on import into the organelle.

The aim of this chapter was to study the characteristics of MRPL45. SInce at the beginning of this project the structure of the human mitoribosome had yet to be published, it was important to confirm the localisation of MRPL45 within the mitoribosome. Subsequently, the importance of this protein was tested by depleting it from different cell lines using siRNA technology. After initial optimisation, the effects of reduced steady-state levels of MRPL45 were assessed. The parameters measured included cell growth and morphology, mitochondrial protein synthesis, stability of the mitoribosome and stability of the mitochondrial mRNA species. The tools (antibody and siRNA) that were to be used throughout these studies were also validated in this chapter.

3.2. Methods

3.2.1. Cell cycle analysis using Flow-cytometry

Cell cycle analysis was performed following propidium iodide staining of nuclear DNA in whole cells. This fluorescent dye binds stoichiometrically to the DNA present in the cell.

Between 200,000 and 500,000 cells were harvested for every sample. In order to retain the dye, cells were fixed with 1 mL of ice-cold 70% ethanol that was added dropwise to the cell pellet and left to incubate at 4ºC for 30 minutes. After that, the pellet was washed twice in phosphate-citrate buffer (Table 3.1 below) and, to ensure that only DNA was stained, it was incubated for 20 minutes at 37ºC with 50 µL of 100 µg/mL RNase A.

Table 3.1 Phosphate-citrate buffer composition.

Reagents	Final concentration
Na_2HPO_4	192 mM
Citric Acid	4 mM

Propidium iodide (200 µL of 50 µg/mL*; Sigma*, cat no P4170) was added to each sample that was then analysed with the *FACSCanto II Flow Cytometer* (*BD Biosciences*) with the help of Dr. Andrew Filby. *FacsDiva8*.0 and *FlowJo* were used to analyse the data collected. The DNA histograms obtained were analysed according to the Watson (Pragmatic) model.

3.3. Results

3.3.1. Localisation of MRPL45

At the beginning of this project, the structure of the human mitoribosome was not available. Therefore, I aimed to confirm the localisation of MRPL45 within mitochondria and then whether it was integrated into the large mitoribosomal subunit. To determine this, mitochondria were isolated from HEK293 wild-type cells and subfractionated (qv 2.7.) in order to separate the different mitochondrial compartments. The success of the fractionation was assessed via western blot with antibodies recognising proteins of the outer membrane (TOM20), inner membrane (NDUFB8) and matrix (GDH) (Fig. 3.1).

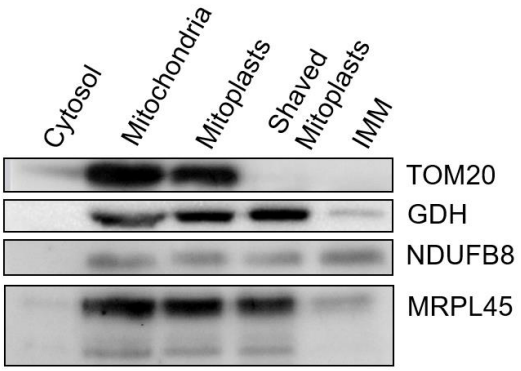

Figure 3.1 Mitochondrial subfractionation to localise MRPL45.

Western blot analysis of proportional amounts of fractions obtained from mitochondria extracted from HEK293 cells. Antibodies targeting TOM20 and NDUFB8 were used as markers for, respectively, OMM and IMM. Antibodies targeting GDH was used as a marker for the matrix fraction. The subfractionation experiment was performed once.

MRPL45 was detected in the mitochondrial fraction, as well as in the mitoplast fraction. This confirmed that the protein is in mitochondria but not in the intermembrane space since this compartment is absent from mitoplasts. The subsequent removal of the OMM, which generated the shaved mitoplasts, did not affect the levels of MRPL45 detected in the fraction. However, the levels of MRPL45 were lower in the IMM fraction. Taken together these data inferred that this protein is mainly found in the mitochondrial matrix. Interestingly, the presence of MRPL45 in the IMM fraction might suggest its interaction with the inner membrane either directly or as a part of a complex. The pattern of MRPL45 was similar to that of GDH, but it is important to specify that the weak signal observed for GDH in the IMM fraction is due to the low level of a membrane-bound form of GDH as previously reported (Rajas F et al., 1996). The detection of MRPL45 showed the presence of an intense signal, corresponding to the predicted size of the full length protein (≈36 kDa), and 2 less intense ones corresponding to approximately 30 kDa.

I aimed to confirm the localisation of MRPL45 within the large mitoribosomal subunit using cell lysate from HEK293 wild-type cells was separated on a linear 10-30% isokinetic sucrose gradient (qv 2.8.). During centrifugation, the components of the lysate were separated according to their density. Twelve fractions were obtained from the gradient and were analysed via western blot (Fig. 3.2).

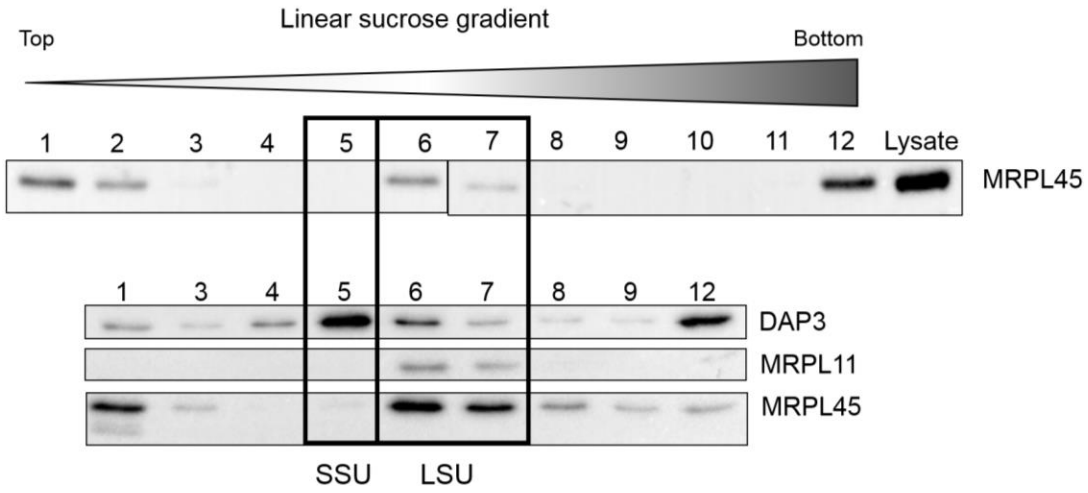

Figure 3.2 Isokinetic sucrose gradient to assess the presence of MRPL45 in the LSU.

Whole cell lysate (700 µg) from HEK293 cells was loaded on top of a 10-30% isokinetic sucrose gradient (qv 2.8.). The 12 fractions obtained after centrifugation were analysed via western blot. mt-LSU and mt-SSU were localised using antibodies against, respectively, MRPL11 and DAP3. The distribution observed for MRPL45 in the figure is representative of 3 biological repeats.

To determine the relative position of the mitochondrial ribosomal subunits, mt-SSU and mt-LSU, antibodies were used against DAP3 and MRPL11 respectively. These data indicated that the mt-SSU was recovered mainly in fraction 5, whereas the heavier mt-LSU was detected mainly in fractions 6 and 7. The lowest sucrose density (fraction 1, lysate with no sucrose) represented the protein or small complexes of low molecular weight, whereas fraction 12 represented the highest sucrose density (30%) and contained heavy complexes or aggregates. MRPL45 was detected in fractions 6 and 7, migrating with other mt-LSU proteins and so was consistent with the protein being a component of the mt-LSU. The proportion of MRPL45 recovered in the heaviest fraction of the gradient potentially indicated the presence of aggregates or incompletely solubilised extract. Since MRPL45 was also detected in fraction 1, it suggested that a proportion is found free or as a part of small complexes. Not all the mitoribosomal proteins show a proportion that is found in the least dense fraction of the sucrose gradient, as observed for MRPL11, which is absent in fraction 1 (Fig. 3.2).

A closer inspection of the western blot analysis of the sucrose gradient experiment revealed the presence of 2 lower molecular species detected by MRPL45 antibody, also observed in Fig 3.1. As previously observed, these signals were less intense than the higher molecular weight one. Surprisingly, the lower MRPL45 signals were detectable exclusively in fraction 1, even though the intensity of the higher molecular weight species was comparable or higher in fractions 6 and 7 compared to fraction 1.

The presence of MRPL45 was also assessed in 143B ρ^0 cells. These cells lack mt-DNA and are cultured in media containing ethidium bromide, in order to suppress a potential subpopulation containing mt-DNA. In the absence of mt-DNA, the mt-ribosomal RNA is not available and therefore the mitoribosomal subunits are unable to fully assemble. MRPL45 levels

were evaluated in lysate from wild-type parental 143B and 143B ρ^0 cells, using the outer membrane protein porin as a loading control (Fig 3.3).

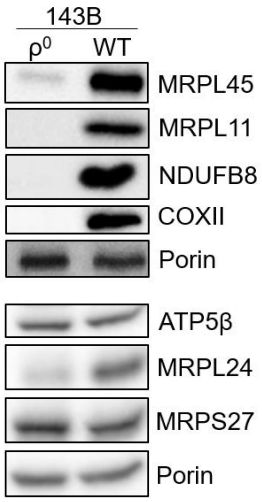

Figure 3.3 Assessment of the presence of MRPL45 and of other mitoribosomal proteins and OXPHOS components in 143B ρ^0 cells.

Western blot analysis was performed on cell lysate (30 µg) from wild-type and ρ0 143B cells. Steady state levels of mitoribosomal proteins (MRPL45, MRPL11, MRPL24, MRPS27) were assessed. Antibodies against NDUFB8, COXII and ATP5β were also visualised. Porin was used to verify the quality of the loading. The figure is representative of 2 biological replicates.

MRPL45 was still detectable in 143B ρ^0 cells, although the steady state level was strongly reduced. In contrast, MRPL11 was undetectable in cells lacking mt-DNA. The steady state level of MRPL24 was also reduced in 143B ρ^0 cells, whereas the level of MRPS27 was unchanged. The absence of the mt-encoded COXII and the component of complex I NDUFB8 confirmed that 143B ρ^0 cells lack of mt-DNA. The steady state level of the component of the F1 of complex V ATP5β was not affected. The signal obtained from porin confirmed the equality of the loading.

3.3.2. Optimisation of MRPL45 depletion

To study the role of MRPL45 in mitochondrial gene expression, the protein was depleted from a number of human cell lines and the consequences on cellular and mitochondrial metabolism were analysed. Transient transfections of targeted siRNAs (MRPL45 siRNA) were used alongside siRNA that was designed not to correspond to any cellular target (NT siRNA).

Initially, the effects of transfection were tested after 3 days (reverse transfection in solution, qv 2.1.5.) with 33 nM siRNA. Reverse transfection was performed in order to increase the surface of the cells in contact with the reagents and therefore the efficiency of the transfection. Because a stable knockdown was not required, siRNA was preferred as silencing tool as opposed to shRNA (short-hairpin RNA). This reagent also avoided the possibly lethal effect due to a constitutive knockdown of MRPL45. Delivery of the siRNA was performed using a lipid carrier, a technique with less detrimental effects on cells when compared to electroporation.

Since it is important to eliminate the possibility of off-target effects, individual siRNAs that target different regions of the same gene transcript were tested. The depletion was performed using 2 different siRNA targeting MRPL45 (Appendix 4), to test whether the reagents gave consistent data, at least 3 independent repeats of each depletion experiment were performed. To eliminate effects due to the use of reagents, cells were also transfected in parallel with 33 nM of NT siRNA, as experimental control.

HEK293 cells were transfected for 3 days by reverse transfection (qv 2.1.5.) with the 2 MRPL45 siRNA and NT siRNA at the same final concentration of 33 nM. After 3 days, cells were harvested and the lysates were analysed via western blot to determine the efficiency of MRPL45 loss and the effects on other MRPs (Fig. 3.4).

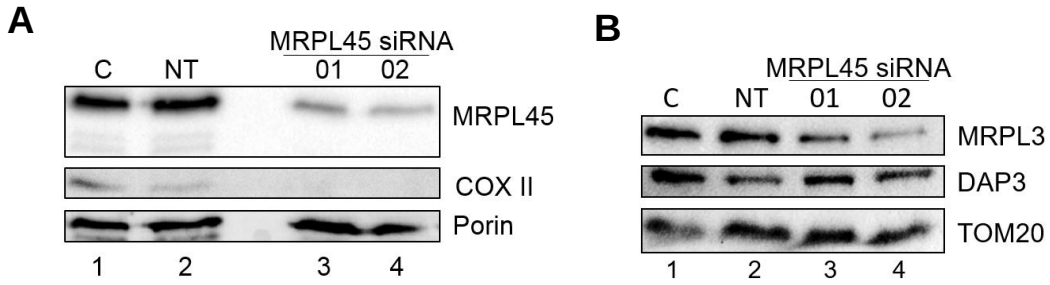

Figure 3.4 Depletion of MRPL45 on HEK293 cells using 2 different siRNA.

HEK293 cells were transfected with MRPL45, NT siRNA or cultured as an untreated control for 3 days. At the end of the incubation, cell lysate (30 µg) was analysed via western blotting. The figures shown is representative of the results obtained. Antibodies against MRPL45 and COXII were detected on membrane A, while membrane B was incubated with components of large (MRPL3) and small (DAP3) mitoribosomal subunits. Porin or TOM20 were used to verify the equality of the loading. The figure is representative of 2 biological replicates.

MRPL45 depletion was efficient with both the tested siRNA (Fig. 3.4A, lanes 3 and 4). Together with the reduction of steady state level of MRPL45, a reduction in the steady state levels of a mitochondrial encoded subunit of complex IV (COXII) was also observed in both the siRNA treatments (Fig. 3.4A, lanes 3 and 4). Porin was used to validate loading. With respect to the mitoribosomal proteins, a reduction of MRPL3 levels was detected in MRPL45 cells depleted using either of the targeted siRNAs, whereas the levels of the mt-SSU protein DAP3 were unchanged compared to controls (Fig. 3.4B, lanes 3, 4 cf lanes 1, 2). The equality of the loading was determined with antibodies targeting TOM20.

Having established that MRPL45 depletion was successful in HEK293 cells using the conditions tested, the depletion studies continued using MRPL45 siRNA02 (SASI_Hs02_00359740, Appendix 4) at a final concentration of 33 nM. Parallel control depletions were performed throughout the study with 33 nM NT-siRNA in order to exclude effects related to reagents present in the transfection rather than the targeted depletion. All the conditions tested were performed in duplicate for every experimental repeat, unless otherwise stated and experimental repeats were performed for all investigations. Although the depletion

was efficient after 3 days, the following studies presented in the chapter were performed over 6 days in order to detect effects due to the depletion of MRPL45 that might not be present after 3 days. Reverse transfection was performed, after 3 days, the cells were retransfected while adherent with the forward transfection method (qv 2.1.5.).

3.3.3. Effects of MRPL45 depletion on cell growth and morphology

The effects of 6 day MRPL45 depletion on cell growth and morphology were assessed on HEK293, HeLa and U2OS cells.

The daily visual inspection of HEK293 cells showed the emergence of large clusters of cells in the sample depleted of MRPL45, whereas the control sample showed an even distribution of cells on the culture surface (Fig. 3.5).

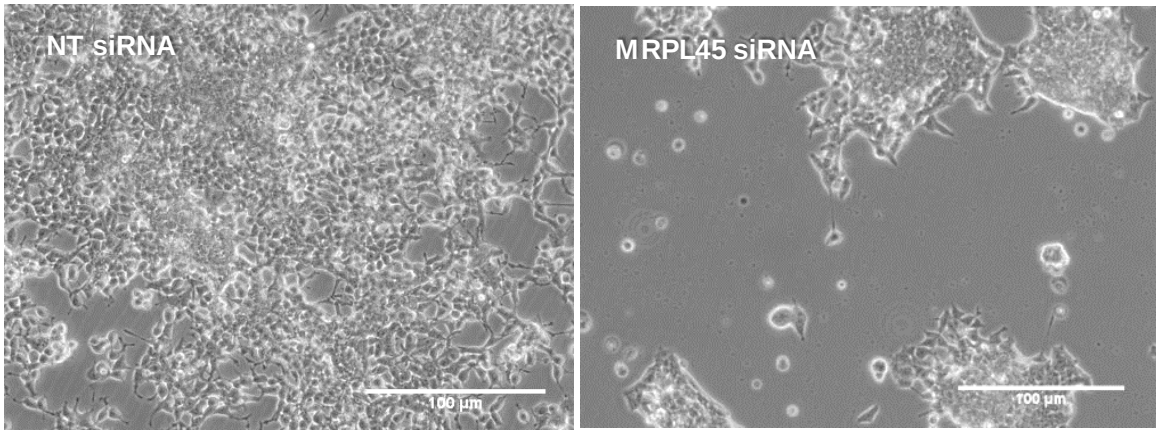

Figure3.5 Effects of MRPL45 depletion on HEK293 cells.

HEK293 cells were visualised with bright field using the inverted Zeiss Axiovert 200M microscope at 10x magnification after 6 days of incubation with NT siRNA (left panel) or MRPL45 siRNA (right panel). Scale bar= 100 µm. The figure are representative of 3 biological replicates.

Due to the presence of clusters, it was not feasible to estimate cell number using a method that depended on calculating the occupied surface area (*IncuCyte*). Therefore, the growth curve for HEK293 cells was obtained by cell counting, which was performed every 48 hours on individual wells set up in parallel at the outset of the experiment (Fig. 3.6). Counting was done in the presence of Trypan blue to exclude dead cells from the cell counts.

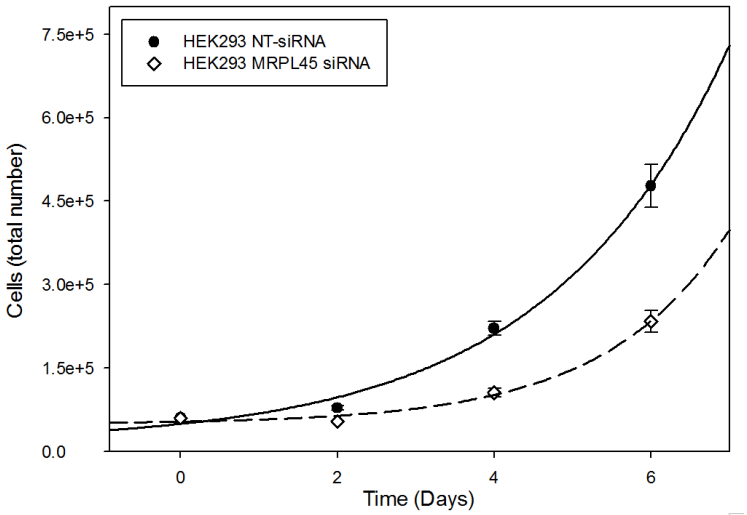

Figure 3.6 Effects of MRPL45 on HEK293 cell growth.

Cell counts were performed in 2 independent experiments on HEK293 cells incubated with NT or MRPL45 siRNA, approximately every 48 hours throughout the depletion and the data obtained were plotted to monitor cell growth.

At day 6, the number of living cells that remained after treatment with MRPL45 siRNA was approximately half the number of living cells recovered for the control sample.

In contrast to HEK293 cells, depletion of MRPL45 in U2OS or in HeLa cells did not cause the formation of clusters of cells, therefore it was possible to monitor cell growth with the *IncuCyte® ZOOM System* (Fig. 3.7). This instrument can be 'trained' to recognise specific cell types and so allows the generation of a growth curve based on the occupied space as a representation of the confluency of adherent cells but does not count the number of cells present in the sample. The number of points that are monitored per well can be selected. For my experiments, images at 12 points/well were taken for every well of a 6-well plate every 3 hours and the confluency was then calculated by the integrated software. A minimum 2 wells for every treatment were prepared and the confluency at every time point was calculated as an average of 12 data points obtained in each individual well. The cells from each well were harvested at the end of the siRNA treatment so that the efficiency of the depletion could be confirmed by western blot analysis (Fig. 3.7; inserts). Depletion in HeLa cells was interrupted at day 5 due to acidification of the media and high confluency of the cells.

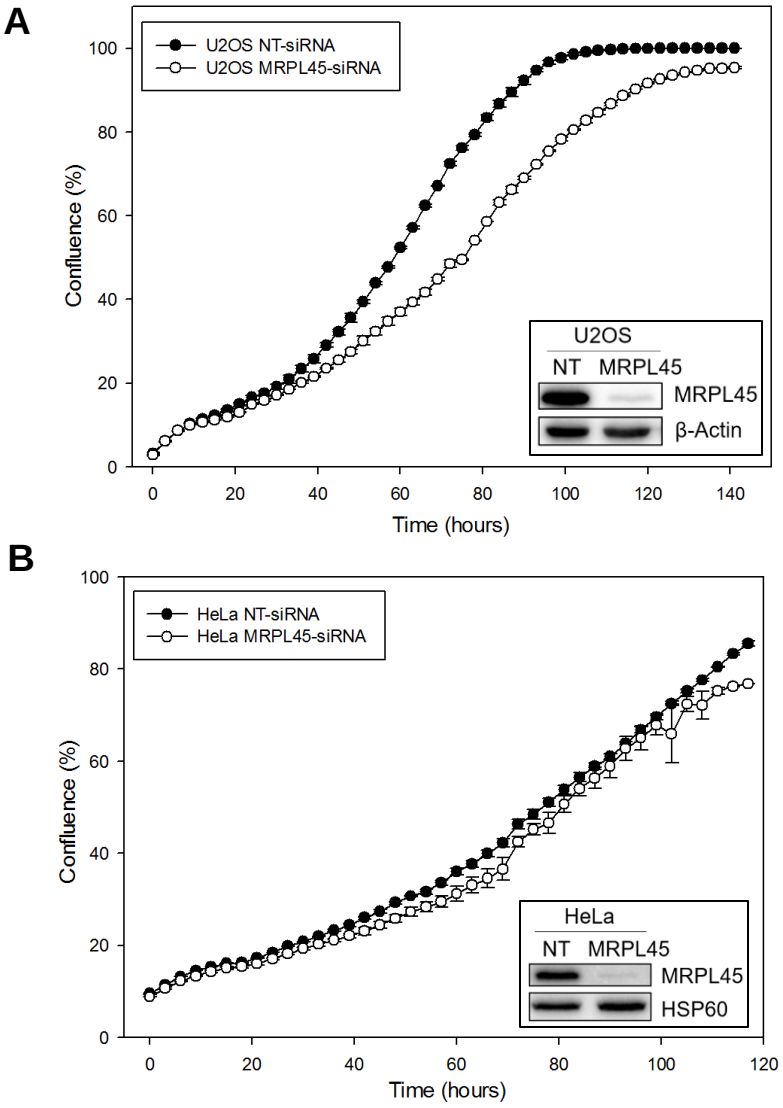

Figure 3.7 U2OS and Hela cell growth was monitored during MRPL45 depletion.

Cell coverage was evaluated every 3 hours through the IncuCyte system for U2OS **(A)** and HeLa **(B)** cells during MRPL45 depletion, and NT siRNA control treatment. Data is presented as a growth curve of calculated confluency over time. The efficiency of the depletion was confirmed via Western blot analysis (inset panels) using antibodies against MRPL45. The levels of β-Actin and HSP60 were used as loading controls. The figures are representative of 2 biological repeats.

The western blot analysis confirmed that the depletion of MRPL45 was efficient in both U2OS and HeLa cells. At this level of depletion, cell growth did not appear to be strongly impaired in U2OS cells, as 100% confluency is reached by the sample depleted of MRPL45 (white circles) with minor delay when compared to the control (black circles) (Fig. 3.7A). For HeLa cells, no growth defect was detected by *IncuCyte* monitoring (Fig. 3.7B).

Cells were also visualised using the *IncuCyte* system. Images after approximately 6 days are shown for U2OS and HeLa cells in Fig. 3.8 A and B.

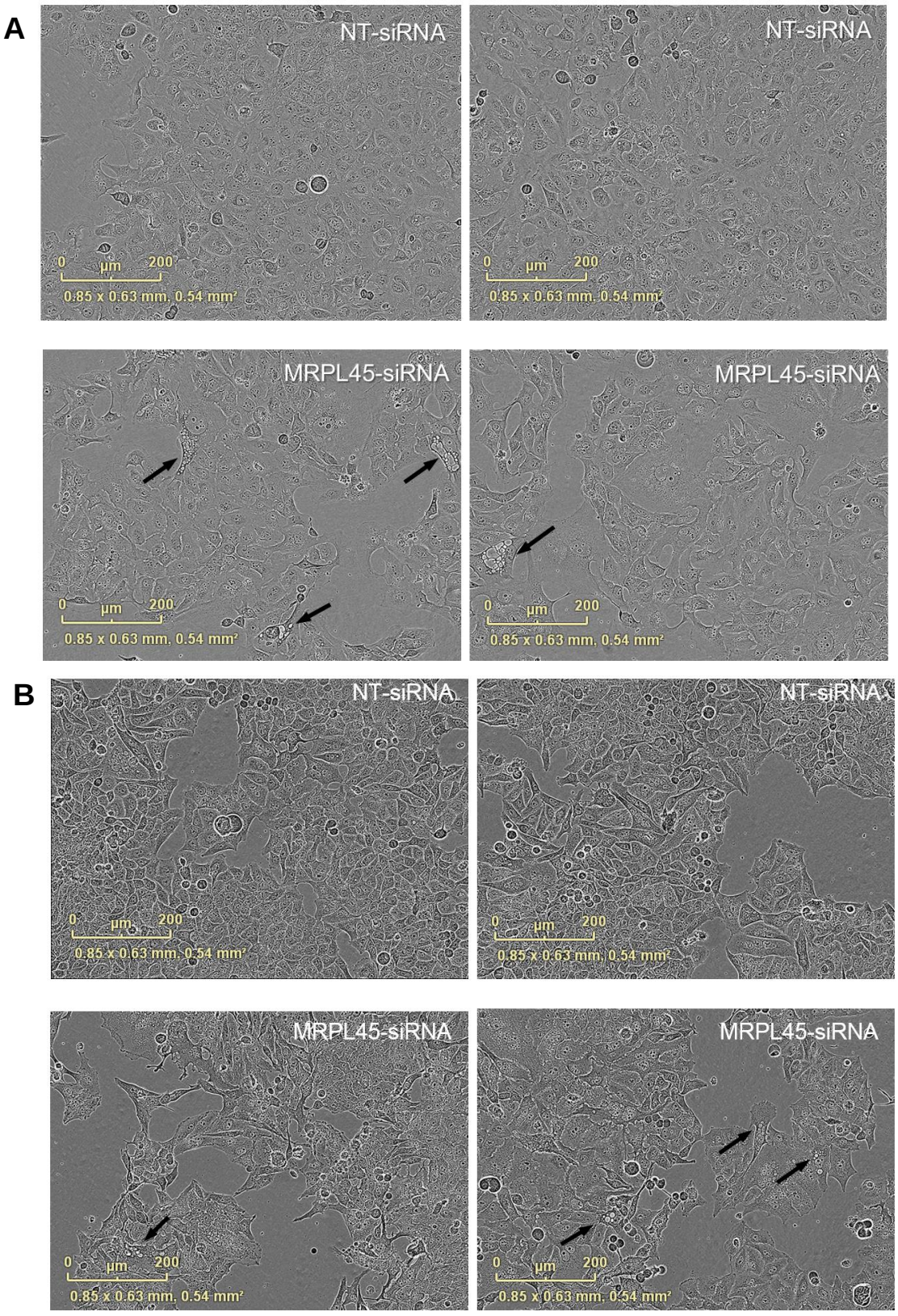

Figure 3.8 U2OS and HeLa cells after 6 days of siRNA treament to deplete MRPL45.

U2OS **(A)** and HeLa **(B)** cells were transfected for 6 days with NT or MRPL45 siRNA and visualised 5 days later. Images were obtained from the IncuCyte system. Cells containing vacuoles are indicated by black arrows. The figures are representative of 3 biological repeats.

A proportion of U2OS and HeLa cells depleted of MRPL45 looked enlarged, with less defined edges and containing vacuoles (Fig. 3.8, indicated by black arrows). These features were less common in the control cells. The enlargement of the cells might also

Interestingly, a major effect on U2OS cell growth could be seen by cell counting when the depletion levels of MRPL45 were so low that western blot could not detect any protein. Representative results of these experiments are illustrated in Fig. 3.9. The growth curve was obtained by manual cell counting performed approximately every 48 hours throughout the 6 days of depletion rather than by *IncuCyte* (Fig. 3.9 A). Cell morphology was evaluated on a daily basis using the inverted microscope (Fig. 3.9 B) and the efficiency of the depletion was confirmed via Western blotting (Fig. 3.9 C).

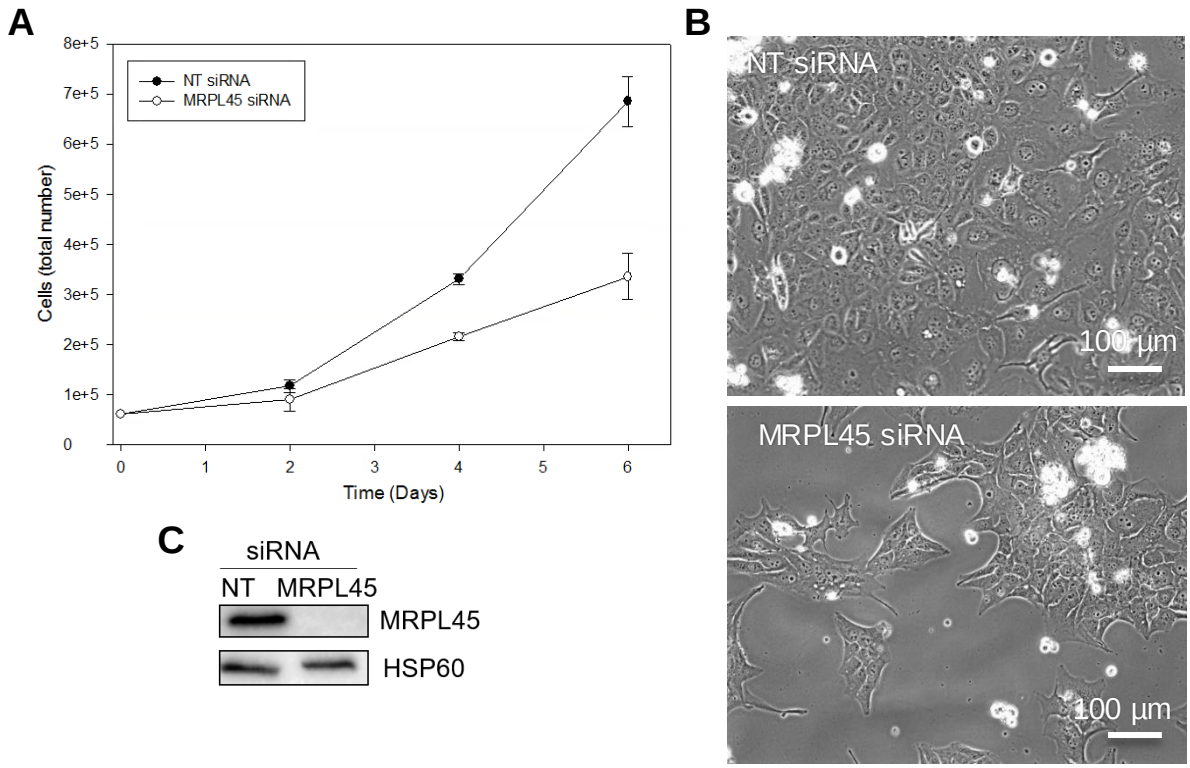

Figure 3.9 Effects of MRPL45 knockdown on U2OS cells upon higher efficiency of the depletion.

U2OS were transfected with NT siRNA or MRPL45 siRNA for 6 days. The growth curve was obtained by cell counting during 6-days depletion of MRPL45 **(A).** Cells were visualised using the inverted microscope at the end of the treatment **(B).** Cell lysates (x µg) were analysed via Western blotting to confirm the depletion. HSP60 was used as loading control **(C).** The data are representative of 2 biological repeats.

When the level of MRPL45 was undetectable via western blot (Fig. 3.9 C), a severe growth defect (Fig. 3.9 A and B) was observed, whereas a milder growth defect was observed when the depletion was less efficient, as shown in Fig. 3.7 A and 3.8 A. Although 2 different methods were used to evaluate cell growth (occupied surface in 3.7 A and number of cells in 3.8 A), a difference in cell growth can be appreciated in the figures of cells obtained in the two different experiments (Fig. 3.8 A and 3.9 B). These data, combined with those previously observed on

U2OS cells depleted of MRPL45, suggest that the effect on cell growth might be finely regulated by the efficiency of the depletion.

As cell growth seemed to be affected, cell cycle analysis was performed on U2OS cells after 6 days of transfection with MRPL45 and NT siRNA. Cells can be attributed to different phases of the cell cycle according to their DNA content. The profile of "healthy" cell growth usually results in the majority of the cells in G1 phase, which will contain the normal amount of genomic DNA (diploid). A smaller proportion of the cell population will be actively replicating DNA (designated S phase) and the remainder will be in late stage of mitosis phase (G2) where the chromosomes have been duplicated and so cells contain twice as much DNA as cells in phase G1. Some cells stick together and so in the sample they were present as doublets. These could be easily identified and excluded from the final analysis. The results (Appendix 7) were analysed and the cells were partitioned into the different phases as shown in the following figure (Fig. 3.10A). The Watson model was preferred to the Dean-Jet-Fox model to analyse the data. The former model makes no assumption on the shape of the S phase, which instead is modelled in the Dean-Jet-Fox model. A sample for each treatment was retained to confirm the efficiency of the knockdown via western blot analysis (Fig. 3.10B).

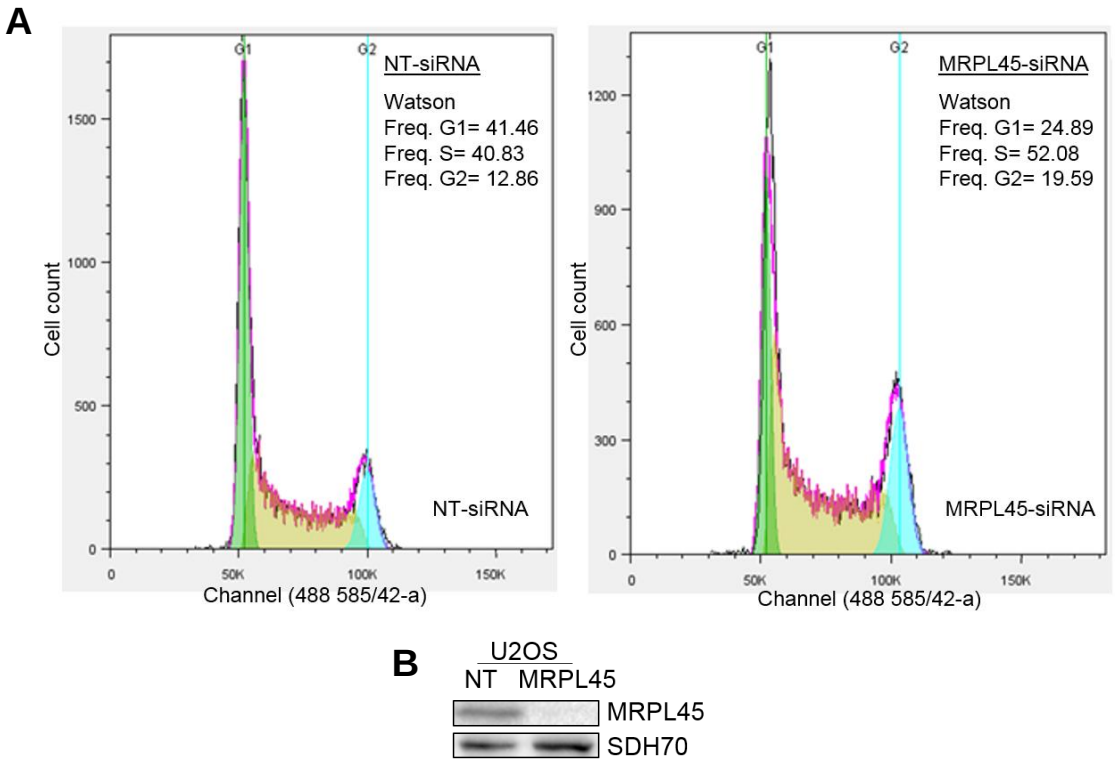

Figure 3.10 Cell cycle analysis of U2OS cells following MRPL45 depletion.

A) Propidium iodide DNA staining was performed on U2OS cells after incubation for 6 days with NT or MRPL45 siRNA. Approximately 100,000 events were collected and the data were analysed and the percentage of cells in phases G1 (green), S (yellow) and G2 (blue) was calculated (Watson model). **B)** Western blot analysis to confirm the efficiency of MRPL45 depletion in the cells used for the cell cycle analysis. SHD70 was used as a loading control. The experiment was performed once.

The western blot analysis confirmed depletion of MRPL45. The cell cycle analysis indicated that when compared to control cells, cells treated with MRPL45 siRNA for 6 days showed an increase in proportion of cells in S (+11%) and G2 (+7%) phases, with a relative reduction of cells in G1 phase (-16.5%). This result might suggest that the cells are proliferating faster or that they are arrested in the middle of duplicating their DNA. In order to discriminate between the 2 possibilities, it would be possible to analyse the S phase using bromodeoxyuridine (BrdU) uptake. This reagent is an analogue of thymidine that is incorporated into DNA during its replication. When a BrdU pulse-chase experiment is performed, it is possible to follow the group of cells that were actively replicating the DNA during the pulse of BrdU staining as they progress through the cell cycle of and understand if the cells were increasing their proliferation or if they were arresting in a particular phase. This experiment was not performed as it was considered not crucial for the project.

3.3.4. Effects of MRPL45 depletion on mitochondrial protein synthesis and the OXPHOS components

As MRPL45 was predicted to be a component of the mitochondrial translation machinery, the effects of its depletion on mitochondrial translation were assessed.

The depletion was performed over a 6-days period, combining reverse transfection with forward transfection (qv 2.1.5.), to analyse the effects observed due to the prolonged absence of the protein. The experiment was performed on different cell lines to determine it this was a physiologically relevant effect and to indicate the reproducibility of the findings in different systems. At the end of the transfection period, cells were lysed and the protein content was analysed via western blot. Cells transfected with NT-siRNA were used as control (Fig. 3.11).

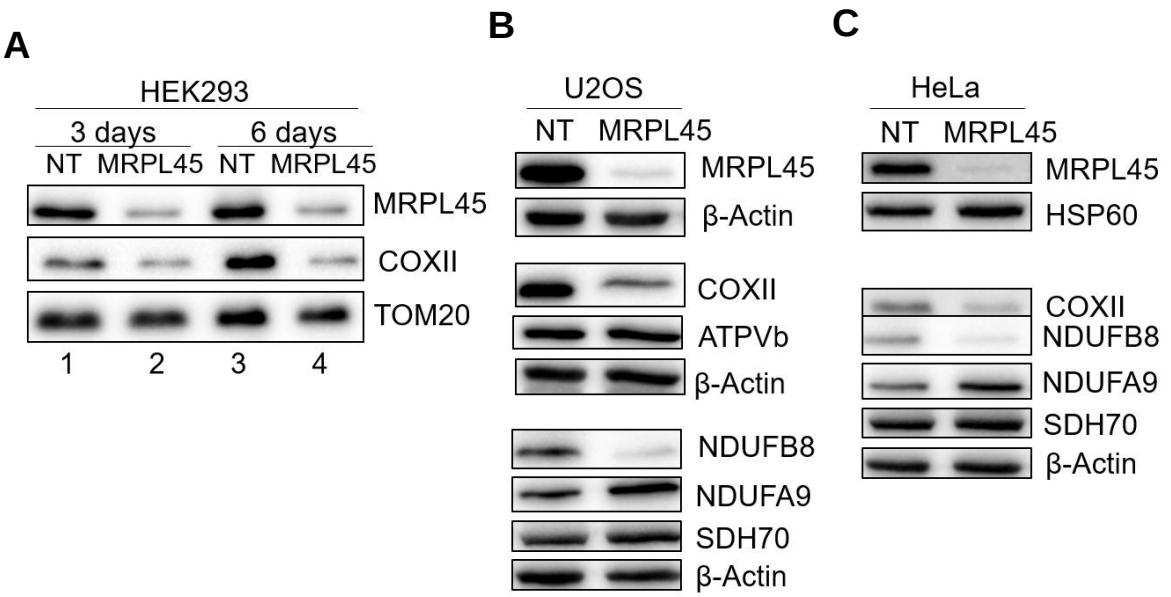

Figure 3.11 Analysis of the steady state level of OXPHOS components following MRPL45 depletion.

HEK293 (**A**;30 µg), U2OS (**B;**30 µg) and HeLa (**C**;30 µg) cells depleted of MRPL45 for 6 days were analysed by Western blot. The efficiency of the depletion was verified with antibodies against the depleted protein. The effects of the depletion on the OXPHOS components were analysed using antibodies against the mitochondrial encoded COXII or nuclear encoded components (ATPVb, NDUFB8, NDUFA9, SDH70). TOM20, HSP60 and β-Actin were used as loading controls. The data shown are representative of 3 biological repeats.

Data obtained for HEK293 cells showed that, together with the reduction of the steady state level of MRPL45, a reduction of the mitochondrial encoded subunit II of complex IV (COXII) was observed. Antibody against the OMM protein TOM20 was used to confirm the equality of the loading (Fig. 3.11A). The results obtained were recapitulated in U2OS and HeLa cells (Figure 3.11 B and C). The steady state level of other OXPHOS components were also assessed in these 2 cell lines following MRPL45 depletion. Together with the reduction of the mitochondrial-encoded protein COXII, a reduction of a nuclear-encoded subunit of complex I (NDUFB8) was observed. This protein is also absent in ρ^0 cells (Fig. 3.3), probably because the mt-encoded components of the complex are needed for its integration within a subcomplex of complex I to stabilise it. This indicates that NDUFB8 is a good surrogate marker to interrogate the state of mitochondrial translation. Unlike NDUFB8, no reduction was detected in the steady-state level of another nuclear encoded component of the same complex, (NDUFA9). No changes were detected in the steady-state level of 2 other nuclear encoded components of the OXPHOS system, SDH70 (Complex II) and ATPVb (Complex V). This result was also expected as both these proteins are present at normal level in ρ^0 cells. HSP60 or β-Actin were used as loading controls.

The OXPHOS deficiency highlighted from western blot analysis after MRPL45 down-regulation was also supported by the acidification of the media observed in the depleted cells (Fig. 3.12).

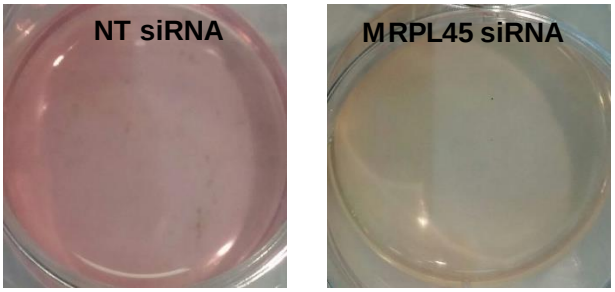

Figure 3.12 MRPL45 down-regulation affects the growth media acidity.
Images of 6-well plates were taken after 6 days of MRPL45 depletion on U2OS cells.

When compared to the control, the media of cells depleted of MRPL45 was more yellow. Phenol red, is a pH indicator that is included as a component of the growth medium. It has a range from 6.2 (bright yellow) to 8.4 (pink/purple). This allows for quick visual assessment of the metabolic status of the cells in culture. The observed change in colour indicated the acidification of the media, probably due to the metabolic switch for ATP production from oxidative phosphorylation to glycolysis in MRPL45 depleted cells. In this condition, glucose is transformed in pyruvate to generate ATP. Due to the failure of the OXPHOS system, pyruvate cannot be further metabolised and is reduced to lactate by the enzyme lactate dehydrogenase, which uses the excess of NADH accumulated as a consequence of the malfunction of the OXPHOS. The release of lactic acid within the media lowers its pH, which leads to the change in colour of phenol red.

3.3.5. Effects of MRPL45 depletion on the stability of LSU and SSU

The steady state level of a mitochondrial encoded protein (COXII) was compromised in the absence of MRPL45 (Fig. 3.11). This was predicted to be caused by a lack of functional mitoribosome, so to investigate if this effect was due to a defect of mitochondrial protein synthesis, the stability of the mitoribosome was examined. Cells were, therefore, depleted of MRPL45 for 6 days and the steady state level of protein components of the mt-LSU and the mt-SSU was assessed via western blot analysis (Fig. 3.13).

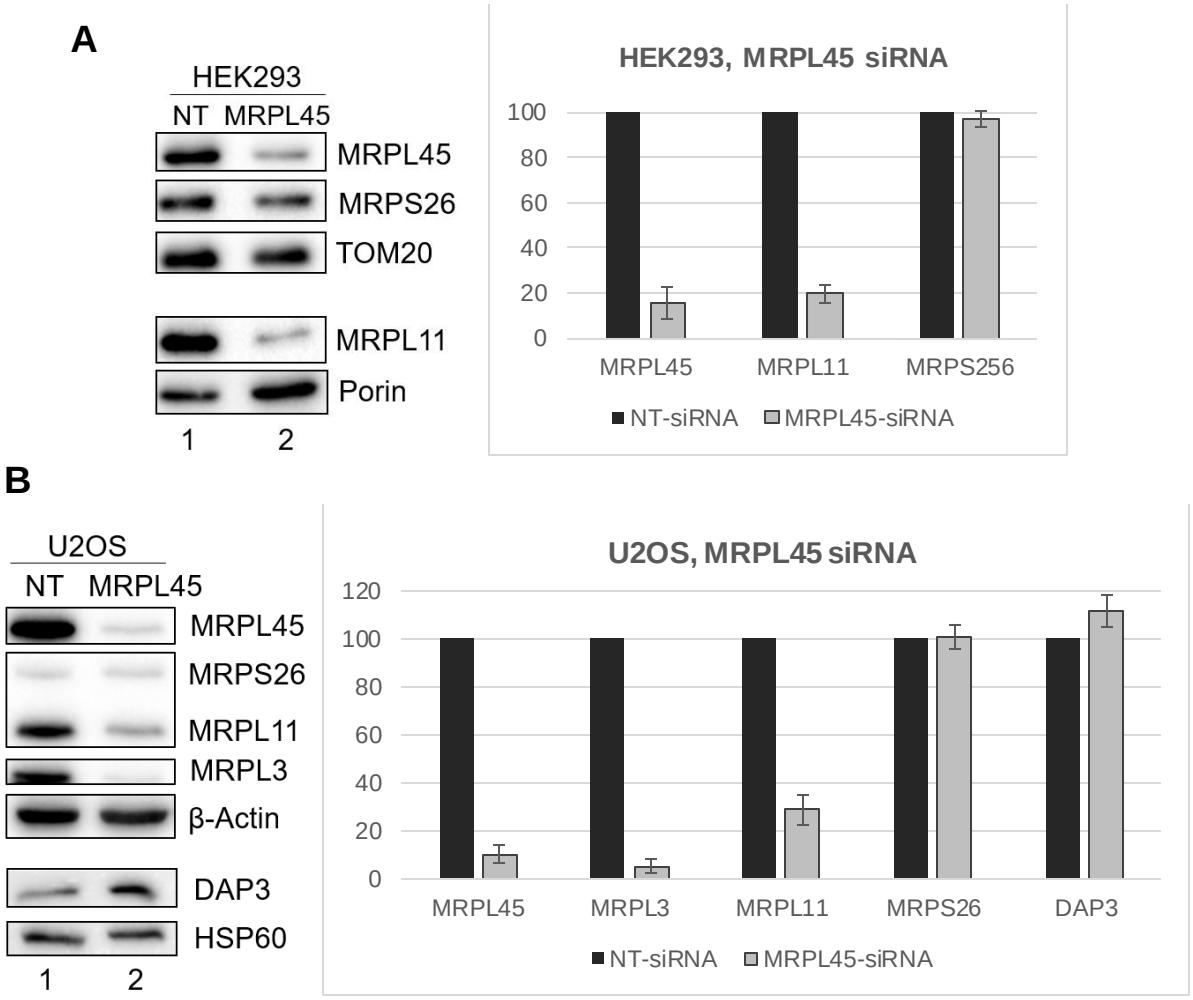

Figure 3.13 Evaluation of the steady state level of proteins of the mt-LSU and mt-SSU in MRPL45 depleted cells.

Western blot analysis was performed after 6 days of MRPL45 depletion in HEK293 (**A**; 30 µg) and U2OS (**B**; 30 µg) cells. Antibodies against MRPS26 and DAP3 were used as markers for the mt-SSU, whereas antibodies against MRPL11 and MRPL3 were used to detect the mt-LSU. Quantification of 3 biological repeats is also presented.

The analysis of the steady state level of components of the LSU following MRPL45 depletion in HEK293 (Fig. 3.13A, lane 2 and bar graph) and U2OS (Fig. 3.13B, lane 2 and bar graph) cells showed a reduction of MRPL11, MRPL3, whereas the SSU proteins tested (MRPS26 and DAP3) were not affected. TOM20, porin, HSP60 and β-Actin were used to verify the equality of the loading.

To further confirm the effects on the stability of the 28S and 39S subunits, the steady state level of the mitochondrial rRNAs (16S and 12S) were evaluated by qPCR (qv 2.3.4.). Total RNA was isolated from U2OS cells after 6 days of MRPL45 depletion or siNT treatment and aliquots (500 ng) from each were then reverse transcribed (qv 2.4.1. and 2.4.2.). An equal proportion of each cDNA (2 µl) was used to programme the qPCR and the data were analysed as reported in 2.3.4. The results are reported in Fig. 3.14 and are representative of 3 biological repeats.

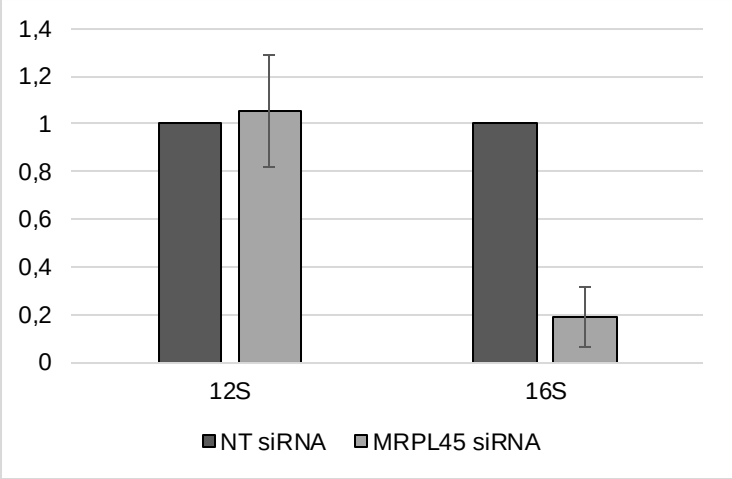

Figure 3.14 Effects of MRPL45 depletion on mt-rRNA.

The levels of 12S and 16S rRNA were quantified after 6 days of MRPL45 depletion via q-PCR reaction for 3 biological repeats. NT-siRNA was used as a control. The cytosolic 18S rRNA was also quantified and used to normalise the data, which were analysed as in 2.3.4.

The qPCR analysis showed a reduction of 16S rRNA, while 12S rRNA was unaffected. This agreed with the western blot data which showed the instability of the mt-LSU, but not of the mt-SSU after depletion of MRPL45.

3.4. Discussion

The results obtained in this chapter have confirmed that MRPL45 is a mitochondrial protein mainly if not exclusively found in the matrix and showing a weak association with the IMM. Two additional bands were detected for the protein in the figure obtained for the sucrose gradient analysis, indicating a possible existence of a cleaved version of this protein. Isokinetic sucrose gradient analysis confirmed that MRPL45 is a component of the mt-LSU, as reported in the structures of the porcine (Greber BJ et al., 2014) and human (Brown A et al., 2014) mt-LSU published after the start of this project. Interestingly, the sucrose gradient analysis also highlighted the presence of an important free pool of protein that is not associated with the mitoribosome. Of all the mitoribosomal proteins that have been analysed in our laboratory, relatively few are well represented in the low density fractions that reflect low molecular weights. Like MRPL45, another mitoribosomal protein that shows a biphasic distribution is MRPL12. Published data show the existence of a proportion of MRPL12 in the first fraction of the sucrose gradient (Surovtseva YV et al., 2011). The same study also claims that the proportion of MRPL12 that is not bound to the mt-LSU is involved in regulation of mitochondrial transcription via interaction with POLRMT. Since MRPL45 shows a similar distribution to MRPL12, it is reasonable to speculate a second unidentified role of MRPL45 within mitochondria. In addition, the lower molecular weight signals detected by MRPL45 antibody were detected only in the first fraction. A recent study by Nouws J et al. (2016) identified that the interaction between MRPL12 and POLRMT is mediated by a cleaved version of this mitoribosomal protein, that is found in fraction 1 of the sucrose gradient analysis of the cited study. It is tempting to speculate the possibility of a second role of cleaved

versions of MRPL45 outside the mitoribosome. This hypothesis could be further explored, although this aspect is not in the scope or time frame of this project.

Because of its proximity to the polypeptide exit site and its structural similarities to the IMM interacting protein TIM44, the importance of MRPL45 for an efficient translation in mitochondria was assessed via siRNA depletion experiments.

The optimisation of the siRNA transfection was performed using multiple siRNA duplexes targeting different regions of the MRPL45 transcript. Since these had similar consequences on cell growth, morphology, and mitochondrial homeostasis it suggested specificity and not off-target effects. A commercially available antibody was used and validated the depletion. The siRNA was therefore selected for further use in my study.

The use of siRNA allows specific depletion of proteins by selectively targeting the mRNA sequence that encodes for the protein of interest. As this approach is not a genetic knockdown, the efficiency can be variable and the depletion is usually not complete. In the experiments performed in this chapter, it emerged that the amount of MRPL45 remaining after the depletion, differently affected the cell growth. Despite there being differences observed in how severe ly cell growth was affected, the cell morphology was affected in all the experiments performed. Whereas HEK293 cells tended to grow in clusters following loss of MRPL45, U2OS and HeLa cells showed a morphology more reminiscent of senescent cells, which could not be clearly confirmed by subsequent experiments on U2OS cells. In addition, cell cycle analysis suggested a longer doubling time. Altogether, these data highlight the importance of MRPL45 for maintaining cellular homeostasis.

Further evidence of the importance of MRPL45 within mitochondria came from the analysis of protein content in the depleted cells. The reduction of the tested mitoribosomal components of the mt-LSU observed in the absence of MRPL45 revealed the crucial role of this protein for the stability and assembly of the large subunit. This is a striking difference from the yeast homologue of MRPL45, Mba1, which is only transiently associated with the mitoribosome and, therefore, not required for the stability of the mt-LSU. As a consequence of the absence of the mt-LSU, the fully assembled mitoribosome is absent and cannot perform mitochondrial translation. This leads to a dramatic reduction of mitochondrial encoded protein as observed in the MRPL45 depletion studies here reported. In the absence of mitochondrial-encoded proteins, the OXPHOS complexes cannot assemble in functional units, leading to the impossibility to create a proton gradient and eventually produce ATP. In these conditions, cells must survive by relying on glycolysis for ATP synthesis.

Unlike the mt-LSU, the mt-SSU did not show instability in the absence of MRPL45, as inferred by the unchanged steady state level of the tested components of the subunit, both protein and rRNA. This result suggests that the assembly and stability of the mt-SSU does not require the presence of the mt-LSU.

Since my data demonstrated the importance of MRPL45 for protein synthesis in mitochondria, its potential involvement as mediator of the interaction with the IMM, as hypothesised earlier, will be investigated in the following chapter.

Chapter 4: Analysis of the interaction of mitoribosome and MRPL45 with the IMM

4.1. Introduction

As described earlier in the general introduction, the 13 products of intramitochondrial translation are all hydrophobic OXPHOS proteins that are inserted in the IMM upon synthesis by the mitoribosome. Due to high hydrophobicity of their products, it is likely that the translating mitoribosomes are found in close proximity to the IMM to avoid the aggregation of the newly synthesised polypeptides, their unfolding and refolding, and to promote their direct integration into the membrane. Previous studies on mammalian mitochondria have reported that approximately 50% of the mitoribosomes are tightly bound to the IMM (Liu M & Spremulli LL, 2000), but how this interaction is mediated is still unclear. As discussed in the general introduction, at present only few mammalian proteins (MPV17L2, OXA1L and LetM1) have been suggested to interact with both the IMM and the mitoribosome, but extensive studies to confirm and characterise their role in this interaction are missing. While the previous chapter was focused on understanding the importance of MRPL45 as a structural component of the mitoribosome, this chapter will study the possible role of the protein in the interaction between mitoribosome and IMM. The location of this protein in close proximity to the polypeptide exit site (as shown in Fig. 1.13, page 29) and its structural similarity with an IMM-interacting protein support the hypothesis of a role of MRPL45 in the interaction with the IMM.

The PFAM (Protein FAMily) database search of MRPL45 suggested that this protein contains a Tim44-like domain located between residues 119 and 263 (RefSeq NP_115727.5). The Tim44-like domain corresponds to a region at the C-terminus of TIM44, a peripheral membrane protein that binds to the IMM and to the TIM23 complex, allowing the translocation of polypeptides through the IMM into the mitochondrial matrix (D'Silva P et al., 2004). The N-terminus of yeast Tim44p was suggested to be involved in the interaction with Tim23p (Schiller D et al., 2008), whereas *in vitro* studies on the C-terminus of both the yeast and the mammalian homologues highlighted the ability of this domain to interact with membrane-like structures. The crystal structures of the C-terminus of both yeast Tim44p (PDB 2FXT (Josyula R et al., 2006)) and human TIM44 (PDB 2CW9 (Handa N et al., 2007)) were previously resolved by Josyula R and Sha B (2006) and Handa N et al. (2007) respectively. The publication of the human mt-LSU structure in 2015 (Brown A et al., 2014) included structural details of MRPL45 (PDB 3J7Y (Brown A et al., 2014), chain d), allowing it to be compared to the structure of human TIM44, shown in Fig. 4.1. Although the cryo-EM studies on the human mt-LSU gave nanometer resolution, it did not fully resolve MRPL45 (resolved residues: 119-200, 207-252, 255-287). The structure of MRPL45 within the mt-LSU obtained from this study is shown in Appendix 15.

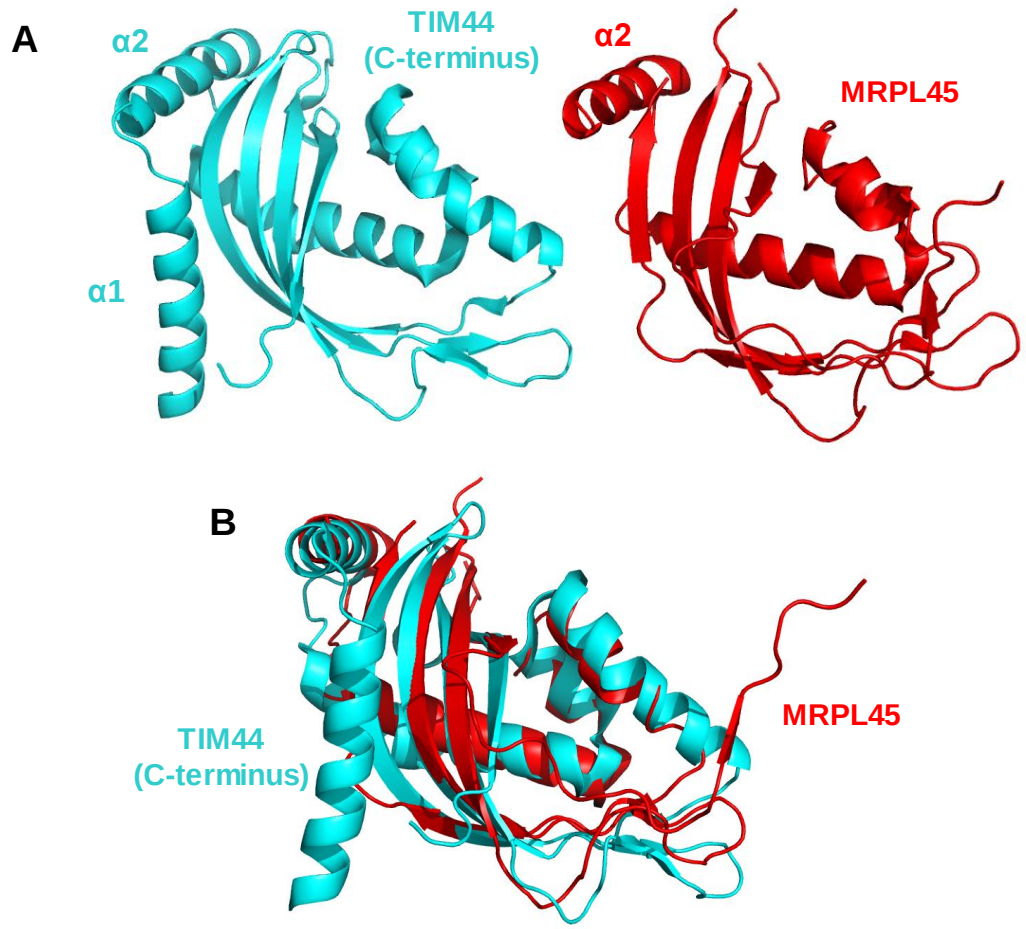

Figure 4.1 Structural comparison of human TIM44 and human MRPL45.

A) The structures of the C-terminus of human TIM44 (cyan, PDB 2CW9 (Handa N et al., 2007)) and the human MRPL45 (red, PDB 3J7Y, chain d (Brown A et al., 2014)) were visualised on Pymol as cartoons. The structure of MRPL45 obtained from the PDB file was not complete and is reported in Appendix 15. **B)** Superimposition of the structures of TIM44 and MRPL45 visualised in Fig. 4.1A.

Figure 4.1 shows the structural similarity between the MRPL45 protein and the C-terminus of human TIM44. Both the proteins present a similar organisation composed of cystatin-like folding, which is defined as helix packed against coiled antiparallel beta-sheet. The 2 proteins share a sequence identity of approximately 11%, with a similarity that reaches approximately 21% (http://www.ebi.ac.uk/Tools/psa/emboss_needle/).

The ability of the C-terminus of human and yeast Tim44 to interact with membranes has been studied *in vitro*. With respect to Tim44p, the C-terminus of this protein was shown to interact with liposomes containing cardiolipin (Marom M et al., 2009), which is the most highly represented acidic phospholipid of the IMM (Comte J et al., 1976). Two hydrophobic regions were detected on the C-terminus of Tim44p, of which 1 is found between 2 α-helices and 1 creates a cavity that is composed of residues Val306, Gly388, Tyr 398 and Phe422. The specific region of the C-terminus of Tim44p involved in the interaction with the membrane was found by studying the interaction of truncated versions of the protein with liposomes (Marom M et al., 2009). The interaction with the membrane-like structures was lost when helix A1 was absent, despite the presence of the

hydrophobic cavity. In the study, the authors claim that the folding of the 2 α-helices A0 and A1 (Fig. 4.2) is involved in the interaction with the model membrane, and that their relative position is important for this interaction.

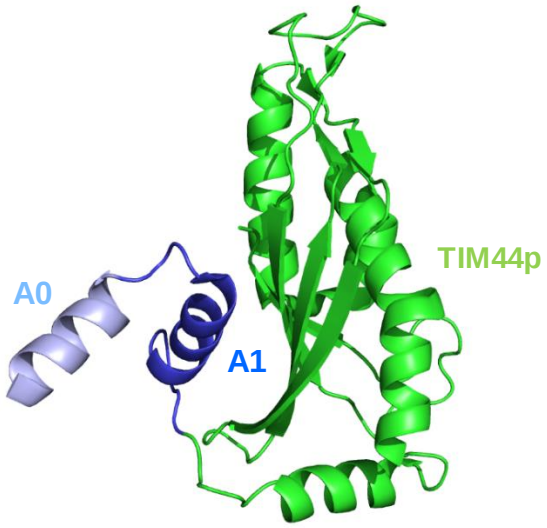

Figure 4.2 Putative membrane-interacting domain of yeast Tim44p

PyMol was used to visualise the structure of yeast Tim44p, shown as cartoon (PDB 2FXT (Josyula R & Sha B, 2006)). The putative membrane-interacting helices are shown in light blue (A0) and blue (A1). The remaining part of the protein is shown in green.

The crystallisation of the C-terminus of human TIM44 was performed by Handa N et al. (2007) using PEG 400 as a precipitant. The resulting structure closely resembles the yeast homologue, with the exception of the C-terminal domain, which presents 1 long helix in human, in contrast with 2 shorter helices found in yeast (Fig. 4.3, indicated by arrows). These domains also differ in the orientation of the helices, with the yeast ones protruding more from the central structure. It has been proposed that upon binding with the membrane, these helices undergo a conformational change, resembling the long helix (α1) found on the human TIM44 (Josyula R & Sha B, 2006).

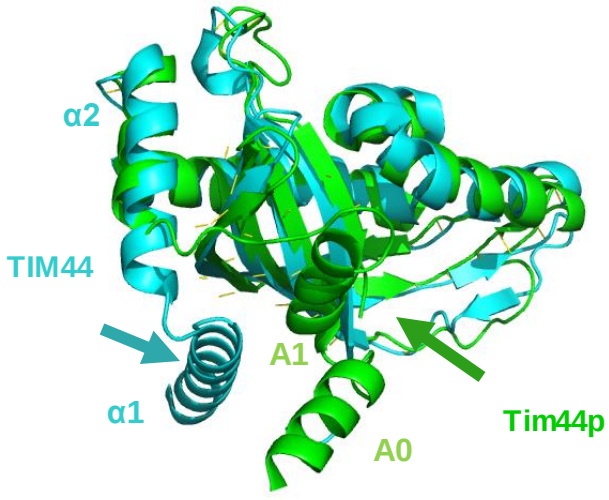

Figure 4.3 Structural comparison of human TIM44 and yeast Tim44p.

Superimposition of human (cyan, PDB 2CW9 (Handa N et al., 2007)) and yeast (green, PDB 2FTX (Josyula R & Sha B, 2006)) Tim44 obtained by automatic structure alignment on PyMol.

In the crystal structure of human TIM44, 2 molecules of PEG were recovered, indicating hydrophobic regions that might act as binding sites with the membrane. One of the PEG molecules recovered was bound to the highly conserved loop present between helices α1 and α2 (Fig. 4.4A, shown in orange, indicating one of the potential membrane binding sites that is very well conserved amongst species (Fig. 4.4B). The PEG molecules also identified another hydrophobic cavity found in the core of the protein, between helices α3, α4, α5 and two β-sheets.

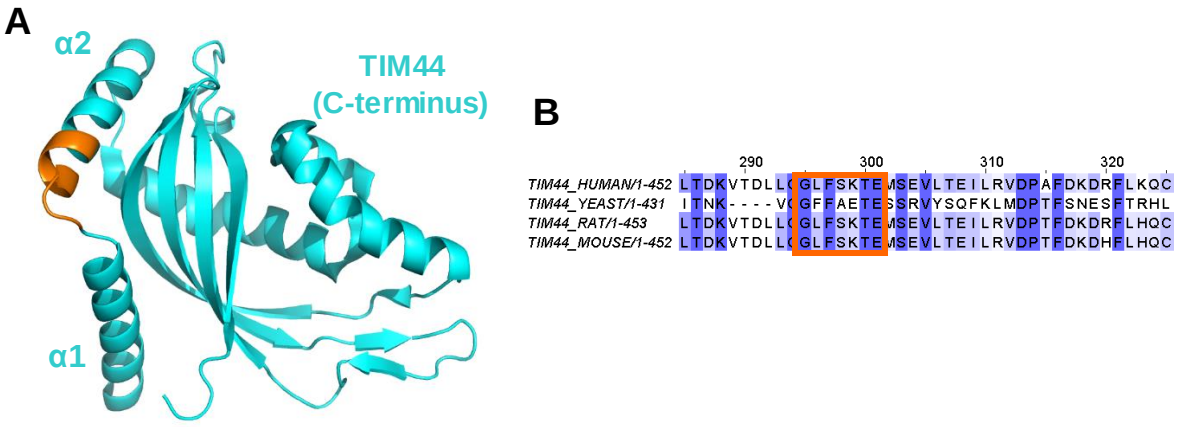

Figure 4.4 Putative membrane interacting domain of the C-terminus of human TIM44 and its conservation amongst different species.

A) Crystal structure of the C-terminus of human TIM44 obtained in PyMol using the published PDB 2CW9 (Handa N et al., 2007). The residues claimed to interact with membrane-like structures (Marom, Safonov et al. 2009) are depicted in orange. **B)** Alignment of Tim44 sequences from different species. The intensity of the blue indicates the degree of conservation of the amino acid sequence. The putative membrane-interacting site is indicated in orange.

Because of its structural similarity to the membrane interacting protein TIM44, MRPL45 might be able to interact with the IMM via the domain corresponding to the one suggested for TIM44 interaction.

In addition to the presence of a Tim44-like domain, studies on the yeast MRPL45 homologue (named Mba1) further support the hypothesis of a role of MRPL45 in the interaction with the membrane. Unlike the mammalian homologue, Mba1 is not a constitutive component of the mitoribosome, but has been suggested to interact tightly with the matrix face of the IMM (Preuss M et al., 2001) and to bind the mitoribosome (Ott M et al., 2006). Studies in yeast showed that Mba1 could be cross-linked with proteins at the polypeptide exit tunnel of the mitoribosome (Gruschke S et al., 2010). Recent studies reported that Mba1 creates a complex with Cox20 to support cotranslational maturation of Cox2 (Lorenzi I et al., 2016). Additional evidence of the Mba1-mediated bridge between the mitoribosome and IMM came in 2015 by cryo-electron tomography studies on yeast that identified 2 contact points between the mitoribosome and the membrane (Pfeffer S et al., 2015). Of these, one was mediated by rRNA and the other one by Mba1. The superposition of the sub-tomogram of yeast mitoribosome and the structure of mammalian mitoribosome presented in the study showed the colocalisation of Mba1 and MRPL45 (Fig 4.5).

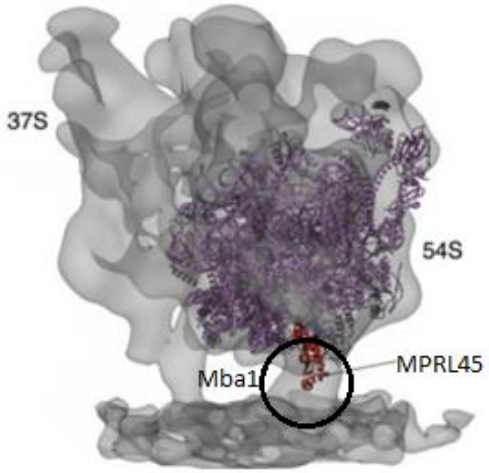

Figure 4.5 Colocalisation of Mba1 and MRPL45 shown by superimposition of the structures of yeast and mammalian mt-LSU.

The cartoon structure of mammalian mt-LSU (PDB 4CE4 (Greber BJ et al., 2014), in purple) was superimposed on the sub-tomogram of yeast 54S mt-LSU ((Pfeffer S et al., 2015), taken with permission from Rightslink, license number 3831330401788). The position of Mba1 within the tomogram is circled. MRPL45 is depicted in red in the mt-LSU structure.

Little is known about how Mba1 interacts with the IMM in yeast. A physical association of this protein with the IMM protein Mdm38 has been reported by (Bauerschmitt H et al., 2010). The homologue of Mdm38 in human is LetM1, a protein that will be discussed in Appendix 17. Briefly, LetM1 is an IMM protein that has been reported to have a role in the maintenance of mitochondrial tubular networks and in the assembly of the supercomplexes of the respiratory chain. This protein has a matrix domain suggested by PFAM to contain a ribosome-binding domain. It is possible that the interaction between Mba1 and Mdm38 described in yeast is conserved between the two respective homologues in human.

In addition to its role as a receptor for the mitoribosome on the membrane, it has been suggested that Mba1 also interacts with mitochondrial translation products, including Cox1, Cox2, Cox3 and Cytb. This protein has been also reported as necessary for the insertion of both mitochondrial and nuclear encoded proteins into the IMM (Preuss M et al., 2001). This observation might support the hypothesis of a second role of MRPL45, as speculated in the previous chapter.

Altogether, the observations presented above support the hypothesis of a role for MRPL45 in anchoring the mitochondrial translation machinery to the IMM, probably aligning the nascent chain of the mt-encoded OXPHOS components with insertases and chaperones, to facilitate the integration into the membrane. MRPL45 might mediate the interaction by binding directly to the IMM (as shown for TIM44) or via the binding with IMM proteins, as suggested for its homologue Mba1.

In the previous chapter, I confirmed the importance of MRPL45 for the stability of the mt-LSU and, as a consequence, for an efficient protein synthesis. In this chapter, I aimed to confirm the interaction of the mitochondrial translation machinery with the IMM in human mitochondria and to

study the possible involvement of MRPL45 in this interaction. For this purpose, a protocol to analyse the interaction was developed and applied in the studies that are presented in this chapter. In order to study the ability of MRPL45 to directly interact with the IMM, cell lines able to inducibly express this protein were prepared. After the characterisation of the phenotype of the cell line was obtained, the direct interaction of MRPL45 with the membrane was studied in cells induced to express the protein in the absence of the assembled mitoribosome. Once the existence of a direct interaction between MRPL45 and the IMM was established, modifications to the protein were engineered to investigate the involvement of certain domains in the interaction.

4.2. Methods

4.2.1. Generation of stable cell lines able to overexpress MRPL45

The ORF encoding MRPL45 was cloned into pcDNA5/FRT/TO, a plasmid that is compatible with the Flp-In TRex system and that allows the inducible overexpression in HEK293 Flp-In TRex cells by addition of tetracycline or doxycycline to the growth media. The multiple cloning site of the plasmid contains a BamHI restriction site that was used to insert the sequence encoding for MRPL45. A complete map of pcDNA5/FRT/TO can be found in Appendix 3.

The plasmid was obtained from an *E. coli* strain previously transformed with the plasmid in our laboratory, purified and digested with *Bam*HI (qv 2.3.7.) (Fig. 4.6).

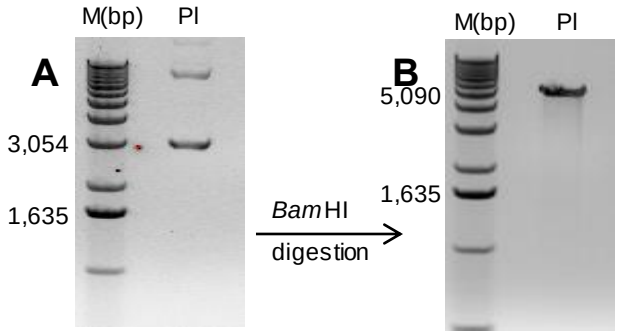

Figure 4.6 pcDNA5/FRT/TO was purified and digested with *Bam*HI.
The extracted plasmid (Pl) was separated on 1.2% agarose gel prior **(A)** and following **(B)** digestion with *Bam*HI. M=marker, Pl=pcDNA5/FRT/TO.

The fragment to be used in the ligation was prepared via PCR using random hexamer primed cDNA obtained from HEK293 cells as template. The primers were designed to amplify the mature MRPL45 mRNA sequence and to insert *Bam*HI restriction sites on either side of the sequence. Three inserts were prepared using different combinations of custom designed primers (Frw1, Rev3; Frw2, Rev3; Frw2, Rev2; listed in Appendix 5), targeting a different region prior or after the ORF of MRPL45. The products obtained were separated on 1.2% agarose gel and after visualisation with UV light, the bands correspondent to the insert size were excised (Fig. 4.7).

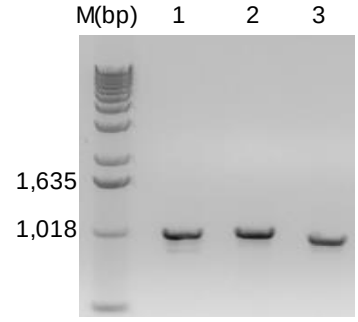

Figure 4.7 Preparation of MRPL45 insert via PCR

DNA electrophoresis on 1.2% agarose gel of purified MRPL45 fragments obtained via PCR reactions. The inserts were obtained with different combinations of primers (1= Frw1, Rev3; 2= Frw2, Rev3; 3= Frw2, Rev2, see Appendix 5). M=size marker.

After digestion with *BamHI* and purification via gel extraction, insert 2 (1,004 bp) was used to perform ligation in pcDNA5/FRT/TO. The product of ligation was used to transform competent cells (qv 2.3.9.) that were plated on LB-agar containing 100 µg/mL of ampicillin for the selection of the transformed cells. After overnight incubation, single colonies were expanded and analysed to verify the presence of the insert within the plasmid. Half of each colony was used in a PCR performed with CMV and BGH primers (sequences in Appendix 5) that span the multiple cloning site of pcDNA5/FRT/TO (qv 2.3.10.). If MRPL45 was not successfully inserted in the plasmid, the fragment obtained from the PCR reaction would have been equal to the distance between CMV and BGH sites on the empty plasmid (338 bp), whereas if the insert was present the length of the amplified DNA would have been of 1342 bp. The products obtained from the PCR were visualised on agarose gels to determine the size of the amplicon (Fig. 4.8).

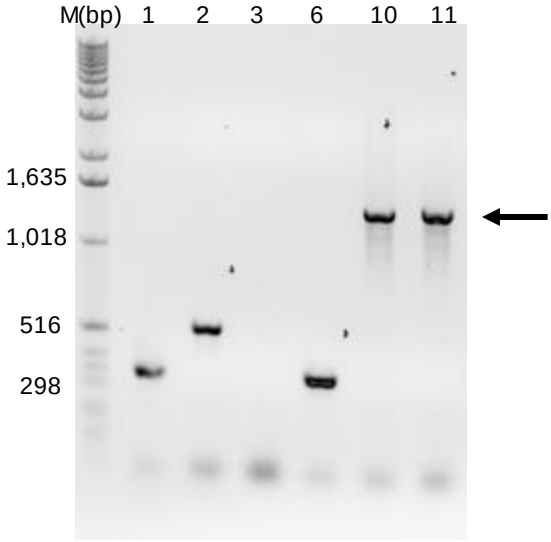

Figure 4.8 PCR amplification of MRPL45 to identify colonies containing successful insertion into pcDNA5/FRT/TO.

The products obtained from the PCR reactions performed using CMV and BGH primers were separated on a 1.2% agarose gel. The arrow indicates the size of the fragments that confirm the success of the ligation reaction. M=size marker, Numbers = colony designation.

The DNA electrophoresis analysis showed that the PCR performed on colonies 10 and 11 produced a fragment of approximately 1,300 bases, indicating that these colonies contained the ORF for MRPL45 ligated into the plasmid.

Due to the use of the same restriction enzyme on both sides of the insert, the orientation of MRPL45 within the plasmid needed to be confirmed. For this, diagnostic digestion was performed on plasmids from colonies 10 and 11. Each plasmid (500 ng) was digested with *Afl*II, a restriction enzyme that cuts both the plasmid and the insert. If the orientation of *MRPL45* is correct, the enzyme will cut 116 bases prior to the end of the insert itself, leading to the formation of a 877 bp fragment. Whilst, if the insert has been ligated in the wrong orientation, the digestion will produce a smaller fragment of 137 bp. In both cases, a bigger fragment (5264 bp and 6004 bp respectively) containing the majority of the vector will be obtained from the digestion (Fig. 4.9A). In order to have a positive control, the plasmids were also linearised via digestion with *Kpn*I, which performed a single cut on the whole MRPL45- pcDNA5/FRT/TO construct. The fragments obtained were analysed on a 1.2% agarose gel (Fig. 4.9B).

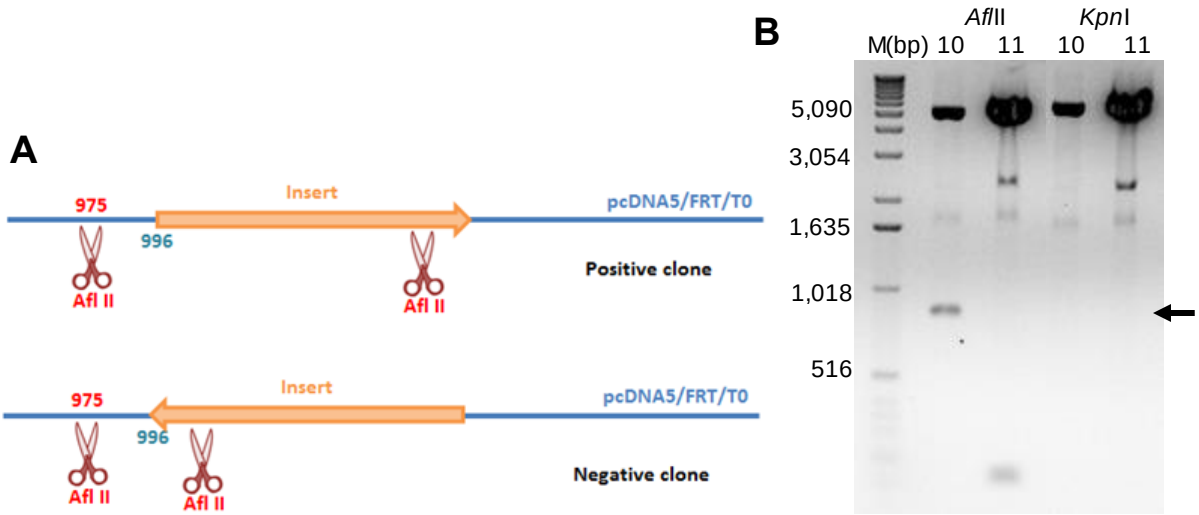

Figure 4.9 Identification of the colony containing the MRPL45 ORF in the correct orientation.

Diagnostic digestion was performed using *Afl*II, which cut the plasmid as represented in **(A)**. The plasmid was also linearised with *Kpn*I and the products obtained from the digestion were on a 1.2% agarose gel **(B)**. The arrow indicates the size of the fragment

The diagnostic digestion showed that colony 10 contained *MRPL45* inserted with the correct orientation into pcDNA5/FRT/TO, as a fragment of approximately 900 bp was obtained by the digestion of the construct with *Afl*II. Subsequently, the plasmid from colony 10 was sequenced to confirm the identity of the sequence. The result obtained also confirmed the absence of mutations in MRPL45 nucleotide sequence cloned in pcDNA5/FRT/TO (Appendix 8). Finally, MRPL45-pcDNA5/FRT/TO was used, together with pOG44m to generate HEK293 Flp-In TRex cells able to overexpress MRPL45 (qv 2.1.6.). Positive transformants were selected through antibiotic resistance and individual clones were expanded and testef fot the ability to overexpress the protein upon induction with tetracycline.

4.2.2. Membrane-Soluble Fraction Protocol Optimization

A reliable protocol to separate membranes from the soluble fraction in mitochondria was required in order to study the interaction of the mitoribosome with the IMM.

The interaction of Mba1 with the IMM had been previously studied in yeast using the "membrane flotation assay" (Ott M et al., 2006). In this assay, intact mitochondrial membranes are disrupted by 3 cycles of freezing in liquid nitrogen and thawing at 37°C and then the membranes are separated from the soluble fraction by centrifugation at high speed using a step gradient containing different concentrations of sucrose. The composition of the IMM of human mitochondria differs from the yeast counterpart, the protocol cannot be directly transferred to be performed on human mitochondria. I, therefore, decided to optimise a method to perform on human mitochondria to separate membranes from the soluble fraction.

After extraction from cells (qv 2.6.), mitochondria were disrupted using different techniques and buffers. The separation of membranes and the soluble fraction was then performed via high-speed centrifugation, of which the duration and g-force needed to be adjusted. The protocol is summarised in Fig. 4.10.

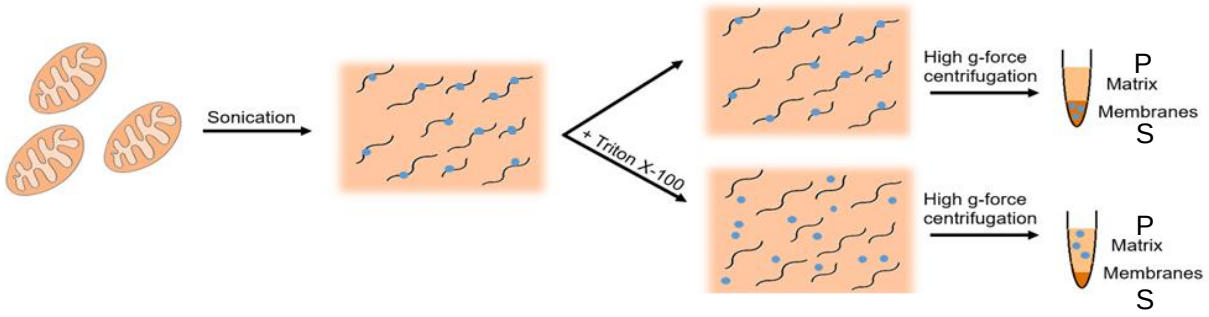

Figure 4.10 Protocol to determine the ability of proteins or complexes to interact with the mitochondrial membranes.

Mitochondria were extracted and their membranes were disrupted by sonication. The sample was then divided in half and one half was incubated with 1.6% (v:v) Triton X-100 to release membrane- and membrane-interacting proteins. After that, the membrane fraction was pelleted by high g-force centrifugation. The matrix sample (S) was retained and the pelleted membranes (P) were resuspended. The samples obtained were analysed via western blot. The blue dots represent membrane and membrane-interacting proteins.

Mitochondrial disruption was performed in 2 different buffers using either sonication or freeze-thaw cycles. Both the methods led to protein degradation when performed on mitochondria resuspended in phosphate-based buffer (potassium phosphate pH 7.4 20 mM, DTT 5mM, KCl 10 mM, $MgCl_2$ 10 mM). Sonication was preferred over freeze-thaw cycles to disrupt mitochondria in sucrose-mannitol buffer (MS buffer, Table 4.1) because the latter, performed by freezing the samples in liquid nitrogen and thawing them on ice led to degradation of proteins. Samples were sonicated on ice for a total time of 1 minute, composed of 10 seconds of activity followed by 50 seconds of rest on ice, to allow the dispersion of the heat generated.

After sonication, a clearing spin was performed to eliminate unbroken mitochondria. The supernatant obtained was expected to be composed of matrix proteins, fragments of mitochondrial membranes and membrane vesicles. The membranes needed to be separated from the soluble components via high-g force centrifugation (100,000 g, 30 minutes at 4ºC). After that, the pellet was resuspended in MS buffer (Table 4.1) and half of it was incubated with high salt concentration (500 mM KCl), which should detach the proteins loosely bound to the IMM, without extracting the integral IMM proteins. Western blot analyses performed with the samples obtained suggested that the salt treatment was not efficient, therefore, another approach was developed.

I thought it was possible to investigate and estimate the interaction of the monosome and its subunit with the membrane by comparing the effects on the composition of the membrane and soluble fractions obtained by high g-force centrifugation in presence or absence of detergent.

The signal detected by western blot analysis of the mitoribosomal subunits in the membrane fraction (P) will be composed of membrane-interacting subunits (or monosome) together with a proportion of the unbound subunits (or monosome) that are pelleted at that g-force due to their weight. The incubation of the sample with a non-ionic detergent (Triton X-100) aimed to release the integral and peripheral membrane proteins so that they would then be detected in the soluble fraction on western blot analysis. The presence of a signal for a protein in the membrane fraction upon treatment with Triton X-100 would suggest that this protein is a part of a heavy complex that is pelleted at the condition used for the high g-force centrifugation. The detection of an integral IMM protein that is not a component of a heavy complex, for example TOM20, was used to confirm the efficiency of the incubation with Triton X-100. If the protein of interest, which is suspected to interact with the membrane, has a different distribution between P and S fractions in the presence or absence of detergent, it is likely that that protein is interacting with the IMM.

In order to limit the precipitation of heavy soluble complexes present in the matrix, a lower g-force needed to be found at which only the membranes are pelleted. For this purpose, the protocol was repeated centrifuging the samples for 30 minutes at 4 different g-forces (50,000, 70,000, 100,000 and 150,000). Mitochondria were extracted and the membranes disrupted by sonication as previously described. After a clearing spin at 11,000 g for 10 minutes at 4ºC, the supernatant was supplemented with 150 mM NaCl and divided into 2 samples of equal volume. One half of each sample was then supplemented Triton X-100 at the final concentration of 1.6% and all the samples were incubated for 30 minutes on ice, with gentle vortexing every 10 minutes. At the end of the treatment, the samples were centrifuged. The pellets obtained from the protocol were resuspended in presence of 0.2% SDS (W/V) at 37ºC in half the volume of the soluble fraction. A comparable volume of the two samples (15 µL for S, and 7.5 µL for P) were analysed via western blot (Fig. 4.11).

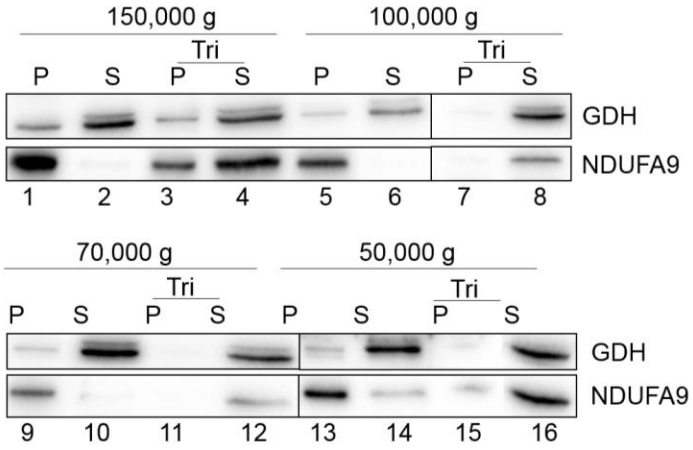

Figure 4.11 Separation of soluble and membrane components in presence or absence of Triton X-100 at 4 different g-force centrifugations.

Western blot analysis of membrane (P) and soluble (S) proteins obtained after disruption of mitochondria with sonication. The initial sample was incubated on ice in the presence or absence of 1.6% of Triton X-100 (Tri). Soluble proteins and membrane proteins were obtained after centrifugation at different g-forces (150,000 g, 100,000 g, 70,000 g and 50,000 g) for 30 minutes at 4°C. GDH was used as marker for the matrix, whereas NDUFA9 was used to confirm the membrane fractions.

The western blot analysis showed that at all the tested g-forces, the matrix protein GDH was found mainly in the soluble fractions. A weak signal was expected in the membrane fractions in absence of detergent because of the ability of one of its isoform to interact with the IMM (Rajas F et al., 1996). Triton X-100 should release the remaining, membrane-interacting, GDH that should be then detected in the soluble fractions (Fig. 4.11, lanes 4, 8, 12, 16). The IMM protein NDUFA9 (a component of respiratory complex I) was predominantly detectable in the membrane fractions in absence of detergent (Fig. 4.11, lanes 1, 5, 9, 13). In presence of detergent, NDUFA9 was relased and detected in the soluble fractions (Fig. 4.11, lanes 4, 8, 12, 16) and should be absent or barely detectable in the membrane fractions (Fig. 4.11, lanes 3, 7, 11, 15). A significant signal for this IMM protein was detected in the membrane fraction when the centrifugation was performed at 150,000 g (Fig. 4.11, lane 3), suggesting that NDUFA9 (and probably the whole complex I) was pelleted at that speed due to its mass. In addition, GDH was also detectable in the same fraction (Fig. 4.11, lane 3), suggesting again that the g-force applied was pelleting a heavy complex containing the hexameric complex of the protein.

At the lower g-force tested (50,000 g) a signal from NDUFA9 was detectable in the soluble fraction in absence of detergent (Fig. 4.11, lane 14), indicating that complex I and likely the membranes were not completely pelleted at this g-force.

Because the 70,000 g centrifugation resulted in an efficient separation of membranes from soluble components, this g-force was selected to be used for the membrane-interaction studies. The final protocol used throughout the study is reported below.

General protocol

Cells were grown in the desired conditions in 75 cm^2 flasks until 80% confluent. Cells were then harvested, mitochondria were extracted (qv 2.6) and resuspended in Mannitol-Sucrose buffer (MS buffer, Table 4.1).

Table 4.1 MS buffer composition.

DTT and PMSF were added immediately prior to use to the buffer, due to their lower stability in aqueous solution.

Reagents	Final concentration
Mannitol	210 mM
Sucrose	70 mM
HEPES, pH 7.8 (*Sigma*, cat no H3375)	20 mM
EDTA	2 mM
DTT	2 mM
PMSF	1mM
EDTA-free protease inhibitor (*Pierce*)	1x

Once fully resuspended, an aliquot of mitochondria was retained for lysis and protein concentration was quantified. The suspension was sonicated on ice in a minimum volume of 800 µL for 1 minute at amplitude 10 with the *Soniprep 150 plus* (*MSE*) doing cycles of 10 seconds of sonication followed by 50 seconds of rest, to avoid overheating of the sample. After the membrane disruption, the sample was centrifuged at 11,000 g for 10 minutes at 4ºC to eliminate unbroken mitochondria. The resulting supernatant was divided into two samples of equal volume. Both the samples were supplemented with 150 mM NaCl. In order to solubilise the membranes, Triton X-100 was added to one of the samples at a final concentration of 1.6% (v:v). The final volume of the two samples was then equalised by addition of MS buffer and the samples were incubated on ice for 30 minutes with occasional gentle vortexing. At the end of the incubation time, the volume of the samples was measured and then moved to polycarbonate tubes (*Beckman Coulter*, cat no 343778). The untreated membranes were separated from the soluble fraction by centrifugation at 70,000g for 30 minutes at 4ºC in the Beckmann ultracentrifuge (rotor TLA120.2). The supernatants were saved for western blot analysis, and the pellets were washed in MS buffer and centrifuged again using the same conditions. The pellet was then resuspended in MS buffer containing 0.2% SDS, in a final volume that was half the volume of the sample measured prior to centrifugation. A volume of 15 µL of every supernatant (S) and 7.5 µL of every pellet (P) were resolved by SDS-PAGE and analysed via western blot. The results were quantified with *ImageLab* (as in 4.2.2.) for every condition tested (presence or absence of detergent) and presented as percentages using the following equations:

Signal P + Signal S= Total signal (corresponds to 100%)

%Signal P= Signal P * 100/ Total signal

%Signal S= 100- %Signal P

4.3. Analysis of the interaction of the mitoribosome with the IMM

The protocol developed in the previous section was used to assess the interaction between the mitoribosome and the IMM in human organelles, an interaction that was previously reported in bovine tissue (Liu M & Spremulli LL, 2000).

HEK293 cells were grown in 75 cm^2 flasks until 80% confluent. Mitochondria were extracted, burst by sonication and then the membranes were separated from the soluble fraction as explained in 4.2.2. Membranes (P) and soluble (S) fractions obtained in presence or absence of Triton X-100 were analysed via western blot (Fig. 4.12A).

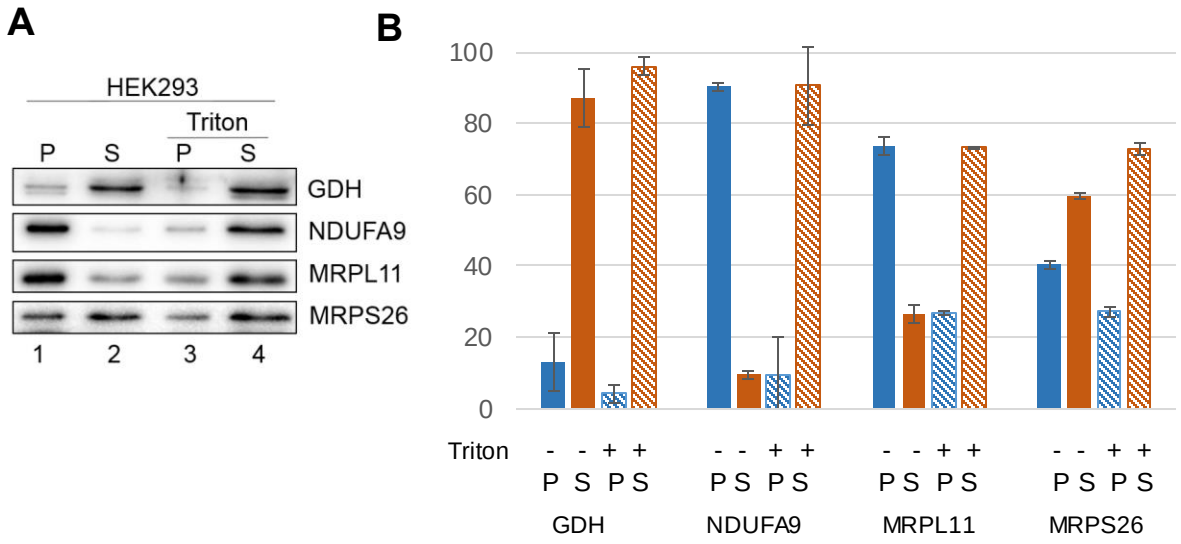

Figure 4.12 Interaction of large and small subunits of the human mitoribosome with the IMM.

A) Representative figure of membrane (P) and soluble (S) fractions obtained in presence or absence of 1.6% Triton X-100 from mitochondria extracted from HEK293 cells (qv 4.2.2) and analysed via western blot. The distribution of the mitoribosome between the two fractions for each treatment was visualised using antibodies against mt-LSU (MRPL11) and mt-SSU (MRPS26) proteins. GDH and NDUFA9 were used as markers for the soluble and the membrane fractions respectively. **B)** Quantification of the western blot results was obtained with ImageLab and calculated as reported in 4.2.2. The results summarise 3 different biological repeats and are shown as percentages.

The efficiency of the protocol was confirmed by the distribution of GDH and NDUFA9. The matrix protein GDH was mainly present in the S fraction for both the conditions tested (Fig. 4.12A, lanes 2 and 4). The component of complex I NDUFA9 was predominantly found in the P fraction in absence of Triton X-100 (Fig. 4.12A, lane 1), whereas its presence was mainly in the S fraction upon solubilisation of the membranes by the detergent (Fig. 4.12A, lane 4).

The partitioning of the mitoribosomal subunit between membrane and soluble fraction was assessed using antibodies against MRPL11 (mt-LSU) and MRPS26 (mt-SSU). The addition of detergent led to release of these 2 proteins, although this was not complete. The presence of approximately 30% of both MRPL11 and MRPS26 in the P fraction upon solubilisation of the membranes with Triton X-100 (Fig. 4.12A, lane 3) suggested that at the g-force used, at least this proportion of mt-LSU and mt-SSU pelleted because of their weight. Subtracting the intensity of

this residual signal (lane 3) from the signal obtained in the absence of detergent for the P fraction (lane 1), it is possible to infer information with respect to the interaction of the subunits with the IMM. My data suggest that al least ≈45% of mt-LSU and at least ≈15% of mt-SSU interacted with the membrane. This observation indicated that at steady state there is a greater association of the mt-LSU with the IMM than there is of the mt-SSU, and that this interaction might happen when the mt-LSU is not associated with the mt-SSU. It is important to notice that a proportion of both the subunits was found in the supernatant in the absence of detergent (Fig. 4.12, lane 2). This suggested that a proportion was not interacting with the membrane.

4.4. Analysis of the interaction of MRPL45 with the IMM

In addition to the analysis of the interaction of the mitoribosome with the IMM, the protocol developed in 4.2.2. was also used to investigate the specific involvement of MRPL45 in this interaction.

To test the possibility of a direct interaction of MRPL45 with the IMM, this mitoribosomal protein needed to be present in mitochondria in the absence of the rest of the mitoribosome. The steady state level of the mitoribosome and of the mitoribosomal proteins can be depleted with incubation of the cells with ethidium bromide. This reagent intercalates into mt-DNA, inhibiting its replication and transcription. As a consequence, the 16S and 12S rRNA encoded by the mitochondria cannot be transcribed and be integrated into the subunits of the mitoribosome. In this condition, the mitoribosome cannot fully assemble and mitoribosomal proteins, including MRPL45, become depleted. A cell line that can be induced to overexpress MRPL45 can be used in these conditions to independently study the interaction of MRPL45 with the IMM. The cell line was generated as reported in 4.2.2. Prior the analysis of the interaction of MRPL45 with the IMM, the effects of the overexpression of the protein were evaluated.

4.4.1. Effects of MRPL45 overexpression

Prior to the use of the MRPL45-HEK293 cell line to test the interaction of MRPL45 with the membrane, the effects of the overexpression on the cellular phenotype were studied.

MRPL45-HEK293 cells were induced for 10 days and cell growth was monitored with the *IncuCyte* system over the overexpression period (Fig. 4.13A). The morphology of the cells after 6 days of overexpression is shown in Fig. 4.13B.

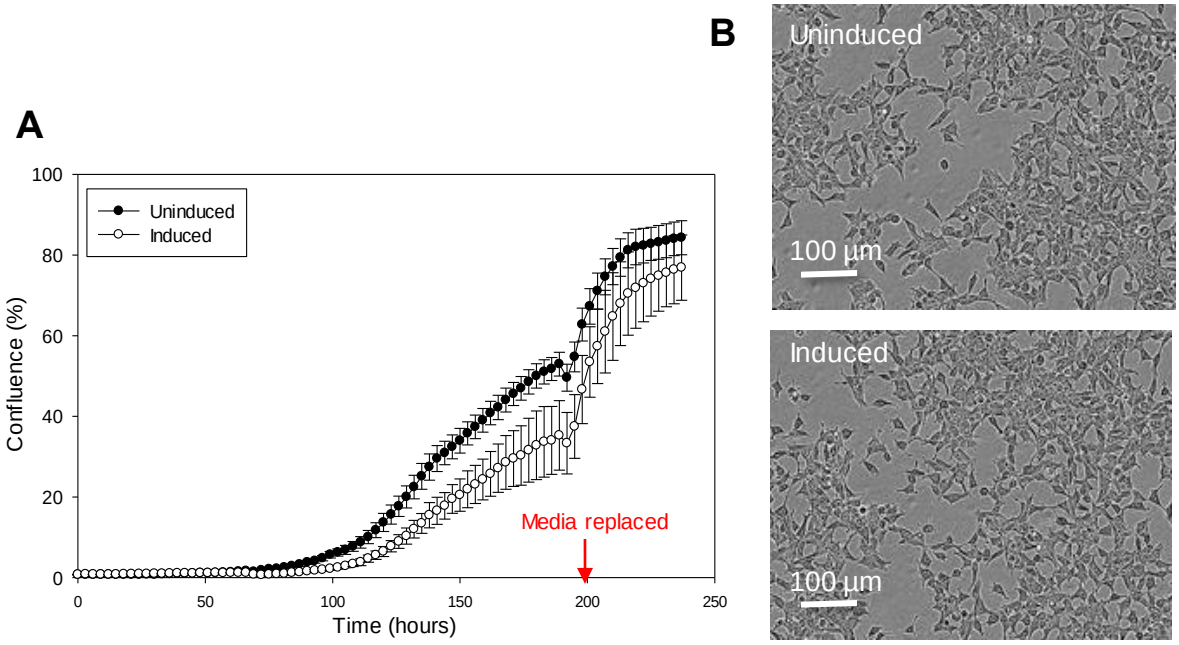

Figure 4.13 Effects of MRPL45 overexpression on cell growth.

A) Cell confluence was measured with the *IncuCyte* system every 3 hours over 10 days of overexpression of MRPL45 in HEK293 Flp-In TRex cells. The red arrow indicates when the media was replaced. **B)** Cell morphology was visualised after 6 days of MRPL45 in HEK293 Flp-In TRex cells. The data are representative of 3 biological repeats.

A mild growth delay was observed in the cell line overexpressing MRPL45 (Fig. 4.13A). Because the overexpression leads to non-physiological levels of this protein, it is possible that this condition causes stress and affects cell homeostasis, causing the mild growth retardation. A minor drop in the growth was present for both the samples due to replacement of the media (Fig. 4.13A, red arrow) caused a minor drop in the growth. No effects were detected on cell shape or morphology (Fig. 4.13B).

The effects on the steady state level of mitochondrial proteins involved in translation were also analysed via western blotting of cell lysate after 10 days of continuous induction of MRPL45 (Fig. 4.14).

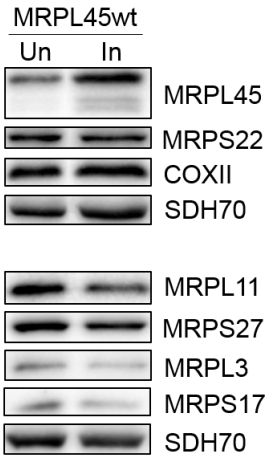

Figure 4.14 MRPL45 overexpression effects on steady state level of mitochondrial proteins involved in mitochondrial translation.

Western blot analysis was performed on lysate obtained after 10 days of MRPL45 overexpression (In) in MRPL45- HEK293 Flp-In TRex. Uninduced cells (Un) were cultured as a control. Levels of MRPL45 overexpression were detected using an antibody targeting the protein. Steady state level of components of mt-SSU (MRPS22, MRPS27, MRPS17) and mt-LSU (MRPL11, MRPL3) were evaluated, as well as the mitochondrial encoded protein COXII. SDH70 steady state levels were used as loading control. The figure is representative of 3 biolgical repeats.

As expected, the overexpression of MRPL45 had no effect the steady state level of COXII, suggesting that protein synthesis in mitochondria was not affected. However, the levels of the mitoribosomal proteins evaluated were mildly affected.

These results suggest that the overexpression of MRPL45 did not cause any major deleterious effect on MRPL45-HEK239 cells.

4.4.2. Analysis of the direct interaction of MRPL45 with the IMM

After the confirmation of the interaction between the mitoribosome and the IMM in 4.3, the ability of MRPL45 to directly interact with the membrane was studied.

MRPL45-HEK293 Flp-In TRex cell line was cultured in two 75 cm^2 flasks using supplemented media containing 250 ng/mL of ethidium bromide for 10 days to deplete mitochondrial DNA. In the last 4 days of ethidium bromide treatment, MRPL45 was overexpressed, by adding of 1 µg/mL of tetracycline to the growth media. The length of the ethidium bromide treatment was considered sufficient to lead to depletion of the assembled mitoribosome. This needed to be confirmed on western blot analysis using antibodies targeting components of mt-SSU and mt-LSU. COXII steady state levels could also be used to further verify the efficiency of the ethidium bromide treatment.

The treatment with ethidium bromide made the cells very delicate, therefore extra care was needed during their growth. Media was replaced every 2 days (or earlier if a change of its colour indicated increased acidity), in order to replace the glucose needed throughout the ethidium bromide treatment for the glycolytic synthesis of ATP. Attention was also paid to the cell

confluence, which was kept below 70%, to avoid cell detachment, which was observed at higher confluency.

At the end of the ethidium bromide treatment, cells were harvested and mitochondria were isolated. Membrane and soluble fractions were separated following the protocol optimised in 4.4.2, with some modification. In particular, the membranes were pelleted at 150,000 g, and no incubation with 1.6% Triton X-100 was performed prior to centrifugation. These modifications were legitimate because, after incubation with ethidium bromide, the mitoribosome was absent and therefore could not sediment during the high speed centrifugation, used to separate membranes from the soluble fraction. The same protocol was also performed in parallel on HEK293 cells, cultured in normal growth media. The samples obtained were analysed on western blot (Fig. 4.15).

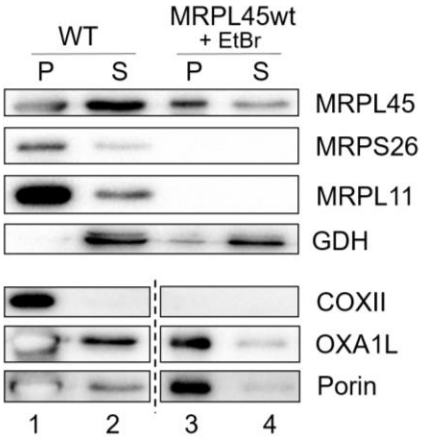

Figure 4.15 Distribution of MRPL45 between membranes and soluble fractions in wild-type cells or in cells overexpressing MRPL45 and treated with ethidium bromide.

Western blot analysis was performed on membranes (P) and soluble (S) fractions obtained from wild type HEK293 cells and HEK293 Flp-In TRex cells overexpressing MRPL45 for the final 4 days of 10 days in ethidium bromide. The efficiency of the separation was assessed with antibodies against the matrix protein GDH and against the membranes protein OXA1L and porin. The success of the overexpression was verified using an antibody against MRPL45 and the efficiency of the ethidium bromide treatment was confirmed with antibodies against COXII, MRPS26 and MRPL11. The dashed line indicated that some lanes have been omitted. The experiment was not replicated.

MRPS26, MRPL11 and COXII were all detectable in the samples obtained from the HEK293 wild type cells (Fig. 4.15, lanes 1 and 2), whereas they were undetectable in either of the fractions obtained for cells grown in ethidium bromide (Fig. 4.15, lanes 3 and 4), confirming the efficiency of the treatment with the intercalating agent. The presence of GDH mainly in the soluble fractions and of OXA1L and porin predominantly in the membrane fractions for both the cell lines confirmed the successful precipitation of the membranes at the g-force used. As the majority of MRPL45 was detected in the membrane fraction in the absence of the assembled mitoribosome, it is likely that MRPL45 is able to interact directly with the IMM.

The overexpression of MRPL45 could potentially cause aggregation of the protein that might be pelleted at the g-force used in the previous experiment. In order to discriminate between the

presence of MRPL45 in the membrane fraction only because of its aggregation, or as a result of its interaction with the IMM, the separation of membrane and soluble fraction was repeated, but this time following the optimised protocol given at 4.2.2. MRPL45- HEK293 Flp-In TRex cells were grown in the same conditions used for the previous experiment (10 days in ethidium bromide with 4 days of MRPL45 overexpression), mitochondria were extracted and the membranes and soluble fraction were separated. If MRPL45 was interacting with the IMM, the addition of 1.6% Triton X-100 would release the IMM-interacting pool of MRPL45 and the distribution of MRPL45 between membranes (P) and soluble fraction (S) should change, showing a difference in the presence or absence of the detergent. The fractions obtained were analysed by western blot (Fig. 4.16A).

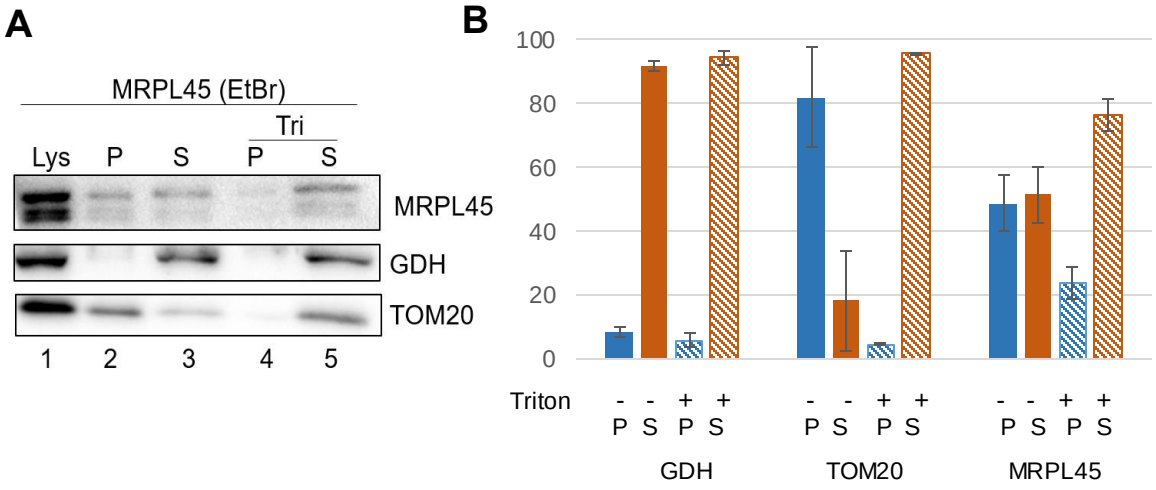

Figure 4.16 Distribution of overexpressed MRPL45 between membrane and soluble fractions in the presence or absence of detergent.

Representative figure of western blot analysis **(A)** performed on mitolysate (Lys), membranes (P) and soluble (S) fractions obtained as in 4.2.2. from HEK293 Flp-In TRex cells overexpressing MRPL45 for 4 days during ethidium bromide incubation (10 days). Half of the suspension of membranes and matrix proteins obtained was incubated with 1.6% Triton X-100 (Tri) prior centrifugation. The success of the overexpression was verified using an antibody against MRPL45. The efficiency of the protocol was assessed with antibodies against the matrix protein GDH and against the membrane protein TOM20. COXII levels were undetectable. Data obtained by western blot for 3 biological repeats were quantified with *ImageLab* as in 4.2.2. and summed up in a bar graph **(B)**.

The matrix protein GDH was present mainly in the S fraction both in the presence and absence of detergent. The presence of the outer membrane protein TOM20 in the S fraction upon addition of Triton X-100 confirmed the success of membranes solubilisation. No signal for either MRPL11 and MRPL26 was detected. The detection of MRPL45 showed that the distribution between P and S fractions changed following the incubation with the detergent. While the protein appeared to be equally divided between the 2 fractions in the absence of detergent (Fig. 4.16A, lanes 2 and 3), the majority of MRPL45 was present in the S fraction upon addition of detergent (Fig. 4.16A, lane 5). The addition of Triton X-100 releases the membrane proteins, as well as the membrane-interacting ones. As a consequence, the release observed for MRPL45 in absence of the assembled mitoribosome suggested that the protein is able to

interact with the membrane directly. The residual signal for MRPL45 found in the P fraction in presence of Triton X-100 might indicate the presence of aggregates. Noticeably, at least the 50% of MRPL45 was found in the supernatant in the absence of detergent. This suggested that a large proportion of MRPL45 was not interacting with the membrane. This could be due either to the saturation of the interaction points (since the high steady state level of the protein), or to the transient nature of the interaction. The quantification of the data obtained from western blot analysis suggested that approximately the 25% of MRPL45 was released by the addition of detergent, suggesting that at least this portion of the population was interacting with the IMM directly or indirectly.

4.5. Discussion

Due to the high hydrophobicity of the products of mitochondrial translation, it is likely that their synthesis is coupled with their insertion into the IMM. A protocol was developed in order to investigate the interaction between the membrane and the mitoribosome or mitoribosomal components. The aim of this protocol was to allow the comparison of the distribution between membranes and the soluble fraction of a protein/complex in the presence or absence of detergent. The optimised protocol showed efficient separation of membranes and membrane-interacting proteins from soluble components as evidenced by the relevant markers (TOM20 or NDUFA9 and GDH, respectively). The addition of Triton X-100 successfully solubilised the membrane and membrane-interacting proteins that were then located in the soluble fraction. From the data obtained via western blot analysis, it was possible to hypothesise the existence of an interaction of a single protein or a group of proteins with the membranes. The main weakness of the process is the absence of a control that can be used to ensure that the membranes and the soluble fraction are equally represented on western blot analyses. In order to generate good quality data, extra care is needed on analysing representative volumes. In particular, the volume of each of the samples needs to be measured prior to high g-force centrifugation and the pellets obtained need to be resuspended in half the volume measured before the centrifugation. I decided to resuspend the pellet in half a volume in case of needing a more concentrated sample for western blot analyses. The volume of supernatant obtained at the end of the protocol does not have to be measured. With this precaution, it will be possible to compare the changes in the distribution of the analysed protein.

The protocol performed on wild type HEK293 confirmed the ability of the human mitoribosome to interact with the IMM, previously described in bovine organelles by Liu M and Spremulli LL (2000). Specifically, my data suggested that under exponential growth conditions approximately 45% of the mt-LSU interacted with the IMM, since this proportion was released by addition of detergent. This data is in agreement with the results published by Liu M and Spremulli LL (2000). On the other hand, a smaller proportion of the mt-SSU (≈15%) was found to interact with the membrane. It is likely that the interaction of the small subunit with the IMM is mediated by the large subunit. Because a higher proportion of mt-LSU was found associated with the membrane,

it is tempting to speculate that the mt-LSU anchors to the membrane first, waiting for the mt-SSU to recruit the mRNA and then join to form the monosome. These experiments also showed that a proportion of mt-LSU and mt-SSU (≈30% and ≈60%, respectively) were not interacting with the membranes.

The key players in the association between IMM and mitoribosome are not yet fully identified. The mitoribosomal protein MRPL45 was suggested to play a role in the interaction because of its structural similarity to the membrane interacting protein TIM44 (Handa N et al., 2007; Marom M et al., 2009) and because recent mt-LSU structures localised it in close proximity to the polypeptide exit site. This position would be ideal to establish membrane-interaction to promote the insertion of mitochondrial translation products, however, it was only identified in 2014 by Greber et al, after I began this study. Characterisation of the yeast homologue, Mba1, confirmed the interaction of this non-mitoribosomal protein with both the IMM and the mitoribosome mitoribosome (Ott M et al., 2006). My protocol, which was designed to investigate membrane interaction, was performed on cells overexpressing MRPL45 in the absence of fully assembled mitoribosomal subunits after incubation with ethidium bromide. It is important to mention that in all the cases when the cells were treated with ethidium bromide (both in this and in the following chapters), a complete precipitation of TOM20 in the pellet fraction in absence of detergent could not be achieved. This effect might be a consequence of the general effect of ethidium bromide on mitochondrial physiology. However, the data obtained showed that a proportion of MRPL45 was released by addition of detergent and that therefore approximately the 25% of the protein was found associated with the membranes, confirming the ability of MRPL45 to directly bind the IMM and, therefore, a role of this mitoribosomal protein as a mediator of the IMM-mitoribosome interaction. A proportion of MRPL45 was not released by the detergent, suggesting the presence of aggregates, which might be due to the heat generated during the sonication used to break the mitochondrial membranes. In absence of detergent, MRPL45 was not completely interacting with the membrane, but approximately 50% was recovered in the free fraction. This suggests that the interaction sites might be saturated due to the high steady-state level of the overexpressed protein, or that the interaction is only transient. The percentage of MRPL45 suggested to interact with the membrane (≈25%) is lower than the one observed for the mt-LSU (≈45%). Because it is likely that more than one interaction is contributing to the association of the mitoribosome with the IMM, it is predictable that the interaction of MRPL45 might be weaker compared to the one of the assembled mt-LSU.

In the following chapter, the modality of interaction of MRPL45 with the IMM will be discussed.

Chapter 5: Investigation of the mode of interaction of MRPL45 with the IMM

The previous chapter confirmed the ability of MRPL45 to interact directly with the IMM. This chapter will investigate the mode of this interaction, which could be mediated by a transmembrane domain, by contact with a membrane protein or by interaction with the phospholipid layer. In order to identify putative membrane-interacting proteins, immunoprecipitation was performed. This was carried out on a cell line that could inducibly overexpress MRPL45FLAG, after proving that the addition of the FLAG-tag did not alter the protein's role.

5.1. Methods

5.1.1. Mass spectrometry analysis

Mass spectrometry was used to identify proteins present in the samples that were obtained via immunoprecipitation (qv 2.9.). Extra care was used to prevent contamination of the samples, which might impact on the quality of the results obtained in the analysis. Together with attention to avoid keratin contamination throughout the protocol, the beads used for the immunoprecipitation where washed, prior to elution, 5 times instead of the 3 reported in the protocol at 2.9.

Once eluted, the samples (1/5) were first analysed via western blotting to confirm the success of the immunoprecipitation. After that, the remainder of the sample was loaded on a 12% SDS-PAG and electrophoresed until the samples had migrated 5 mm into the resolving gel. At that point the plates containing the SDS-PAGE were wrapped and taken to Dr Achim Treumann for proteomic analysis (NUPPA, Newcastle University).

The samples were digested with the filter-aided sample preparation (FASP) method (Winiewski JR et al., 2009). This method allows a wide proteome coverage (including membrane proteins) by solubilising the samples in 4% SDS and then replacing the detergent, which is not compatible with mass spectrometry analysis, with urea via filtration. This method was also demonstrated to be efficient in the detection of membrane proteins via mass spectrometry.

The data received reported the ID of the protein identified, the sum of raw spectrum identity (log(I)), the number of peptides found (rI) and the expectation of finding the protein stochastically (log(e)).

5.1.2. Generation of a cell line able to express MRPL45FLAG

The addition of a FLAG-tag at the C-terminus of MRPL45 will result in a useful tool to investigate the interactome of the protein via immunoprecipitation, as well as to generate

mutants that will be easily distinguished from the endogenous MRPL45 via the detection with an anti-FLAG antibody.

*Bam*HI was used as restriction site to introduce *MRPL45FLAG* into pcDNA5/FRT/TO. The same plasmid prepared for the previous cloning (Fig. 4.9) was used to introduce the sequence encoding for the FLAG-tagged protein. The insert was prepared via PCR starting from cDNA from HEK293 cells using the the primers Frw1 and Rev1FLAG (Appendix 5), of which the reverse primer contained the nucleotide sequence that encodes the FLAG-sequence (aspartic acid - tyrosine - lysine - aspartic acid - aspartic acid - aspartic acid - aspartic acid - lysine). DNA-electrophoresis of the product obtained PCR showed that the insert was successfully amplified (Fig. 5.1).

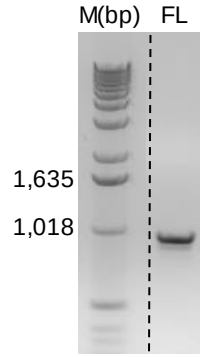

Figure 5.1 MRPL45FLAG insert was prepared via PCR.

A purified insert obtained from PCR reaction with Frw1 and Rev1FLAG primers was separated in a 1.2% agarose gel to confirm recovery and purity. M=marker, Fl=MRPL45FLAG insert.

After digestion with *Bam*HI, *MRPL45FLAG* was ligated into pcDNA5/FRT/TO (qv 2.3.9.). Of the 36 colonies obtained by transformation, no positive colony was identified using the cracking gel technique (qv 2.3.10.). Both ligation and transformation were repeated, but without success. One of the possibilities for the failiure in MRPL45FLAG cloning was the incomplete digestion of the insert. A successfully digested fragment for insertion was therefore obtained using the *PCR-script Amp Cloning Kit* (qv 2.3.11.). This method allows excision of the insert after cloning into a p*PCR-script* vector. After digestion, the insert was gel-purified and used for cloning into the plasmid of interest. MRPL45-FLAG obtained from the previous PCR reaction was ligated with the pPCRscript Amp SK(+) plasmid and the product was used to transform competent cells. The positive colonies were screened using a 'cracking gel' and the plasmids extracted from putatively positive, which were then digested with *Bam*HI and analysed via DNA electrophoresis (Fig. 5.2).

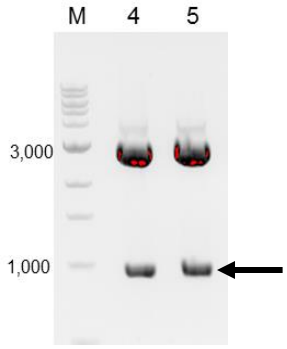

Figure 5.2 Digestion of MRPL45FLAG-pPCRscript Amp SK(+) plasmid

The plasmids obtained from colonies 4 and 5 were digested with *Bam*HI and the products were visualised on 1.2% agarose gel. M=size marker, numbers=PCRscript colonies.

Two products were obtained from *Bam*HI digested, of which the faster migrating one (≈1000 bp) corresponded to the insert. The insert obtained from colony 4 was gel-purified and used to ligate *MRPL45FLAG* into pcDNA5/FRT/TO (qv 2.3.9.). The colonies obtained after transformation of the competent cells (qv 2.2.2.) were screened to confirm the presence of the insert by visualisation of the products obtained for the PCR reaction using CMV and BGH primers on agarose gel (Fig. 5.3A) (qv 2.3.10.). The colonies containing the insert were further analysed using the diagnostic digestion shown in Fig. 4.12 (page 87), and the products were visualised on an agarose gel (Fig. 5.3B).

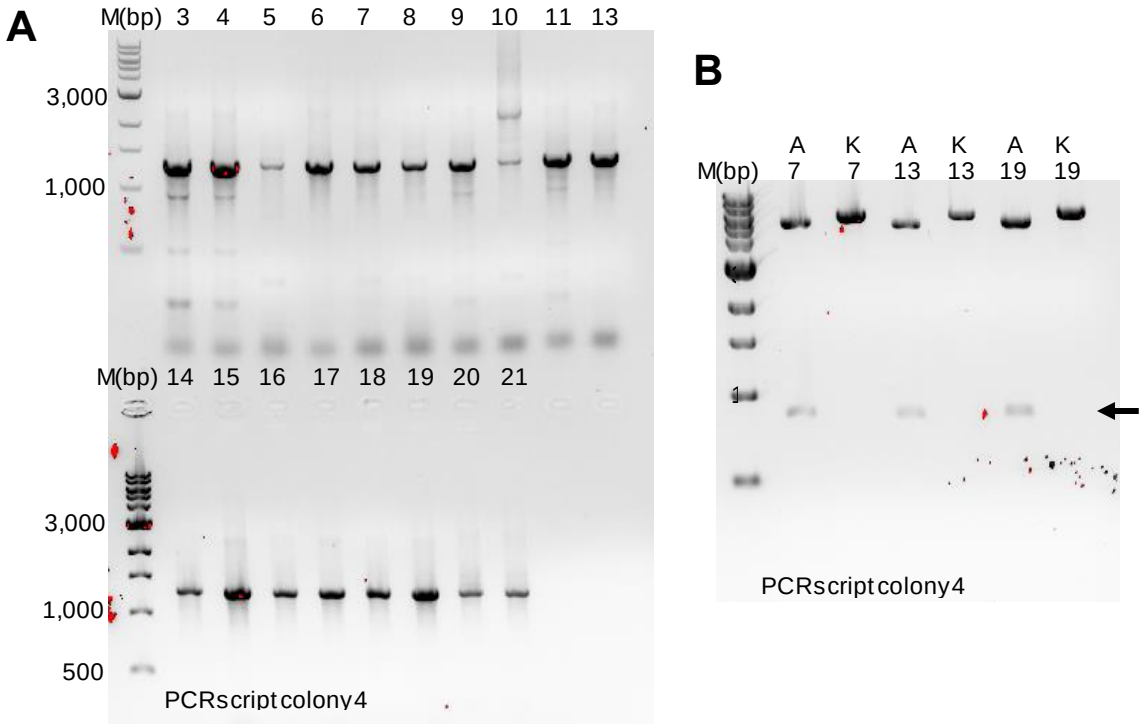

Figure 5.3 Colony screening to identify colonies positive for MRPL45FLAG transformation.

1.2% agarose gels were used to visualise the products of the PCR performed on colonies transformed with MRPL45FLAG-pcDNA5/FRT/TO using BGH and CMV primers **(A)** and the results of diagnostic digestion with *Afl*II [A] **(B)** on selected positive colonies from panel A. Plasmids were also linearised by digestion with *Kpn*I.[K] M= size marker, numbers= colonies.

All the colonies tested contained the insert, as the analysis indicated by the presence of a ≈1300 bp fragment, compatible with the presence of the insert (≈1000 bp) between CMV and BGH primer sites (344 bp). Colonies 7, 13 and 19 derived from PCRscript fragment 4 were further analysed with diagnostic digestion and all presented the correct orientation of MRPL45FLAG, as suggested by the ≈900 bp fragment formed after digestion with *Afl*II. The plasmid obtained from colony 7 was sequenced using CMV and BGH primers to confirm the absence of mutations. While the sequences obtained from the forward primer (CMV) showed 100% of identity, the one obtained from the reverse primer (BGH) showed a mutation that led to an alteration of the encoded amino acid sequence. The altered amino acids was the last one found before the FLAG-tag (p.A306T). Due to its close proximity to the end of the protein sequence, I made the assumption that this mutation would not cause improper folding of MRPL45FLAG.

HEK293 Flp-In TRex cells were then transfected with the plasmid as explained in 2.1.6. The antibiotic-selected clones were expanded and the overexpression verified. Positively-expressing clones were further expanded to prepare samples for long-term storage in liquid nitrogen.

5.2. Effects of MRPL45-FLAG overexpression

If the C-terminus of MRPL45 has an essential role in anchoring the mitoribosome to the IMM, the introduction of a FLAG-tag at the C-terminus of MRPL45 might disrupt this interaction and have effects on mitochondrial translation and cells homeostasis.

First, the integration of MRPL45FLAG into the assembled mt-LSU needed to be verified. For this purpose, an isokinetic sucrose gradient analysis was performed (qv 2.8) on MRPL45FLAG-HEK293 Flp-In TRex cell lysate after 4 days of overexpression. The 12 fractions obtained were analysed via western blotting (Fig. 5.4).

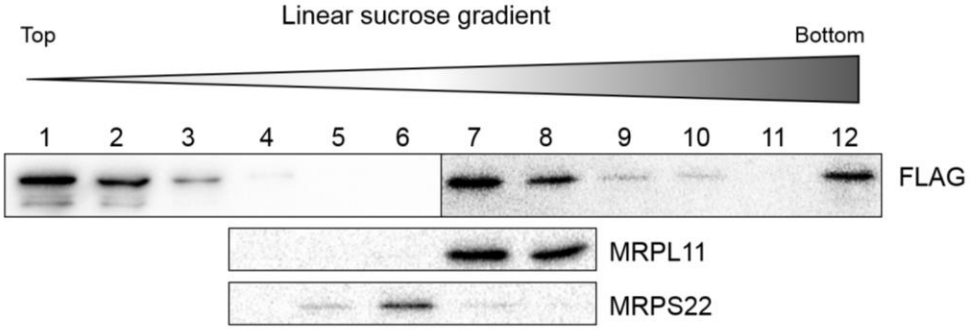

Figure 5.4 Analysis of the integration of MRPL45FLAG into mt-LSU.

10-30% isokinetic sucrose gradient was performed on MRPL45FLAG- HEK293 Flp-In TRex cells (700µg) after 4 days of induction. Aliquots (10 µL) of each of the 12 fractions were resolved on a 12% SDS-PAGE and analysed via western blotting. The distribution of the mt-LSU and mt-SSU was assessed for the central fractions using antibodies against MRPL11 and MRPS22 respectively. The distribution of MRPL45FLAG was verified using an antibody targeting the FLAG-tag. The experiment was not replicated.

The western blot analysis showed that the FLAG-tagged protein was successfully integrated in the mt-LSU, as shown by the co-localisation of MRPL11 and FLAG in fractions 7 and 8. A pool of MRPL45FLAG was also found in fractions 1 and 2, indicating that it was unassociated (free), this was expected due to the overexpression of the protein. The presence of the protein in the bottom fraction of the gradient indicated the presence of high molecular weight particles that are likely to be aggregates. The results obtained from this experiment suggested that the FLAG-tag on MRPL45 did not prevent either its integration into the mt-LSU or the assembly of the subunit itself. Interestingly, a second product was detected with the FLAG antibody, suggesting a possible N-cleavage of MRPL45. As observed in the sucrose gradient analysis of wild type HEK293 cells (Fig. 3.2, page 58), this second signal was detectable only in the first 2 fractions of the gradient, indicating that this form might not be integrated in the mitoribosome. This second signal was also detected with MRPL45 antibody in HEK293. The sucrose gradient analysis on wild type HEK293 showed that the second signal was found in the least dense fraction of the gradient and was not detected in the fractions corresponding to the mt-LSU. It is tempting to speculate that this cleaved form of MRPL45 might play a second role in mitochondria

As MRPL45FLAG was shown to be efficiently integrated into the mt-LSU, the effects on cell growth and mitochondrial protein content were assessed. MRPL45FLAG- HEK293 Flp-In TRex cells were induced for 10 days. Cell confluence was monitored with the *IncuCyte* system (Fig. 5.5A) and the correspondent whole cell lysates were analysed via western blotting (Fig. 5.5B).

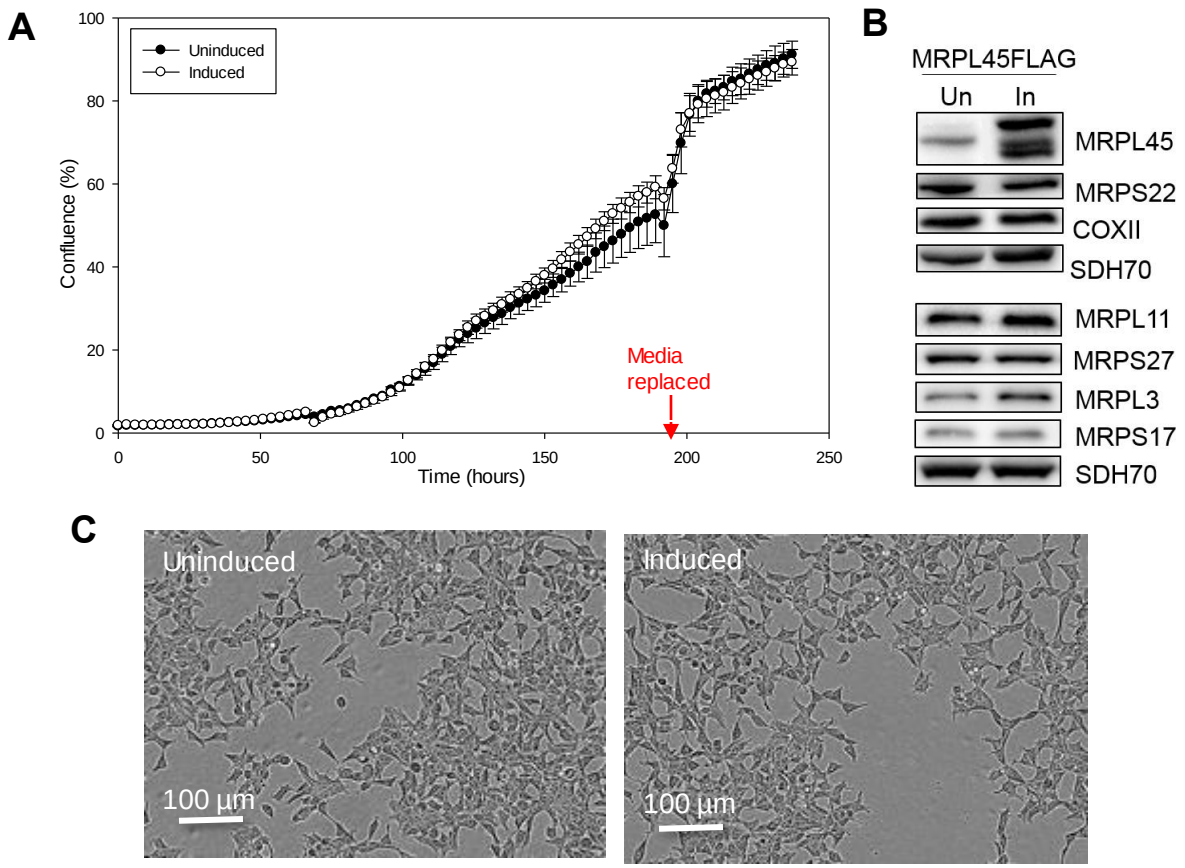

Figure 5.5 Effects of MRPL45FLAG overexpression on HEK293 Flp-In TRex cell growth and on components of the mitoribosome.

MRPL45FLAG- HEK293 Flp-In TRex cells were induced for 10 days and their confluence was monitored with the *Incucyte* system **(A).** Cell lysates obtained from these uninduced and induced cells were resolved on by 12% SDS-PAGE and then analysed via western blotting **(B)**. Antibodies against the mt-LSU (MRPL45, MRPL11, MRPL3) and mt-SSU (MRPS22, MRPS27, MRPS17) proteins were used. The steady state level of the mitochondrial-encoded protein COXII was also evaluated. Nuclear-encoded SDH70 levels were detected to verify the equality of the loading. Cell morphology after 6 days of overexpression is also presented **(C)**. The figures are representative of 3 biological repeats.

The overexpression of MRPL45FLAG had no effect on cell confluency throughout the 10 days of monitoring. A minor drop in the growth was present for both the samples due to replacement of the media (Fig. 5.5A, red arrow). The overexpression was successful as shown by the presence of an intense signal at a higher molecular weight signal observed after incubation with MRPL45 antibody. Two lower molecular weight signals were also detected with the FLAG antibody, suggesting that the protein was subjected to an N-cleavage. The overexpression had no effects of the steady state level of the components of the mt-SSU evaluated, whereas the steady-state level of the mt-LSU components seemed mildly upregulated. These results suggested that the stability of the subunits was not compromised by the overexpression of MRPL45FLAG. The level of COXII was also unaffected, suggesting that the overexpression had no observable effect on mitochondrial protein synthesis.

These results confirmed that the introduction of a FLAG-tag on MRPL45 has no detectable negative effects on the stability of the mt-LSU or mitochondrial translation.

5.3. Analysis of the direct interaction of MRPL45FLAG with the IMM

In order to test the ability of MRPL45FLAG to interact directly with the IMM, membranes were separated from the soluble fraction following the ethidium bromide treatment optimised in 4.2.2, after 10 days of ethidium bromide incubation with overexpression of the tagged protein during the last 4 days of the treatment. The mito-lysate and the fractions obtained in the absence and presence of 1.6% Triton X-100, were analysed via western blot (Fig. 5.6A).

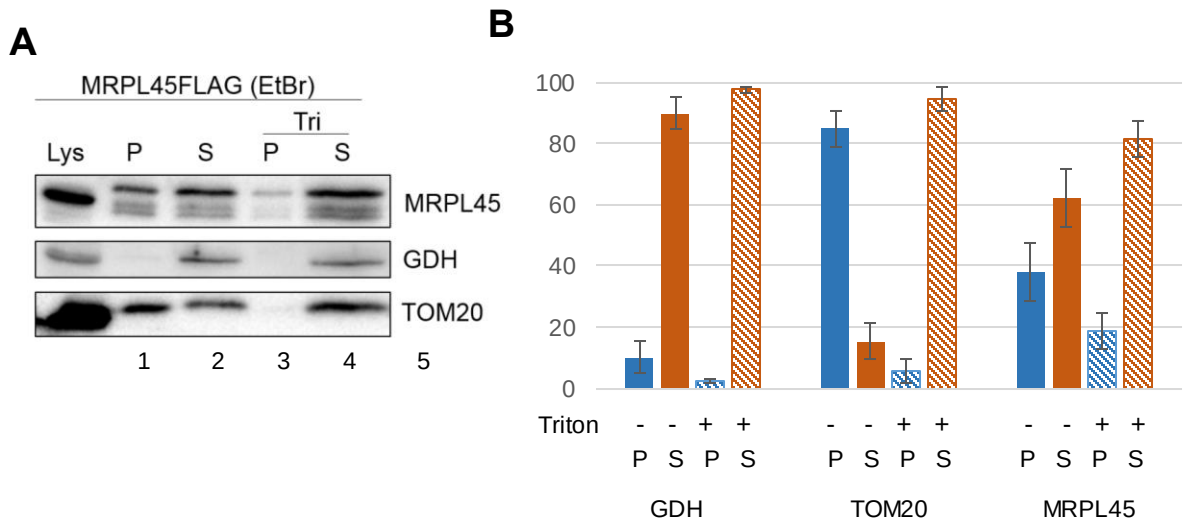

Figure 5.6 Distribution of MRPL45FLAG between membranes and soluble fraction in the absence of assembled mitoribosome.

A) Representative figure of western blot analysis performed on mito-lysates (Lys), membranes (P) and the soluble fractions (S) obtained as in 4.2.2. from HEK293 Flp-In TRex cells overexpressing MRPL45FLAG for 4 days during ethidium bromide incubation (10 days). Half of the membranes and matrix proteins obtained were incubated with 1.6% Triton X-100 (Tri) prior to centrifugation. The success of the overexpression was verified using an antibody against MRPL45. The efficiency of the separation protocol was assessed with antibodies against the matrix protein GDH and against the membrane protein TOM20. COXII levels were undetectable. **B)** Quantification of 3 biological repeats of the protocol was performed from the western blot analysis using *ImageLab* as explained in 2.5.5.

The efficiency of the subfractionation protocol was demonstrated using antibodies against GDH and TOM20. The matrix protein GDH was recovered mainly in the supernatant (Fig. 5.6A, lanes 3 and 5), whereas the OMM protein TOM20, which is predominantly present in the membrane fraction in absence of Triton X-100 (Fig. 5.6A, lane 1), was solubilised after incubation with the detergent, ending up in the S fraction (Fig. 5.6A, lane 5). The detection of MRPL45 showed a change of distribution of MRPL45FLAG upon incubation with Triton X-100, which suggested the ability of the protein to maintain its interaction with the IMM despite the presence of the FLAG-tag. It is important to notice that a proportion of TOM20 was detected in the S fraction, in absence of Triton X-100 (Fig. 5.6A, lane 3). This was observed in every experiment where the cells were incubated with ethidium bromide and could indicate that the membrane fraction was not completely pelleted. Quantification performed on biological repeats of the experiment (Fig.

5.6B) suggested that about 40% of MRPL45FLAG is found in the P fraction in absence of detergent and that its addition effected the release from the membrane of at least 20% of the protein. A small proportion of MRPL45FLAG was not solubilised by the addition of detergent. This could be due to the presence of aggregates. In addition, it is important to notice that approximately 40% of MRPL45FLAG was present in the soluble fraction in the absence of detergent. As previously mentioned for MRPL45 (Fig. 4.16, page 92), it is possible that a proportion of the protein in not interacting with the IMM either because of the saturation of the membrane-interacting points, or because the interaction was transient. Despite this, the solubilisation of the protein after addition of detergent confirmed its ability to interact with the IMM.

5.4. Characterisation of the interaction of MRPL45 with the IMM

The interaction between MRPL45 and the IMM might be due to the presence of a transmembrane domain, as well as mediated by a direct contact with the phospholipid layer or by the interaction with a membrane protein.

The possibility of the presence of a transmembrane domain was investigated by calculating the hydrophobicity of the protein using the Kyte-Doolittle method (Kyte J et al., 1982). Thanks to this method it is possible to predict the transmembrane domains in a protein of interest. Every amino acid has a hydropathy score that has been experimentally calculated and which depends on its characteristics and on the amino acids found in close proximity. The result of the prediction is shown in a graph presenting the hydropathy score in function of the window position, which correspond to the amino acid sequence. The window size (which is the number of residues evaluated at once) needs to be set. When this is set to 19, the presence of peaks over 1.6 will identify putative transmembrane regions and scores above 0 will indicate hydrophobic regions. Since the cleavage of the leader sequence of MRPL45 had not been confirmed yet, the prediction of the presence of hydrophobic domains was performed on the full-length MRPL45. The hydropathy plot is shown in Fig. 5.7.

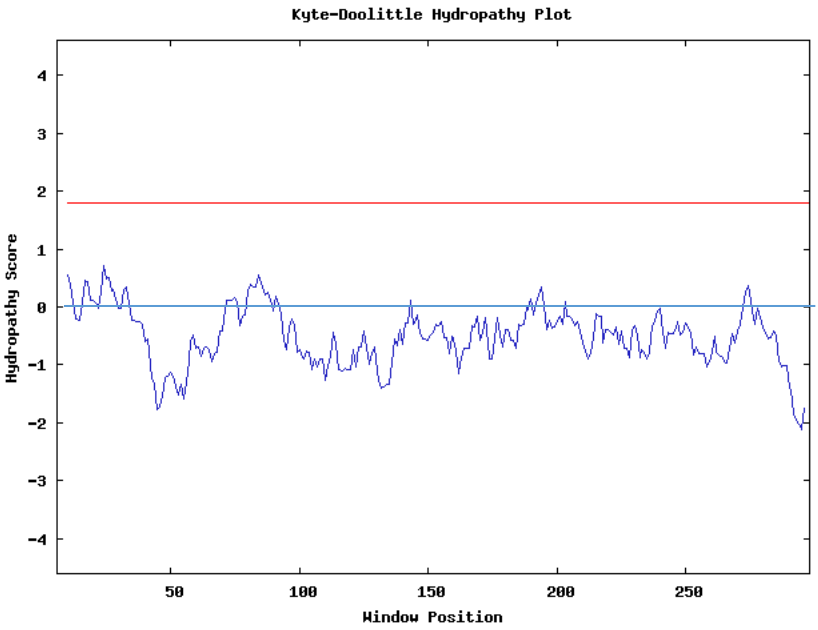

Figure 5.7 Hydrophobicity of MRPL45 calculated with the Kyte-Doolittle method.

Hydropathy scores were assigned to MRPL45 to highlight the presence of hydrophobic regions and transmembrane domains. The window was set at 19. Regions above 0 (blue line) are hydrophobic and the ones above the red line (at the score of 1.6) indicate the possible presence of transmembrane domains.

The presence of peaks above 0 (blue line) indicated the presence of only a few hydrophobic regions. As no peak reached 1.6 (red line), no transmembrane domains were predicted.

Because the presence of transmembrane domains of MRPL45 was unlikely, the possibility of its interaction with IMM proteins was assessed. For this purpose, the interactome of the protein was studied via immunoprecipitation studies on MRPL45FLAG. In order to discriminate between IMM proteins interacting with the monosome or directly with MRPL45, cells were incubated with ethidium bromide. This reagent made mt-rRNA unavailable, resulting in the lack of assembled mitoribosomal subunits. In absence of the ethidium bromide treatment, the whole mitoribosome will be co-immunoprecipitated with MRPL45FLAG, together with mitoribosome-interacting (but not necessarily MRPL45-interacting) proteins.

First of all, the efficiency of the immunoprecipitation was verified on HEK293-MRPL45FLAG cells cultured in growth media and overexpression of the recombinant protein for 3 days (by addition of 1 µg/mL tetracycline). MRPL45FLAG was immunoprecipitated from mitochondria via the FLAG-tag following the protocol in 2.9. The removal of the immunoprecipitated proteins from the beads was performed at 95°C for 3 minutes in 100 µL of 1x sample buffer (qv 2.5.4). The experiment was also performed on HEK293 cells as a negative control. The result of the experiment was analysed via silver staining (40 µL of each sample) and western blot analysis (40 µL of each sample) (Fig. 5.8).

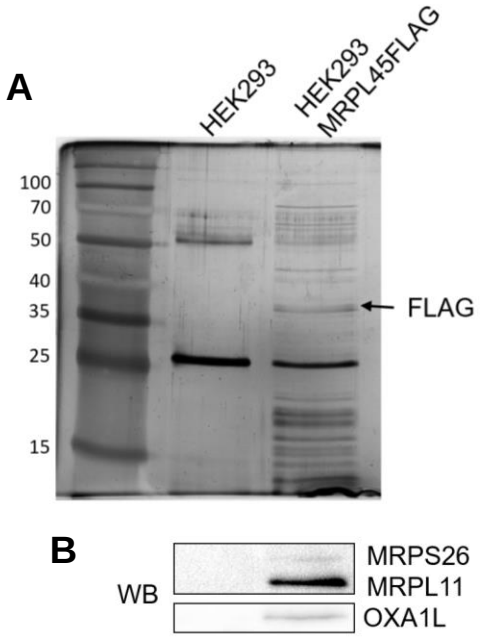

Figure 5.8 Immunoprecipitation of MRPL45FLAG

Silver staining of a 12% SDS-PAGE **(A)** of samples (40 µL) from FLAG immunoprecipitation from HEK293 and HEK293-MRPL45FLAG cells (3 days induction). The same samples were also analysed via western blotting **(B),** using antibodies against MRPS26, MRPL11 and OXA1L. Two biological replicates of the experiment were performed.

The samples obtained from FLAG immunoprecipitation from HEK293-MRPL45FLAG mitochondria showed the presence of co-immunoprecipitated proteins when compared to the wild type cells, suggesting the success of the immunoprecipitation experiment. The signals observed at approximately 50 and 25 kDa represent the light and heavy chain of the antibody found on the beads and are therefore present in the sample obtained from HEK293 cells. The signal observed above 35 kDa for the HEK293-MRPL45FLAG sample might correspond to the FLAG-tagged protein. The western blot analysis confirmed the presence of a component of the mt-LSU (MRPL11) and a component of the mt-SSU (MRPS26), as well as the presence of OXA1L, an IMM protein previously suggested to interact with the mitoribosome (Haque ME et al., 2010).

Because the immunoprecipitation via the FLAG-tag was successful, the experiment was repeated on the same cell line, following ethidium bromide treatment. Wild-type HEK293 cells were also incubated with the intercalating agent and used as a control. Each cell line was grown in 75 cm^2 flasks in presence of 250 ng/mL of ethidium bromide for 10 days. During the last 4 days of treatment, 1 µg/mL of tetracycline was added to HEK293-MRPL45FLAG to induce the overexpression of the protein. The cells were then harvested, and mitochondria were extracted, lysed and used for the immunoprecipitation experiment. A proportion (15 µg) of mitolysate was retained for western blot analysis. The elution of the immunoprecipitated proteins from the beads was performed at 95°C for 3 minutes in 50 µL of 1x sample buffer (qv 2.5.5.) as elution with the 3x FLAG peptide did not efficiently displace the MRPL45FLAG from the beads. The samples (one third of the final volume) were analysed via western blot (Fig. 9). HEK293 cell lysate was also

loaded as a control for the efficiency of the ethidium bromide treatment. The sample was also analysed via mass spectrometry to identify the proteins that co-immunoprecipitated with MRPL45FLAG (Appendix 13).

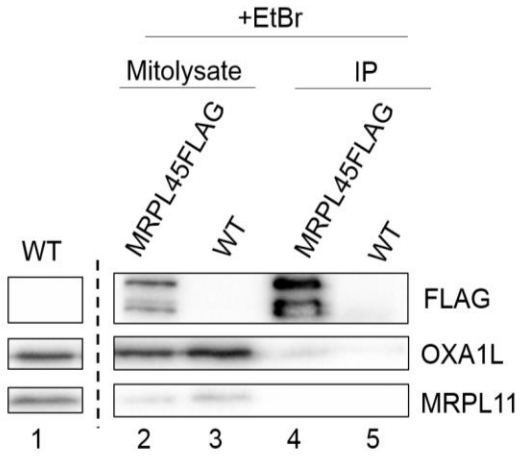

Figure 5.9 Immunoprecipitation of MRPL45FLAG from ethidium bromide treated cells.

Western blot analyses performed on mitolysates (15 µg) and FLAG-immunoprecipitated samples (25 µL of 50 µL elution volume, IP) from HEK293 (WT) and HEK293-MRPL45FLAG, both incubated with ethidium bromide for 10 days and with overexpression of the FLAG-tagged protein in HEK293-MRPL45FLAG for 4 days. Mitolysate from untreated HEK293 cells was also loaded as a control (lane 1). Antibodies against FLAG were used to confirm the presence of MRPL45FLAG; antibodies against MRPL11 and OXA1L were also used. The dashed line indicates that intervening lanes from the same blot have been omitted. Two biological replicates of the experiment were performed.

The FLAG-tagged protein was efficiently expressed (Fig. 5.9, lane 2) and immunoprecipitated (Fig. 5.9, lane 4). The steady state level of MRPL11 was reduced in the ethidium bromide treated cells (Fig. 5.9, lanes 2 and 3) when compared to the control (Fig. 5.9, lane 1), confirming the success of the treatment. MRPL11 was not detectable in the immunoprecipitated sample (Fig. 5.9, lane 4). No proteins were detected in the sample immunoprecipitated from wild type HEK293 cells incubated with ethidium bromide (Fig. 5.9, lane 5). A weak signal was detected for OXA1L in the sample obtained from immunoprecipitation of MRPL45FLAG (Fig. 5.9, lane 4).

In order to further identify the proteins that interact with MRPL45FLAG, the sample obtained from the immunoprecipitation experiments on HEK293 and HEK293-MRPL45FLAG cells, in presence of ethidium bromide, were also analysed via mass spectrometry (qv 5.1.1.) and are listed in Appendix 13. For every protein identified, 3 values were reported: the sum of raw spectra (log(I)), the number of peptides found (rI) and the expectation of finding the protein stochastically (log(e)). The data were sorted according to this last value, setting -2 as cut off point. Protein identified with a log(e) major than -2 have a 1 in 100 chance of a stochastic protein assignment. The experiment was repeated twice using 2 different controls, either HEK293 cells or induced HEK293-MRPS27FLAG cells, each after ethidium bromide treatment. For the biological repeat,

the cell line overexpressing MRPS27FLAG was used. This was a better control for the experiment since MRPS27 is a mitochondrial protein.

The proteins identified in the second biological repeat were limited. Several mitochondrial proteins were detected the proteomic analysis. Amongst these were chaperones (mt-HSP70, HSP60, etc), but these were also identified in the control samples. OXPHOS components were present, as well as several matrix proteins. It is likely that several of these proteins were interacting non-specifically since several were also detected in the control samples. No IMM proteins that might be the membrane partners of MRPL45 were identified. The most interesting proteins identified were prohibitin, prohbitin 2 and stomatin-like protein 2. The latter was reported to interact with prohibitin and prohibitin 2 (Christie DA et al., 2011), which form a large, multimeric ring complex in the IMM (Nijtmans LG et al., 2002). Prohibitin was reported as a component of the nucleoids that was able to interact with mtDNA but also with the mitoribosome (He J et al., 2012). However, prohibitin was also identified in the control sample, with a different ensemble identifier. Interestingly, neither LetM1 nor OXA1L were detected.

The mass spectrometry data obtained from the first biological repeat of the immunoprecipitation experiment showed the presence of 2 mitoribosomal proteins in the sample obtained from HEK293-MRPL45FLAG. These 2 proteins, MRPL39 and MRPL24, are found in close proximity of MRPL45.

Previously in this chapter, I demonstrated that the addition of a FLAG-tag at the C-terminus of MRPL45 did not affect neither protein synthesis nor mitoribosome assembly and that is also did not affect the ability of MRPL45 to bind the membrane. In order to confirm that the FLAG-tag was not disrupting the interaction of MRPL45 with putative membrane proteins, the immunoprecipitation was repeated on cells overexpressing wild type MRPL45.

First, the ability of MRPL45 antibody to perform the immunoprecipitation was assessed. HEK293-MRPL45 cells were induced for 3 days in 75 cm^2 flasks. Once 80% confluent, the cells were harvested and mitochondria extracted. The immunoprecipitation was performed with MRPL45 antibody (5 µg) immobilised on magnetic beads (30 µg) (qv 2.9.) and incubated with the lysate after removal of the excess of antibody. Western blot analysis was performed to investigate the result of the immunoprecipitation (Fig. 5.10).

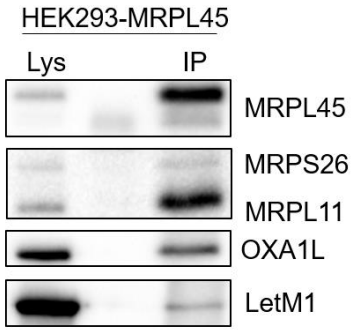

Figure 5.10 Immunoprecipitation of MRPL45 to identify the presence of components of the mitoribosome

Western blot analyses of cell lysate (≈30 µg) and immunoprecipitated samples (half of the final volume) from HEK293-MRPL45 after 3 days of induction. The success of the immunoprecipitation was confirmed with antibodies against MRPL45. The blot was interrogated with antibodies against MRPL11 and MRPS26 and OXA1L and LetM1. The experiment was performed once.

The immunoprecipitation of MRPL45 was successful, as shown by the presence of MRPL45 in the eluted sample. The mitoribosome (represented by MRPL11 and MRPS26) was also successfully immunoprecipitated. A major enrichment of the mt-LSU protein MRPL11 was detected, when compared to the mt-SSU protein MRPS26, suggesting that a bigger proportion of mt-LSU was precipitated when compared to the mt-SSU. The IMM protein OXA1L was well represented in the eluted sample, indicating its interaction with the mitoribosome. A weak signal was also detected for the IMM protein LetM1.

Because MRPL45 antibody was efficient in immunoprecipitation of its target, the experiment was repeated on HEK293-MRPL45 in the absence of assembled mitoribosome. Cells were grown in 75 cm^2 flasks for 10 days in ethidium bromide (250 ng/mL), with overexpression of MRPL45 during the last 4 days. Half of the resulting mitolysate was incubated with magnetic beads coated with either antibodies against MRPL45 or MNKI. MNKI is a protein involved in cytosolic translation and was used as experimental control. The bound proteins were eluted from the beads in 50 µL of 1x sample buffer after incubation at 95°C for 3 minutes. A proportion (1/3) of the eluted volume was analysed via western blot, together with 30 µL of whole cell lysate (Fig. 5.11).

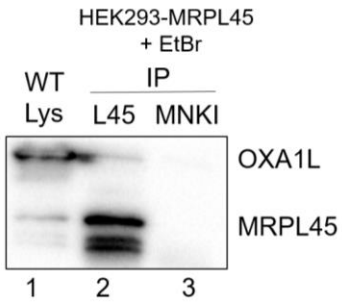

Figure 5.11 Immunoprecipitation of MRPL45 in cells incubated with ethidium bromide.

Western blot analyses performed on HEK293 cell lysate (30 µg, lane 1) and the samples obtained from immunoprecipitation of MRPL45 (lane2) or MNK1 (lane 3) from HEK293-MRPL45 cells incubated with ethidium bromide for 10 days and with overexpression of MRPL45 for 4 days. Antibodies against MRPL45 were used to confirm the success of the immunoprecipitation. Antibodies against OXA1L were also used. The figure is representative of 3 biological repeats.

The immunoprecipitation of MRPL45 was efficient (Fig. 5.11, lane 2). A weak signal was detected for OXA1L in the sample immunoprecipitated with MRPL45 (Fig. 5.11, lane 2), as previously observed for MRPL45FLAG immunoprecipitation in presence of ethidium bromide (Fig. 5.9). No signals for either OXA1L or MRPL45 were detected in the control immunoprecipitation (Fig. 5.11, lane 3). Unfortunately, the mass spectrometry analysis that was also performed on the samples identified only few proteins for both the biological repeats performed (Appendix 14). None of the proteins identified were putative membrane candidates that would be predicted to mediate the interaction.

5.5. Is MRPL45 part of a subcomplex formed during mt-LSU biogenesis?

The proteomic studies performed on HE293-MRPL45FLAG cells after ethidium bromide treatment identified the presence in the immunoprecipitated sample of 2 mitoribosomal proteins (Appendix 13). These 2 proteins are MRPL39 and MRPL24, and are found in direct contact of MRPL45 (Fig. 5.12).

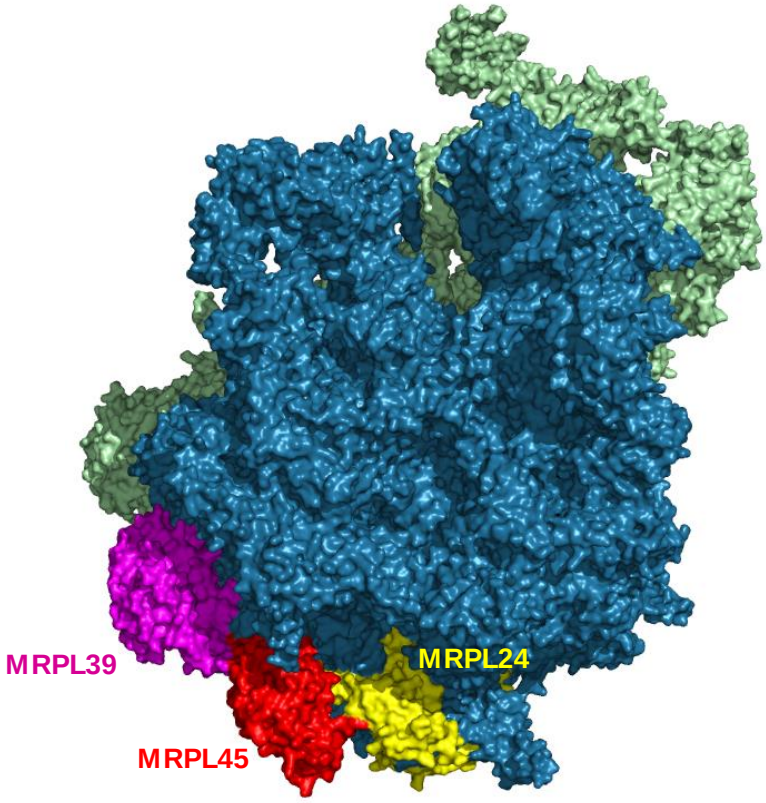

Figure 5.12 Localisation of MRPL45, MRPL24 and MRPL39 within the mt-LSU.

The mt-LSU (PDB 3J7Y (Brown A et al., 2014)) is represented on *PyMol* as surface in desaturated blue. MRPL45 (red), MRPL39 (magenta), MRPL24 (yellow) are highlighted. The mt-SSU is shown in desaturated green.

The biological replicate of the experiment failed to identify these proteins. Despite this, since the only mitoribosomal proteins identified in the sample are ones that are found on either side on MRPL45, it was tempting to speculate that MRPL45, MRPL24 and MRPL39 form a subcomplex

that might represent one of the steps of mitoribosome biogenesis. To test this hypothesis, the level of MRPL24 and MRPL39 were analysed in ethidium bromide treated wild-type HEK293 cells and compared to HEK293-MRPL45FLAG cells also treated with ethidium bromide for 10 days, with overexpression of the recombinant protein in the last 4 days of ethidium bromide treatment. Because MRPL45, MRPL24 and MRPL39 appeared to form a subcomplex, a hypothesis could be that the overexpression of MRPL45FLAG in presence of ethidium bromide might lead to increased steady state levels of the other 2 mitoribosomal proteins when compared with wild type cells also incubated with the intercalating agent. The samples were analysed via western blotting (Fig. 5.13).

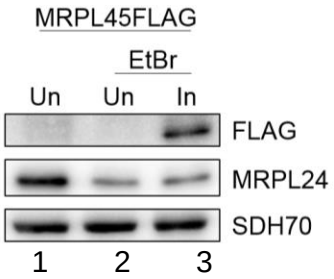

Figure 5.13 Steady state level of MRPL24 after ethidium bromide treatment, in presence or absence of MRPL45FLAG overexpression.

Western blot analysis was performed on cell lysates (≈30 µg) obtained from uninduced HEK293-MRPL45FLAG untreated (lane1) or those incubated with 250 ng/mL of ethidium bromide for 10 days with (lane 2) or without (lane 3) induction of MRPL45FLAG during the last 3 days of the treatment. The efficiency of the overexpression was confirmed with antibodies against FLAG. The quality of the loading was detected with antibodies against SDH70. The figure is representative of 2 biological repeats.

The western blot analysis did not show an increase in the steady state level of MRPL24, indicating that the overexpression of MRPL45FLAG does not increase the expression or stability of this protein. The success of the overexpression was proved with antibodies against the FLAG-tag and the equality of the loading was confirmed with antibodies against the IMM protein SDH70. The blot was also interrogated with an antibody for MRPL39, but no signal was detected.

5.6. Discussion

The ability of MRPL45 to interact directly with the inner mitochondrial membrane was demonstrated in chapter 4. This chapter aimed to clarify the mode of this interaction. For this purpose, a cell line able to inducibly overexpress MRPL45FLAG was prepared.

The FLAG tag was inserted at the C-terminus of the protein. The overexpression of MRPL45FLAG did not affect the steady state level of mitochondrial protein, cell morphology or growth rate. The sucrose gradient analysis performed after overexpression of the protein showed its integration in the mt-LSU, suggesting that the addition of the FLAG did not prevent the protein from being assembled in this subunit. Although these results suggest that the homeostasis of the cells was not affected, no information of the ability of MRPL45FLAG to interact directly with the IMM could be inferred. Because of the importance of a concomitant insertion of the mtDNA

encoded proteins in the IMM with translation, it is likely that more anchoring points cooperate to secure the interaction between the IMM and mitoribosome, as previously shown in yeast (Pfeffer S et al. 2015). It is therefore possible that the interaction of the whole monosome is maintained despite the absence of one (or more) of these anchoring points. The ability of MRPL45FLAG to associate directly the IMM was assessed using the protocol developed to study membrane interaction, under conditions of overexpression of the tagged protein in absence of the fully assembled subunits of the mitoribosome. The data obtained confirmed that the FLAG-tagged protein retained the ability to directly bind the IMM.

The results obtained for MRPL45FLAG suggested that the addition of a FLAG-tag at the C-terminal of MRPL45 did not affect the role of MRPL45. As a consequence, in the following chapter, two MRPL45 constructs presenting a FLAG-tag will be prepared to identify the domain of MRPL45 involved in the interaction with the IMM. Due to the FLAG-tag, these will be easily discerned from the endogenous protein. In chapter 6, immunoprecipitation of MRPL45FLAG (via the FLAG) will be used to identify putative membrane proteins that might be interacting directly.

Concerning the interaction of MRPL45 with the membrane, the prediction of hydrophobic domains of MRPL45 did not suggest the presence of transmembrane domains, indicating that the interaction was likely to be either with an IMM protein or with the phospholipidic bilayer. The mass spectrometry analysis performed on the samples obtained by immunoprecipitation of MRPL45FLAG or MRPL45 did not identify any putative interacting membrane proteins, although western blot analysis did identify a weak signal for OXA1L in the immunoprecipitated sample. This might indicate a non-stoichiometric interaction between MRPL45 and OXA1L. Despite this, no convincing evidence was found to substantiate the existence of a IMM protein that could mediate the interaction with MRPL45. Therefore, it might be that MRPL45 interacts directly with the inner mitochondrial membrane. However, it is important to remember that despite the mass spectrometry method used to analyse the immunoprecipitated samples being efficient in detecting membrane proteins, it is possible that some proteins were not detectable using this technique.

Interestingly, of the 80 proteins present in the human mitoribosome, in absence of the assembled mt-LSU, only MRPL39 and MRPL24 were co-immunoprecipitated with MRPL45FLAG. These 2 proteins are found on either side of MRPL45 and the recent cryo-EM structure of the human mt-LSU (Brown A et al., 2014). Unfortunately, it was not possible to replicate this result.

To date, the steps involved in the assembly process of the mt-LSU are still poorly defined. It is possible that MRPL45, MRPL24 and MRPL39 constitute a subcomplex of the large subunit, which might be stable in the absence of the 16S rRNA and the other mitoribosomal proteins. If this were the case, the overexpression of MRPL45FLAG in the absence of assembled mt-LSU would be expected to lead to the increase of the steady state levels of MRPL24 and MRPL39, stabilised by complexing with MRPL45FLAG. Because this effect was not observed, it is unlikely that these 3 proteins compose a subcomplex of the mt-LSU. The co-immunoprecipitation of MRPL39 and MRPL24 with MRPL45 might simply confirm the direct interaction of these proteins.

Chapter 6: Investigation of putative membrane-interacting domains of MRPL45

6.1. Identification of the putative membrane-interactive domains and their analysis via modification of the protein sequence

The previous chapter confirmed the ability of MRPL45 to bind directly to the IMM. In order to further investigate this interaction, alterations were introduced into the candidate membrane-binding domains of MRPL45.

The changes introduced into the first construct were based on the observation that the helix α2 (residues 118-129) and the following unstructured sequence (residues 130-136) of MRPL45 (RefSeq NP_115727.5) were the most protruding domain in the structure of the human mitoribosome (Brown A et al., 2014) (Fig. 6.1).

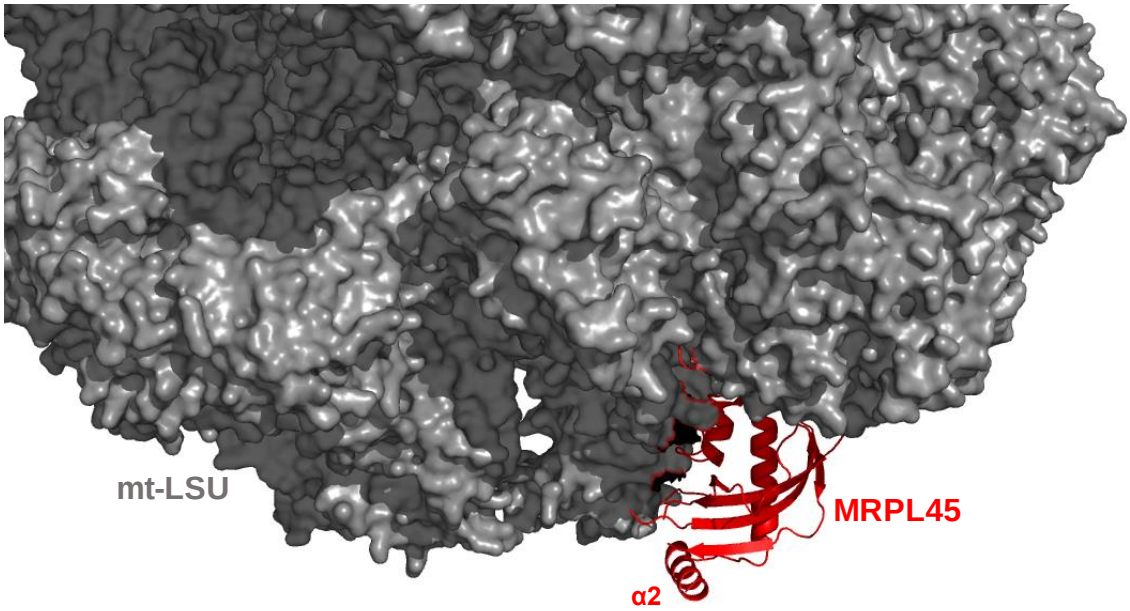

Figure 6.1 Visualisation of the position of MRPL45 within the large subunit of the human mitoribosome.

The figure was obtained using PyMol from the PDB file 3J7Y (Brown A et al., 2014). The mt-LSU surface is visualised in grey, whereas MRPL45 is depicted as cartoon in red. Helix α2 is labelled.

In order to investigate the contribution of this MRPL45 domain in the interaction with the membrane, the polar or charged amino acids present were mutated to alanine. This amino acid has a methyl group as a side chain, which is not bulky and not reactive, and it is therefore commonly used in mutation analyses to evaluate the contribution of specific amino acids. In this construct, the mutated residues were Gln 119, Arg 123, Arg 124, Lys 126, Asp 127, Tyr 128 Lys 133 Lys 135 and Asp136 (Fig. 6.2A, indicated in yellow) and are all found at the beginning of what is identified as the 'Tim44-like' domain of MRPL45. Asp129 was not mutated into alanine since its chain was not protruding towards the outside of the structure and was therefore predicted to

be unlikely to be involved in the membrane interaction. The construct will be identified in this study as MRPL45FLala. Although the substitution with alanine should not perturb the formation of the helix, the potential effects of these mutations on the secondary structure of the domain were predicted using JPred4 (Drozdetskiy A et al., 2015), and the results are shown in Fig 6.2B.

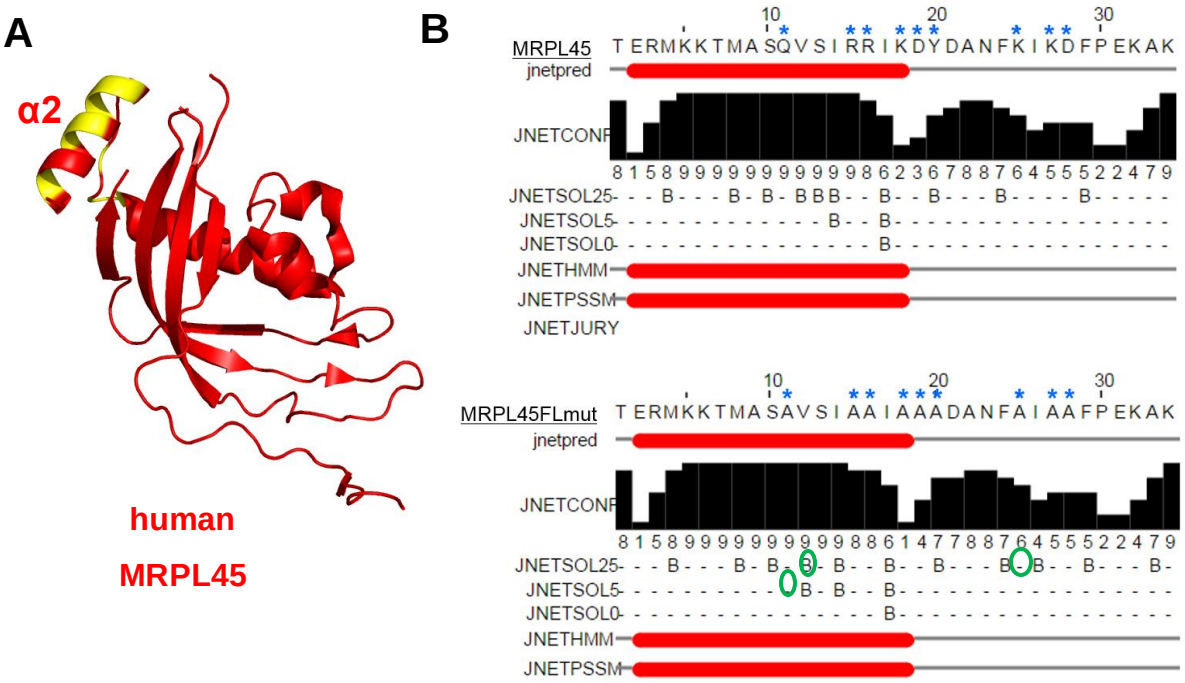

Figure 6.2 Mutated residues on the most protruding domain of MRPL45 and their effect on the secondary structure.

A) Visualisation of residues mutated (yellow) on MRPL45. The cartoon representation was obtained from chain d of the PDB file 3J7Y. **B)** Prediction of the effects of the mutations on the secondary structure with JPred4 (Drozdetskiy A et al., 2015). Jnetpred indicates the consensus prediction generated from several methods and its confidence is reported at JNETCONF. JNETSOL25, 5 and 0 predict the solvent accessibility, where 'B' indicates a buried residue. The differences are circled in green. The structure prediction was also predicted using the Hidden Markov Model (JNETHMM) and the Position-Specific Scoring Matrix prediction (JNETPSSM). For the structure prediction models used, the red tubes indicate helices. The mutated residues in the MRPL45 sequence are indicated by a blue asterisk.

The mutations performed are not predicted to alter the secondary structure of the domain, but might have an effect on the solvent accessibility of some residues, highlighted in green in Fig. 6.2B.

To evaluate the importance of the mutated residues, the conservation of the domain subjected to mutations was inferred from the alignment of the available sequences of MRPL45 from different species (Fig. 6.3). The amino acids mutated in MRPL45FLala are indicated by asterisks.

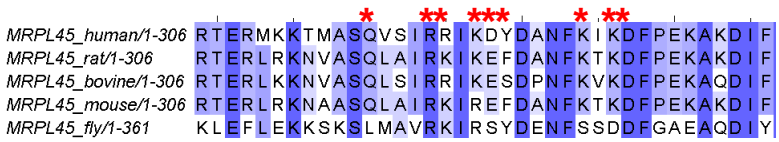

Figure 6.3 Conservation of the mutated area of MRPL45 throughout different species.

The sequences of MRPL45 available were aligned using Jalview (ClustalWS) and the residues were coloured with a different intensity of blue according to their conservation. The residues mutated in MRPL45FLala are indicated by asterisks.

The mutations (Fig. 6.3, indicated by asterisks) resulted to be localised in a relatively conserved domain of MRPL45, which suggests an importance for the protein stability or function.

In order to investigate membrane-interaction of MRPL45, a second construct was also generated. This was based on the homology with TIM44, but also on the structure of porcine MRPL45 available thanks to the cryo-EM structure recently released (Greber BJ et al., 2014). The cryo-EM studies on the porcine mt-LSU were able to obtain a better resolution for MRPL45 than the one obtained for the human subunit. Porcine MRPL45 highlighted the presence of another helix (named α1) N-terminal proximal to the previously discussed helix α2 (Fig. 6.4).

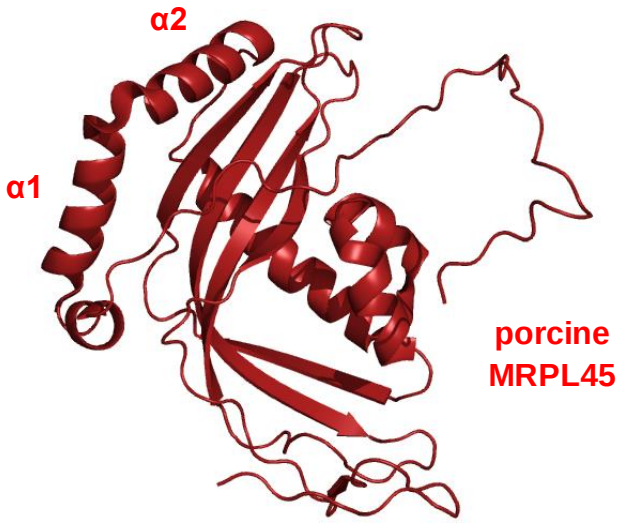

Figure 6.4 Structure of porcine MRPL45.

The structure of MRPL45 was obtained from the cryo-EM structure of porcine mt-LSU and visualised in Pymol as cartoon, from the PDB file 4V1A (Greber BJ et al., 2014).

The helix α1 closely resembles the helix α1 found in human TIM44 (Fig. 4.1, page 76). Human and porcine MRPL45 are very conserved, therefore the presence of helix α1 in human MRPL45 is highly likely. Its presence was assessed analysing the amino acid sequence via Phyre2 to predict the secondary structure of the full length MRPL45. The prediction program generated a PDB file that was then visualised in PyMol (Fig. 6.5).

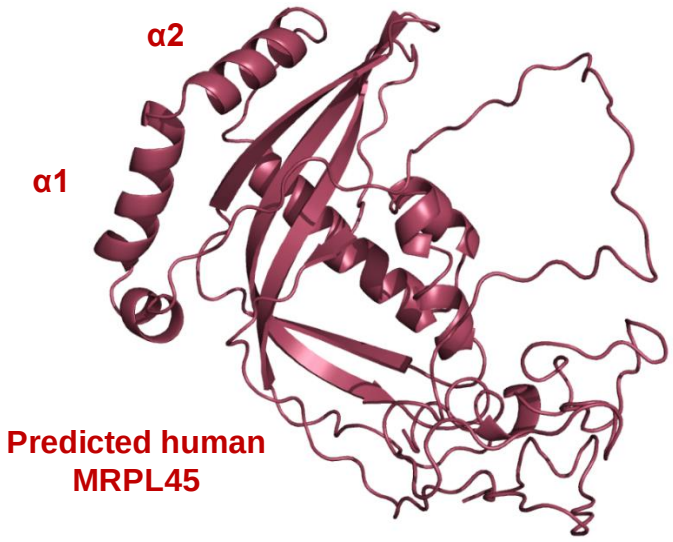

Figure 6.5 Prediction of the structure of the full length human MRPL45.

Cartoon representation of the full structure of MRPL45, obtained in PyMol using the PDB file generated by the structure prediction of Phyre2 (Kelley LA et al., 2015).

The prediction of the full structure of MRPL45 hypothesised the presence of another helix ahead of the helix α2, resolved in the cryo-EM structure. This helix will correspond to the helix α1 present in the porcine homologue and also present in human TIM44 (as helix α1).

As mentioned in the introduction of chapter 4, studies on yeast Tim44 suggested that the folding of helices A0 and A1 (Fig. 4.2, page 77, corresponding to α1 and α2 in human TIM44 and MRPL45) is important for membrane interaction of this protein. In addition, crystallographic studies on the C-terminus of human TIM44 highlighted the presence of 2 hydrophobic cavities within the structure. In particular, a molecule of PEG was recovered in between helices α1 and α2 (residues 289-295, Fig. 4.4A highlighted in orange, page 78). These residues are widely conserved in the same protein across species (Fig. 4.4B, page 78) and the corresponding region of MRPL45 (Fig. 6.6, green box, residues 104-110) appears to be also relatively conserved across different species.

Figure 6.6 Conservation of the putative binding domain of TIM44 across its homologue MRPL45 in different species.

The sequences of MRPL45 available for different organisms were aligned using Jalview (ClustalWS) and the residues were coloured with a different intensity of blue according to their conservation. The domain of interest is indicated by a green box.

A different approach was used to investigate the possible role of this conserved region in the interaction with the membrane. Instead of mutations of residues, the domain between 1 and 117 was deleted. This construct will be referred to as MRPL45FLΔ and will be discussed in 6.4.

This chapter will focus on the generation of the cell lines expressing MRPL45FLala and MRPL45FLΔ, and on the evaluation of the ability of these proteins to be integrated in to the mt-LSU and to directly interact with the IMM. These experiments aim to identify domains of importance for the function of MRPL45.

6.2. Methods

6.2.1. Site-directed mutagenesis

It is possible to quickly generate mutations, insertion or deletions using a technique called site-directed mutagenesis. The modifications are inserted by primers that are complementary to the template DNA around the region to modify. The mutations were introduced using the *QuikChange II Site-Directed Mutagenesis* Kit (*Argilent,* cat no 200523). This kit allows to introduce the modifications directly on a plasmid, using a PCR-like reaction that will synthesise the new mutated plasmid. The reaction was carried out as follows:

Table 6.1 Composition (A) and conditions (B) of the site directed mutagenesis.

The reaction was carried out using the QuickChange II Site-Directed Mutagenesis kit (Argilent) in ProFlex™ PCR machine (*Thermo Scientific*).

A

Reagents	Final concentration/amount
10x Reaction buffer	1x
dNTPs mix (from the kit)	2 µL
100 µg/µL sense primer	125 µg/µL
100 µg/µL anti-sense primer	125 µg/µL
Template plasmid	50 ng
PfuUltra DNA polymerase (2.5 U/µl)	1.25 U
DI water	Up to 25 µL

B

Reaction	Temperature	Duration	
Initial denaturation	95ºC	30 sec	
Denaturation	95ºC	1 min	
Annealing	Dependent on the primers	1 min	**x 20**
Extension	68ºC	1 min/kb plasmid	

Since the mutated plasmid was generated by the reaction *in vitro,* newly generated DNA will not be methylated, unlike the parental one. This difference in methylation state was used to selectively digest the parental plasmid with Dpn1, leaving the newly synthesised plasmid with

the generated mutations intact. The digestion was performed at 37ºC for 90 minutes by addition of 0.5 µL of 10 U/µL *Dpn*I (present in the kit). The product (4 µL) was then used to transform supercompetent cells (XL1- Blue cells, *Agilent*), following the protocol in 2.2.2., and plated on LB-agar containing the appropriate antibiotic for selection. The plate was finally grown at 37ºC overnight to allow the growth of transformed colonies.

6.2.2. *In vitro* transcription

This protocol was used to prepare mRNA transcripts for *in vitro* translation. A PCR product of the gene of interest was prepared (qv 2.3.3.) using cDNA or previous plasmids as a template and the primers listed in Appendix 5. The sense primer used will contain the SP6 promoter (5'-ATT-TAG-GTG-ACA-CTA-TAG-3'), needed to initiate *in vitro* transcription. The product obtained was purified with the *QIAquick PCR Purification Kit* (*Quiagen*, cat no 28104) and then used for the *in vitro* transcription. The reaction was carried out using the *AmpliScribe T7 High Yield Transcription* kit (*Epicentre,* cat no AS2607), mixing the reagents in the same order shown in Table 6.2 with care to avoid RNase contamination.

Table 6.2 Composition of the *in vitro* transcription reaction performed with *AmpliScribe T7 High Yield Transcription* kit.
The reagents were added in the same order as the one listed in this table.

Reagents	Amount
RNase-free water	Up to 20 µL
10x SP7 buffer	2 µL
100 mM ATP	1 µL
100 mM CTP	1 µL
100 mM GTP	1 µL
100 mM UTP	1 µL
100 mM DTT	2 µL
RiboSafe	0.5 µL
DNA (from PCR reaction)	1 µg
SP6 Enzyme solution	2 µL

The mixture was incubated at 37°C for 2 hours. After that, the RNA was precipitated using ammonium acetate. After addition of 20 µL of 5 M ammonium acetate, the sample was incubated for 15 minutes on ice. The RNA was then pelleted by centrifugation at 10,000 g at 4°C for 15 minutes. The supernatant was discarded and the pellet was resuspended 200 µL of 75% ethanol. The sample was then centrifuged again at 10,000 g at 4°C for 15 minutes. The supernatant was discarded again, and the pellet was resuspended in 10 µL of RNase-free water with the addition of 1 µL of RNase inhibitor (*RiboSafe*). The quality of the sample (1/10) was checked on 1% denaturing agarose gel (qv 6.2.4.). The sample was stored at -80°C.

6.2.3. *In vitro* translation

The translation of the RNA transcribed *in vitro* was performed using the following mixture:

Table 6.3 Composition of *in vitro* translation reaction.

Reagents	Amount
Rabbit reticulocyte lysate	10 µL
^{35}S-Met easy tag protein mix	3.5 µL (35 µCi)
25 µM Amino acids minus Met	0.5 µL
In vitro transcribed RNA	Up to 5 µL
RiboSafe	0.5 µL
Nuclease-free water	Up to 20 µL

The reaction was incubated at 30°C for 1 hour. Sample buffer was added to every sample, which were heated to 95°C for 3 minutes. The samples were resolved on a 12% SDS-PAGE gel. The gel was fixed overnight in a solution composed of 30% methanol, 10% acetic acid and 3% glycerol and then vacuum dried in between filter paper at 65°C for 2 hours. The signals for the translated products were detected using the *Typhoon FLA 9500* system and ImageQuant software (*GE Healthcare*), after exposition of the gel to a PhosphorImage screen for 1 day.

6.2.4. Denaturing agarose gel for RNA electrophoresis

All the equipment to be used for the electrophoresis was soaked in DEPC water and 3% H_2O_2 for 1 hour and then rinsed twice with DEPC water. The samples were prepared as in Table 6.4A and incubated at 55ºC for 15 minutes. After that, every sample was mixed with 1 µL of 2 mg/mL ethidium bromide and 2.2 µL of loading dye (Table 6.4B).

Table 6.4 Preparation of samples for RNA electrophoresis (A) and 10X MOPS composition (B).

A

Reagents	Amount
10x MOPS	2 µL
37% Formaldehyde (*Sigma*, cat no F1635)	3 µL
Formamide (*Sigma*, cat no F7503)	7 µL
RNA	x µL
DEPC H_2O	Up to 20 µL

B

Reagents	Final concentration
MOPS (*Sigma*, cat no M1254)	400 mM
CH_3COONa	100 mM
EDTA	10 mM

The samples were run on a 1% denaturing agarose gel (Table 6.5) in order to separate RNA species of different molecular weight.

Table 6.5 Denaturing agarose gel (1%) for RNA electrophoresis

Reagents	Final concentration
Agarose	1%
DEPC H_2O	87.5%
Warmed up until the agarose melts, then added	
10x MOPS	1x
37% Formaldehyde	0.925%

Once solidified, the samples were loaded and the gel was run at 50-60 V until the needed separation of the components was reached. At the end of the electrophoresis, the samples quality and migration was checked by imaging the gel with the *ChemiDoc* system.

6.3. Investigation of the importance of the α2 helix of MRPL45

6.3.1. Generation of stable cell lines able to express mutant MRPL45FLAG (MRPL45FLala)

The mutant MRPL45FLAG construct (MRPL45FLala) was personally designed (Appendix 6) and then commissioned to the *GeneArt* service (*Thermo Scientific*), who synthesised the fragment and cloned it into a plasmid carrying kanamycin resistance, named pMK. To allow the study of the mutant protein in the absence of the endogenous MRPL45, silent mutations in the sequence targeted by siRNA02 (Appendix 4) were introduced so that MRPL45FLala mRNA cannot be bound with this siRNA. As MRPL45FLAG was shown to interact with the IMM (Fig. 5.6, page 101), a FLAG tag at the C-terminus of this construct was also added. This will allow to use the anti-FLAG antibody on western blot analysis to easily discriminate the mutant MRPL45 from the endogenous counterpart. The sequence of MRPL45FLala designed was delimited by 2 *Bam*HI restriction sites, to allow the extraction of the insert from the delivered pMK plasmid and it subsequent cloning into pcDNA5/FRT/TO. MRPL45FLala-pcDNA5/FRT/TO was used to transfect HEK293 Flp-In cells to express the protein under tetracycline control.

Because of problems in its production, the construct delivered was not sequence-verified. The MRPL45FLala-pMK plasmid (20 ng) was transformed into competent cells (qv 2.2.2.). Positive colonies were expanded in LB media containing 50 µg/mL kanamycin and the plasmid was extracted. The plasmid obtained (3 mg) was digested with *Bam*HI (qv 2.3.7.) in a final volume of 20 µL, and the products of the digestion (1 µL) was resolved on a 1.2% agarose gel to assess the efficiency of the reaction (Fig. 6.7).

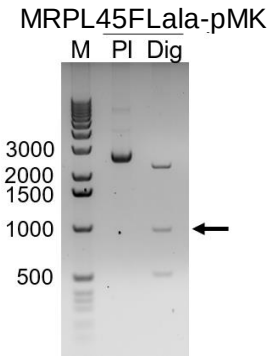

Figure 6.7 Products of MRPL45FLala-pMK digestion with *Bam*HI.

MRPL45FLala-pMK (3 mg) obtained from GeneArt (Appendix 6) were digested with *Bam*HI (20 µL final volume) and 1 µL (Dig) was resolved on a 1.2% agarose gel. The undigested plasmid (PI) was also loaded on the gel. The size of the desired product is indicated by the arrow.

The DNA electrophoresis analysis showed the presence of 3 species after digestion of MRPL45FLala-pMK with *Bam*HI. Together with the heaviest species (≈ 2300 bp) that corresponded to the pMK empty plasmid, 2 lighter forms were detected. One species at approximately 1000 bp matched the size expected for MRPL45FLala insert (984 bp) (Fig. 6.7, indicated by the arrow), whereas the smallest band of approximately 500 bp was an unexpected product of the digestion. The remaining volume of the reaction was resolved on a new agarose gel and the species corresponding to ≈ 1000 bp was excised. After gel extraction, the desired insert was ligated into *Bam*HI-digested pcDNA5/FRT/TO and then used to transform competent cells as previously described. In order to discriminate colonies successfully transfected with MRPL45FLala-pcDNA5/FRT/TO from the ones containing the empty plasmid, half of every expanded colony was analysed using the cracking gel technique (qv 2.3.10.) (Fig. 6.8).

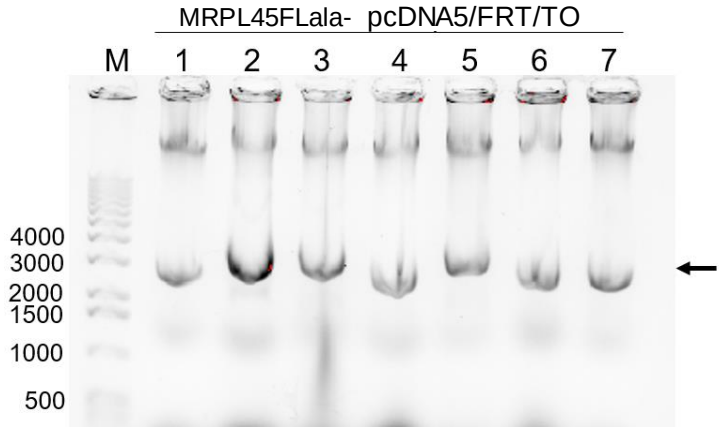

Figure 6.8 Identification of colonies positively transformed with MRPL45FLala-pcDNA5/FRT/TO.

Cracking gel technique (qv 2.3.10.) was used on expanded colonies obtained from the transformation of α-competent cells with MRPL45FLala-pcDNA5/FRT/TO. The black arrow identifies the higher products that indicates the colonies containing the insert within pcDNA5/FRT/TO.

The figure showed that colonies 2, 3 and 5 presented a band corresponding to the plasmid that was heavier than other colonies (1, 3, 6, 7). This indicates that colonies 2, 3 and 5 are likely to contain a copy of the plasmid with MRPL45FLala successfully inserted in the cloning site.

Because the same restriction site was used at either side of the insert, diagnostic digestion was performed to identify the colonies containing the insert with the correct orientation. At this purpose, the plasmid was extracted from colonies 2, 3 and 5 and 500 ng of each plasmid were digested either with *Afl*II or simply linearized by digestion with *Kpn*I. *Afl*II will cut the plasmid 21 bases ahead of *BamH*I site and the correctly-oriented insert at 848 bases from the insertion site. As a consequence, the formation of a heavy fragment of ≈5 kb and one of ≈850 bp upon digestion with *Afl*II will identify colonies containing the insert in the wanted orientation. In case a fragment of ≈100 bp was present instead of the ≈850 bp, the correspondent colony will contain a plasmid with the insert in the wrong orientation. The products of every digestion were analysed via DNA electrophoresis (Fig. 6.9).

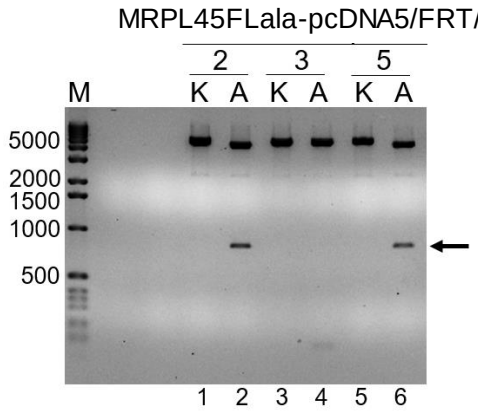

Figure 6.9 Diagnostic digestion of MRPL45FLala-pcDNA5/FRT/TO.

MRPL45FLala-pcDNA5/FRT/TO from colonies 2, 3 and 5 was digested with either *Kpn*I (K) or *Afl*II (A) to, respectively, linearize the plasmid or investigate the orientation of the insert. The samples were resolved on a 1.2% agarose gel together with a size marker (M). The presence of a band at ≈ 800 bp will indicate the correct orientation of the insert and is indicated by an arrow.

The digestion of the plasmids obtained from colonies 2 and 5 with *Afl*II produced a fragment of approximately 800 bp (Fig. 6.9, lanes 2 and 6, indicated by an arrow), indicating the correct orientation of the insert within the plasmids of these colonies. The smaller band detected for the same digestion performed on MRPL45FLala-pcDNA5/FRT/TO extracted from colony 3 suggested that this colony contained the insert with the wrong orientation (Fig. 6.9, lane 4). All the plasmids were successfully linearized by *Kpn*I.

Prior generation of a cell line able to express MRPL45FLala, the sequence of the insert within pcDNA5/FRT/TO was verified (qv 2.3.10.). The sequence obtained confirmed the identity of the construct designed (Apprendix 10), therefore the plasmid was used to transfect HEK293 Flp-In cells (qv 2.1.6.). After antibiotic selection, single colonies were expanded and samples were prepared for long term storage in liquid nitrogen.

6.3.2. Effects of MRPL45FLala expression

The ability of HEK293-MRPL45FLala to express the protein was tested. Three different clones able to express the mutant protein were tested. Since the data obtained were in agreement between the different clones, only one will be represented in the following figures. Cell growth was monitored as cell confluence for 6 days using the *IncuCyte* system (Fig. 6.10A). Cell lysate obtained after induction with tetracycline for 3 days was analysed via western blotting (Fig. 6.10B). The cell morphology after 5 days is shown in Fig. 6.10C.

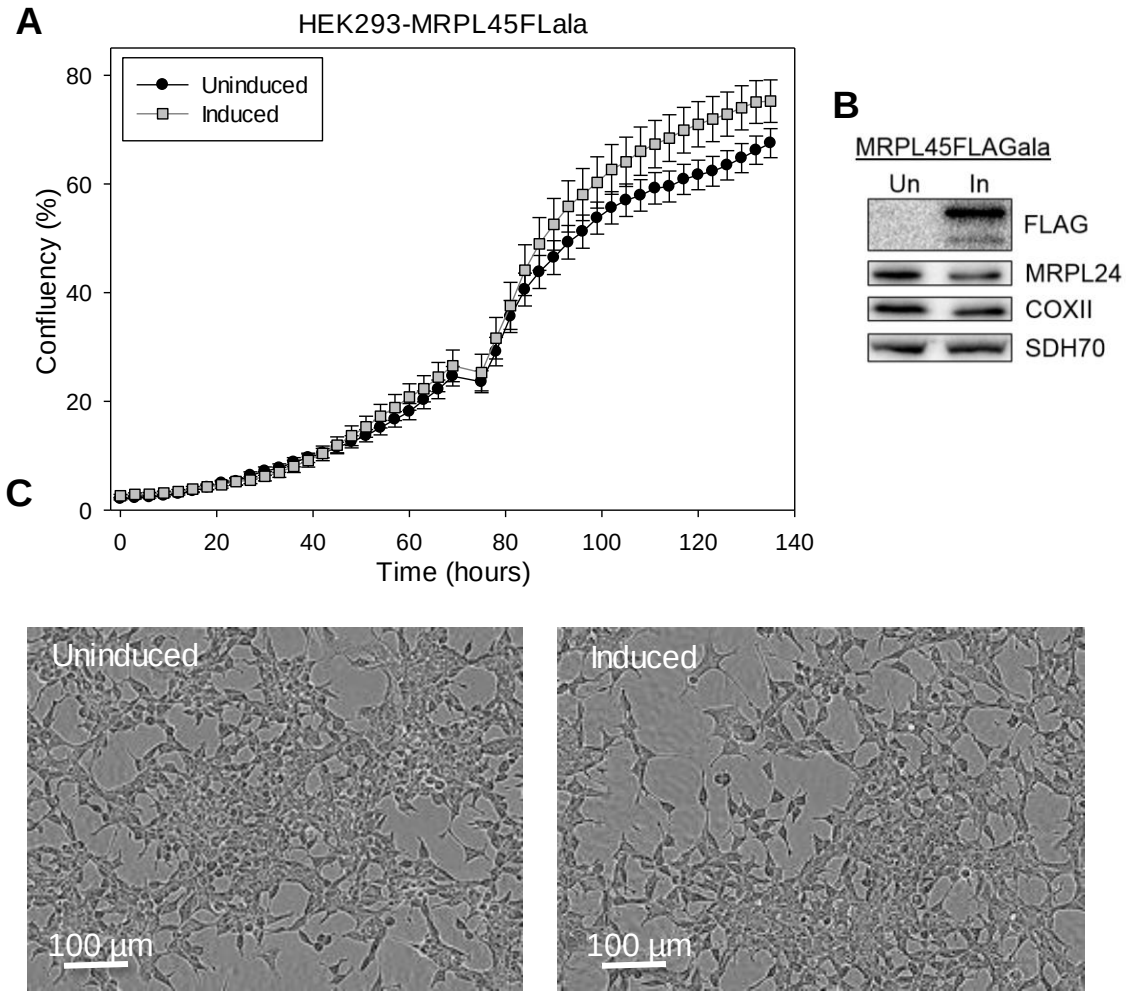

Figure 6.10 Effects of the expression of MRPL45FLala in HEK293 cells on steady state level of mitochondrial proteins and on cells growth.

HEK293-MRPL45FLala cells were induced for 6 days with the addition of 1 µg/mL of tetracycline. Uninduced cells were also grown in parallel. Cell growth **(A)** was monitored by confluency estimate every 3 hours throughout the experiment (2 biological repeats). Representative figure of western blot analysis **(B)** performed on lysate (≈30 µg) obtained from uninduced and induced HEK293-MRPL45FLala cells after 3 days of induction. Antibodies against FLAG were used to detect the expression of the mutant protein. Steady state levels of the mitoribosomal protein MRPL24 and of the OXPHOS component COXII were also evaluated. SDH70 was used as a loading control. Cell morphology after 5 days of induction is also shown **(C)**. The results are representative of 3 biological repeats.

The expression of the FLAG-tagged mutant protein did not affect cell growth over a 6 days' period (Fig. 6.10A). Cell morphology also appeared unaltered (Fig. 6.10C). The expression of MRPL45FLala was successful (Fig. 6.10B). The FLAG antibody detected the presence of 2 species, also previously observed for the detection with the same antibody on cell lysate from induced HEK293-MRPL45FLAG cells (Fig. 5.5B, page 100). Since its detection was through the FLAG peptide at the C-terminal, this lower Mr species was assumed to be an N-terminal cleavage of the protein performed upon or after import. It is important to notice that the detection of the FLAG-tagged product required a long exposure of the membrane (≈ 16 seconds), which indicate a low steady-state level of the protein. This was also observed comparing the steady state level of MRPL45FLala and MRPL45FLAG after 3 days of induction (Fig. 6.27). It is possible, indeed, that the mutations generated on MRPL45 affected the stability of the protein, although they were not predicted to significantly disturb the secondary structure of the protein (Fig. 6.2). The western blot analysis also suggested a mild reduction of the steady state level of the mt-LSU components MRPL24 and of the mtDNA-encoded COXII. The equality of the loading was confirmed with the detection of SDH70.

In order to exclude that the low steady-state level of MRPL45FLala observed was due to problems in the expression of the correspondent mRNA, qPCR was performed on cDNA obtained from reverse transcription of total RNA from uninduced and induced (3 days) HEK293-MRPL45FLala cells. The level of the transcripts was evaluated with primers targeting MRPL45 that will, therefore, also measure the endogenous expression of MRPL45 in both the samples. The levels of COXII mRNA and 16S rRNA were also measured. The data were normalised on the level of 18S rRNA and the result are shown in the following figure.

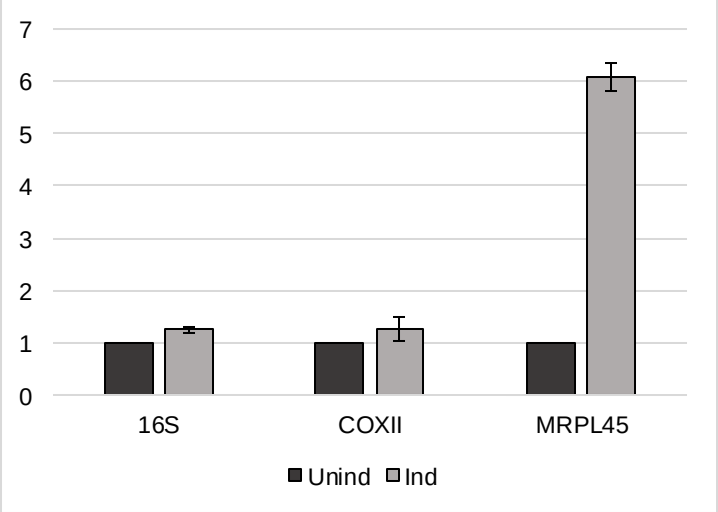

Figure 6.11 Levels of 16S rRNA, COXII mRNA and MRPL45 mRNA upon MRPL45FLala induction.

qPCR was performed on cDNA obtained by HEK239-MRPL45FLala uninduced or induced with 1 µg/mL of tetracycline for 3 days. The level of MRPL45 were evaluated, together with the levels of the 16S mt-LSU rRNA and the mt-encoded COXII mRNA. The results shown were normalised to the cytosolic 18S rRNA. The values correspond to 2 biological repeats.

The expression of MRPL45FLala caused an increase of approximately 6 folds of the total level of MRPL45 mRNA (endogenous + mutated) when compared to the uninduced sample (endogenous), indicating that the expression of the mRNA of MRPL45FLala was successful. No relevant effects were detected on the levels of 16S and COXII mRNA. This result supports the hypothesis of a reduced stability of the mutant protein.

The low steady-state level of MRPL45FLala might be due to a failure of its targeting to mitochondria. It is important to remember that the length of the targeting sequence of MRPL45 (as well as its cleavage) has not been confirmed to date. The mutations generated are located relatively far from the N-terminal, in particular between residues 119 and 136. To confirm the localisation of the mutated protein within mitochondria, cell lysate and mitochondrial lysate were prepared from HEK293-MRPL45FLala induced for 3 days. The presence of the mutant protein within mitochondria would be confirmed by its enrichment (expected of approximately 5 times) in the mitochondrial lysate when compared to the cell lysate. After protein estimation with the Bradford assay, the same amount of cell lysate and mitochondrial lysate was resolved on a 12% SDS-PAGE gel and analysed via western blotting (Fig. 6.12).

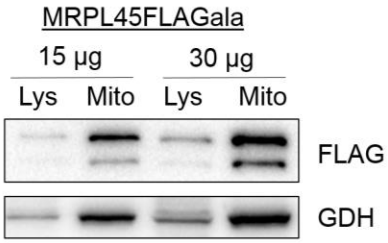

Figure 6.12 Enrichment of MRPL45FLala in mitochondrial lysate.

Western blot analysis was performed on cell lysate and mitochondrial lysate (both ≈15 and ≈30 µg) obtained from HEK293-MRPL45FLala after induction for 3 days with 1 µg/mL of tetracycline. Antibodies against FLAG were used to detect the expression of the mutant protein. The steady state level of the matrix protein GDH were also evaluated. The experiment was not replicated.

A distinct enrichment of MRPL45FLala was observed in the mitochondrial lysate (Fig. 6.12, lanes 2 and 4) when compared to the same amount of cell lysate (Fig. 6.12, lanes 1 and 3). A very similar pattern was observed for the matrix protein GDH, indicating that the FLAG-tagged mutant protein is efficiently targeted to mitochondria.

It is possible that the low steady-state level of MRPL45FLala could be due to a fast degradation of the protein. One of the roles of mitochondrial proteases is degrading misfolded and damaged proteins. Several mitoproteases have been identified to date (Quirós PM et al., 2015). From these, Lon protease homologue (LONP) and Clp protease proteolytic subunit (CLPP) are 2 of the main proteases suggested to be important for quality-control in the mitochondrial matrix. In the attempt to increase the steady state level of MRPL45FLala, depletion of either of these 2 proteases was performed. Because of the importance of proteases in the homeostasis of cells, the depletion was carried out only for 3 days, both on induced cells,

and on induced cells also depleted of MRPL45. The cell lysates obtained at the end of the treatment were analysed via western blotting (Fig. 6.13).

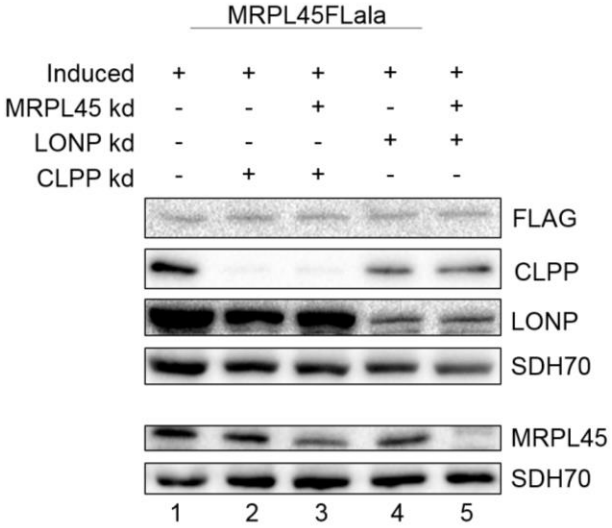

Figure 6.13 Depletion of proteases LONP or CLPP in cells overexpressing MRPL45FLala, in presence or absence of endogenous MRPL45.

HEK293-MRPL45FLala were induced for 3 days and then depleted for 6 days of either CLPP (lanes 2,3) or LONP (lanes 4,5), with or without concomitant depletion of endogenous MRPL45 (lanes 3,5 and 2,4 respectively). The expression of MRPL45FLala was continued during the depletion. Induced cells were also incubated for 6 days with NT-siRNA as a control (lane 1). The cell lysates (≈30 µg) obtained were analysed via western blotting. The level of MRPL45FLala were detected with an antibody targeting the FLAG-tag. The efficiency of the depletions was assessed with antibodies against CLPP, LONP and MRPL45. The level of the nuclear encoded SDH70 were used as a loading control. The experiment was not replicated.

The western blot analysis showed that the depletion of CLPP and LONP were efficient (Fig. 6.13, respectively lanes 2,3 and 4,5). When MRPL45 depletion was present, this was also efficient (Fig. 6.13, lanes 3,5). No effects on the steady state level of the FLAG-tagged protein were detected. Both in presence or absence of endogenous MRPL45, depletion of the proteases CLPP and LONP did not affect the steady state level of MRPL45FLala, indicating that there are not involved in its degradation.

6.3.3. Integration of MRPL45FLala in the mitochondrial large mitoribosomal subunit

The mutations generated on MRPL45 might affect its ability to be integrated into the mt-LSU or to interact with the IMM. To test the first possibility, lysate (700 µg) obtained after 3 days of expression of MRPL45FLala was analysed on a 10-30% isokinetic sucrose gradient to separate the components according to their molecular weight and, therefore, isolate the mitoribosomal subunits. Western blot analysis was performed on 1/10 of each of the 11 fractions collected (Fig. 6.14).

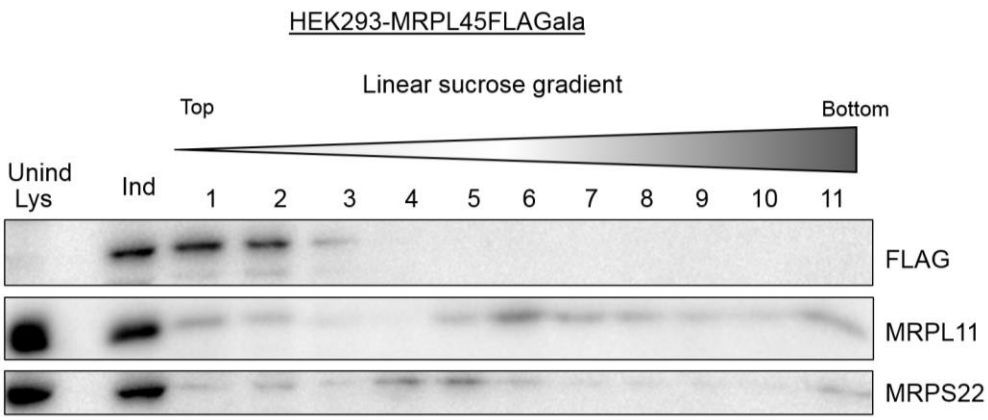

Figure 6.14 Sucrose gradient analysis of HEK293-MRPL45FLala after 3 days of induction.

Cell lysate (≈700 µg) obtained from HEK293-MRPL45FLala after 3 days of induction with 1 µg/mL of tetracycline was analysed on a 10-30% isokinetic sucrose gradient. A proportion (1/10) of the 11 fractions obtained was analysed via western blot, together with ≈40 µg of lysate from uninduced and induced cells. Antibodies against FLAG were used to detect the distribution of the mutant protein. Antibodies against MRPL11 and MRPS22 were used to investigate the distribution in the different fraction of, respectively, mt-LSU and mt-SSU. The figure is representative of 2 biological repeats.

The mt-LSU was identified mainly in fraction 6, while the small subunit was enriched in fractions 4 and 5 (Fig. 6.14). No signal from the FLAG antibody was detected in the fractions corresponding to the mt-LSU and MRPL45FLala seemed to localise mainly in fraction 1 and 2. It is important to remember that, for the overexpression of MRPL45FLAG (Fig. 5.4, page 98), a signal from the fractions corresponding to the mt-LSU was clearly observed when a comparable amount of sample (1/10 of a fraction, from 700 µg of cell lysate loaded on the gradient) was analysed via western blotting. MRPL11 and MRPS22 were used to localise, respectively, mt-LSU and mt-SSU along the sucrose gradient.

Routinely, only 1/10 of every fraction obtained in the sucrose gradient analysis is resolved on SDS-PAGE. Because the steady-state level of MRPL45FLala appeared to be low, I thought possible that the lack of signal in fraction 6 was due an undetectable amount of protein in the sample analysed via western blot. At this purpose, the fractions (from 5 to 8) corresponding to the mt-SSU and mt-LSU in Fig. 6.14 were TCA-precipitated (qv 2.5.3.) to further confirm the absence of the FLAG-tagged protein. The whole resuspended sample was analysed via western blot (Fig. 6.15).

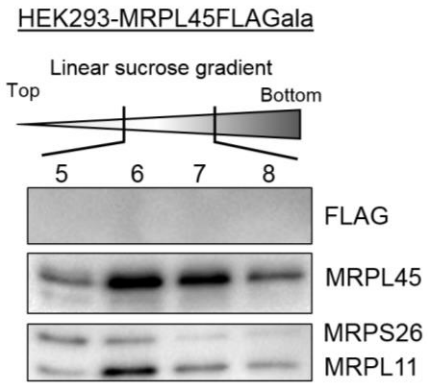

Figure 6.15 Sucrose gradient analysis of fractions 5 to 8 from induced HEK293-MRPL45FLala after TCA-precipitation.

Cell lysate (≈700 µg) was obtained from HEK293-MRPL45FLala after 3 days of induction with 1 µg/mL of tetracycline and analysed on a 10-30% isokinetic sucrose gradient. Fractions 5 to 8 were TCA precipitated and analysed via western blot. Antibodies against FLAG were used to detect the distribution of the mutant protein. Antibodies against MRPL11 and MRPS26 were used to investigate the distribution in the different fraction of, respectively, mt-LSU and mt-SSU.

While MRPL11 and MRPS26 were localised, respectively, mainly in fractions 6 and 5, no signal was detected from the FLAG-antibody in any of these fractions (Fig. 6.15), even at high exposure times (up to 1 minute). Antibodies against MRPL45 confirmed the presence of the endogenous MRPL45 mainly in fraction 6 and 7.

Despite the failure of MRPL45FLala to integrate in the mt-LSU upon induction, I decided to test the possibility of its integration in absence of the endogenous protein. As shown in chapter 3, MRPL45 is essential for assembled mt-LSU. In the absence of this protein, therefore, mitochondria can only assemble mt-LSU by utilising the mutated MRPL45FLala. HEK293-MRPL45FLala cells were induced for 3 days with 1 µg/mL of tetracycline. Cells were then harvested and 1,000,000 cells were seeded in 75 cm^2 flasks. MRPL45 depletion was carried out with siRNA02 at 33 nM for 6 days (reverse and forward transfection, qv 2.1.5.). The expression of the FLAG-tagged mutant protein was continued during the depletion. Because silent mutations have been generated in *MRPL45FLala* in the site targeted by siRNA02 will not be targeted by the siRNA and therefore it will still be expressed. At the end of the treatment, cells were harvested and 700 µg of cell lysate were analysed on a 10-30% isokinetic sucrose gradient. The 11 fractions obtained were TCA-precipitated (qv 2.5.3.) to concentrate the sample and facilitate the visualisation of the FLAG-tagged protein and used for a western blot analysis (Fig. 6.16A). In parallel HEK293 cells were depleted of MRPL45 for 6 days, as an experimental control (Fig. 6.16B).

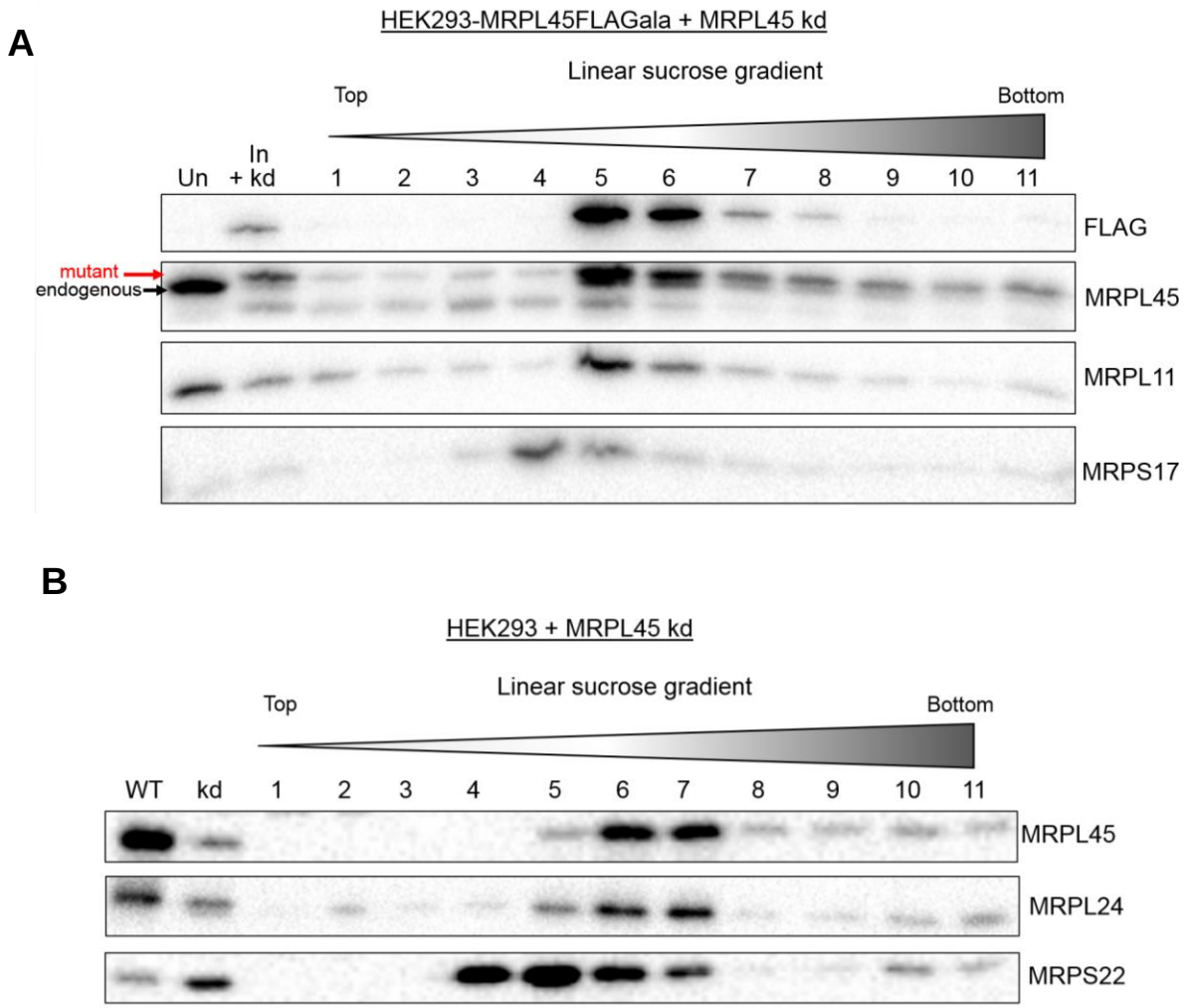

Figure 6.16 Sucrose gradient analysis of HEK293-MRPL45FLala

A) HEK293-MRPL45FLala cells were induced for 3 days and then depleted of MRPL45 for 6 days (siRNA02, 33 nM final concentration), continuing the induction. At the end of the treatment, cells were harvested and 800 µg of cell lysate were separated on a 10-30% isokinetic sucrose gradient. The 11 fractions obtained from the gradient were TCA precipitated and then loaded on a 12% SDS-PAGE gel for western blot analysis. Cell lysate (≈40 µg) from uninduced cells and from the treated cells were also loaded on the gel. The steady state level of the FLAG-tagged protein was detected first. After that, antibodies against MRPL45 and MRPL11 were used to localise the mt-LSU, whereas the mt-SSU was localised with antibodies against MRPS17. The figure is representative of 2 biological repeats. **B)** HEK293 cells were depleted for 6 days of MRPL45 (siRNA02, 33 nM final concentration) were used as an experimental control for A). Cell lysates from untreated HEK293 (WT) and from depleted cells (kd) were analysed via western blotting together with the 11 TCA-precipitated fractions obtained from the 10-30% isokinetic sucrose gradient analysis. Antibodies against MRPL45 and MPRL24 were used to visualise the m-LSU, while antibodies targeting MRPS22 were used to detect the mt-SSU.

The expression of the protein was successful, as shown by the presence of a signal for the FLAG antibody in the lysate from the treated cells (Fig. 6.16A, 'Ind+kd'). Unlike the previous sucrose gradient (Fig. 6.14), a signal from the FLAG-tagged protein was clearly detected in fractions 5 and 6 (Fig. 6.16A) and was co-localised with the signal obtained for the mt-LSU (MRPL11). It is important to notice that no signal for the FLAG-tagged protein was detected in the first fractions of the gradient, suggesting that all the induced protein was completely

integrated in the subunit. The incubation of the western blot in Fig. 6.16A with MRPL45 antibody will detect both the signal due to the endogenous protein and to the induced MRPL45FLala protein. Its detection showed the presence of 3 species. The slowest migrating species, absent in the uninduced lysate, corresponds to the mutant protein, while the intermediate species correspond to the endogenous protein. The most rapidly migrating species represents the N-terminal cleaved MRPL45 (see above). The endogenous MRPL45 was mainly present in the uninduced lysate and hardly detectable in the induced and depleted lysate. Because the signal of the endogenous MRPL45 was weak in the induced and depleted sample, it is possible to conclude that the depletion was efficient. Depletion of MRPL45 reduced the level of this protein as well as the steady state level of MRPL11, when compared to the uninduced and non-depleted sample (Fig. 6.16A, 'Un' and 'In+kd', respectively). The mt-SSU protein MRPS22 was mainly recovered in fraction 4. The control experiment performed on HEK293 cells depleted of MRPL45 showed that, despite the reduction of the steady state level of both MRPL24 and MRPL45 upon depletion, a proportion of these proteins is still located in the mt-LSU (Fig. 6.16B). In both Fig. 6.16 A and B, despite the depletion of MPRL45 being successful, the signal detected for components of the mt-LSU in the western blot analysis appeared relatively strong. It is, indeed, important to remember that every fraction has been concentrated via TCA-precipitation and that a large amount of cell lysate (700 µg) was loaded on top of the gradient.

MRPL45FLala was successfully integrated within the mt-LSU in the absence of the endogenous protein, but no information was available from the previous experiment on the ability of mt-LSU containing MRPL45FLala to form a translating monosome. This was verified on HEK293-MRPL45FLala cells induced for 9 days and depleted of endogenous MRPL45 in the last 6 days of induction. Uninduced cells were also incubated with NT-siRNA or MRPL45-siRNA for 6 days. At the end of the treatment, cells were visualised at the microscope (Fig. 6.17A) and the cell lysate obtained for every sample was analysed via western blot (Fig. 6.17B).

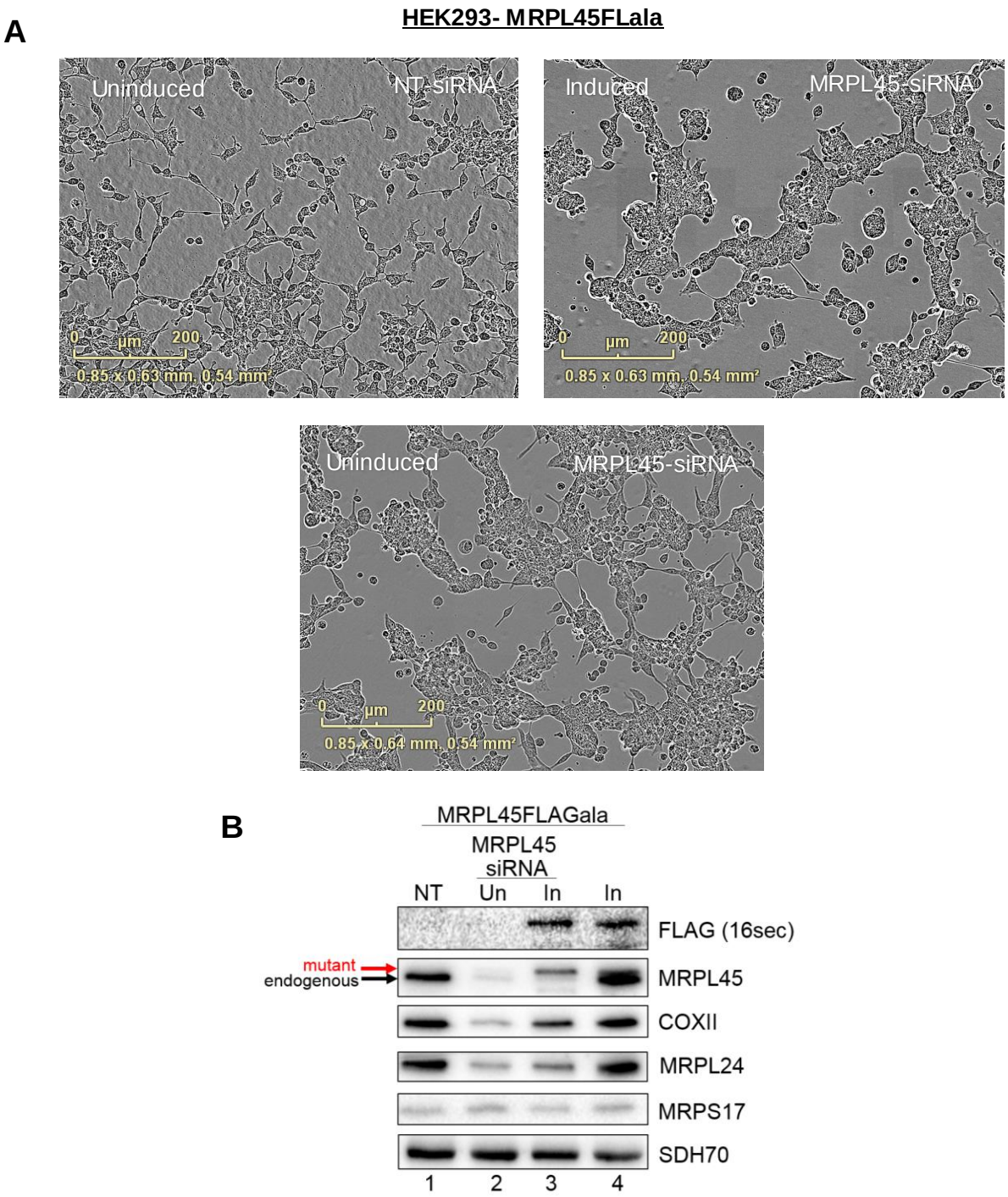

Figure 6.17 Effects on MRPL45 depletion on induced HEK293-MRPL45FLala cells.

MRPL45 depletion was performed using siRNA02 on HEK293-MRPL45FLala uninduced or induced with 1 µg/mL of tetracycline. NT-siRNA was used as a control on uninduced cells. Cells were visualised at the microscope **(A)** and cell lysates was analysed via western blot **(B)**. The efficiency of the induction was assessed with antibodies targeting the FLAG-tag, while the steady-state level of MRPL45 was used to verify the efficiency of the depletion. Antibodies against MRPL24 and MRPS17 were also used to assess the effects on, respectively, mt-LSU and mt-SSU. The steady state level of the mt-encoded COXII was also detected. The IMM protein SH70 was used as a loading control. The results are representative of 2 biological repeats.

The depletion of MRPL45 was efficient, as shown in Fig. 6.17B lane 2 by the reduced steady state level of MRPL45. Although the expression of MRPL45FLala was efficient (Fig. 6.17B, lanes

3 and 4), a long exposure was needed to detect the signal, suggesting the low steady state level of the protein both in presence and in absence of the endogenous MRPL45. It is important to also notice that the steady state level of MRPL45FLala was lower than the level of endogenous MRPL45 present in the sample treated with NT-siRNA (Fig. 6.17B, lanes 3, 1 respectively). As shown in chapter 3, and confirmed by the results obtained in Fig. 6.17B lane 2, the depletion of MRPL45 depletion affects the steady state level of the mt-LSU, leading to an impairment of mitochondrial translation. This phenotype was partially rescued by the expression of the mutant protein, as shown by the increase of the steady state level of MRPL24 and COXII (Fig. 6.17B lane 3), when compared to the sample obtained from the uninduced cell line after depletion of the endogenous MRPL45. This result suggests that the mutations generated on MRPL45 are not affecting the possibility to generate an actively translating monosomes. Despite the partial rescue observed upon expression of MRPL45FLala, the cells were organised in clumps, as observed for MRPL45 depletion on uninduced cells (Fig. 6.17A).

6.3.4. Rescue of MRPL45 depletion phenotype

The previous section showed that MRPL45FLala can be integrated in the mt-LSU and that its expression is able to partially rescue the phenotype observed upon MRPL45 depletion. It is possible that the full rescue was not obtained because of the low steady state level of this protein. To support this hypothesis, a full rescue of the phenotype was attempted by depletion of MRPL45 with siRNA02 in cells able to express MRPL45FLAG from mRNA containing silent mutations in the region targeted by siRNA02. The silent mutations designed are reported in Fig. 6.18. This experiment will also further validate the results obtained with the siRNA used in chapter 3 of this thesis.

Figure 6.18 Silent mutation generated on MRPL45 at the sequence targeted by siRNA02.
Silent mutations (red) were introduced in MRPL45 sequence in the region targeted by siRNA02 (blue). The amino acid sequence correspondent is also reported in bold.

Silent mutations were generated on MRPL45FLAG-pcDNA5/FRT/TO prepared in chapter 4, using site-directed mutagenesis (qv 6.2.1.). The primers used for the reaction were *MRPL45sisilmutsense* and *MRPL45sisilmutanti-s* (Appendix 5). The annealing temperature used was 70ºC, and the extension had a duration of 10 minutes for every cycle. After transformation of the product in supercompetent cells, the colonies obtained were expanded on a fresh LB-agar plate containing 100 µg/mL of ampicillin and then expanded in liquid LB media to perform plasmids extraction. Two of the plasmids obtained were sequenced (qv 2.3.10.) and confirmed the presence of the mutations on the sequence targeted by siRNA02 (Appendix 11).

MRPL45FLsil-pcDNA5/FRT/TO was used, together with pOG44, to transfect HEK293 Flp-In cells and generate a cell line able to overexpress MRPL45FLsil. After antibiotic selection, the expanded single colonies obtained were induced for 3 days with 1 µg/mL of tetracycline. The results for one of the colonies are shown in the following western blot analysis (Fig. 6.19A). The effects of the overexpression on cell growth were monitored over 6 days with the *IncuCyte* system (Fig. 6.19B). The phenotype of the cells after 5 days of expression is showed in Fig. 6.19C.

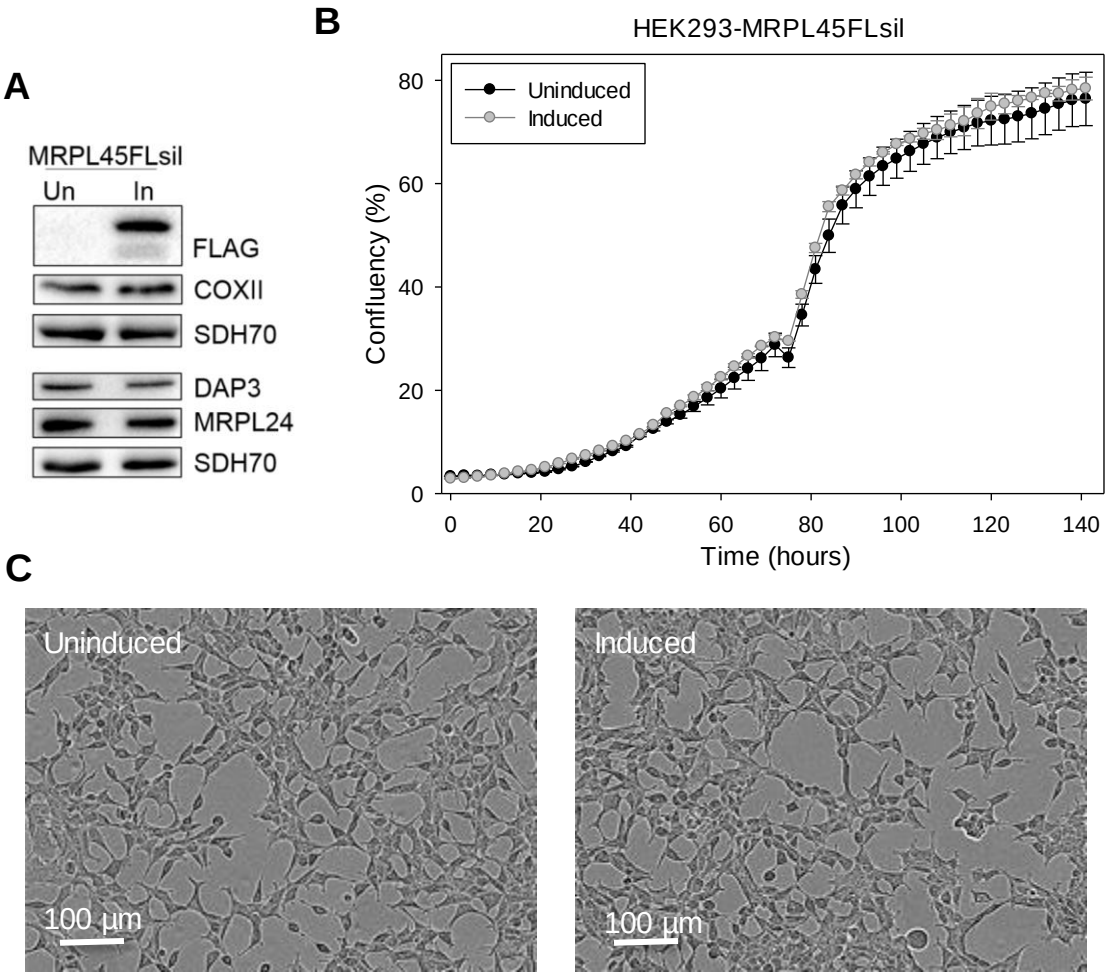

Figure 6.19 Effects of MRPL45FLsil overexpression on mitochondrial proteins and on cells growth.

Western blot analysis **(A)** was performed on cell lysates obtained from HEK293-MRPL45FLsil cells uninduced or induced for 3 days. Cell growth was monitored **(B)** during the induction of MRPL45FLsil for 6 days (2 biological repeats). The effects on morphology after 5 days of overexpression **(C)** are also reported. The results are representative of 3 biological repeats

The expression of the protein was very efficient and no effects were observed on the steady state level of the mitoribosomal protein MRPL24 or the mt-encoded COXII (Fig. 6.19A). The levels of DAP3 appeared slightly reduced in the induced sample. SDH70 confirmed the equality of the loading. Cell growth, evaluated as cell confluence, was also unaffected by the overexpression of the protein over a period of 6 days (Fig. 6.19B).

The levels of overexpression of MRPL45FLsil mRNA were evaluated with qPCR from total RNA extracted from HEK293-MRPL45FLsil uninduced and induced for 3 days with 1 µg/mL of tetracycline. The levels of 18S rRNA, 16S mt-rRNA, COXII mRNA and MRPL45 mRNA were evaluated using the primers in Appendix 5. The data were normalised to 18S rRNA and the results are represented in the following bar graph.

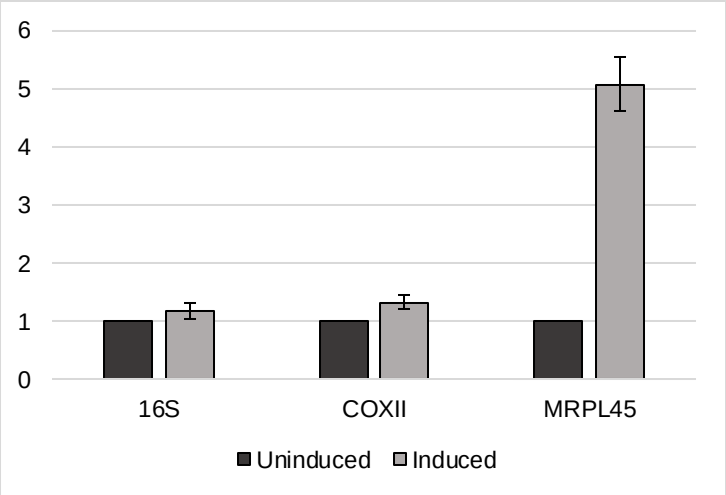

Figure 6.20 Levels of 16s mt-rRNA, COXII mRNA and MRPL45 mRNA after overexpression of MPL45FLsil.

qPCR was performed on cDNA obtained from HEK239-MRPL45FLsil uninduced or induced for 3 days. The level of MRPL45 were evaluated, together with the levels of the 16S mt-LSU rRNA and the mt-encoded COXII mRNA. The results shown were normalised to the cytosolic 18S rRNA. The values correspond to 2 biological repeats.

The qPCR showed an overexpression of MRPL45FLsil of more than 5-folds, a value that resemble the one observed for MRPL45FLala (Fig. 6.20).

The ability of MRPL45FLsil to rescue the phenotype observed for MRPL45 depletion was tested. HEK293-MRPL45FLsil cells were induced for 3 days and then depleted for 6 days with MRPL45 siRNA02, continuing the induction of the FLAG-tagged throughout the depletion. NT-siRNA was used as an experimental control on uninduced cells. To confirm the efficiency of the depletion, uninduced cells were also depleted of MRPL45. At the end of the treatment, cells were visualised at the microscope (Fig. 6.21A). Cell lysates were finally analysed via western blotting (Fig. 6.21B).

A

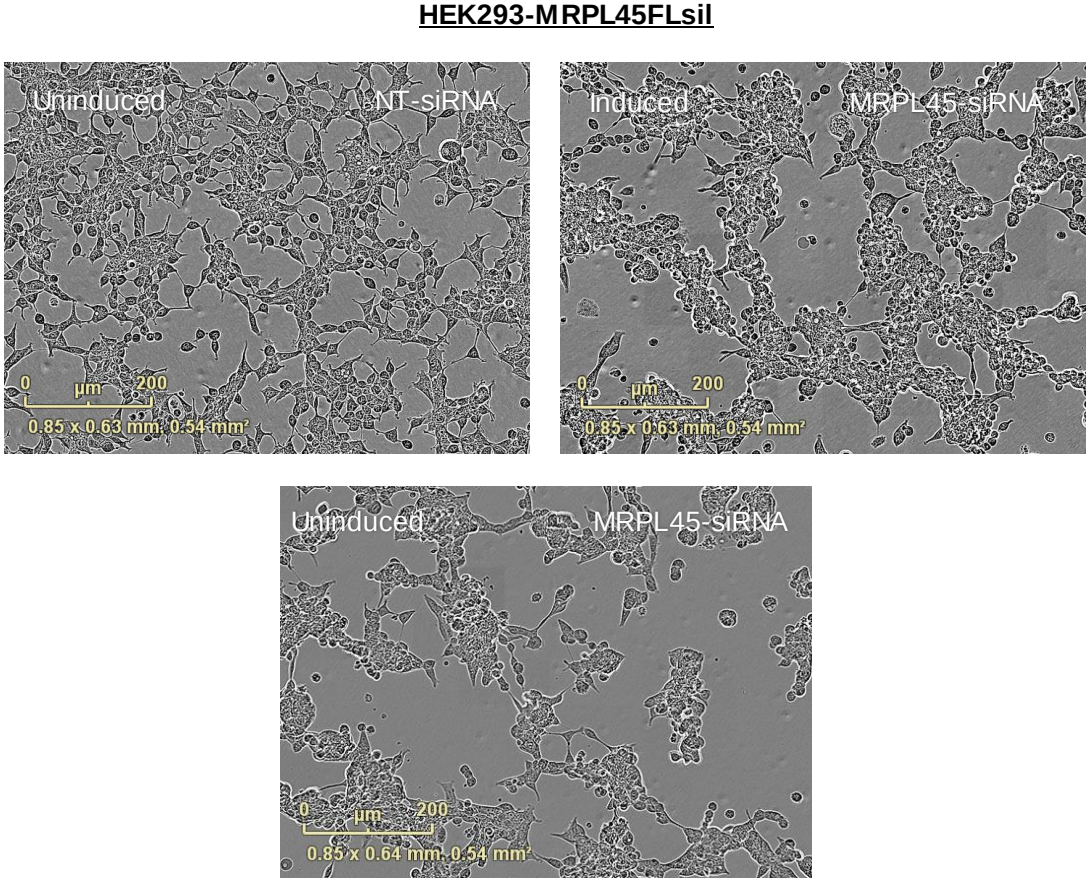

B

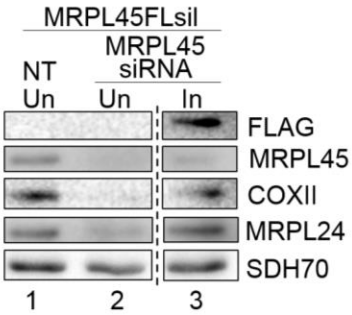

Figure 6.21 Effect of MRPL45 depletion in cells overexpressing MRPL45FLsil.

MRPL45 depletion was performed using siRNA02 on HEK293-MRPL45FLsil uninduced or induced with 1 µg/mL of tetracycline. NT-siRNA was used as a control on uninduced cells. Cells were visualised at the microscope **(A)** and cell lysates was analysed via western blot **(B)**. Antibodies against FLAG-tag were used to confirm the overexpression. The level of MRPL45, MRPL24 and the mt-encoded COXII were also assessed. SDH70 was used as loading control. The data shown are representative of 2 biological repeats. Lane1: NT-siRNA on uninduced cells, Lane 2: MRPL45-siRNA on induced cells, Lane3: MRPL45-siRNA on induced cells. The dashed line indicates the omission of lanes.

The western blot analysis showed that the overexpression of MRPL45FLsil was efficient. Because the FLAG-tagged protein migrates at a higher molecular weight than the endogenous one, it was possible to verify the efficiency of MRPL45 depletion using MRPL45 antibody. The depletion was efficient as indicated by the weak signal detected for MRPL45 (Fig. 6.21B, lane 2, 3). When MRPL45 was depleted in uninduced cells (Fig. 6.21B, lane 2), the level of the tested

mitoribosomal protein and the level of the mt-encoded COXII were also reduced (Fig. 6.21B, lane 2), as previously reported in chapter 3. Upon overexpression of MRPL45FLsil both mitoribosmal protein and COXII were rescued and their steady state level was increased (Fig. 6.21B, lane 3) when compared to the depletion alone. SDH70 confirmed the equality of the loading. On the other hand, the visualisation of cells at the microscope revealed that the overexpression of MRPL45FLsil is not able to completely reverse the effects observed on cells morphology upon MRPL45 depletion because in the induced and depleted sample the cells were still associated in clusters (Fig. 6.21A). It is therefore possible to conclude that MRPL45FLAG containing silent mutations in the region targeted by siRNA02 was able to rescue the phenotype observed for MRPL45, with the exception of the effect observed on cells morphology. This result further validated the effects of MRPL45 depletion on mitoribosomal protein reported in chapter 3.

6.3.5. Interaction of MRPL45FLala with the mitochondrial IMM

Since MRPL45FLala was shown to partially rescue the phenotype of MRPL45 depletion, I decided to investigate the ability of the mutated protein to interact with the IMM. For this, the protocol developed in chapter 4 to allow the investigation of membrane interaction was used.

Because the interaction of the mt-LSU with the IMM might be mediated by other proteins than MRPL45, the ability of MRPL45FLala to directly interact with the membrane was also assessed. For this, HEK293-MRPL45FLala cells were grown in ethidium bromide for 10 days to deplete the assembled mitoribosome. During the last 3 days of treatment, the expression of the mutant protein was induced in 1 µg/mL of tetracycline. At the end of the treatment, mitochondria were extracted and membrane and soluble fractions were separated following the protocol in 4.2.2. Soluble (S) and membrane (P) fractions obtained in absence or presence of detergent were analysed via western blotting (Fig. 6.22).

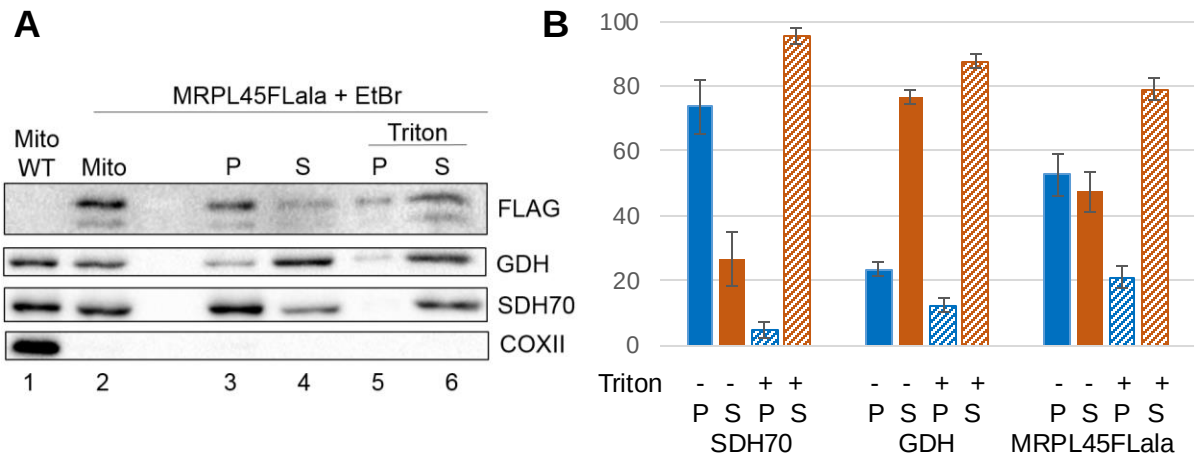

Figure 6.22 Distribution of MRPL45FLala between soluble and membrane fraction in cells incubated with ethidium bromide.

A) Representative figure of western blot analysis performed on samples from membrane-soluble fraction protocol (qv 4.2.2.) performed on HEK293-MRPL45FLala cells incubated with 250 ng/mL of ethidium bromide for 10 days, with induction of the protein during the last 3 days of the treatment. Mitochondria from the treated cells (lane 2) and from HEK293 cells (lane 1) were analysed via western blot together with the membrane (P, lanes 3, 5) and soluble (S, lanes 4, 6) fractions obtained from the protocol in presence or absence of 1.6% Triton. Antibodies against GDH and SDH70 were used to confirm the success of the protocol. Antibodies against COXII were used to confirm the efficiency of the ethidium bromide treatment. The success of the induction and the distribution of MRPL45FLala between soluble and membrane fraction were detected with antibodies targeting the FLAG-tag. **B)** Quantification of 2 biological repeats of membrane-soluble fraction protocol.

The absence of COXII in the mitochondria extracted from HEK293-MRPL45FLala cells after incubation with ethidium bormide confirmed the efficiency of the treatment (Fig. 6.22A, lane 2). The expression of MRPL45FLala was also successful, as confirmed by the presence of a signal from the FLAG antibody in the treated mitochondria (Fig. 6.22A, lane 2). The matrix protein GDH was mainly detected in the soluble fractions (Fig. 6.22A, lanes 4, 6). The IMM protein SDH70 was mainly found in the pellet in absence of detergent and was solubilised in its presence (Fig. 6.22A, lanes 3 and 6, respectively). A proportion of SDH70 was detected in the soluble fraction in absence of detergent (Fig. 6.22A, lane 4). This was observed in every protocol performed on cells treated with ethidium bromide, independently on the marker used to localise the membrane fraction. The detection of the FLAG-tagged protein showed a partial solubilisation in presence of Triton (approximately 30%), suggesting the ability of MRPL45FLala to interact with the IMM. Just above the 20% of MRPL45FLala was detected in the pellet after solubilisation with Triton X-100 (Fig. 6.22A, lane 5). This might be due to aggregation resulting from the heat generated during sonication, used to disrupt the mitochondrial membranes, or to the presence of the protein associating with very large complexes. It is also important to observe that MRPL45FLala was also detected in the supernatant in absence of detergent (Fig. 6.22A, lane 4), suggesting that a proportion of MRPL45FLala is not interacting with the membrane.

The ability of the mt-LSU containing MRPL45FLala to interact with the membrane was also tested. At this purpose, HEK293-MRPL45FLala cells were grown in 75 cm^2 flasks under

induction with 1 µg/mL tetracycline for 3 days, before performing MRPL45 depletion with siRNA02 for 6 days (forward and reverse transfection, qv 2.1.5.). The induction was carried on over the depletion period. At the end of the treatment, cells were harvested, mitochondrial extracted and the interaction of the mt-LSU containing MRPL45FLala was investigated with the membrane-soluble fraction protocol (qv 4.2.2.). The efficiency of the depletion of MRPL45 and of the induction were confirmed by western blot analysis (Fig. 6.23A). A comparable amount of membrane (P) and soluble (S) fractions obtained in absence and presence of 1.6% Triton were analysed via western blotting (Fig. 6.23B). Because the signal expected from the FLAG-tagged protein was expected to be low, twice the usual amount of P and S samples were loaded. The results obtained for different biological repeats were quantified and represented in Fig. 6.23C.

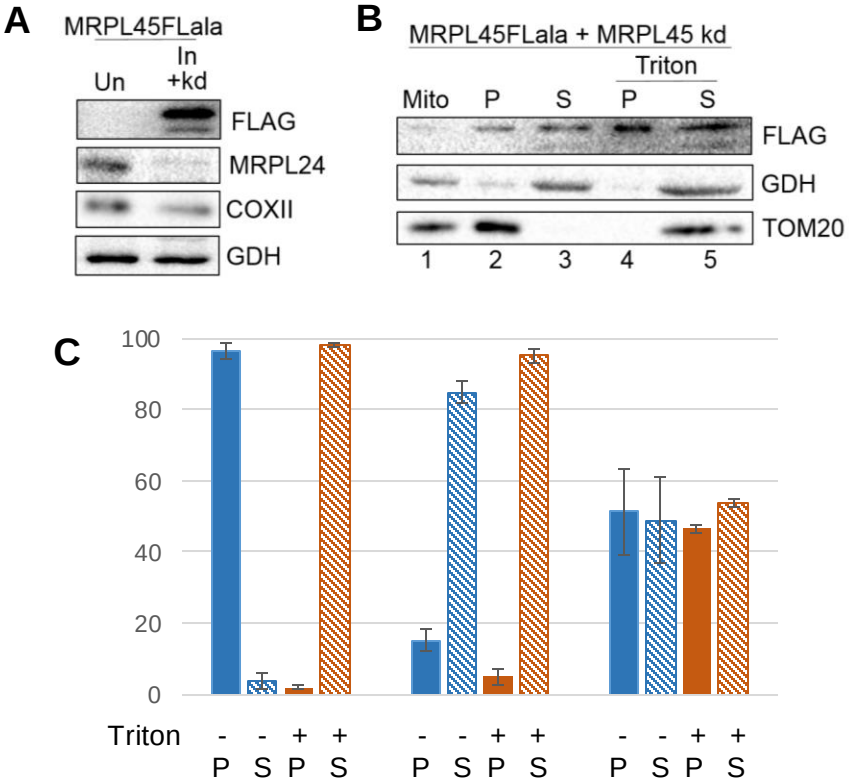

Figure 6.23 Distribution of MRPL45FLala between membrane and soluble fraction in absence of endogenous MRPL45.

HEK293-MRPL45FLala cells were induced for 3 days and then depleted of MRPL45 for 6 days, continuing the induction. Mitochondria were extracted and membrane and soluble fraction were prepared in presence or absence of 1.6% Triton X-100 as in 4.2.2. **A)** Western blot analysis was performed on uninduced and treated cell lysates to confirm the efficiency of the depletion and the induction. Antibodies against the FLAG-tag were used, together with antibodies targeting MRPL24 and COXII. GDH was used as loading control. **B)** Representative figure of western blot analysis was performed for membrane (P, 15 µL) and soluble (S, 30 µL) fractions obtained from the protocol. Mito-lysate (15 µg) was also loaded. The success of the protocol was assessed with detection of a matrix protein (GDH) and a OMM protein (TOM20). The signal from MRPL45FLala was detected with an antibody targeting the FLAG-tag. **C)** Quantification of 2 biological repeats of the membrane-soluble protocol.

The western blot analysis performed on cell lysates (Fig. 6.23A) confirmed the success of the induction, as showed by the presence of a signal for MRPL45FLala. In chapter 3, I reported that depletion of MRPL45 leads to reduction of mt-LSU components, affecting mitochondrial

translation. Because of the reduction in steady state level of MRPL24 and COXII upon depletion of MRPL45 (Fig. 6.23A, 'In+kd'), I deduced that the depletion was efficient. The western blot analysis performed on membrane-soluble fraction protocol (Fig. 6.23B) confirmed the success of the protocol. The matrix protein GDH was detected in the S fractions both in absence and in presence of detergent (Fig. 6.23B, lanes 3,5). The IMM protein TOM20 was only detected in the P fraction in absence of detergent (Fig. 6.23B, lane 2) and was completely solubilised by its addition (Fig. 6.23B, lane 4). This shows that the membrane (and membrane-interacting) proteins were successfully pelleted at the force applied and that the treatment with 1.6% Triton X-100 successfully solubilised the membrane proteins. The signal detected for MRPL45FLala was equally divided between P and S both in presence and in absence of detergent, as also shown quantification of biological repeats (Fig. 6.23C). This result indicates that no significant solubilisation occurred after the addition of Triton X-100. This might be the consequence of aggregation due to the heat generated in the sonication used to disrupt mitochondria. The detection of a signal for MRPL45FLala in the supernatant in absence of detergent (Fig. 6.23B, lane 3) indicates that a considerable amount of the protein (approximately 50%) is not interacting with the membrane.

6.4. Investigation of the importance of the α1 helix of MRPL45

6.4.1. Generation of stable cell lines able to express truncated MRPL45FLAG (MRPL45FLΔ)

As described in paragraph 5.1, it is likely that human MRPL45 presents helix α1 and it is possible that this is involved in the interaction of MRPL45 with the IMM. To test this hypothesis, the first 117 amino acids of MRPL45 were deleted. This truncation will remove the targeting sequence, therefore the Su9 presequence was added to promote mitochondrial localisation. The Su9 presequence is a 69 amino acids presequence of subunit 9 of *Neurospora crassa* F0-ATPase. It has been widely used to target proteins to mitochondria and is double-cleaved in the mitochondrial matrix. Two alanine were added as a spacer between the Su9 presequence and the beginning of the truncated MRPL45. A FLAG-tag was added at the C-terminal of MRPL45, since its addition did not show any effect on the ability of the protein to be integrated in the mt-LSU (Fig. 5.4, page 98) and to interact with the IMM (Fig. 5.6, page 101). This will allow an easier discrimination between the endogenous and the mutated protein.

The Su9 presequence was obtained from a pcDNA5/FRT/TO plasmid containing the insert Su9-RelE, previously prepared in our laboratory by Dr. Dennerlein. Digestion of this plasmid with *BssH*II and *Not*I removed the RelE sequence, that can then be replaced by MRPL45FLΔ. The Su9-RelE- pcDNA5/FRT/TO plasmid was extracted from transformed competent cells and digested at 37ºC for 1 hour with *BssH*II and *Not*I (1 µL each) in a final volume of 20 µL of 1x NEB3 buffer. The efficiency of the digestion was verified on DNA gel electrophoresis (Fig. 6.24). The insert was prepared in a PCR reaction using the primers in Appendix 5 from HEK293 cDNA.

The forward primer (*L45trFrw*) was used to introduce the restriction site (*BssH*II) to join the truncated MRPL45 to the Su9 presequence and the 2 alanine that precede the amino acid 118 of MRPL45. The reverse primer (*L45trRev*) introduced the FLAG-tag sequence at the end of MRPL45 and the second restriction site (*Not*I), needed for the insertion in the digested Su9-pcDNA5/FRT/TO. The insert generated was composed of ≈600 bp. The result of the PCR reaction was visualised on 1.2% agarose gel electrophoresis (Fig. 6.24).

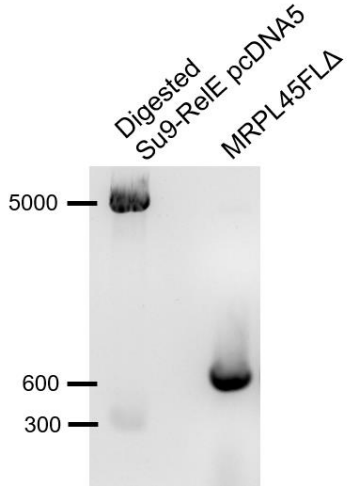

Figure 6.24 Digestion of Su9-RelE-pcDNA5/FRT/TO and preparation of MRPL45FLΔ insert.

The products obtained from digestion of Su9-RelE-pcDNA5/FRT/TO with *Not*I and *BssH*I were separated on a 1.2% agarose gel, together with the result of the PCR reaction set up to prepare MRPL45FLΔ insert with *L45trFrw* and *L45trRev*, using MRPL45FLAG-pcDNA5/FRT/TO as template.

The agarose gel showed the presence of two bands upon digestion of the plasmid. Both the bands corresponded to the expected sizes of the RelE insert (lower band, ≈300 bp) and Su9-pcDNA5/FRT/TO (higher band, ≈5000 bp). The PCR reaction product showed the presence of a band at ≈600 bp, which corresponded to the expected size of the insert. The higher band obtained for the digested plasmid and the band derived from the PCR reaction were excised and the DNA was extracted.

The MRPL45FLΔ insert was ligated into Su9-pcDNA5/FRT/TO (qv 2.3.9.), and the product was used to transform competent cells, as previously described. Prior generation of a cell line able to express MRPL45FLΔ, the insert contained between *BGH* and *CMV* was sequenced (qv 2.3.10.). The sequence obtained confirmed the identity of the construct designed (Apprendix 12), therefore the plasmid was used together with pOG44 to transfect HEK293 Flp-In cells (qv 2.1.6.). After antibiotic selection, single colonies were expanded, prepared for long term storage in liquid nitrogen and used for the following experiments.

6.4.2. Effects of the expression of MRPL45FLΔ

The ability of HEK293-MRPL45FLΔ to express the truncated protein was tested. After 3 days of induction, cells were harvested and cell lysate was analysed via western blotting (Fig. 6.25A).

Cell growth was also monitored every 3 hours over a 6-days period with the *IncuCyte* system (Fig. 6.25B). Cell morphology after 5 days of induction is also shown in Fig. 6.25C.

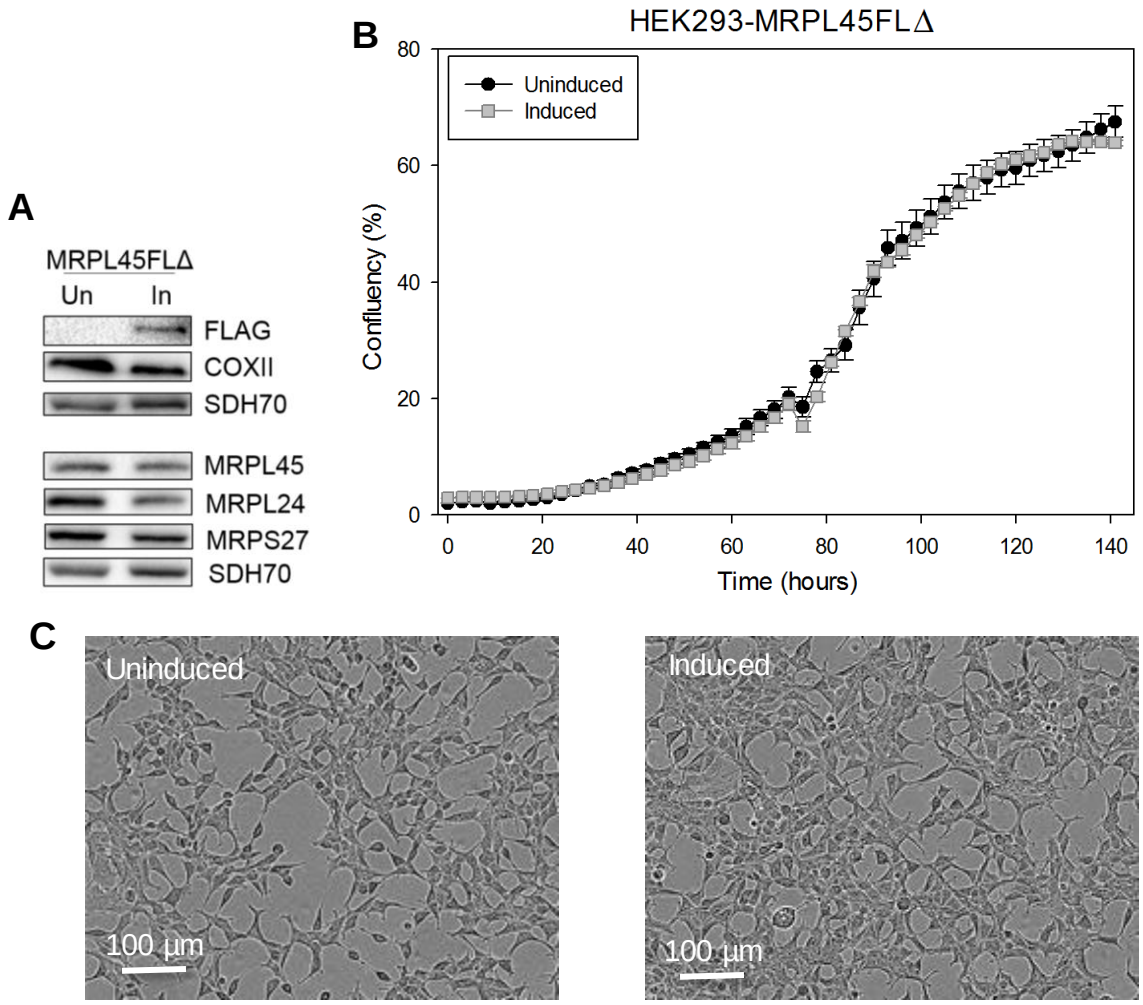

Figure 6.25 Effects of the expression of MRPL45FLΔ on mitochondrial proteins level and cell growth.

Western blot analysis **(A)** was performed on HEK293-MRPL45FLΔ cells expressing the truncated protein after 3 days. Uninduced cells were used as a control. The efficiency of the overexpression was verified using antibody against the FLAG-tag. The steady state level of the mt-encoded COXII, as well as of components of the mitoribosome (MRPL45, MRPL24, MRPS27) were also evaluated. The nuclear-encoded SDH70 was used as a loading control. Cell growth **(B)** was also monitored as confluency every 3 hours over 6 days of induction of MRPL45FLΔ. Cell morphology after 5 days is also shown **(C).** The results are representative of 2 biological repeat.

The expression of the recombinant protein was efficient, although a long exposure needed to detect it. This might indicate that, as observed for MRPL45FLala, the steady state level of MRPL45FLΔ might be low. The levels of COXII and of the mitoribosomal protein tested appeared to be slightly reduced. SDH70 detection showed that the loading was not perfectly equal, suggesting that the induced sample was slightly more loaded. Cell growth was unaffected upon overexpression of MRPL45FLΔ over a 6-days period (Fig. 6.25B). Cell morphology also appeared normal (Fig. 6.25C).

Because the targeting sequence of the endogenous MRPL45 was not present in the truncated version, but instead the protein was targeted to mitochondria using the Su9 sequence, it was necessary to confirm the localisation of the protein in these organelles. At this purpose, cell lysate and mitochondrial lysate were prepared from HEK293-MRPL45FLΔ induced for 3 days, and then loaded on a western blot (Fig. 6.26).

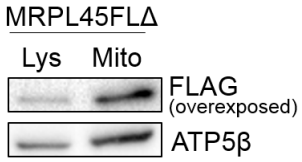

Figure 6.26 Enrichment of MRPL45FLΔ in mitochondria.

The same amount (30 µg) of cell lysate and mitochondria obtained from HEK293-MRPL45FLΔ cells was analysed via western blotting. Antibodies against the FLAG-tag were used to confirm the success of the expression of the recombinant protein. The steady state level of the subunit of complex V ATP5β was also evaluated. The experiment was not replicated.

The mitochondrial fractions clearly showed an increase in the signal detected from the FLAG antibody when compared to the cell lysate. The same pattern was observed for the mitochondrial protein ATP5β, suggesting that the Su9 presequence successfully targets MRPL45FLΔ to the organelle.

The low steady state level detected for MRPL45FLΔ after induction resembles the one observed for MRPL45FLala, as shown in the following western blot analysis of cell lysates obtained from HEK293-MRPL45FLala, HEK293-MRPL45FLΔ and HEK293-MRPL45FLsil after induction for 3 days. Cell lysate from wild-type HEK293 cells was also loaded (Fig. 6.27).

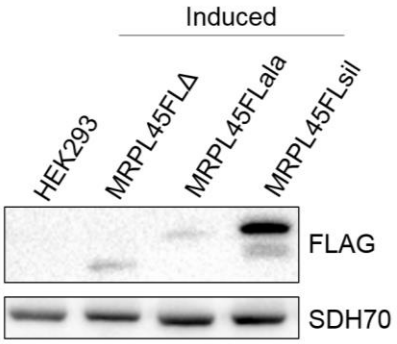

Figure 6.27 Levels of different MRPL45 mutants after 3 days of induction.

Western blot analysis performed on cell lysates (≈30 µg) from HEK293 cells and from induced HEK293-MRPL45FLala, HEK293-MRPL45FLΔ and HEK293-MRPL45FLsil (3 days, 1 µg/mL tetracycline). The steady state levels of the induced proteins were detected with antibodies targeting their FLAG-tag. SDH70 was used as a loading control.

The detection of the FLAG-tagged proteins confirmed that the level of expression of MRPL45FLΔ were similar to the level observed for MRPL45FLala. Both are considerably lower than the one obtained for the FLAG-tagged protein only presenting silent mutations (MRPL45FLsil).

During the detections of the previous western blots, I noticed that the size observed for MRPL45FLΔ was of approximately 30 kDa. This molecular weight matches the size predicted for Su9-MRPL45FLΔ (30.5 kDa) and is considerably bigger than the one expected after cleavage of the Su9 presequence (≈23 kDa). The observed size for MRPL45FLΔ is reported in the following figure.

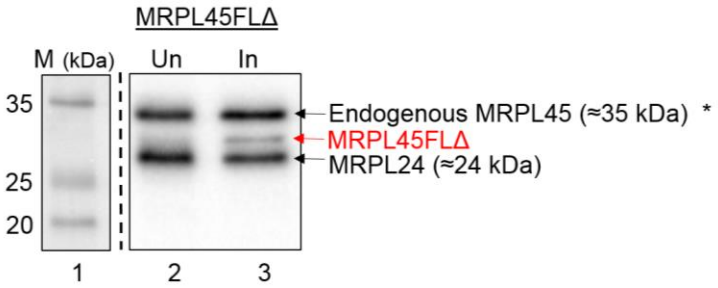

Figure 6.28 Observed molecular weight for MRPL45FLΔ.

Representative figure of western blot analysis of cell lysate (≈30 µg) from uninduced and induced HEK239- MRPL45FLΔ cells. Antibodies against MRPL45 and MRPL24 were used. A proportion of the protein ladder (M, lane 1) was carefully aligned to the western blot to indicate the migration of the species observed.

* = Molecular weight of the full-length product (unknown length of transit peptide)

MRPL45FLΔ was present in the cell lysate obtained from induced cells (Fig. 6.28, lane 1 indicated by the red arrow) and was detected between the endogenous MRPL45 and MRPL24. To date, the length of the transit peptide of MRPL45 is unknown, but the full-length protein is of approximately 35 kDa. The cleavage of the transit peptide of MRPL24, composed of only 9 amino acids, lead to a protein of approximately 24 kDa. These observations suggest that MRPL45FLΔ should have a molecular weight between 35 and 24 kDa, which will be higher that the molecular weight of 23 kDa predicted upon cleavage of the Su9 presequence.

Although the Su9 has been widely used to target proteins to the mitochondrial matrix, I decided to confirm that this presequence is effectively cleaved after the import of the protein. Therefore, MRPL45FLΔ was *in vitro* translated, in order to compare the migration on 12% SDS-PAGE gel with the migration of the protein expressed in HEK293-MRPL45FLΔ detected with the FLAG antibody. The mRNA needed for the *in vitro* translation was prepared by *in vitro* transcription. Su9-MRPL45FLΔ- pcDNA5/FRT/TO was used as a template in a PCR reaction to generate the DNA fragment that was then transcribed to RNA. The forward primer used for the PCR (*SP6-Su9-L45Frw*) contained the SP6 promoter that is used by RNA polymerase to start transcription in vitro, while the reverse primer (*SP6-Su9-L45trRev*) was complementary to the FLAG-tag present at the end of the MRPL45FLΔ construct. The primers used were (Appendix 5). The PCR reaction was carried out as in 2.3.3., using either 65 ºC or 67 ºC as annealing temperature. The products obtained were resolved on a 1.2% agarose gel (Fig. 6.29).

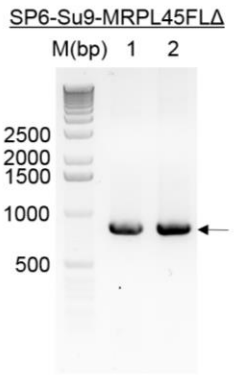

Figure 6.29 Product of PCR to synthesise SP6-Su9- MRPL45FLΔ.

MRPL45FLΔ- pcDNA5/FRT/TO was used as a template in a PCR using the primers SP6-Su9-L45trFrw and SP6-Su9-L45trRev (Appendix 5). Either 65 ºC (lane 1) or 67 ºC (lane 2) were used as annealing temperature. The products obtained were resolved on a 1.2% agarose gel and visualised at the ChemiDoc. The desired product is indicated by the arrow.

Both the annealing temperatures tested efficiently produced a single product of the expected size (831 bp). The product obtained at 65 ºC was purified and then *in vitro* transcribed (qv 6.2.2.). To confirm the efficiency of the reaction, the product obtained (1 µL) was resolved on a 1% agarose denaturing gel (qv 6.2.4.), together with 1 µg and 2 µg of total RNA. The gel was then visualised at the *ChemiDoc* system (Fig. 6.30).

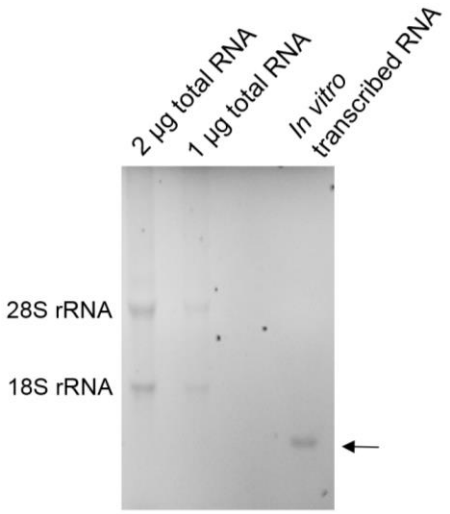

Figure 6.30 Visualisation of the product of *in vitro* transcription of SP6-Su9-MRPL45FLΔ.

In vitro transcription was performed as in 6.2.2. to obtain SP6-SU9-MRPL45FLΔ. The product (1 µL) was resolved on a 1% agarose denaturing gel (qv 6.2.4.) and visualised at the *ChemiDoc*. Total RNA (1 µg and 2 µg) were also loaded on the gel as a reference for size and quantity. The desired product is indicated by the arrow.

The transcription was successful as demonstrated by the presence of a single band in the product of the reaction (indicated by an arrow in Fig. 6.30). The 2 bands detected for the total RNA represented the cytosolic 28S and 18S rRNA, whose approximate sizes are 5 kB and 1.9 kB, respectively. The band observed in the *in vitro* transcription product was lower than the 18S

band, in agreement with the expected size of Su9-MRPL45FLΔ (831 bp), The intensity of the band for Su9-MRPL45FLΔ was comparable with the ones observed for the 2 µg of total RNA, suggesting a high amount of RNA in the sample obtained by *in vitro* transcription.

The Su9-MRPL45FLΔ RNA was used to perform *in vitro* translation (qv 6.2.3.). RNA encoding for mouse Su9-DHFR was also translated as a control. Cell lysates from HEK293 cells and from cells expressing either MRPL45FLAG or MRPL45FLΔ were resolved on a 12% SDS-PAGE gel, together with samples obtained from *in vitro* translation. The gel was divided and the proportion containing the lysates samples was transferred on a PVDF membrane for western blotting, while the remaining part (containing the *in vitro* translated products) was fixed, vacuum-dried and exposed for detection of the radioactive products as described in 5.2.3 (Fig. 6.31). The migration of the protein visualised were compared to the protein ladder.

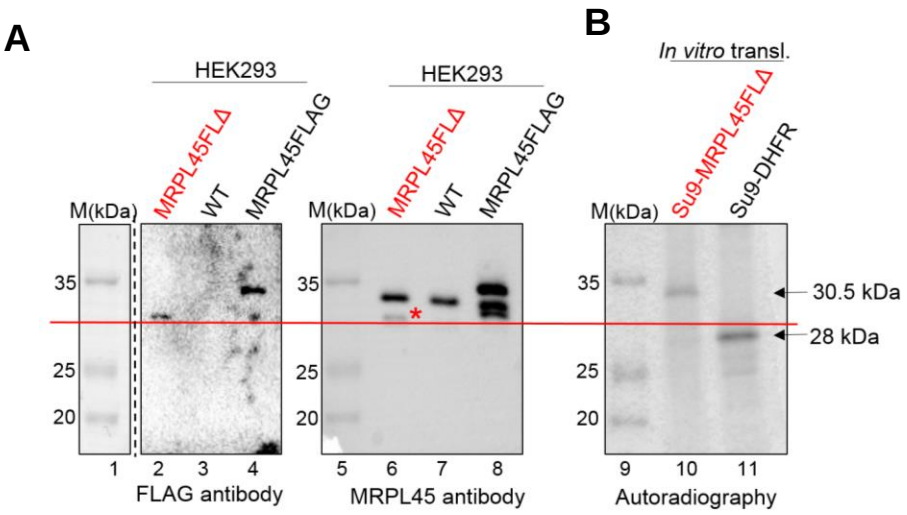

Figure 6.31 Migration of MRPL45FLΔ from cell lysate compared to migration of *in vitro* translated Su9-MRPL45FLΔ.

Cell lysates (≈30 µg) from HEK293, induced HEK293-MRPL45FLΔ and induced HEK293-MRPL45FLAG, as well as the product of *in vitro* translation of Su9-MRPL45FLΔ (1 µL, lane 10) and Su9-DHFR (2 µL, used as a control, lane 11), were resolved via 12% SDS-PAGE. The proportion of the gel containing the lysates was transferred on a PVDF membrane for western blot analysis **(A)**. The efficiency of the overexpression was detected with antibodies against the FLAG-tag (lanes 2, 3, 4). Subsequently, antibodies against MRPL45 were used (lanes 6, 7, 8). The red asterisk represents the induced MRPL45FLΔ in lane 5. The experiment was not replicated.

The proportion of the gel containing the *in vitro* translated products (lanes 10, 11) was fixed overnight and then vacuum-dried. The gel was finally exposed at the PhosphorImage screen to visualise the result **(B)**. The size of Su9- MRPL45FLΔ and Su9-DHFR is also reported. The protein ladders for both the western blots and the radio-labelled detection are also shown (M, lanes 1, 5, 9). Lane 1 was carefully aligned with the detection observed for the FLAG-tag antibody. A red line was drawn just below the MRPL45FLΔ product observed in the protein lysate. The experiment was not replicated.

MRPL45FLΔ was detected with the FLAG antibody (Fig. 6.31A, lane 2, above the red line) and corresponded to a molecular weight of approximately 30 kDa. A signal for MRPL45FLAG was also detected with this antibody just below 35 kDa (Fig. 6.31A, lane 4). The following incubation of the membrane with MRPL45 antibody showed the endogenous protein at

approximately 33 kDa, detected in all the 3 samples (Fig. 6.31A, lanes 6, 7, 8). Upon detection of MRPL45, 2 additional bands were detected in lane 8. Of these, one corresponded to the endogenous protein, while the other is likely to be a cleaved MRPL45, also observed in the previous chapters. The success of the *in vitro* translation was confirmed by the presence of a band above 25 kDa, which corresponded to the expected size of 28 kDa for Su9-DHFR (Fig. 6.31B, lane 11). Concerning the translation of Su9-MRPL45FLΔ, a single species was detected at approximately 34 kDa (Fig. 6.31B, lane 10), when compared to the protein ladder (Fig. 6.31B, lane 9). The molecular weight of Su9-MRPL45FLΔ is of approximately 30.5 kDa, lower than the one observed. This might suggest an inaccurate migration of the protein ladder. Despite this, the migration observed for Su9-MRPL45FLΔ is evidently different for the one observed for the protein induced in HEK293-MRPL45FLΔ cells (Fig. 6.31A, lane 2, also indicate by a red line), suggesting that the Su9 presequence is efficiently cleaved upon import of the protein.

The migration observed for the 30.5 kDa Su9-MRPL45FLΔ (Fig. 6.31B, lane 10) is close to the one observed for the endogenous MRPL45 (Fig. 6.31A, lane 7). As previously mentioned, the exact size of the targeting sequence of MRPL45 is still unknown. *Mitoprot* II, an online tool that calculates the N-terminal protein region that might correspond to the transit peptide (Claros MG et al., 1996), predicted a cleavage site for the presequence 42 amino acids from the N-terminal. This cleavage will lead to a protein of approximately 30 kDa, which appears to be in agreement with the migration observed for the endogenous MRPL45 (Fig. 6.31A, lane 7).

6.4.3. Integration of MRPL45FLΔ in the mitochondrial large mitoribosomal subunit

The ability of MRPL45FLΔ to be integrated in the mt-LSU was verified via isokinetic sucrose gradient analysis, as performed for MRPL45FLala. HEK293-MRPL45FLΔ cells were induced for 3 days and the cell lysate obtained (700 µg) was loaded on top of a 10-30% isokinetic sucrose gradient (qv 2.8.). As for MRPL45FLala, the steady state level of MRPL45FLΔ was very low, therefore the 11 fractions obtained from the sucrose gradient analysis were TCA-precipitated (qv 2.5.3.) and then loaded on a 12% SDS-PAGE and analysed via western blotting (Fig. 6.32).

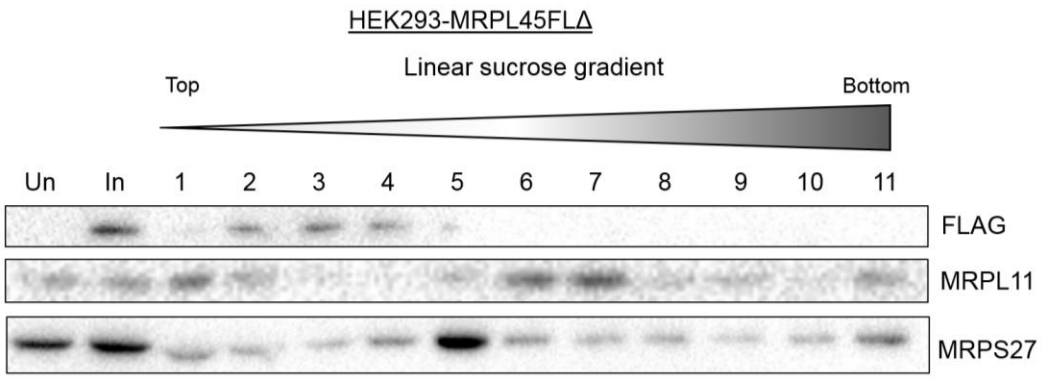

Figure 6.32 Distribution of MRPL45FLΔ on isokinetic sucrose gradient.

Representative figure of western blot analysis performed on the 10-30% isokinetic sucrose gradient analysis of cell lysate (≈700 µg) from induced HEK293-MRPL45FLΔ. The 11 fraction collected were TCA-precipitated, resolved on a 12% SDS-PAGE and analysed via western blotting. Cell lysate from the induced cells (50 µg) was also loaded on the gel. The efficiency of the overexpression was confirmed with antibodies against the FLAG-tag. The distribution of mt-LSU was detected with antibodies against MRPL24 and MRPL11, while antibodies against MRPS27 were used to localise the mt-SSU. Representative of 2 biological repeats.

The western blot analysis showed that the majority of the mutant protein was localised in the first fractions of the gradient. These were not corresponding to the fractions containing the mt-LSU, identified by MRPL11 mainly in fractions 6 and 7 (Fig. 6.32). The mt-SSU was instead localised in fraction 5 by detection of MRPS27.

In section 6.3.3., MRPL45FLala showed the ability to integrate within the mt-LSU in absence of endogenous MRPL45 and to partially rescue the phenotype observed for MRPL45 depletion. The possibility of MRPL45FLΔ to follow the same pattern was tested. The integration of MRPL45FLΔ within the mt-LSU in absence of the endogenous protein was tested via isokinetic sucrose gradient analysis. After 3 days of induction with 1 µg/mL of tetracycline, 1,000,000 HEK293-MRPL45FLΔ cells were seeded in 75 cm^2 flasks and depleted of MRPL45 with siRNA02 at 33 nM for 6 days (reverse and forward transfection, qv 2.1.5.), continuing the expression of the FLAG-tagged mutant protein. The sequence targeted by MRPL45-siRNA02 is localised within the region deleted in MRPL45FLΔ, therefore the siRNA will not target the mutant protein. At the end of the treatment, cells were harvested and 700 µg of cell lysate were analysed on a 10-30% isokinetic sucrose gradient. The 11 fractions obtained were TCA-precipitated (qv 2.5.3.) to concentrate the sample and facilitate the visualisation of the FLAG-tagged protein and used for a western blot analysis (Fig. 6.33A). A proportion (50 µg) of the cell lysate loaded on the gradient was also analysed, together with 50 µg of cell lysate from uninduced HEK393-MRPL45FLΔ. The same experiment was performed on HEK293 cells, as a control (Fig. 6.33B)

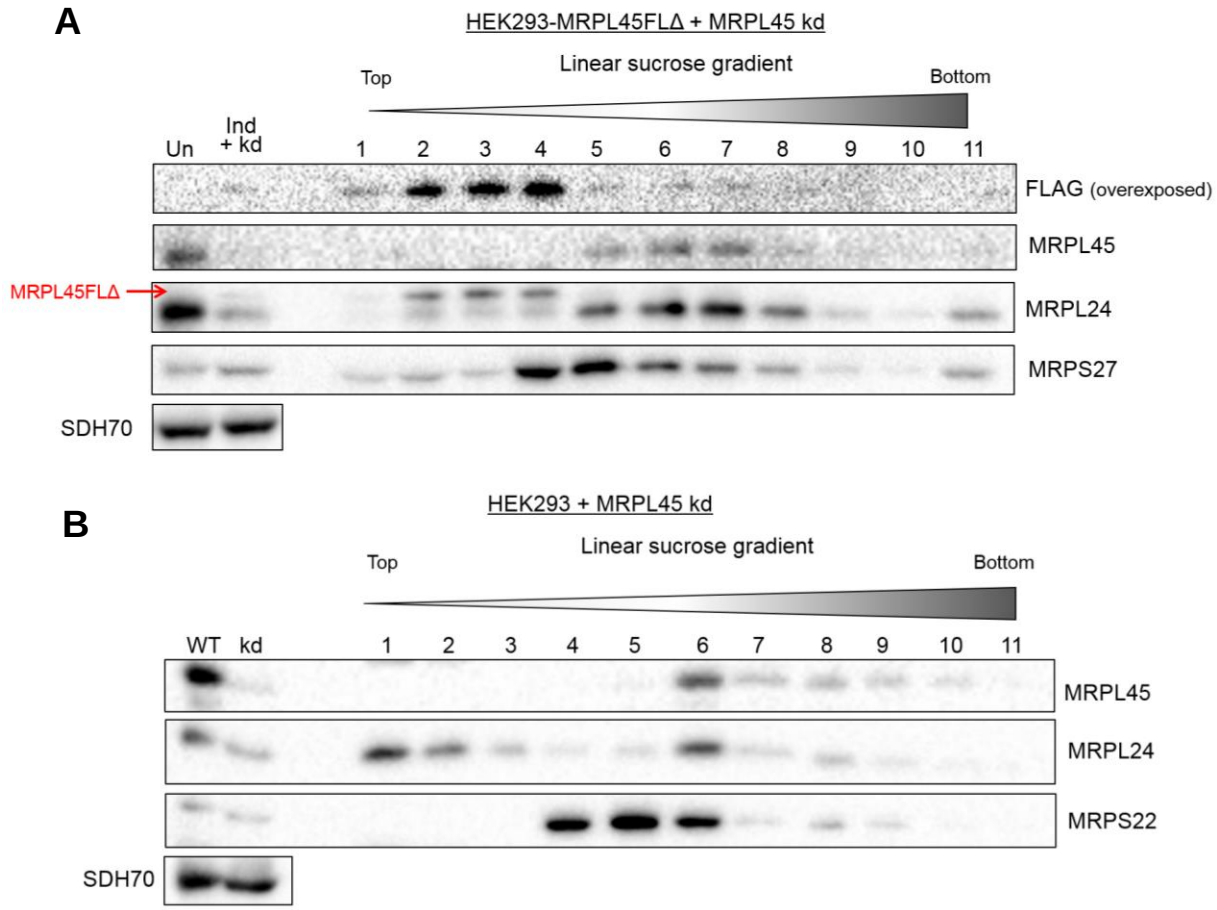

Figure 6.33 Distribution of MRPL45FLΔ on isokinetic sucrose gradient in absence of endogenous MRPL45.

A) HEK293-MRPL45FLΔ cells were induced for 3 days and then depleted of MRPL45 for 6 days (siRNA02, 33 nM final concentration), continuing the induction. At the end of the treatment, cells were harvested and 700 µg of cell lysate were separated on a 10-30% isokinetic sucrose gradient. The 11 fractions obtained from the gradient were TCA precipitated and then loaded on a 12% SDS-PAGE gel for western blot analysis. Cell lysate (≈30 µg) from uninduced cells and from the treated cells were also loaded on the gel. The steady state level of the FLAG-tagged protein was detected first. After that, antibodies against MRPL45 and MRPL24 were used to localise the mt-LSU, whereas the mt-SSU was localised with antibodies against MRPS27. SDH70 was used to confirm the equality of the loading of the cell lysates. The signal obtained from SDH70 thought the gradient was omitted. The figure is representative of 2 biological repeats. **B)** HEK293 cells were depleted for 6 days of MRPL45 (siRNA02, 33 nM final concentration) were used as an experimental control for A). Cell lysates from untreated HEK293 (WT) and from depleted cells (kd) were analysed via western blotting together with the 11 TCA-precipitated fractions obtained from the 10-30% isokinetic sucrose gradient analysis. Antibodies against MRPL45 and MPRL24 were used to visualise the m-LSU, while antibodies targeting MRPS22 were used to detect the mt-SSU. SDH70 was used to confirm the equality of the loading of the cell lysates. The signal obtained from SDH70 thought the gradient was omitted.

The efficiency of depletion was confirmed by the reduction of the steady state level observed for MRPL45 when compared to uninduced and non-depleted cells (Fig. 6.33A). As reported in chapter 3, depletion of MRPL45 led to reduction of assembled mt-LSU. In agreement with this, a reduction of the steady state level of MRPL24 was observed upon depletion of MRPL45. Despite this, a signal form MRPL24 was detected in the sucrose gradient analysis, with an

enrichment in fraction 6 and 7, signalling that a proportion of the mt-LSU was still present (Fig. 6.33A). This can be expected as the depletion of MRPL45 was not complete as a small amount of the protein was still present. In fact, detection of MRPL45 also confirmed an enrichment of this protein in fraction 6 and 7 (Fig. 6.33A). It is important to remember that the fractions of this sucrose gradient have been TCA-precipitated and that, therefore, the signal from detected by MRPL24 and MRPL45 appeared very strong despite their depletion. The control experiment performed on HEK293 cells confirmed the distribution of MRPL24 and MRPL45 observed throughout the gradient upon depletion of MRPL45 (Fig. 6.33B). MRPS27 (Fig. 6.33A), not reduced by the depletion, was localised mainly in fractions 4 and 5, identifying the distribution of the mt-SSU throughout the 10-30% isokinetic sucrose gradient. Detection of MRPL45FLΔ via the FLAG-tag showed that the majority of the protein was localised in fractions 2, 3 and 4 of the gradient. A minor fraction of MRPL45FLΔ appeared to be integrated with the mt-LSU since a weak signal for the FLAG-tagged protein was observed in fractions 6 and 7 (Fig. 6.33A). The presence of the mutant protein in lighter fractions (2, 3, 4) but not in free fraction (1) suggested the possibility that this protein is present in complexes.

The ability of MRPL45FLΔ to rescue the MRPL45 depletion phenotype was also tested. HEK293-MRPL45FLΔ cells were induced for 3 days and then depleted of MRPL45, continuing the expression of the mutant protein. As control, uninduced cells were also treated with either NT- or MRPL45- siRNA for 6 days. At the end of the incubation, cells were visualised at the microscope (Fig. 6.34A) and then the cell lysates were analysed via western blotting (Fig. 6.34B).

A

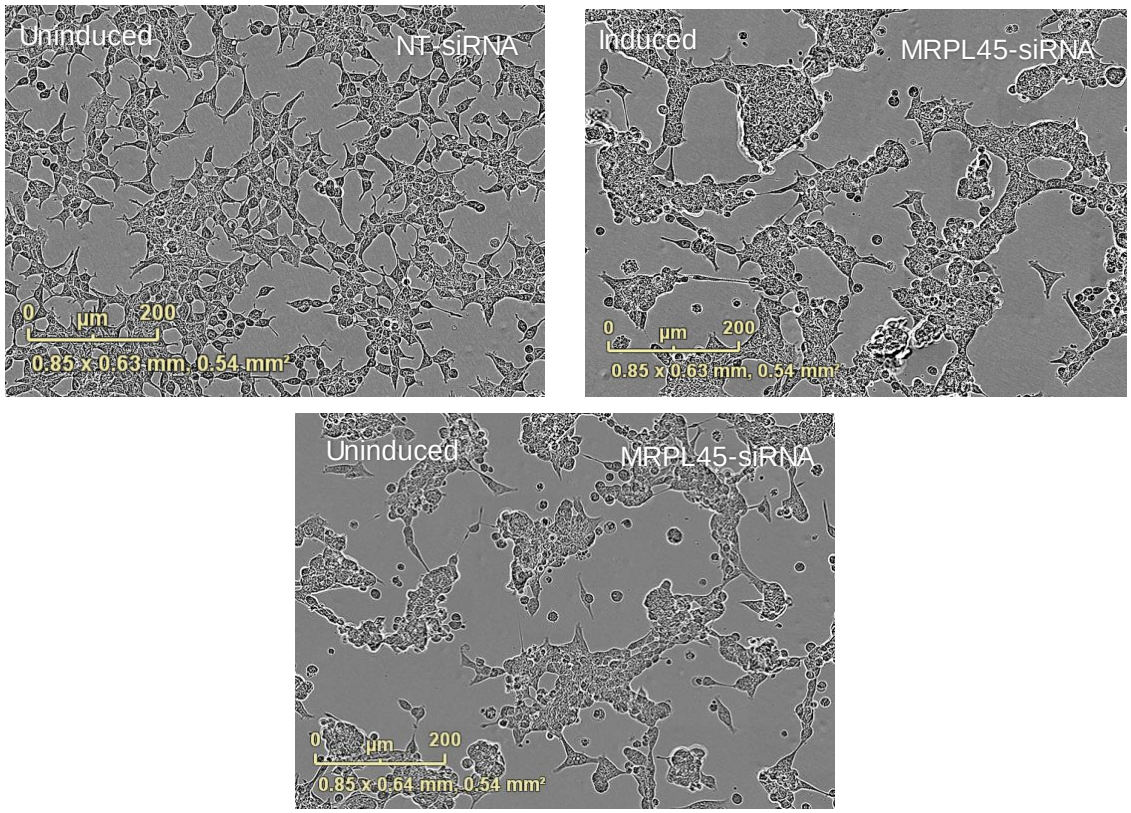

B

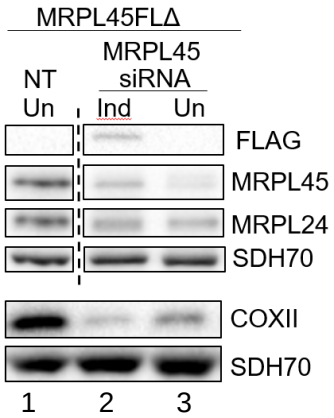

Figure 6.34 Effects of the expression of MRPL45FLΔ in cells depleted of endogenous MRPL45 on cell growth and mitochondrial translation.

HEK293-MRPL45FLΔ cells were induced for 3 days and then incubated with 33 nM MRPL45-siRNA for 6 days, continuing the induction of the mutant protein. In parallel, uninduced cells were also incubated with either NT- or MRPL45-siRNA for 6 days, as a control. At the end of the treatment the cells were visualised **(A)** and cell lysates were analysed via western blotting **(B)**. The efficiency of the overexpression and of the depletion were confirmed with antibodies against the FLAG-tag and MRPL45, respectively. The steady-state level of the mitoribosomal protein MRPL24 and of the mt-encoded protein COXII were also detected. SDH70 was used to confirm the quality of the loading. The results are representative of 2 biological repeats. The dashed line indicates the omission of lanes.

The expression of the mutant protein was confirmed with the detection of a signal from the FLAG-tag (Fig. 6.34B, lane 2). The reduction of MRPL45 steady state level observed confirmed the efficiency of the depletion (Fig. 6.34B, lane 2, 3). No rescue of MRPL24 or COXII, which steady state level was reduced in MRPL45 depleted cells (Fig. 6.34B, lane 3) was observed

upon overexpression of MRPL45FLΔ. The equality of the loading was confirmed by SDH70. This result agrees with a marginal integration of MRPL45FLΔ within the mt-LSU observed upon depletion of endogenous MRPL45 (Fig. 6.33).

6.4.4. Interaction of MRPL45FLΔ with the mitochondrial IMM

To test if the domain of MRPL45 deleted in MRPL45FLΔ was important for the interaction with the membrane, the protocol developed in the previous chapter was performed after expression of MRPL45FLΔ in absence of assembled mitoribosomal subunit. HEK293-MRPL45FLΔ cells were incubated with 250 ng/mL of ethidium bromide for 10 days, with induction of the mutant protein during the last 3 days of the incubation. Cell were harvested, mitochondria were extracted and membrane and soluble fraction were separated following the protocol explained in 4.2.2. Because of the low steady state level of MRPL45FLΔ, twice as much material as usually analysed was loaded on a 12% SDS-PAGE for subsequent western blot analysis (Fig. 6.35).

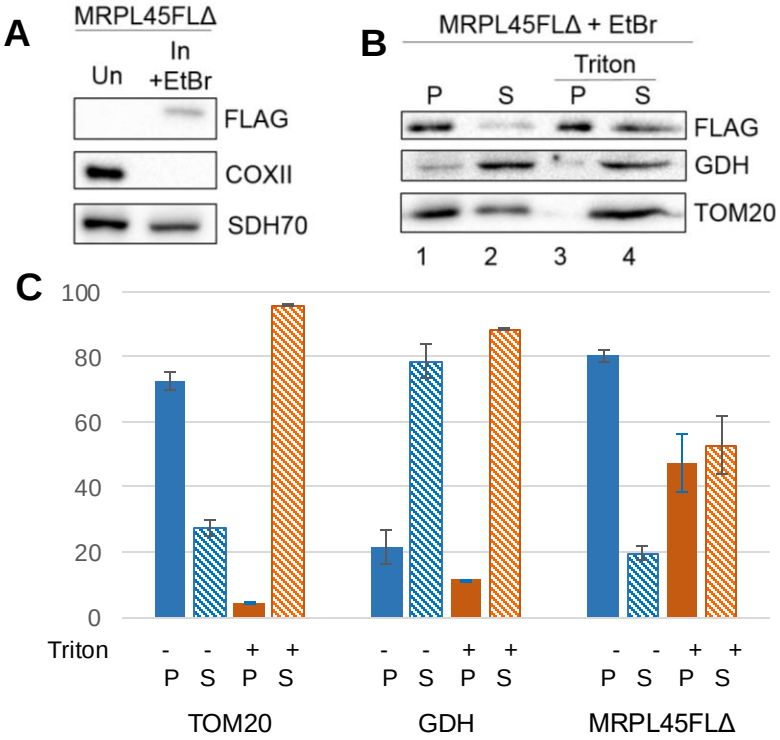

Figure 6.35 Distribution of MRPL45FLΔ between membrane and soluble fractions after treatment of the cells with ethidium bromide.

HEK293-MRPL45FLΔ cells were incubated with 250 ng/mL ethidium bromide for 10 days, with induction of the recombinant protein for the last 3 days. Mitochondria were extracted and membrane and soluble fraction were prepared in presence or absence of 1.6% Triton X-100 as in 4.2.2. **A)** Western blot analysis was performed on uninduced and treated cell lysates to confirm the efficiency of the ethidium bromide treatment as well as the induction. Antibodies against the FLAG-tag were used, together with antibodies targeting COXII. SDH70 was used as loading control. **B)** Representative figure of western blot analysis performed for membrane (P, 15 µL) and soluble (S, 30 µL) fractions obtained from the protocol. The success of the protocol was assessed with detection of a matrix protein (GDH) and the OMM protein TOM20. The signal from MRPL45FLala was detected with an antibody targeting the FLAG-tag. **C)** Quantification of 2 biological repeats of the membrane-soluble protocol.

The western blot analysis of the cell lysates (Fig. 6.35A) confirmed the induction of MRPL45FLΔ. The efficiency of the ethidium bromide treatment was confirmed by the absence of COXII in the treated cells. The membrane-soluble protocol was successful. The matrix protein GDH was mainly detected in the soluble fractions both in absence and in presence of detergent (Fig. 6.35B, lanes 2, 4). The OMM protein TOM20 was used as marker for the membrane fraction. This protein was mainly detected in the pellet fraction in absence of Triton X-100 (Fig. 6.35B, lane 1), although a signal was also detected in the supernatant (Fig. 6.35B, lane 2). This was observed for every membrane-soluble fraction experiment performed on cells incubated with ethidium bromide. Upon treatment with Triton X-100, the OMM protein was completely solubilised (Fig. 6.35B, lane 4). Detection of the FLAG-tagged protein showed a partial solubilisation upon treatment with the detergent, quantified as approximately 30% from different biological repeats (Fig. 6.35C). This result suggests that, despite the absence of 117 residues at the N-terminal, MRPL45 can still interact with the IMM. It is important to notice that approximately the 50% of MRPL45FLΔ was detected in the pellet fraction after incubation with the detergent. Since SDH70 showed that the solubilisation of the membranes was successful, the induced protein might aggregate or be a component of a large complex which is pelleted at the g-force used. In addition, a signal for the mutant protein was detected in the soluble fraction in absence of Triton X-100 (Fig. 6.35B, lane 2), suggesting that a small pool of protein (approximately 20%) did not interact with the membrane.

6.5. Discussion

This chapter focused on the investigation of the domain of MRPL45 putatively involved in the interaction with the membrane. For this, 2 different mutants of MRPL45 were generated and induced in HEK293 cells. The mutations were proposed according to the structural data available on human MRPL45 and on the interaction with the membrane of human and yeast TIM44, which share structural homology with MRPL45.

The first construct, MRPL45FLala, contained mutations in the most protruding domain in the structure of human MRPL45 resolved to date (α2 helix). After induction, the steady state level of the protein appeared very low. The qPCR analysis confirmed that the mRNA level for MRPL45 were increased 6 fold upon induction, suggesting that the low level observed was probably due to instability of the protein. In an attempt to increase the levels of MRPL45FLala, 2 of the main proteases important for quality-control in the mitochondrial matrix (CLPP and LONP) were individually depleted. In both cases, no increase of the level of the mutant protein was observed. Although CLPP and LONP are 2 of the main proteases suggested to be important for quality-control in the mitochondrial matrix, it is not possible to exclude that another protease might be involved in its degradation within mitochondria. It is also possible that the mutant proteins could be degraded in the cytosol after their synthesis, reducing the amount of these proteins targeted to mitochondria.

In presence of endogenous MRPL45, MTPL45FLala was not integrated in the mt-LSU and was found free or in complexes of small molecular weight. When the endogenous protein was depleted, instead, the mutant protein was completely integrated in the mt-LSU. In this scenario, a higher steady state level than the one observed for induction in wild type cells was expected for MRPL45FLala, since the protein was integrated in the mt-LSU and potentially less accessible to degradation from proteases. Instead, no increase in the level of the mutant protein was observed. This might have been due either to a relatively fast turnover of the mt-LSU, which did not allow the accumulation of the subunit containing the mutated protein, or to the lower stability of the mt-LSU containing MRPL45FLala. The lack of integration of MRPL45FLala in presence of the endogenous protein could be due to a less favourable integration of the mutant protein. This will lead to free MRPL45FLala that, consequently, might be quickly degraded, explaining the low steady state level observed for the protein. It is also possible that the integration of the mutant protein was less probable due to its lower abundancy. It will be possible to discriminate between these 2 hypothesis performing a less efficient depletion of MRPL45 (for example by lowering the final concentration of siRNA used) and detect the steady state level of COXII via western blot. If the steady state level of this OXPHOS protein will be lower than in the control sample, the experiment will indicate that a higher amount of MRPL45 will be needed to assemble enough mt-LSU to assure the synthesis of the 'normal' amount of COXII. However, despite this uncertainty, the experiments showed that the mutation of charged amino acids to alanine performed in the α2 helix did not prevent the mutated MRPL45 from its integration in the mt-LSU

When integrated in the mt-LSU, MRPL45FLala was shown to partially rescue the phenotype observed upon depletion of the endogenous protein, suggesting that the mutations generated on MRPL45 are not affecting the possibility to generate an actively translating monosome. The rescue of MRPL45 depletion phenotype was clear, but not complete. The possibility of a complete rescue was confirmed by overexpression of a construct containing silent mutations in the sequence targeted by the siRNA used (MRPL45FLsil). This result also validated the phenotype obtained for MRPL45 depletion in chapter 3. The partial rescue observed by MRPL45FLala might be due to a lower abundancy of mt-LSU available in this condition when compared to wild type cells. In chapter 3, I demonstrated that MRPL45 is necessary for the assembly of the mt-LSU. As a consequence, it is possible that the amount of MRPL45FLala available upon induction is limiting the amount of mt-LSU that can be assembled and that, therefore, not enough mitoribosomes are offered to restore the normal level of mitochondrial translation. A partial rescue was also observed for MRPL24, supporting the idea that a reduced amount of assembled mt-LSU is present.

The ability of MRPL45FLala to interact with the membrane was tested after depletion of mtDNA and, therefore, of assembled mitoribosomal subunits. In this condition, the expressed MRPL45FLala was able to interact directly with the membrane. Solubilisation of the membrane fraction obtained with the membrane-soluble fraction protocol developed in chapter 4 suggested that at least the 30% of the protein is interacting with the membrane. A small proportion of the protein was recovered in the soluble fraction in absence of detergent. This could indicate that the

interaction is transient and that therefore not the whole pool of MRPL45FLala was interacting with the membrane. From this experiment, it was possible to conclude that the mutation of the helix α2 of MRPL45 did not affect the ability of the protein to directly bind the IMM, therefore another domain of MRPL45 is mediating the interaction with the membrane of MRPL45FLala.

The ability of the mt-LSU containing MRPL45FLala to interact with the membrane was also tested. No significant interaction was detected and, upon solubilisation of the membranes with detergent, approximately the 50% of the MRPL45FLala was detected in the pellet fraction. This result suggest that MRPL45FLala is likely to be part of heavy complexes. One possibility is that these complexes could be aggregates formed by the heat generated by sonication, performed on ice and used to disrupt the mitochondrial membranes. It is also possible that MRPL45FLala could be recognised by chaperones while integrated in the mt-LSU, which might associate and increase the molecular weight of the subunit. In addition, the presence of a signal for the FLAG-tag in the soluble fraction in absence of detergent suggested that approximately 50% of the protein did not interact with the membrane, suggesting that the interaction of the mitoribosome might have been compromised. Despite this experiment was not able to show an interaction of the mt-LSU containing MRPL45FLala, the previous experiment performed on induced cells in absence of assembled ribosome clearly confirmed the ability of the mutant protein to interact with the IMM.

Since MRPL45FLala failed in identifying the domain involved in membrane-interaction, I designed a second construct lacking the first 117 amino acids (MRPL45FLΔ). This resulted in the deletion of an α-helix and of a following loop predicted to be present on human MRPL45 and suggested as an interacting point with the membrane for TIM44. The deletion did not included the domain modified in MRPL45FLala. The mitochondria-targeting sequence of MRPL45 was lost with the deletion, but the protein was successfully targeted to mitochondria using the Su9 presequence. The steady state level of MRPL45FLΔ was very low and comparable with the one observed for MRPL45FLala.

During the detection of MRPL45FLΔ I noticed that this migrated at approximately 30 kDa when the protein ladder was used as a reference, a molecular weight which corresponded to the full-lenght Su9-MRPL45FLΔ. I demonstrated that the product containing the presequence migrates at a higher molecular weight, confirming, therefore, that the presequence is efficiently cleaved upon import of the protein. Noticeably, the endogenous MRPL45 migrates at a molecular weight very close to the one observed for Su9-MRPL45FLΔ. A cleavage site for the 35 kDa full-length MRPL45 has not been confirmed to date. This observation suggests that MRPL45 presents a transit peptide of approximately 5 kDa, which is cleaved within mitochondria. This will be in agreement with the predicted cleaving site at approximately 40 residues from the N-terminal of the protein.

In the presence of endogenous MRPL45, MRPL45FLΔ was not integrated into the mt-LSU and was localised in the low-density fractions of the sucrose gradient analysis, suggesting its association within small complexes. Depletion of endogenous MRPL45 in cells overexpressing

MRPL45FLΔ did not severely affect the distribution of the mutated protein in the sucrose gradient analysis, although a small proportion colocalised with the mt-LSU, indicating a possible integration. To support the lack of integration, no rescue of the MRPL45 depletion phenotype was observed upon MRPL45FLΔ expression, as opposed to the partial rescue observed by MRPL45FLala. Despite a signal was present in the free-fraction of the sucrose gradient analysis, the majority of MRPL45FLΔ was recovered in the low density fractions, indicating that the mutant protein might be present in a complex. It is possible that this complex corresponds to a partially assembled mt-LSU. It will be possible to explore this theory with immunoprecipitation studies on HEK293-MRPL45FLΔ cells expressing the protein in absence of endogenous MRPL45.

Despite no rescue was observed upon induction of MRPL45FLΔ in cells depleted of MRPL45, the results obtained from the membrane-soluble fraction protocol suggested that the truncated protein retains the ability to interact with the membrane. The protocol, performed on cells expressing MRPL45FLΔ in absence of assembled mt-LSU, showed that approximately 30% of MRPL45FLΔ is able to interact with the membrane. As for MRPL45FLala, and in the previous chapter for MRPL45wt and MRPL45FLAG, MRPL45FLΔ (≈20%) was detected in the soluble fraction in absence of detergent, suggesting that a proportion of the protein was not interacting with the membrane and that, therefore, the interaction might be transient. In presence of detergent, approximately 45% of MRPL45FLΔ was still present in the pellet, suggesting the presence of aggregates.

The results obtained for MRPL45FLΔ suggest that the protein is not integrated in the mt-LSU, although a small proportion might be integrated in absence of endogenous MRPL45. This cannot be due to a lack of interaction with the IMM, since MRPL45FLΔ retained the ability to interact with the IMM. It is possible that the deleted domain is important to establish interactions crucial for the assembly of the mt-LSU.

Unfortunately, it was not possible to identify the domain of MRPL45 involved in membrane interaction since both MRPL45FLala and MRPL45FLΔ maintained their ability to interact with the IMM. Comparison of the integration of these 2 proteins within the mt-LSU performed by sucrose gradient analysis, suggested that the the domain included in the first 117 amino acids (deleted in MRPL45FLΔ) is important for the assembly of the mitoribosomal large subunit.

Chapter 7: The role of the inner mitochondrial membrane protein OXA1L in mitochondrial translation

7.1. Introduction

The inner mitochondrial membrane is one of the most protein-rich membranes in eukaryotic cells. It is composed of both nuclear and mitochondrial encoded protein, all of which need to be integrated into the membrane itself.

In bacteria, there are inner membrane proteins (IMP) that are inserted co-translationally. The nascent IMP is recognised by a signal recognition particle (SRP) (Keenan RJ et al., 2001), which targets the ribosome to the membrane. The IMP can then interact with the SecYEG complex (Rapoport TA, 2007) that cooperates with YidC membrane insertase to fold, assemble and insert the IMP (du Plessis DJF et al., 2006; Kol S et al., 2009; Scotti PA et al., 2000). It addition to its cooperation with SecYEG, YidC is also able to insert several IMPs (Samuelson JC et al., 2000; van der Laan M et al., 2004) and has been found associated with the ribosome in bacteria (Kedrov A et al., 2013; Kohler R et al., 2009), supporting its role in co-translational insertion.

Mitochondria lack of both SRP and SecYEG complex (Glick BS et al., 1996), but have maintained the ability to insert IMPs in the IMM. In mammals, the only protein known to date to be involved in the insertion of nascent proteins from the matrix of IMP is OXA1L (OXidase Assembly 1-Like). This protein is a member of the YidC/Alb3/Oxa1 membrane protein insertase family (Hennon SW et al., 2015) and it was first identified in yeast as important for the assembly of complex IV (Bonnefoy N et al., 1994; Keil M et al., 2012). Subsequently, Oxa1 was also reported to be important for the assembly of complex V (Altamura N et al., 1996), helping the formation of the transmembrane domain (Jia L et al., 2007). It has been reported that both Oxa1 and YidC are able to dimerise and form pores in the membrane helping the translocation of IMPs (Kohler R et al., 2009; Krüger V et al., 2012). Yeast Oxa1 is suggested to play a role in the insertion of the mitochondrial-encoded Atp6, Atp9, Cox1, Cox2, Cox3 and Cyb, but also appears to have a role in the insertion of nuclear-encoded IMM proteins (Hell K et al., 1998; Hildenbeutel M et al., 2012; Stiller SB et al., 2016). Another member of the YidC/Alb3/Oxa1 family, named Cox18, was shown to be important in yeast for the insertion of the C-terminal of Cox2 (Saracco SA et al., 2002). Its human homologue, (hCox18) shares 25% identity and 45% similarity with the yeast counterpart (Sacconi S et al., 2005) but its role remains unclear.

Because of the role of Oxa1 in the insertion of mt-encoded proteins, it was suggested that this protein is in direct contact with the mitochondrial protein synthesis machinery. This hypothesis was validated by the following studies that showed the co-localisation of Oxa1 with the yeast mt-LSU on sucrose gradients and identified the importance of the C-terminus in this interaction (Jia L et al., 2003). Crosslinking experiments were able to identify the presence in close proximity to Oxa1 of the yeast mitoribosomal proteins Mrp20 (human MRPL23) (Jia L et al., 2003) and Mrp40 (human MRPL24) (Jia L et al., 2009), which are found at the polypeptide exit site (PES) of yeast

mt-LSU. The interaction with the PES would facilitate a seamless integration of the hydrophobic products of mitochondrial translation into the IMM. The ability of Oxa1 to bind the ribosome was also confirmed *in vitro* by Cryo-EM studies that determined the 3D structure of Oxa1 (and YidC) bound to bacterial ribosomes (Kohler R et al., 2009). This study showed that the insertases interact with the ribosome in the proximity of the ribosomal PES and that the positively charged C-terminal domain is involved in this interaction.

The Cryo-EM studies on Oxa1 and YidC suggested a similarity between the structure and function of these proteins. The members of the YidC/Alb3/Oxa1 family are composed of a conserved core of 5 transmembrane helices (Hennon SW et al., 2015) and the human OXA1L is not an exception. This 48 kDa IMM protein also presents a C-terminal domain found in the matrix, which has been cross-linked *in vitro* to the mitoribosomal proteins MRPL13, MRPL20, MRPL29, MRPL48, MRPL49 and MRPL51 (Haque ME et al., 2010). Thanks to the recent release of the structure of the mitoribosome, it is now possible to identify the position of these proteins within the structure (Fig. 7.1). Of these, only MRPL29 is found in close proximity of the PES, a location predicted to be ideal for membrane-interaction. Several of the proteins that form crosslinks are not localised on the surface. None of the interactions with MRPL23 and MRPL24 that were observed for the yeast Oxa1 (Jia L et al., 2003; Jia L et al., 2009), were reported by Haque et al with mammalian mitoribosomes.

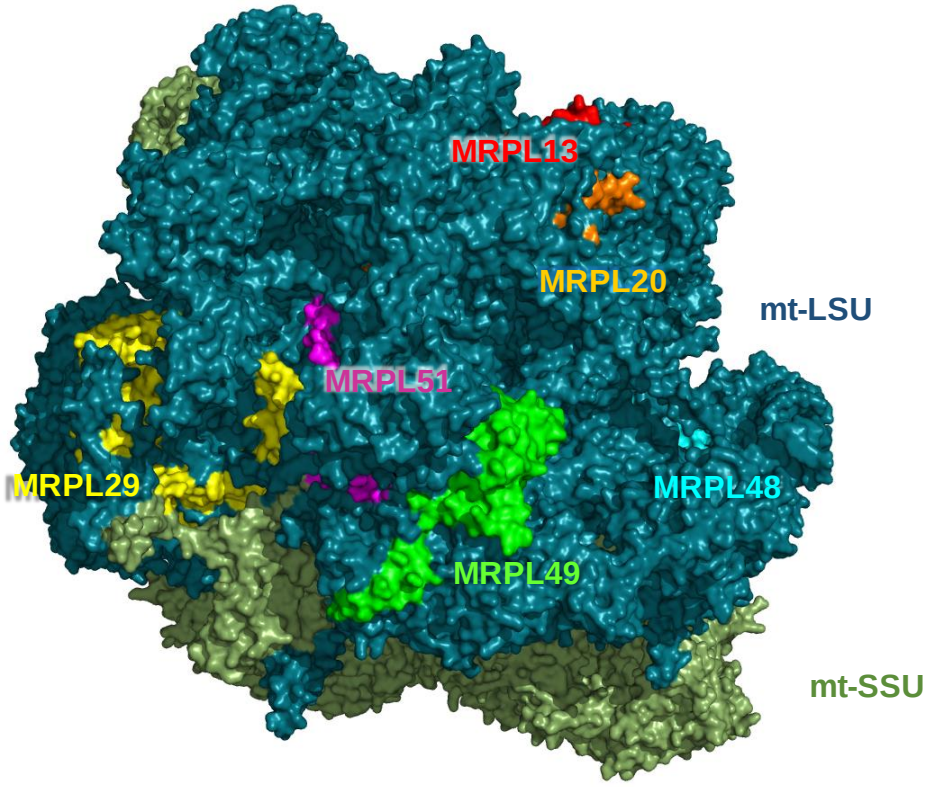

Figure 7.1 Positions of the mitoribosomal protein that co-immunoprecipitated with human OXA1L.

Localisation within the mitoribosome of mitoribosomal proteins that co-immunoprecipitate with OXA1L as reported by Haque et al (PDB 3J9M). The small subunit is depicted in desaturated green, while the large subunit is in blue. Theimmunoprecipitated mitoribosomal proteins are highlighted in different colours (MRPL13=red, MRPL20=orange, MRPL29=yellow, MRPL48=cyan, MRPL49=green, MRPL51=magenta).

Depletion studies of OXA1L in human cell lines suggested the importance of this protein for the assembly of complexes I and V (Stiburek L et al., 2007). OXA1L depletion did not affect the other partially mt-encoded OXPHOS complexes. If this unexpected result will be confirmed, it will suggest that other insertases different from OXA1L must be involved in the insertion of mt-encoded subunits of complex III and IV.

Due to the possibility of a central role of OXA1L in the insertion of the mt-encoded proteins in the IMM and in the interaction with the mitoribosome, I decided to characterise the effects of the depletion of this protein in human mitochondria and to investigate its importance for mitochondrial translation.

7.1.1. OXA1L structure

A better understanding of the structure of OXA1L can be useful to give insight on its function or to infer the importance of particular domains and residues.

Human OXA1L, yeast Oxa1 and bacterial YidC were aligned using Clustal Omega. Oxa1 and OXA1L share 31.44% identity, whereas Oxa1 or OXA1L and YidC share 17.14% and 18.48% identity respectively. It is important to mention that several non-identical residues have maintained a certain degree of conservation of the physical proprieties.

OXA1L is composed of 5 transmembrane helices and a C-terminal domain that protrudes in the matrix and has been reported to be important for the interaction with the ribosome (Table 7.1). Because 3 isoforms of OXA1L have been identified due to alternative splicing, the longer isoform identified as Q15070-1 (435 aa) will be used as a reference.

Table 7.1 Topology of OXA1L.

The analysis was based on the information predicted for the longer isoform of the protein (Q15070-1) by *Uniprot*.

Residues	From – To (aa seq)	Structure/Localisation
1 – 113	MAMG – SFAE	Intermembrane space
114 – 134	LGLG – FMHV	Transmembrane helix (α1)
135 – 139	DLGLP	Matrix
140 – 160	WWGA – PLTV	Transmembrane helix (α2)
161 – 212	TGQR – HGIK	Intermembrane space
213 – 233	LYKP – FFIA	Transmembrane helix (α3)
234 – 260	LREM – TVSD	Matrix
261 – 281	PIYI – ELGA	Transmembrane helix (α4)
282 – 299	ETGV – VIRM	Intermembrane space
300 – 320	MPLI – MYWL	Transmembrane helix (α5)
321 – 435	SSNL – DTLG	Matrix

At present, no structure is available for either mammalian OXA1L or yeast Oxa1. The structure of human OXA1L was predicted Phyre2, and the result is shown in Fig. 7.2.

Figure 7.2 Predicted secondary structure of human OXA1L.

The structure of OXA1L was predicted using Phyre2 on the full length isoform of OXA1L (435 aa) and visualised as cartoon on Pymol. High confidence was obtained in the structure between residues 101 and 331 (blue), due to the similarity with the bacterial protein YidC.

The prediction of the structure of OXA1L between residues 101 and 331 had 100% confidence (Fig. 7.2, blue) and was based on several YidC crystal structures available (Kumazaki K et al., 2014; Kumazaki K et al., 2014; Wickles S et al., 2014). This domain of OXA1L represents ≈25% identity with the YidC sequence. The confidence represents the probability that the match between the sequences analysed and the template is a homology, and does not represent the accuracy of the model. The high-confidence structure corresponds to the transmembrane domain of the protein. Unfortunately, a good prediction could not be obtained for the matrix domain of the protein.

7.2. OXA1L and the interaction with the mitoribosome

As discussed in the introduction of this chapter, the C-terminus of OXA1L protrudes in the matrix and has been crosslinked *in vitro* to a number of mt-LSU proteins. As previously mentioned, all the proteins suggested to interact with OXA1L (Haque ME et al., 2010), with the exception of MRPL29, are distributed at a distance from each other throughout the mt-LSU and not always easily accessible from the solvent. Since this study was performed *in vitro,* I decided to confirm the interaction with mitoribosomal proteins via immunoprecipitation from HEK293 cells. HEK293-MRPL45FLAG cells (qv 5.2) and HEK293 cells with a FLAG tagged MRP protein from the mt-

LSU, ICT1FLAG, were grown in 75 cm^2 flasks and induced for 3 days. At the end of the induction, mitochondria were extracted and the immunoprecipitation was performed via the FLAG-tag (qv 2.9). The elution samples (1/3 of the total volume eluted) were analysed via western blotting (Fig. 7.3). The FLAG-immunoprecipitation was also performed on wild type HEK293 as an experimental control.

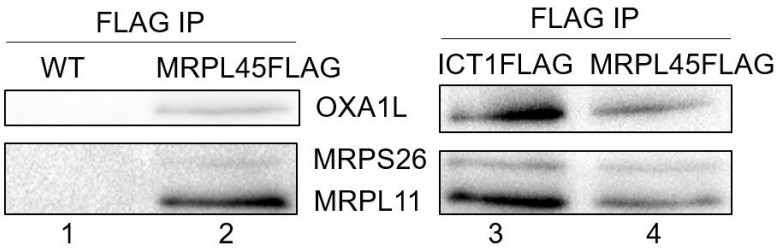

Figure 7.3 Immunoprecipitation of ICT1FLAG and MRPL45FLAG to investigate the potential interaction with OXA1L.

Western blot analysis of the eluted protein (1/3 of the total sample) from FLAG-immunoprecipitation from HEK293 (lane 1), HEK293-ICT1FLAG (lane 3) and HEK293-MRPL45FLAG (lane 2, 4) cells, after 3 days of induction. Wild type HE293 cells were used as a control (lane 1). The presence of the mitoribosome was assessed with antibodies targeting MRPS26 and MRPL11. The steady state levels of OXA1L was also investigated. The figure is representative of 2 biological repeats.

The mitoribosome was efficiently immunoprecipitated both via ICT1FLAG and MRPL45FLAG, as indicated by the presence of MRPL11 and MRPS26. OXA1L was also detected in both samples, confirming its interaction with the mitoribosome. The specificity of the IP was confirmed since no signal was detected from the sample obtained from wild type HEK293 cells (Fig. 7.3, lane 1).

7.3. Effects of OXA1L depletion

OXA1L depletion was performed using siRNA using the lipofectamine technology as for depletion of MRPL45. The siRNA used was a SmartPool composed of a mixture of 4 siRNA (*Dharmacon*, cat no M-012696-00, Appendix 4), in which each siRNA was designed to reduce off target complementarity. To further reduce these effects, the SmartPool mix was used at a final total concentration of 33 nM. Because it is composed by 4 siRNA, each individual siRNA is at the lower concentration (≈8 nM), further reducing the chances of off target effects. The consequences of 6 days OXA1L depletion on U2OS cell growth and morphology was monitored with the *IncuCyte* system (Fig. 7.4). NT-siRNA was used as an experimental control.

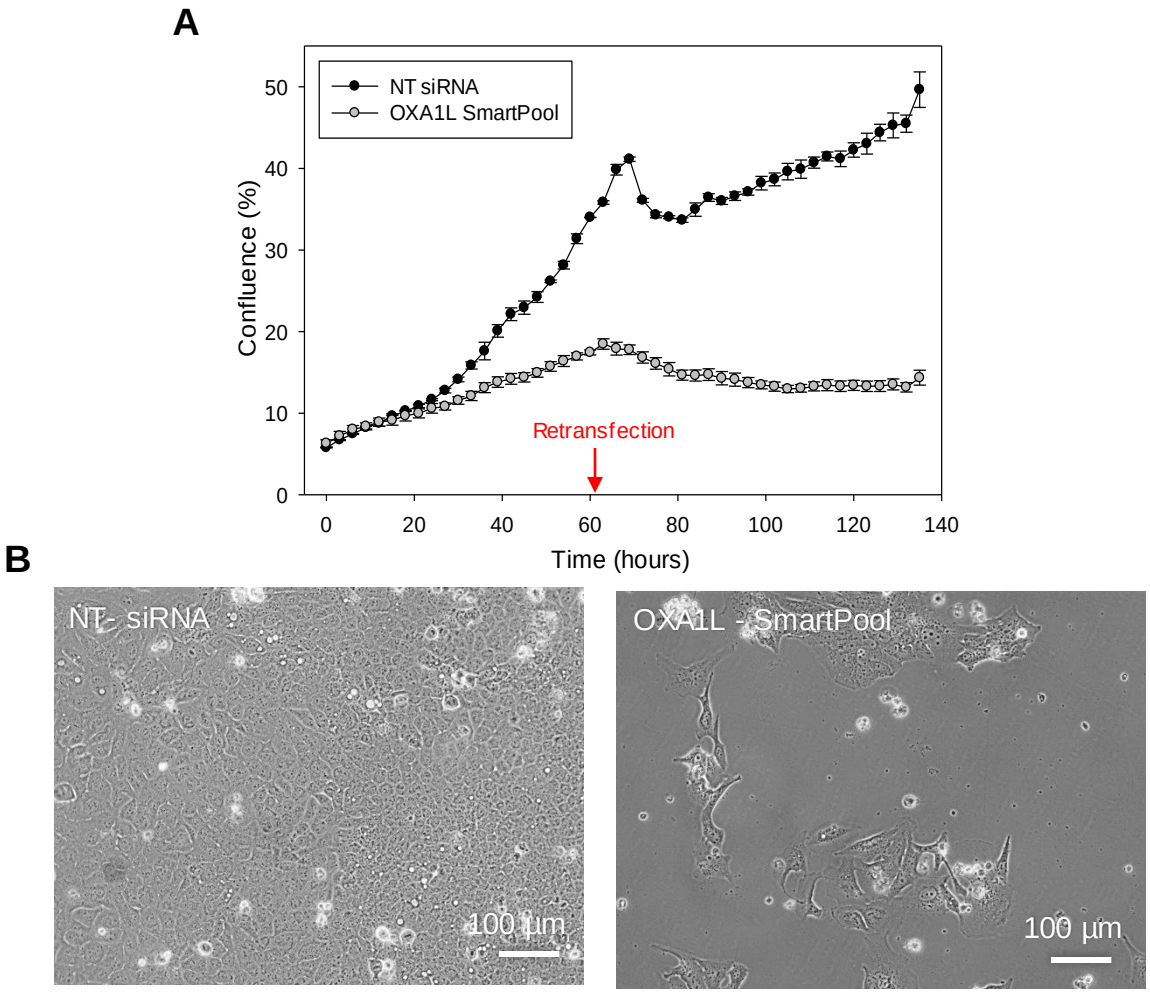

Figure 7.4 Effect on cells growth of OXA1L depletion.

Cell growth was monitored over 6 days of OXA1L depletion by SmartPool siRNA. **A)** Growth was measured as a consequence of cell confluency, calculated by the *IncuCyte* system. The time of restransfection is indicated by a red arrow. **B)** Cells were visualised 6 days after incubation with NT-siRNA or OXA1L siRNA. The images are representative of 3 biological repeats.

OXA1L depletion severely affected cell growth. After 2 days, the cell confluency was decreasing, suggesting cells death (Fig. 7.4A). The severe effect on cells growth was also noticeable from visual inspection of cells (Fig. 7.4B). The steady state level of mitochondrial proteins was then analysed by western blotting (Fig. 7.5).

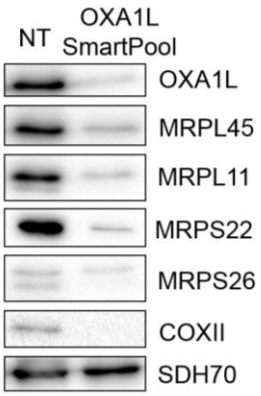

Figure 7.5 Effects of OXA1L depletion on steady state level of mitochondrial protein using SmartPool siRNA.

Representative figure of western blot analysis performed on cell lysate (≈30 µg) after 6 days of incubation with either NT-siRNA or OXA1L SmartPool siRNA. The steady state level of OXA1L and of components of the mt-LSU (MRPL45, MRPL11) and mt-SSU (MRPS26, MRPS22) were evaluated, as well as the steady state level of the mtDNA-encoded protein COXII. Antibodies against SDH70 were used as loading controls. Three biological repeats of the experiment were performed.

The western blot analysis showed a very efficient depletion of OXA1L (Fig. 7.5). This depletion appeared to reduce the steady state levels of mitoribosomal components of both the mt-LSU and mt-SSU, suggesting an instability of the mitoribosome in absence of OXA1L and therefore its possible involvement in the biogenesis of both subunits. As a consequence, mitochondrial translation was affected, as confirmed by the reduced steady state levels of the mt-encoded COXII. The quality of the loading was verified with antibodies targeting the IMM protein SDH70.

Due to the unexpected reduction of the steady state level of both the mitoribosomal subunits observed upon OXA1L depletion, and to disprove the hypothesis of an off target effect, I decided to test the effect of the individual siRNAs present in the SmartPool (Appendix 4). Each siRNA was tested at a final concentration of 33 nM, which is routinely used in our laboratory. U2OS cells were incubated with OXAsi01, OXAsi02, OXAsi03 or OXAsi04 for 6 days (reverse and then forward transfection at day 3). NT-siRNA was used as experimental control. The effects of the depletion on cell morphology and their confluency was monitored over the time course (Fig. 7.6).

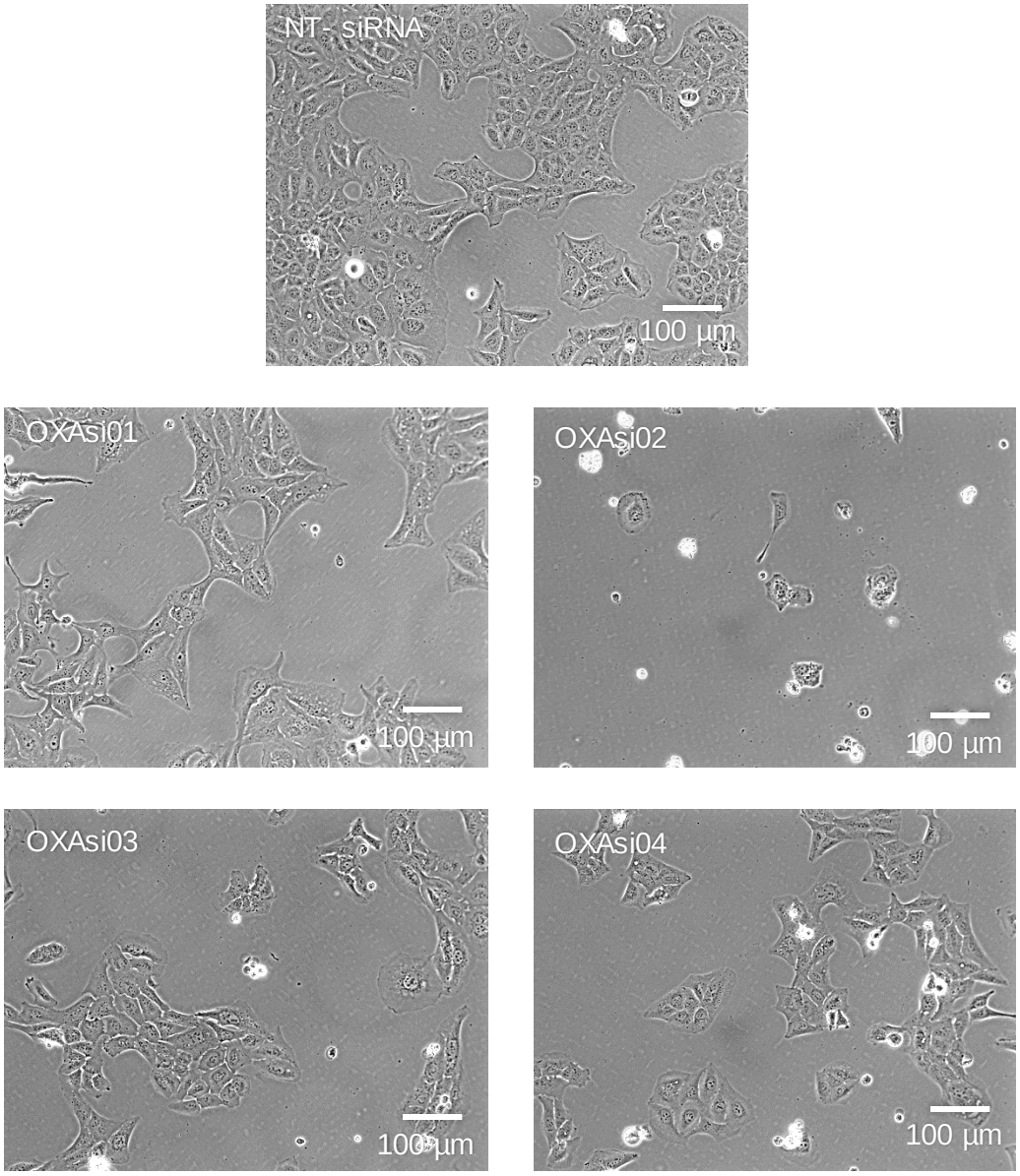

Figure 7.6 Effects on cell growth and morphology of individual OXA1L SmartPool-siRNAs.

Representative figure (2 biological repeats) of U2OS cells depleted of OXA1L for 6 days using 4 different siRNA at the final concentration of 33 nM and visualised at the inverted microscope on day 6.

Examination at the microscope of depleted cells showed a reduction of cell growth for all the tested siRNA, with the most dramatic effect observed for OXAsi02. Cells incubated with OXAsi02 were smaller and round when compared to the one incubated with NT-siRNA.

Since cell growth was affected by OXA1L depletion with all the siRNAs tested, the effects of OXA1L depletion on mitochondrial protein content was analysed via western blotting (Fig. 7.7). The sample obtained from cells treated with OXAsi02 was not enough to allow its analysis with this technique.

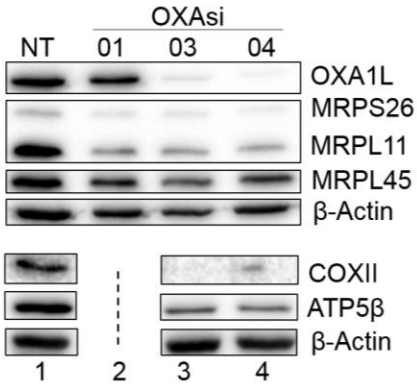

Figure 7.7 Effects of 6 days OXA1L depletion using 3 different siRNAs.

Cell lysates (≈30 µg) following incubation with 3 different siRNAs (33 nM) targeting OXA1L were analysed via western blotting. A representative image of 2 biological repeats is shown. NT-siRNA was used as a control (lane 1). The efficiency of the depletion was verified with antibodies against OXA1L. The effect on the steady state level of the mitoribosomal proteins MRPS26, MRPL11 and MRPL45 was also determined. On a different western blot, the effects of the depletion of OXA1L on ATP5β and COXII levels were detected for cells treated with OXAsi03 and 04. β-Actin was used as a loading control for both the membranes. The dashed line indicates that some lanes were excised from the figure.

A weak signal for OXA1L was detectable in samples obtained from cells treated with OXAsi03 and OXAsi04 (Fig. 7.7, lanes 3, 4), while a strong signal, comparable to the one observed for the NT siRNA was detected for the sample depleted with OXAsi01 (Fig. 7.7, lane 1 vs 2), suggesting the inefficacy of this siRNA. The siRNAs 1, 3 and 4 had a similar effect on the mitoribosomal proteins tested, with a reduction of steady-state level of MRPS26, MRPL11 and MRPL45. Due to the inefficacy of OXAsi01 in depleting OXA1L, it is likely that the reduction of the steady state level observed for mitoribosomal protein with this siRNA (Fig. 7.7, lane 2) was due to an off target effect. OXAsi03 and OXAsi04 also reduced the steady state level of ATP5β, a component of the F1 of complex V.

The off target effects are usually when the complementarity between the siRNA and the target RNA is lower than 100%. Therefore, the off target effects tend to be reduced at lower siRNA concentration. Since the sequence of the siRNAs found in the SmartPool became available after their purchase, the sequences of OXAsi01, 02, 03 and 04 were analysed using BLAST to identify other possible targets different from OXA1L (http://blast.ncbi.nlm.nih.gov/).

OXAsi01 was not successfully depleting OXA1L but showed a reduction of mitoribosomal proteins. The 73% of its sequence also matched *DDX46* and *FBXO38*, involved in splicing and ubiquitination, respectively. In the match obtained, 73% of OXAsi02 showed a 100% identity to *HLF*, which encodes for a protein that regulates a complex involved in upregulation of anti-apoptotic genes and downregulation of pro-apoptotic ones. It is possible that the effect observed on cell growth upon depletion with OXAsi02 was due to the unwanted targeting of the transcript encoding for this protein. OXAsi03 targets *PANK1* mRNA with 73% of query coverage and 100% identity. This protein is involved in the first step of coenzyme A synthesis, important for the metabolism of fatty acids and the oxidation of pyruvate in the citric acid cycle. This siRNA also

targets with 68% of query coverage and 100% identity 2 transcripts encoding proteins that have been suggested to act as transcription activators (*ZNF711* and *SIX4*), although their role is still not confirmed. Finally OXAsi04 had 73% query coverage of *DMRTA1,* which encodes for a protein suggested act as a transcription factor.

To investigate the possibility of off target effects for OXAsi03 and OXAsi04, the depletion of OXA1L was performed at different concentration of siRNA (33 nM, 16 nM and 8 nM) on U2OS cells for 6 days, to identify the lowest siRNA concentration that successfully depletes OXA1L and detect the effects on mitoribosomal protein steady state levels at the different concentrations. Cell growth was monitored via the *IncuCyte* system (Fig. 7.8A) and, at the end of the depletion, cells were collected and analysed via western blotting (Fig. 7.8B).

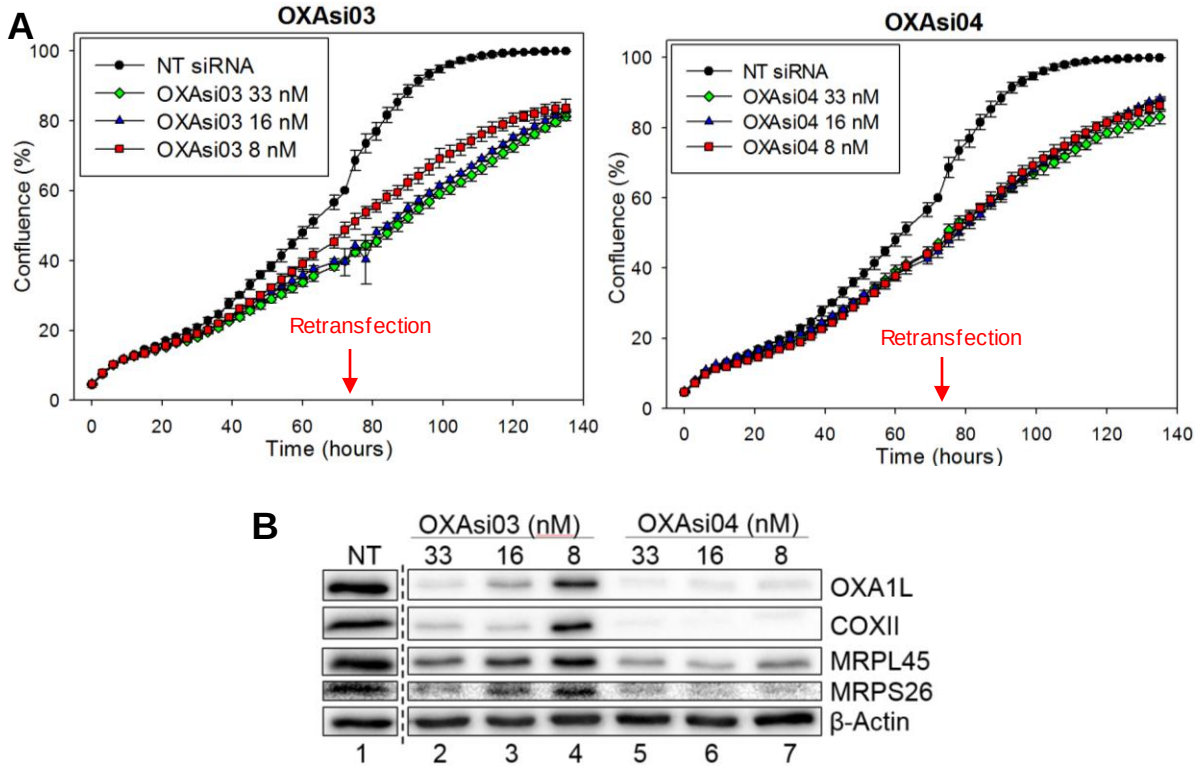

Figure 7.8 Effects of OXA1L depletion using different concentrations OXAsi03 or OXAsi04.

U2OS cells were independently incubated for 6 days with 2 different siRNA targeting OXA1L (OXAsi03, OXAsi04), each at 3 different final concentrations (33 nM, 16 nM and 8 nM). **A)** Cell growth was monitored by cell confluency using the *IncuCyte*. The retransfection time is indicated by red arrows. **B)** Western blot analysis was performed on cell lysate (≈30 µg). The efficiency of the depletion was assessed with antibodies targeting OXA1L. Steady state levels of the mt-encoded protein COXII as well as mitoribosomal proteins MRPL45 and MRPS26 were also visualised. The equality of the loading was controlled using antibodies targeting β-Actin. The figures are representative of 2 biological repeats. The dashed line indicates that some lanes were omitted from the figure.

Cell growth was mildly delayed by both OXAsi03 and OXAsi04, independent of the siRNA concentration used to perform the depletion (Fig. 7.8A). However, western blot analysis highlighted a different efficiency of OXA1L depletion for the concentrations of the 2 siRNA tested. OXAsi03 was very efficient in depleting OXA1L at 33 nM (Fig. 7.8B, lane 2), but the depletion was

lower at 16 nM (Fig. 7.8B, lane 3) and lower still at 8 nM (Fig. 7.8B, lane 4), showing a graded effect. The same trend was observed for the steady state level of COXII, MRPL45 and MRPS26. A higher steady-state level of COXII, MRPL45 and MRPS26 was observed when at 8 nM OXAsi03 (Fig. 7.8B, lane 3) when compared to 16 nM (Fig. 7.8B, lane 4), and the steady state level of the protein tested in the latter was higher than the same protein detected after depletion with 33 nM OXAsi03 (Fig. 7.8B, lane 2). This result suggest that the effect observed on the mitoribosomal protein was related to the efficiency of the depletion of OXA1L, implying that an off target effect with the use of OXAsi03 was unlikely. Concerning OXAsi04, a similar level of depletion and a similar effect on the steady state level of COXII, MRPL45 and MRPS26 was observed at all the concentration tested (Fig. 7.8B, lanes 5,6,7). In particular, COXII was severely reduced, and MRPL45 and MRPS26 were also reduced. Because the use of lower concentrations of siRNA will reduce the chances of off target effects (Caffrey DR et al., 2011), it is unlikely that the effects observed on the mitoribosomal proteins are off target.

Because OXAsi04 was still very efficient at the final concentration of 8 nM, lower concentrations (4 and 2 nM) were also tested. U2OS cells were depleted of OXA1L for 6 days using OXAsi04 at 16, 8, 4 and 2 nM. The results were analysed via western blot (Fig. 7.9).

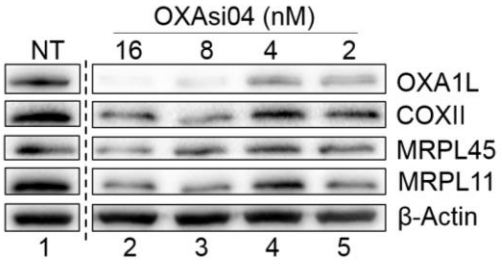

Figure 7.9 OXA1L depletion with OXAsi04 at different concentrations.

Western blot analysis of cell lysate (≈ 30 µg) obtained from U2OS cells incubated for 6 days with OXAsi04 at 16, 8, 4 or 2 nM (final concentration). NT siRNA was used as control. The efficiency of the depletion was assessed with antibodies against OXA1L. The steady state level of the mt-encoded COXII and of the mitoribosomal protein MRPL45 and MRPl11 was also assessed. β-Actin was used as a loading control. The dashed line indicates that some lanes were omitted from the figure. The experiment was not replicated.

The signal detected for β-Actin (Fig. 7.9) suggested that the loading of lane 5 was lower compared to the other lanes. The western blot analysis confirmed the efficiency of OXA1L depletion obtained with OXAsi04 at 8 nM (Fig. 7.9, lane 3). OXA1L was still depleted at the final concentrations of 4 (Fig. 7.9, lane 4) and 2 (Fig. 7.9, lane 5) nM, although the efficiency was lower. As observed for OXAsi03 in Fig. 7.8B, at lower efficiency of depletion (4 and 2 nM, Fig. 7.9, lanes 4,5) a more intense signal for COXII, MRPL45 and MRPL11 was observed, when compared to 16 or 8 nM of OXAsi04 (Fig. 7.9, lanes 2, 3). This result supported the direct correlation between the steady state level of the protein detected and OXA1L, suggesting that the result observed is not due to an off target of the siRNA.

Stiburek et al suggested that OXA1L was important for the assembly of complex I and V (Stiburek L et al., 2007), proposing that the impaired biogenesis of the F1-ATP synthase as a

result of OXA1L knockdown in HEK293 could derive form the impaired assembly or membrane integration of the nuclear-encoded subunit c of F0. In order to investigate this possibility, OXA1L depletion was performed in 143B ρ^0 cells. If the reduction observed for ATP5β was due to a lack of integration of subunit c, a reduction of the steady state level of this component of complex V would be detected in 143B ρ^0 cells.

These cells lack mtDNA but have no growth defect or altered morphology. Their mitochondrial membrane potential is lower than the parental 143B cells and it is maintained mainly by an incomplete F0F1-ATP synthase (Appleby RD et al., 1999; Buchet K et al., 1998), by the adenosine carrier (Buchet K & Godinot C, 1998) and by mitochondrial chloride intracellular channel (Arnould T et al., 2003). If any of these components is inhibited, the membrane potential drops. The complete F0F1-ATP synthase is absent in ρ^0 cells as a consequence of the absence of the mt-encoded subunit ATP6 and ATP8, but the F1 complex is intact in ρ^0 and is present at the same level observed for 143B cells (qv Fig. 3.3, page 59). In ρ^0 cells, about half of the F1 is associated with the IMM, probably through the nuclear-encoded subunit c of F0 (Carrozzo R et al., 2006; García JJ et al., 2000).

OXA1L was depleted in 143B ρ^0 cells for 6 days using OXAsi03 or 04 at the final concentration of 33 nM. Cell growth was monitored during the depletion and the lysate obtained was analysed via western blotting (Fig. 7.10). The reduction in the steady state level of the F1 complex was detected by western blot analysis, although, since the importance of this component to maintain the membrane potential of this cell line, a reduction in its level will affect cell growth.

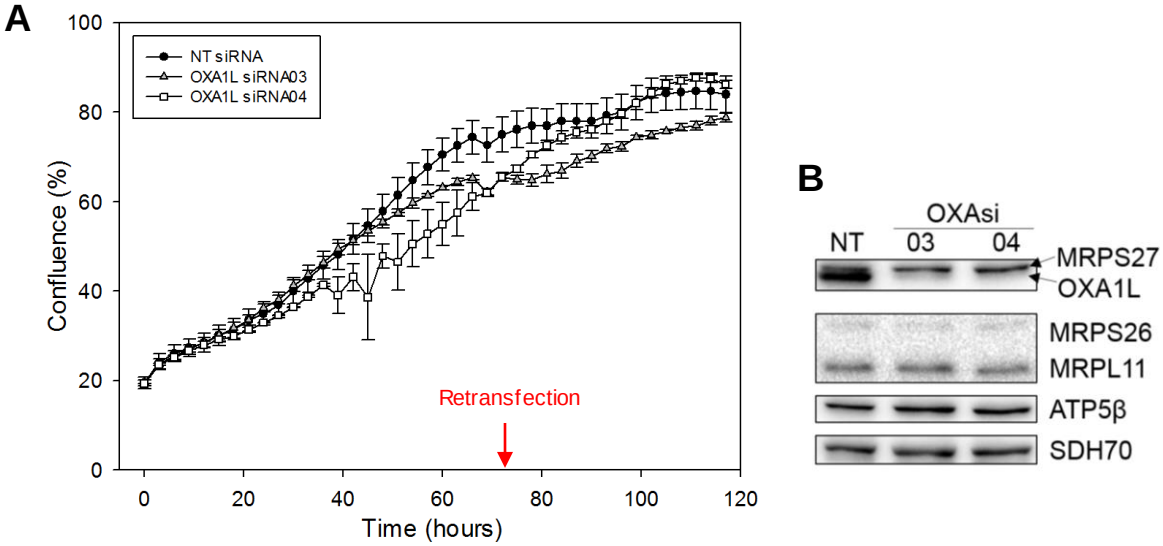

Figure 7.10 Effects of OXA1L depletion in 143B ρ^0 cells.

143B ρ^0 cells were transfected for 6 days with NT-siRNA or OXAsi03/04 at the final concentration of 33 nM. **A)** Representative figure of cell growth, monitored during the depletion as cell confluence using the *IncuCyte* system. The retransfection time is indicated by a red arrow. **B)** Representative figure (2 biological repeats) of western blot analysis performed on cell lysates (≈30µg) obtained after incubation with targeting and non-targeting siRNAs. The efficiency of the depletion was evaluated with antibodies against OXA1L. The steady state level of mitoribosomal proteins (MRPS26, MRP27, MRPL11) was also tested. Antibodies against ATP5β were used to assess the steady state level of the F1 subunit of complex V. SDH70 was used as a loading control.

No effects on cell growth were observed for ρ^0 cells depleted of OXA1L (Fig. 7.10A). The western blot analysis performed on the samples confirmed that the level of OXA1L were dramatically reduced for both the OXA1L siRNA tested (Fig. 7.10B). Depletion of OXA1L did not affect the steady-state level of ATP5β, suggesting that the stability and assembly of the F1 of complex V is not dependent on the insertion by OXA1L of nuclear-encoded components of the F0.

The steady-state level of several mitochondrial ribosomal proteins in ρ^0 cells is lower than the one observed in the parental cell line (qv Fig. 3.3, page 59). Despite this, no reduction in the steady state level of mitoribosomal proteins was observed upon depletion of OXA1L when compared to the NT control. This observation further disproved the possibility that the effect observed on mitoribosomal proteins for OXA1L depletion in U2OS cells was due to an off target effect.

7.4. Confirmation of the absence of off targets effects from OXA1L siRNAs

OXA1L depletion unexpectedly affected both the large and small subunits of the mitoribosome. The previous paragraph suggested that the results observed were not likely to be due to off target effects. In order to confirm the robustness of the results obtained with OXAsi03 and 04, I decided to perform rescue experiments on U2OS cells. If the reduction of the level of mt-LSU and mt-SSU was due to OXA1L depletion, the transfection with OXAsi03 or 04 on cells overexpressing OXA1L should not affect the steady state level of mitoribosomal proteins.

To perform this experiment, OXA1L containing silent mutations at the target sites for the siRNAs (OXA1Lsilmut) needed to be cloned into pcDNA5/FRT/TO, which was then used to perform a stable transfection in U2OS Flp-In cells.

7.4.1. Cloning and overexpression of OXA1L

The OXA1Lsilmut construct was designed personally and synthesised by *GeneArt* (*Thermo Scientific)* (Appendix 6). Silent mutations were performed at the targets for all the 4 siRNAs present in the SmartPool and *Hind*III restriction sites were added at either site of the construct to allow its cloning into pcDNA5/FRT/TO.

OXA1L-pMK-RQ (10 ng) was transformed into bacterial competent cells (qv 2.2.2.) and single colonies were expanded in LB media containing 50 µg/mL of kanamycin. The plasmid was extracted and 2 µg were digested with *Hind*III (qv 2.3.7.) to obtain the OXA1L insert (≈ 1.3 Kb) (Fig. 7.11A). pcDNA5/FRT/TO was also digested with *Hind*III, and then dephosphorylated. The success of the digestion was verified via DNA electrophoresis on 1.2% agarose gel (Fig. 7.11B).

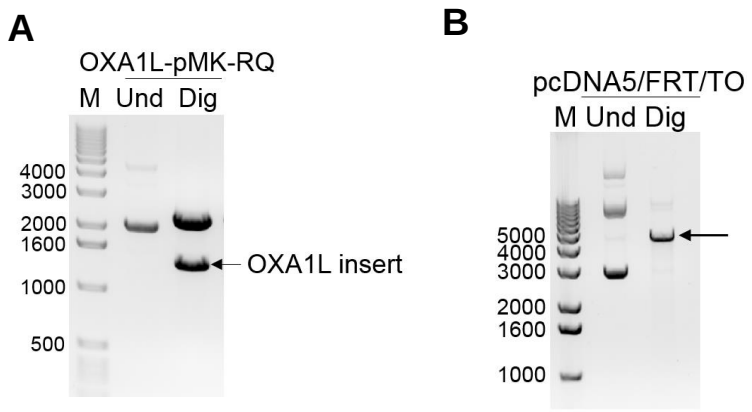

Figure 7.11 Digestion of OXA1L-pMK-RQ and pcDNA5/FRT/TO with *Hind*III.

A) OXA1L-pMK-RQ (2 µg) was digested with *Hind*III at 37°C for 1 hour and then run on a 1.2% agarose gel, together with an undigested sample as control. The lower signal (≈ 1.3 Kb) corresponds to the insert, successfully digested by the restriction enzyme. **B)** pcDNA5/FRT/TO was digested for 1 hour at 37°C. The linearisation of the plasmid was verified on 1.2% agarose gel.

The band corresponded to OXA1L was excised from the gel and the DNA was extracted using the *Qiagen* kit. The insert and the plasmid were then ligated (qv 2.3.9.) and transformed into competent cells (qv 2.2.2.). Single colonies were amplified on a new LB-agar plate and analysed on a cracking gel (qv 2.3.10.) to distinguish colonies containing the plasmid with inserted OXA1L from colonies containing the empty plasmid (Fig. 7.12).

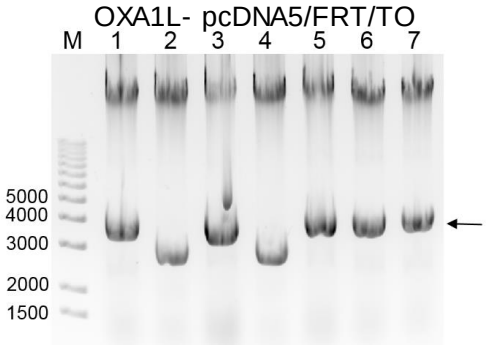

Figure 7.12 Identification of colonies containing OXA1L within pcDNA5/FRT/TO.

Cracking gel technique was performed (qv 2.3.10.) on colonies obtained after transformation of competent cells with OXA1L- pcDNA5/FRT/TO. The gel was visualised to identify colonies containing OXA1L- pcDNA5/FRT/TO plasmid (indicated by the arrow) from colony containing the empty plasmid.

The cracking gel analysis showed the presence of a higher molecular weight species for colonies 1, 3, 5, 6, 7, indicating a larger plasmid likely to contain OXA1L (Fig. 7.12, indicated by an arrow). Since the same restriction enzyme on both sides of the insert a diagnostic digestion was performed to identify colonies containing the insert in the correct orientation. Plasmids extracted from colonies containing the OXA1L insert were digested with *BamH*I. In the case of correct orientation of the insert, the restriction enzyme would digest the insert 523 bases from its beginning, and the plasmid 17 bases from *Hind*III, generating 2 fragments of 842 bp and approximately 5.6 kbp. If the insert was present in the wrong orientation, the digestion would result in 2 fragments of 540 bp and approximately 5.9 kbp (Fig. 7.13).

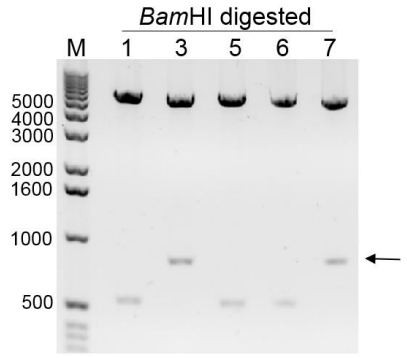

Figure 7.13 Diagnostic digestion of OXA1L-pcDNA5/FRT/TO.

Plasmids (500 ng) extracted from colonies presenting OXA1L insert within pcDNA5/FRT/TO were digested with BamHI to identify the colonies containing the insert in the right orientation. The products of each digestion (2 µL) were resolved on a 1.2% agarose gel. The arrow indicates the expected size of the fragment obtained by the digestion of OXA1L-pcDNA5/FRT/TO containing the insert in the correct orientation.

Because the OXA1L insert, commissioned to *Geneart* (*Thermo Scientific),* was sequence verified by the company, the plasmid was directly used to transfect U2OS-FlpIn cells, together with pOG44 (qv 2.1.6.). After selection in hygromycin^{B} and kanamycin, colonies were isolated and tested for the ability to overexpress OXA1L. After 3 days of overexpression, cells were lysed and the protein content analysed via western blotting (Fig. 7.14A). Cell growth upon overexpression of OXA1L was also monitored for 6 days (Fig. 7.14B).

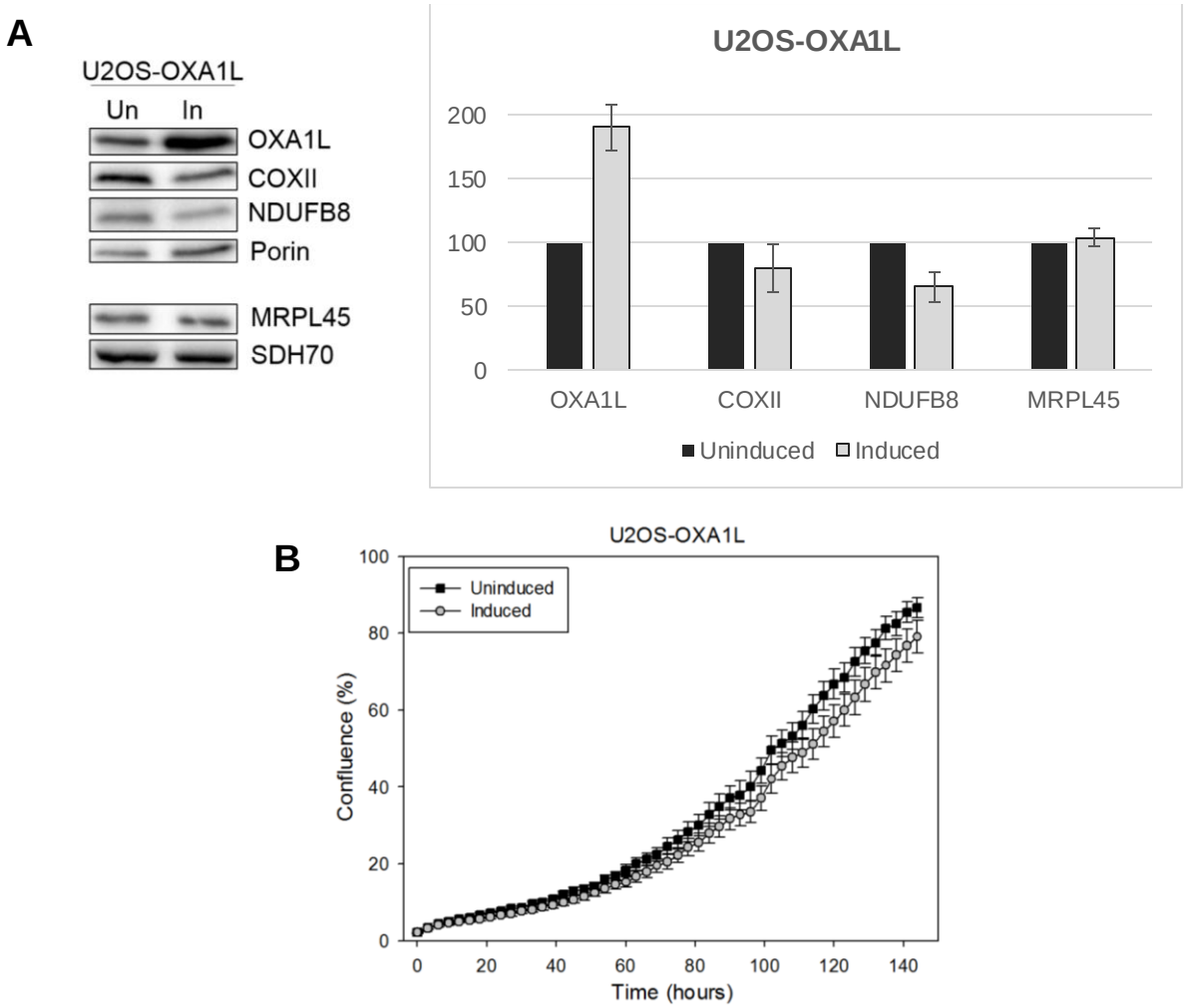

Figure 7.14 Effects on mitochondrial protein of OXA1L overexpression in U2OS cells.

A) Western blot analysis performed on U2OS-OXA1L cell lysate after 3 days of overexpression of OXA1L. Cell lysate from uninduced cells was also analysed. Antibodies against OXA1L were used to confirm the induction. The steady state level of the OXPHOS components COXII and NDUFB8 was also detected, as well as the level of the mitoribosomal protein MRPL45. Porin and SDH70 were used as a loading control. The bar graph shows the quantification obtained from 3 biological repeats. **B)** Cell growth of uninduced or induced U2OS –OXA1L. Cell growth was represented as confluence, measured over 6 days every 3 hours by the *IncuCyte* system. The data presented are representative of 3 biological repeats.

The detection of OXA1L confirmed the efficiency of the overexpression (Fig. 7.14A). The induced sample presented a reduction of the levels of COXII and NDUFB8 when compared to the uninduced control. The steady-state level of MRPL45 was unaffected by the overexpression. Porin and SDH70 were used as loading controls. No effects of OXA1L overexpression were observed on cell growth (Fig. 7.14B).

7.4.2. Rescue experiments on OXA1L siRNA depletion

The U2OS cell line able to overexpress OXA1L upon tetracycline induction, prepared as in the previous paragraph, was used to confirm that the effect observed on the steady state level

of mitoribosomal proteins was due to the absence of OXA1L upon transfection with OXAsi03 and OXAsi04.

U2OS-OXA1L cells were induced for 3 days and then depleted of OXA1L for 6 days either with OXAsi03 (33 nM final concentration) or OXAsi04 (16 nM final concentration). In parallel wild-type U2OS were also depleted of OXA1L. These cells were used instead of the uninduced U2OS-OXA1L to exclude the possibility of a less efficient depletion due to leaky expression of OXA1L. The induction was continued during the depletion. At the end of the experiment, cells lysates were analysed via western blotting (Fig. 7.15).

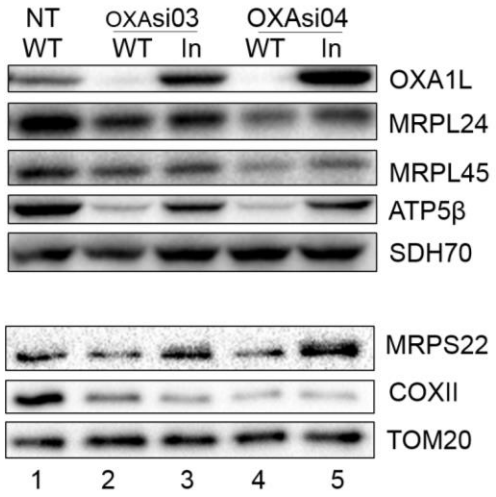

Figure 7.15 Rescue of OXA1L depletion phenotype by overexpression of modified OXA1L immune to the siRNA.

Western blot analysis was performed on cell lysates from U2OS-OXA1L cells induced for 3 days and then depleted of OXA1L for 6 days, whilst continuing the induction. In parallel U2OS cells were incubated with either non-targeting siRNA, OXAsi03 (33 nM) or OXAsi04 (16 nM) for 6 days. The efficiency of the depletion was detected with antibodies against OXA1L. The level of the mitoribosomal proteins MRPL24, MRPL45 and MRPS22 was also measured. The level of the OXPHOS proteins COXII and ATP5β was also detected. SDH70 and TOM20 were used as loading controls. The experiment was not replicated.

The western blot analysis confirmed the efficiency of the depletion of OXA1L (Fig. 7.15, lanes 2 and 4) as well as its rescue (Fig. 7.15, lanes 3 and 5) with both the siRNA used. As observed in the previous experiments, depletion of OXA1L caused reduction of the steady state level of mitoribosomal proteins and OXPHOS components. Upon overexpression of OXA1L (Fig. 7.15, lanes 3 and 5), a clear rescue of the level of ATP5β was observed. Full rescue was also observed for the levels of MRPS22. A partial rescue of MRPL45 and MRPL24, instead, was observed, especially using OXAsi04. No significant rescue was observed for COXII. This might be due to the partial rescue of the mitoribosomal protein, which might limit the amount of assembled mt-LSU and, therefore, not restoring completely mitochondrial translation. The quality of the loading was detected with antibodies against SDH70 and TOM20.

7.5. A role for OXA1L in human disease?

7.5.1. Characterisation of mitochondrial defects in OXA1L patient

During the course of my studies, the laboratory of Professor Rob Taylor identified a patient with mitochondrial disease and biallelic variants in the *OXA1L* gene.

The patient was a 5-year-old boy born to unrelated parents. He had other 4 unaffected siblings as well as a sister who died at 12 months of unknown causes. His main clinical symptoms included severe encephalopathy, hypotonia, developmental delay (both motor and cognitive) and motor axonal neuropathy. He also presented with iron deficiency anaemia and obesity. The patient died in hospital due to complications related to his condition. Sequential COX/SDH reactions identified COX-deficient fibres (Fig. 7.16), whilst assessment of respiratory chain complex activities in Newcastle showed a decrease in complex IV activity in isolation.

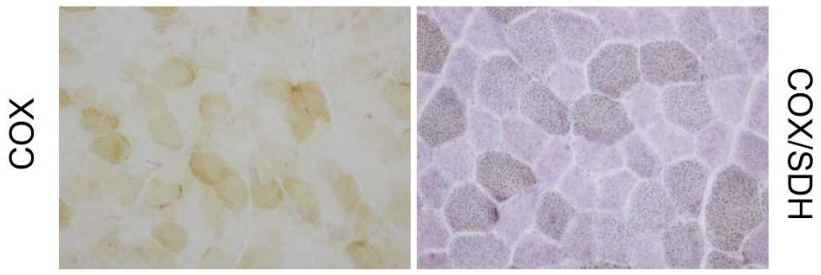

Figure 7.16 COX and COX/SDH reactions in muscle from a patient with mutations in *OXA1L*.

Transverse sections of muscle tissue (10µm) were reacted to assess the activity complex IV (COX) and complex II (SDH). The figures from the individual COX reaction (left) and COX/SDH reaction (right) are represented, highlighting decreased activity. Courtesy of Professor Rob Taylor

A complete screen of his mitochondrial genome (studies performed in Newcastle and Zaragoza) failed to identify causative mutations, as did a diagnostic screen of several nuclear genes known to be implicated in isolated COX-deficiency. Whole exome sequencing identified two novel variants in *OXA1L* (RefSeq Gene NG_051068.1) (c. 500_507dup (p. S170Qfs*18) and c. 620G>T (p. C207F) which segregated with disease in the family and were predicted to be pathogenic by a range of *in silico* tools (Sift, http://genetics.bwh.harvard.edu/pph2/) and were absent in the exome data set present in ExAC (http://exac.broadinstitute.org/).

According to the topography of OXA1L presented in Table 7.1, the identified mutations affected an intermembrane space domain found between the transmembrane helices α2 and α3. This might affect the stability of the protein. The steady state levels of mitochondrial proteins in the patient fibroblast were analysed via western blotting (Fig. 7.17).

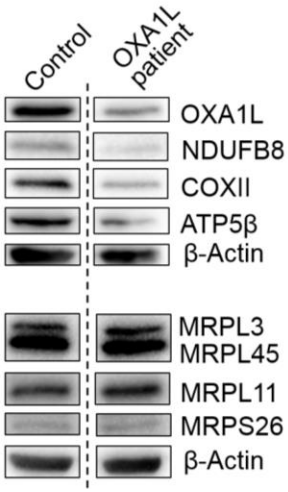

Figure 7.17 Steady state level of mitochondrial proteins in immortalised fibroblast from a patient carrying mutations in *OXA1L* gene.

Western blot analysis was performed from control (M0528-12) and OXA1L patient immortalised fibroblasts. The steady state level of OXA1L was assessed as were the steady state levels of components of the OXPHOS system (NDUFB8, COXII and ATP5β). On a separate western blot, the levels of the mitoribosomal proteins MRPL3, MRPL45, MRPL11 and MRPS26 were detected. For both the membranes, β-Actin was used as loading control. The dashed line indicates that some lanes were omitted from the figure.

The western blot analysis showed a reduced steady-state level of OXA1L, indicating that the mutations, occurring in an intermembrane domain, are affecting the stability of the protein. Despite that, approximately 40% of OXA1L was detected in the patient fibroblasts. Lower steady state levels of NDUFB8, COXII and ATP5β suggested decreased levels of complex I, IV and V, respectively. The levels of the mitoribosomal proteins were not affected. These data were confirmed by western blots performed by Dr Kyle Thompson on the same cell lines.

7.6. Discussion

While several published works investigated the role of yeast Oxa1, few data are available on the human homologue. This chapter focused on improving our understanding of the role of this protein in mitochondrial translation.

Yeast Oxa1 is reported to interact with the mitoribosome (Jia L et al., 2003; Jia L et al., 2009). The main data reporting an interaction between OXA1L and the mitoribosome comes from *in vitro* studies reported by Haque et al, who crosslinked OXA1L to several components of the mt-LSU. I confirmed the ability of OXA1L to interact with the mitoribosome *in vivo* via immunoprecipitation of 2 different mt-LSU components. Identifying the mitoribosomal partner of the interaction was not possible by immunoprecipitation. In case of a successful immunopreciptation of OXA1L, it is likely that the whole mt-LSU, and not only the mitoribosomal proteins directly interacting with OXA1L, will co-immunoprecipitate, making it impossible to identify direct interactions with this protein. The identification of the binding site of OXA1L on the mitoribosome *in vivo* might be achievable with the the use of high-resolution microscopy which

will allow the visualisation of the interaction and the identification of the mt-LSU proteins is in direct contract with OXA1L.

Oxa1 was named after the discovery of its role in complex IV assembly in yeast (Bonnefoy N et al., 1994; Keil M et al., 2012). Since then, Oxa1 has been reported to be involved in the insertion of both mitochondrial and nuclear encoded proteins (Hell K et al., 1998; Hildenbeutel M et al., 2012; Stiller SB et al., 2016). Depletion of human OXA1L was reported to affect the assembly of complex I and V, while the other OXPHOS complexes appeared unaffected (Stiburek L et al., 2007). Due to this unexpected observation and to the the role of OXA1L in anchoring the mitoribosome to the IMM, I decided to investigate the effects of its depletion.

First, a pool of 4 siRNA (SmartPool) targeting different positions in the OXA1L mRNA sequence was used to deplete the protein. Every siRNA present in the pool was selected and optimised by *Dharmacon* to increase the specificity and reduce the off target effects (Anderson EM et al., 2008; Birmingham A et al., 2006; Jackson AL et al., 2006). The final concentration of siRNA routinely used in our laboratory is 33 nM. The use of this final concentration of SmartPool allowed to use a lower concentration (8.25 nM) for every individual siRNA found in the mix. Since most the off target effects are due a partial complementarily of the siRNA with an unintended target, the use of a lower concentration of reagent will further reduce the chances of off target effects (Jackson AL et al., 2010). The depletion of OXA1L performed with the SmartPool severely affected cell growth. At the protein level, reduction of components of the large and, unexpectedly, small subunits of the mitoribosome were detected. COXII was undetectable. The depletion of mitoribosomal proteins suggested that OXA1L could play a role in the assembly of the large, but also of the small subunit of the mitochondrial translation machinery. Further confirmation of this surprising result were needed in order to exclude that the phenotype observed was due to off targets. To this purpose the 4 siRNA present in the SmartPool were individually tested. While OXAsi01 was not efficiently depleting OXA1L, OXAsi02 was lethal. OXAsi01 also led to the reduction of the steady state levels of mitoribosomal proteins, despite its inefficiency in depleting OXA1L. This result suggested that the depletion of the mitoribosomal proteins observed with the SmartPool might be due to an off target effect of OXAsi01. However, depletion with OXAsi03 and 04 led to an efficient depletion of OXA1L and showed reduction in the steady state level of both mt-SSU and mt-LSU proteins. This result might indicate that OXA1L causes depletion of mitoribosomal proteins, since this result was observed for both OXAsi03 and OXAsi04. Interestingly, a depletion of the complex V protein ATP5β was also observed, in agreement with the data published by Stiburek et al. Cell growth was only marginally delayed by OXAsi03 and 04, suggesting that the negative effect on growth observed with the use of the SmartPool siRNA was probably due to OXAsiA02.

The sequences of OXAsi02, 03 and 04 were analysed with BLAST to identify possible targets different from OXA1L. The analysis suggested that OXAsi02 might lead to cell death because 73% of its sequence aligns to mRNA encoding for HLF, involved in the regulation of apoptosis.

OXAsi03 and 04 showed a possible off target on transcriptions factors, which could have an impact on cells homeostasis.

Further confirmation of the results observed with OXAsi03 and OXAsi04 were needed, therefore these siRNA were tested at lower concentrations. OXAsi03 was less efficient at 16 nM. In this condition, the reduction observed for mitoribosomal proteins, and COXII, was also less pronounced, reflecting the lower efficiency of the depletion. At a final concentration of 8 nM of OXAsi03, only a partial depletion of OXA1L was observed, with a steady state level of COXII and mitoribosomal proteins tested that was higher than the one observed for depletion at 16 nM. The efficiency of OXAsi04 was almost unchanged at 33 nM, 16 nM or 8 nM and at all these concentrations, a similar depletion of COXII and mitoribosomal proteins was detected. Lower concentrations of OXAsi04 (4 and 2 nM) showed a less efficient depletion of OXA1L, with less reduction of the levels of mitoribosomal proteins and COXII, as observed for OXAsi03. These experiments highlighted a relationship between the efficiency of OXA1L depletion and levels of COXII and the mitoribsomal components tested, suggesting a relationship between the two effects and the unlikeliness of off target effects. To further validate the data obtained from the depletion experiments, a cell line able to overexpress OXA1L upon tetracycline induction was prepared, in the attempt to rescue the phenotype observed by the depletion. The protein was successfully overexpressed but, unfortunately, the overexpression had an effect on the steady state level of OXPHOS components, which appeared reduced. The rescue experiment was perfomend, but a full rescue of the levels of mitoribosomal proteins and ATP5β was not obtained. This might be due to the negative effects of OXA1L overexpression observed. Interstingly, no rescue of COXII depletion was observed. Further considerations on this are found later in this discussion.

As observed by Stiburek et al, the depletion of OXA1L reported in this chapter showed a reduction of the steady state level of ATP5β. This protein is a component of the F1 of complex V found in the matrix and which associates with F0 of the same complex via subunit c. F1 is completely nuclear-encoded and assembled independently from F0 (Tzagoloff A, 1969). A downregulation of F1 is rarely observed in cases of impaired mitochondrial translation. Stiburek et al suggested that the reduction of ATP5β observed upon OXA1L depletion could be due to the lack of insertion of subunit c of the F0, since yeast Oxa1 has been reported to mediate the insertion of Atp9 (homologue of human subunit c). If the reduced stability of F1 was due to this, a reduction of ATP5β should be observed in OXA1L depletion performed on 143B ρ^0 cells. These cells lack of mtDNA but maintain the membrane potential also thanks to a partially assembled complex V (Appleby RD et al., 1999; Buchet K & Godinot C, 1998). In these cells, F1 is intact and approximately half ~~of it~~ is reported to interact with the membrane via subunit c (Carrozzo R et al., 2006; García JJ et al., 2000). If the reduction of ATP5β observed upon depletion of OXA1L is due to impairment of subunit c insertion into the membrane, the depletion of OXA1L in cells should also reduce the level of ATP5β, affecting the membrane potential of the mitochondria and therefore the homeostasis of the cell. Upon depletion of OXA1L, no effects

on 143B ρ^0 cell growth was observed and the steady state level of ATP5β was unchanged. Although this result gave no information on the membrane insertion of subunit c, it suggested that the instability observed for ATP5β by Stiburek et al (and also in this thesis) cannot be due to an improper integration of subunit c into the inner mitochondrial membrane. In support of this, published data reported that depletion of subunit c did not affect the steady state level of another F1 subunit (ATP5α), confirming that subunit c is not important for the stability of the F1 (Bonora M et al., 2013). The mechanism underlying the reduction of ATP5β levels upon depletion in cells containing mtDNA is not clear. Interestingly, despite the steady state level of most of the mitoribosomal components being lower 143B ρ^0 cells, no further reductions were observed upon depletion of OXA1L, supporting the idea that their reduction in U2OS is linked to the depletion of OXA1L.

While performing the OXA1L depletion studies, I became aware of a patient with mitochondrial disease and biallelic variants in the gene encoding this protein. The patient was compound heterozygous for two *OXA1L* variants, with both the mutations affecting one of the intermembrane domains inbetween 2 transmembrane helices. Muscle histochemistry highlighted COX-deficiency, supporting the hypothesis derived from the depletion studies performed on U2OS cells that OXA1L plays a role ~~of~~ in complex IV assembly. Fibroblasts presented a minor OXPHOS defect, which was compensated by an increase of glycolysis. Western blot analysis performed on immortalised patient fibroblasts indicated a reduction of the steady state level of OXA1L to approximately 40% of the control cell line. A reduction of the steady state level of components of complex I, IV and V was detected. Reduction of complex I and V was in agreement with the observations of Stiburek et al. for OXA1L depletion on HEK293 cells. Depletion of complex V (ATP5β) was also reported upon depletion of OXA1L in this chapter. The effects of the depletion on components of complex I were not tested. In agreement with the depletion experiments reported in this chapter, complex IV (COXII) was also reduced in the patient cell line, supporting the idea of a role of OXA1L in the assembly of this complex. The steady state levels of the mitoribosomal proteins was not reduced in the OXA1L patient fibroblasts. It is important to specify that, when the depletion experiments were perfomed with siRNA (lower concentrations) that led to a steady state level of OXA1L comparable with the levels detected in the patient, there was no significant effect on the steady state levels of mitoribosomal proteins. This result is in agreement with the phenotype observed in the patient fibroblasts. Work on the OXA1L patient is currently continuing (Dr Kyle Thompson and Professor Rob Taylor, unpublished case).

Interestingly, rescue of the OXA1L patient phenotype was attempted by colleagues, without success and is currently being repeated by Dr Kyle Thompson. This, together with the data obtained for depletion or overexpression of OXA1L, suggests that there is a narrow range at which there is an optimal level of this protein, and it might be important to maintain this for correct cellular homeostasis.

Although the rescue experiment of the OXA1L depletion phenotype on U2OS cells did not successfully increase the level of COXII, the reduction in the steady state level of this protein with both the siRNAs tested, and the presence of COX deficiency in the patient fibroblasts and muscle, support the role of OXA1L in the assembly of complex IV.

The reduction of mitoribosomal components observed with OXA1L depletion suggests that this protein might be involved in the assembly of both the large and the small mitoribosomal subunit. OXA1L might be directly involved in the assembly or might be important for membrane insertion of other unknown proteins that might have a key role mitoribosomal assembly.

Chapter 8: Concluding remarks

The work presented in this thesis focused on the characterisation of the role of 2 mitochondrial proteins, MRPL45 and OXA1L, in mitochondrial translation. The main focus was human MRPL45, a constituent of the mitochondrial ribosome that was suggested to be involved in the important interaction of the mitoribosome with the inner mitochondria membrane. Data generated during my project made a connection with and led into work on the IMM protein OXA1L, which in yeast is defined as a mitoribosome-interacting protein and as an insertase that contributes to the assembly of some OXPHOS components.

The data obtained for the 2 proteins are summarised in the sections below.

8.1. MRPL45

Studies presented here demonstrated the importance of the mitoribosomal protein MRPL45 for the homeostasis of cells. Depletion of this protein highlighted its central role in the stability and the assembly of the mt-LSU. In the absence of MRPL45, the mt-LSU failed to assemble, suggesting an involvement of MRPL45 in the first steps of the its assembly process. As a consequence of the reduced levels of mt-LSU, mitochondrial translation was impaired and an increase in the glycolytic activity, necessary to provide the ATP for the cell to survive, was observed.

Once the importance of MRPL45 was established, I focused my attention on investigating the ability of this protein to interact with the membrane. At the beginning of this study, the only information available on the possibility of membrane-interaction of this protein was its structural homology with the membrane-interacting protein TIM44. However, relatively soon after, the first structure of the mammalian mt-LSU was released and localised MRPL45 in close proximity of the polypeptide exit site (Greber BJ et al., 2014), further supporting its potential role in the association of the mt-LSU with the membrane. In order to study membrane-association, I developed a protocol that was used to test membrane-interaction. First, this protocol was used to confirm the ability of human mt-LSU to interact with the IMM, as previously suggested by Liu M and Spremulli LL (2000). Through the application of the developed protocol on cells overexpressing MRPL45, I demonstrated the ability of MRPL45 to interact directly with the membrane in the absence of pre-assembled mitoribosomal subunits.

Cell lines able to inducibly overexpress MRPL45FLAG were prepared in order to study the interactome of the protein. The addition of the FLAG-tag at the C-terminus of the protein did not affect its integration in the mt-LSU and did not inhibit the ability of the protein to directly interact with the IMM. The overexpression of another MRPL45FLAG construct, carrying silent mutations in the sequences targeted by the siRNA used to deplete the endogenous protein, confirmed the ability to obtain a full rescue of the depletion phenotype. This result further confirmed that the addition of the FLAG-tag did not affect the function of MRPL45 and validated the phenotype observed upon depletion of the endogenous protein.

No transmembrane domains were predicted within the MRPL45 protein sequence, and the mass spectrometry analysis of the sample obtained from the immunoprecipitation of MRPL45FLAG in absence of assembled mt-LSU failed to identify any membrane proteins that might interact with MRPL45 to mediate the interaction. A parallel experiment performed on untagged overexpressed MRPL45 also did not identify any strong candidate interacting proteins. In contrast, samples from both immunoprecipitations analysed by western blot prior to the mass spectrometry analysis, detected a weak signal from OXA1L. This might suggest a non-stoichiometric interaction with MRPL45, but using a sensitive technique the protein would be expected to be detected by mass spectrometry, which it was not. The lack of consistent and convincing data on the existence of a partner membrane protein for the interaction with MRPL45 suggests the probability that the interaction of MRPL45 is direct with the phospholipid layer.

In this study, I also investigated the domain of MRPL45 that is putatively involved in the interaction with the membrane. Examining the information available on the structure of human MRPL45 I decided to express a version of the protein containing mutations of the charged amino acids present in the most protruding domain of the protein (α2-helix) by changing these to alanine (MRPL45FLala). Although the steady state level of the protein was very low, it was efficiently targeted to mitochondria. Isokinetic sucrose gradient analyses showed that upon expression MRPL45FLala was not integrated into the mt-LSU, but that it could be used as a component of the subunit only when the endogenous MRPL45 was absent. Consistent with this, the expression of the mutant protein in the absence of the endogenous MRPL45, by siRNA depletion, showed a partial rescue of the phenotype. This was probably because the relatively low levels of available MRPL45FLala was limiting the assembly of the mt-LSU. However, since MRPL45FLala was able to interact with the membrane, it suggested that the mutated domain was not involved in the direct interaction of the protein with the IMM.

Since the first MRPL45 mutant examined did not identify the domain involved in membrane interaction, I designed a new construct, based on the structural homology with the membrane-interacting protein TIM44. The new mutant (MRPL45FLΔ) lacked the first 117 amino acids (N-terminal of the α2-helix) and was efficiently targeted to mitochondria by addition of the Su9 presequence, which I demonstrated to be efficiently and accurately cleaved upon import. Unfortunately, the steady state of this protein was also very low. Unlike the previous mutant studies, MRPL45FLΔ was not efficiently integrated within the mt-LSU, even when the endogenous protein was absent. Unexpectedly, this protein maintained the ability to interact with the mitochondrial membrane. Although the studies that I performed on mutant variants of MRPL45 did not successfully identify the domain of MRPL45 involved in membrane interaction, investigation of MRPL45FLΔ suggested that the deleted domain is important for the assembly of the protein within the mt-LSU.

Since it was not possible to identify the domain of MRPL45 responsible for membrane-interaction, different MRPL45 mutants could be prepared to analyse their ability to interact with the membrane, using the protocol developed during this project.

In addition, the improvement of electron microscopy techniques might allow the visualisation of the membrane-bound mitoribosomes and the identification of other components that might be involved in this important interaction.

The data presented in this project suggested a central role of MRPL45 in the assembly of the mitoribosome, a process is still undefined. Once the components of the assembly machinery will be identified, it will be possible to study the mechanism of the assembly of the mitoribosome by replicating it *in vitro.*

8.2. OXA1L

The data presented in this thesis showed for the first time *in vivo* that the IMM protein OXA1L interacts with the mitoribosome, since this was successfully co-immunoprecipitated with 2 different mitoribosomal proteins. This interaction had been already confirmed in yeast, but it was previously reported in human only by *in vitro* studies (Haque ME et al., 2010).

Subsequently, depletion of OXA1L was performed to study its involvement in mitochondrial translation. This was performed with a pool of 4 siRNA and resulted, unexpectedly, in a reduction of the steady state level of components of both the mt-LSU and the mt-SSU. The result was confirmed by independently using 2 of the siRNA present in the pool, suggesting that the observed effect was genuine. In addition, the reduction of the mitoribosomal components observed upon depletion of OXA1L could be rescued upon overexpression of the protein, further confirming the robustness of these results. From my studies it was not clear if the OXA1L has a direct role in the assembly of the subunits or if this effect was due to the failure in the insertion or the import of other mitochondrial proteins that play a role in the process of mitoribosome biogenesis. Due to the reduction of the steady state levels of mitoribosomal subunits following OXA1L depletion, it was not possible to investigate the effects on the interaction of the mitoribosome in absence of this IMM protein.

Depletion of OXA1L also led to a reduction of on the steady state levels of both complex IV and V. Depletion of complex IV could be related to an impairment of mitochondrial translation following the reduction of mitoribosomal proteins. Reduction of the steady state levels of complex V was also observed by Stiburek et al, who, in contrast to my data, did not find any effect on complex IV. A reduction in the steady state levels of COXII was shown in my study upon depletion with 2 different siRNA, although its levels were not restored by the overexpression of the protein. In parallel with these studies, the characterisation of the phenotype of a patient carrying a compound heterozygous mutation for OXA1L were performed. These also identified a deficiency in this complex IV, suggesting the involvement of OXA1L in the assembly and stability of complex IV. COX/SDH staining performed on skeletal muscle samples highlighted the presence of COX negative fibres, and a reduction of the steady state levels of the COXII component of complex IV was detected in immortalised fibroblasts samples by western blot. This analysis also showed that the steady state level of OXA1L was reduced to approximately 40% in the patient immortalised

fibroblasts, as well as a reduction of the steady state levels of NDUFB8 (Complex I) and ATP5β (Complex V). No reduction of mitoribosomal proteins was detected. These results suggest that OXA1L plays a role in the assembly of complexes I, IV and V, and that when a proportion of OXA1L is present, there are no effects on the assembly of the mitoribosomal subunits. Further biochemical characterisation of the patient's phenotype is currently under investigation.

In this study, it was not possible to identify the mitoribosomal proteins that are directly interacting with OXA1L, since a successful immunoprecipitation of OXA1L will lead to the co-precipitation of the whole mitoribosome. The proteins in direct contact with OXA1L could be identified in the future with the use of advanced electron microscopy techniques that might be able to visualise the interaction. Another method that could be used to identify binding partners of OXA1L is the proximity labelling combined to affinity purification and mass spectrometry analysis. For example, if a fusion protein composed of OXA1L and biotin protein ligase can be expressed in human cells without affecting the role of OXA1L, biotinylation of neighbour proteins can be obtained *in vivo*. These biotinylated proteins can then be collected by affinity purification and identified via mass spectrometry. This method could potentially also contribute to the identification of the role of OXA1L in the assembly of complexes I, IV and V. In addition, it will be interesting to identify the mechanism by which OXA1L is directly or indirectly involved in the assembly of the mitoribosomal subunits. In order to understand OXA1L role in this process, more information on this is needed.

The data presented in this thesis has provided new information on MRPL45 and OXA1L and their role in post-transcriptional mitochondrial gene expression. Although this has improved our understanding of this process that is crucial for cell viability, a deeper knowledge of mitochondrial biology is essential to understand the molecular mechanisms underlying mitochondrial dysfunction.

Appendices

Appendix 1: Nomenclature of mitoribosomal proteins

The new nomenclature (Greber BJ et al., 2016) contains a letter before the number which identifies universal ('u'), bacterial-homologue ('b') and mitochondrial-specific ('m') proteins. In case of the universal and bacterial-homologue proteins, the number is followed by the letter 'm' to refer to the mitochondrial protein.

mt-SSU	
Old name	**New name**
MRPS2	uS2m
MRPS5	uS5m
MRPS6	uS6m
MRPS7	uS7m
MRPS10	uS10m
MRPS11	uS11m
MRPS12	uS12m
MRPS14	uS14m
MRPS15	uS15m
MRPS16	bS16m
MRPS17	uS17m
MRPS18b	mS40
MRPS18c	bS18m
MRPS21	bS21m
MRPS22	mS22
MRPS23	mS23
MRPS24	uS3m
MRPS25	mS25
MRPS26	mS26
MRPS27	mS27
MRPS28	bS1m
MRPS29 (DAP3)	mS29
MRPS31	mS31
MRPS33	mS33
MRPS34	mS34

mt-LSU	
Old name	**New name**
MRPL1	uL1m
MRPL2	uL2m
MRPL3	uL3m
MRPL4	uL4m
MRPL9	bL9m
MRPL10	uL10m
MRPL11	uL11m
MRPL12	bL12m
MRPL13	uL13m
MRPL14	uL14m
MRPL15	uL15m
MRPL16	uL16m
MRPL17	bL17m
MRPL18	uL18m
MRPL19	bL19m
MRPL20	bL20m
MRPL21	bL2m
MRPL22	uL22m
MRPL23	uL23m
MRPL24	uL24m
MRPL27	bL27m
MRPL28	bL28m
MRPL30	uL30m
MRPL32	bL32m
MRPL33	bL33m

MRPS35	mS35
MRPS37 (CHCHD1)	mS37
MRPS38 (AURKAIP1)	mS38
MRPS39 (PTCD3)	mS39

MRPL34	bL34m
MRPL35	bL35m
MRPL36	bL36m
MRPL37	mL37
MRPL38	mL38
MRPL39	mL39
MRPL40	mL40
MRPL41	mL41
MRPL42	mL42
MRPL43	mL43
MRPL44	mL44
MRPL45	mL45
MRPL46	mL46
MRPL47	uL29m
MRPL48	mL48
MRPL49	mL49
MRPL50	mL50
MRPL51	mL51
MRPL52	mL52
MRPL53	mL53
MRPL54	mL54
MRPL55	bL31m
MRPL57	mL63
MRPL58 (ICT1)	mL62
MRPL59 (CRIF1)	mL64
MRPS30 (PDCD9)	mL65
MRPS18a	mL66
/	mL57
/	mL58
/	mL59
/	mL60
/	mL61

Appendix 2: Antibodies

The primary and secondary antibodies used in this study are listed in the following tables:

Primary antibodies	Dilution	Company, Cat. No
α-FLAG	1:2,000	*Sigma*, F1804
ATP5b	1:1,000	*Abcam*, Ab14730
β-actin	1:10,000	*Sigma*, A1978
CLPP	1:1,000	*Abcam*, Ab124822
COXII	1:1,000	*Eugene*, A6404
DAP3	1:1,000	*Abcam*, Ab11328
GDH	1:500	Custom synthesised
HSP60	1:5,000	*BD biosciences*, 611562
ICT1	1:1,000	*Proteintech group*, 10403-1-AP
LetM1	1:2,000	*Proteintech group*, 16024-1-AP
LONP	1:1,000	*Sigma*, HPA002192
MRPL3	1:1,000	*Abcam*, Ab39268
MRPL11	1:1,000	*Cell signalling techn*., D68F2
MRPL24	1:1,000	*Proteintech group*, 16224-1-AP
MRPL45	1:1,000	*Proteintech group*, 15682-1-AP
MRPS17	1:1,000	*Proteintech group*, 18881-1-AP
MRPS22	1:1,000	*Proteintech group*, 10984-1-AP
MRPS26	1:1,000	*Proteintech group*, 15989-1-AP
MRPS27	1:1,000	*Proteintech group*, 17280-1-AP
NDUFA9	1:1,000	*Abcam*, Ab14713
NDUFB8	1:1,000 1:1,000	*Invitrogen*, A31857 *Abcam*, Ab110242
OXA1L	1:1,000	*Proteintech group*, 21055-1-AP
Porin	1:10,000	*Abcam*, Ab 14734
TOM20	1:1,000	*Santa Cruz*, Sc-11415
SDH70	1:1,000	*Abcam*, Ab14715

Secondary antibodies	Dilution	Company, Cat. no
Rabbit	1:3,000	*Dako*, P0399
Goat	1:2,000	*Dako*, P0260
Mouse	1:2,000	*Dako*, P0449

Appendix 3: Plasmids

The following plasmids were used in this study:

- pcDNA™5/FRT/TO *(Invitrogen)*. Vector designed for use in Flp-In™ systems. It contains a multiple cloning site under tetracycline control. It also contains ampicillin and hygromycin B resistance genes. used to select clones respectively in bacteria and human cell lines.

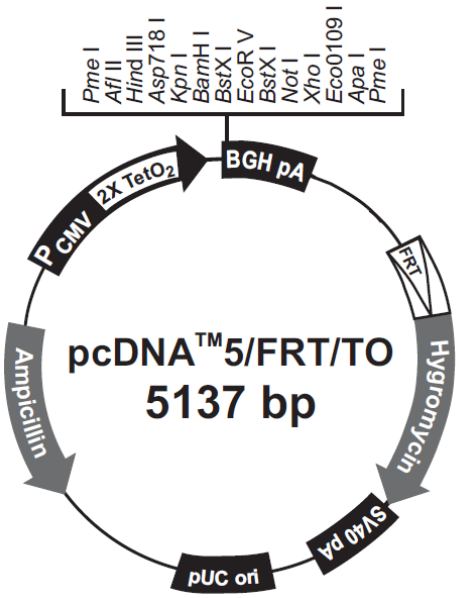

- pOG44 *(Invitrogen).* Flp-recombinase expression vector designed for use in Flp-In™ System in co-transfection with pcDNA™5/FRT/TO. It encodes ampicillin resistance for selection of positive transformed bacteria.

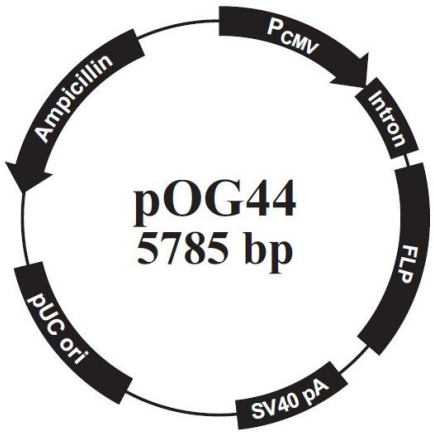

- pMK-RQ *(Thermo Scientific)*. Vector containing the custom synthesised gene from GeneArt (*Thermo Scientific)*. It encodes kanamycin resistance.

Appendix 4: Small interfering RNA

Protein knockdown was obtained using the following small interfering RNA (siRNA):

Target	Company	Catalogue no	Referred to as	Sequence sense fragment (5'-3')
MRPL45	Sigma-Aldrich	SASI_Hs02_00359740	siRNA02	GACUGAUAGAGAGAACUGA
		SASI_Hs01_00089760	siRNA01	GAGUAUGUUGUAUUCGAAA
OXA1L	Dharmacon	M-012696-01	OXAsi01	UAACGUGGCUUUACAGAUU
		M-012696-02	OXAsi02	GGAAACCGCUGACCACACG
		M-012696-03	OXAsi03	CAGGAGACCAUAUUGAGUA
		M-012696-04	OXAsi04	CAAGUAUCCUGUCUCCGGA
		Smartpool M-012696-00	SmartPool	Mixture of M-012696-01. M-012696-02. M-012696-0. M-012696-04
CLPP	Qiagen	SI00083650	CLPP siRNA	CGAUGCAGUACAUCCUCAATT
LONP	Qiagen	SI00068488	LONP siRNA	CGCGCUUUAUCAAGAUUAUTT

Appendix 5: DNA oligonucleotides

The following DNA-oligonucleotides were used for PCR reactions. They were personally designed and then synthesised by *Eurogentec*.

Product	Use	DNA oligonucleotide 5'- 3'
MRPL45 and mutants	PCR, preparation of inserts for cloning.	Frw1 CTC-TAT-GGA-TCC-ATG-GCA-GCC-CCC-ATA-CC
		Frw2 CTC-TAT-GGA-TCC-CTT-TGC-GGG-AAC-AAG-ATG-G
		Rev1FLAG CTC-TAT-GGA-TCC-CTA-CTT-ATC-GTC-GTC-ATC-CTT-GTA-ATC-GGC-TAG-CTG-AGG-CTT-CTG-G
		Rev2 CTC-TAT-GGA-TCC-CTA-GGC-TAG-CTG-AGG-CTT-CTG-G
		Rev3 CTC-TAT-GGA-TCC-GAG-ACT-TCA-AAG-CTT-CCA-GC
		L45trFrw CAC-ACA-GCG-CGC-CGC-AGC-TGC-ATC-ACA-AGT-GTC-AAT-CCG-G
		L45trRev ACA-CAC-GCG-GCC-GCC-AAG-AAG-CCT-CAC-TTG-TCG-TCA-TCG-TCT-TTG-TAG-TCG-GCT-AGC-TGA-GGC-TTC-TGG
MRPL45FLsil	Site-directed mutagenesis	MRPL45sisilmutsense CAA-AGG-AGG-GTT-TAA-TCG-AAA-GAA-CTG-AAC-G
		MRPL45sisilmutanti-s CGT-TCA-GTT-CTT-TCG-ATT-AAA-CCC-TCC-TTT-G
MRPL45	qPCR	L45qP1Frw CTC-AGT-CCG-CAG-CTA-TAG-TTC
		L45qP1Rev GAA-ACA-TAG-GCA-TCA-AAT-ATA-CCA-G
MRPL45FLΔ	In vitro transcription	SP6-Su9-L45Frw ATT-TAG-GTG-ACA-CTA-TAG-CAC-ACC-TCG-AGA-CCA-TGG
		SP6-Su9-L45Rev AAG-CCT-CAC-TTG-TCG-TCA-TCG-TCT-T

Other DNA oligonucleotides, already in use in our laboratory, were also used in this study:

Product	Use	DNA oligonucleotide 5'- 3'
18S	qPCR	Frw GTA-ACC-CGT-TGA-ACC-CCA-TT
		Rev CCA-TCC-AAT-CGG-TAG-TAG-CG
12S	qPCR	Frw ACA-CTA-CGA-GCC-ACA-G
		Rev ACC-TTG-ACC-TAA-CGT-C
16S	qPCR	Frw CCA-ATT-AAG-AAA-GCG-TTC-AAG
		Rev CAT-GCC-TGT-GTT-GGG-TTG-ACA
COXII	qPCR	Frw CTT-AGA-ACC-AGG-CGA-C
		Rev GTC-GTG-TAG-CGG-TGA-A
BGH	PCR Colony screening	Rev TGA-AAG-GCA-CAG-TGC-AGG
CMV	PCR Colony screening	Frw CGC-AAA-TGG-GCG-GTA-GGC-GTG

Appendix 6: Synthetic genes

Two construct were synthesised from GeneArt™ (*Thermo Scientific)* and were used for the cloning of mutated OXA1L (A) and MRPL45FLala (B). Both the genes were integrated in pMK-RQ form *Thermo Scientific.* Two restriction site were included at both ends of each gene to allow its isolation from pMK-RQ and its cloning into pcDNA™5/FRT/TO.

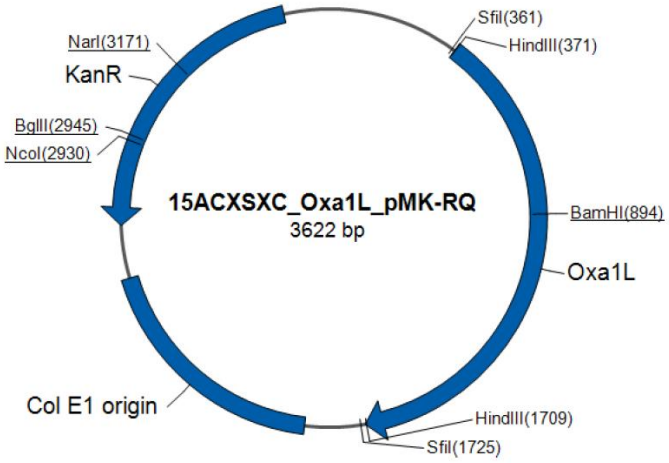

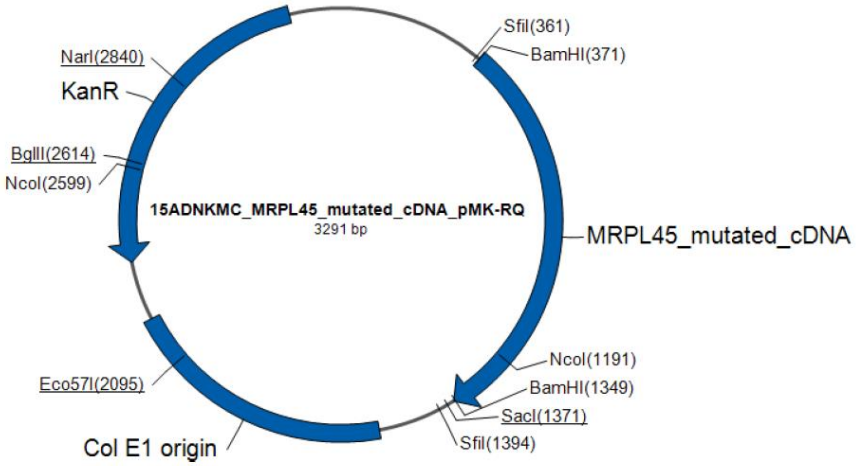

Gene	Sequence
OXA1Lsilmut	*AAGCTT*CCTCTTCCGGGCAAA**ATG**GCGATGGGACTAATGTGCGGACGCCGG GAGCTTCTGCGCTTGCTACAGTCCGGGCGTCGGGTCCACAGCGTCGCAGGG CCCTCGCAATGGCTTGGGAA**G**CC**A**CT**T**AC**T**AC**C**CGGCTCCTATTCCCAGCAG CCCCGTGCTGCTGTCGCCCACACTACCTCTTCCTTGCGGCTTCCGGCCCCC GCAGCCTCAGTACCTCTGCTATCTCTTTTGCAGAAGTCCAGGTTCAGGCCCC TCCTGTTGTTGCTGCAACTCCCTCACCCACAGCAGTACCTGAGGTGGCTTCT GGAGAGACTGCAGATGTAGTCCAAACTGCTGCAGAGCAGAGCTTCGCTGAA CTGGGGCTGGGGTCATACACCCCAGTGGGACTGATCCAGAATTTACTGGAAT TTATGCATGTTGATCTGGGCCTACCTTGGTGGGGGGCCATTGCTGCATGTAC AGTCTTTGCCCGCTGCCTGATTTTTCCTCTCATCGTGACGGGCCAGCGAGAG GCAGCCAGGATCCACAATCACTTGCCAGAGATCCAGAAGTTTTCCAGTCGAA TCAGAGAGGCCAAGTTAG**CAGG**G**GA**T**CA**C**AT**C**GA**A**TA**TTACAAGGCTTCCTC GGAGATGGCACTTTACCAGAAAAAACATGGTATTAAACTCTATAAACCTCTCA TTCTCCCTGTGACTCAGGCCCCAATCTTCATCTCCTTCTTCATTGCTTTGAGA GAGATGGCCAACCTTCCTGTGCCCAGCCTGCAGACAGGTGGCCTCTGGTGG TTCCAGGATCTCACGGTATCCGATCCCATCTACATATTACCACTGGCAGTCAC TGCTACAATGTGGGCTGTTCTTGAGCTAGGTGCTGAGACAGGTGTGCAAAGT TCTGACCTTCAGTGGATGAGAAATGTCATCAGAATGATGCCCCTGATAACCTT GCCCATAACCATGCATTTCCCCACGGCAGTGTTTATGTACTGGCTCTCCTCC AATTTGTTTTCCCTGGTCCA**G**GT**G**TC**T**TG**C**CT**T**CGGATTCCAGCAGTACGCA CTGTACTTAAAATCCCCCAGCGTGTTGTACATGACCTGGACAAATTACCTCCA CGGGAAGGCTTCCTAGAGAGCTTCAAAAAAGGCTGGAAAAATGCTGAAATGA CGCGTCAGCTGCGAGAGCGTGAACAACGCATGCGGAATCAGTTGGAGCTAG CAGCCAGGGGTCCTTTACGACAGACCTTTACCCACAACCCTCTCCTACAACC TGGAAAGGATAACCCTCCCAATATCCCTAGCAGCAGCAGCAAACCAAAGTCA AAGTATCCCTGGCACGACACACTTGGC**TGA**CTTATATTC*AAGCTT*
MRPL45FLala	*GGATCC*TTGCGGGAACAAG**ATG**GCAGCCCCCATACCTCAAGGGTTCTCTTGT TTATCGAGGTTTTTGGGCTGGTGGTCTCGGCAGCCAGTTCTGGTGACTCAGT CCGCAGCTATAGTTCCAGTAAGAACTAAAAAACGTTTCACACCTCCTATTTATT CAACCTAAATTTAAAACAGAAAAGGAGTTTATGCAACATGCCCGGAAAGCAG GATTGGTTATTCCTCCAGAAAAATCGGACCGTTCCATACATCTGGCCTGTACA GCTGGTATATTTGATGCCTATGTTCCTCCTGAGGGTGATGCACGCATATCATC TCTTTCAAAGGAGG**G**C**C**TT**A**TTGA**A**AG**G**AC**C**GAACGAATGAAGAAGACTATG GCATCA**GCA**GTGTCAATC**GCCGCU**ATA**GCAGCCGCU**GATGCCAACTTT**GCU** ATA**GCAGCC**TTCCCTGAAAAAGCTAAGGATATCTTTATTGAAGCTCACCTTTG TCTAAATAACTCAGACCATGACCGGCTTCATACCTTGGTAACTGAACACTGTT TTCCAGACATGACTTGGGACATCAAATATAAGACCGTCCGCTGGAGCTTTGT GGAATCTTTAGAGCCCTCTCATGTTGTTCAAGTTCGCTGTTCAAGTATGATGA ACCAGGGCAACGTGTACGGCCAGATCACCGTACGCATGCACACCCGGCAGA CTCTGGCCATCTATGACCGGTTTGGCCGGTTGATGTATGGACAGGAAGATGT ACCCAAGGATGTCCTGGAGTATGTTGTATTCGAAAAGCAGTTGACAAACCCC TATGGAAGCTGGAGAATGCATACCAAGATCGTTCCCCCATGGGCACCCCCTA AGCAGCCCATCCTTAAGACGGTGATGATCCCTGGCCCTCAGCTGAAACCAGA AGAAGAATATGAAGAGGCACAAGGAGAGGCCCAGAAGCCTCAGCTAGCC**GA** **CTACAAAGACGATGACGACAAG**TGA**TGACAAAAATGACT*GGATCC*

Legend: FLAG tag; siRNA target; *Restriction site*; Start/Stop codon; Changes to wild type

Appendix 7: Flow Cytometry analysis of MRPL45 depletion on HEK293

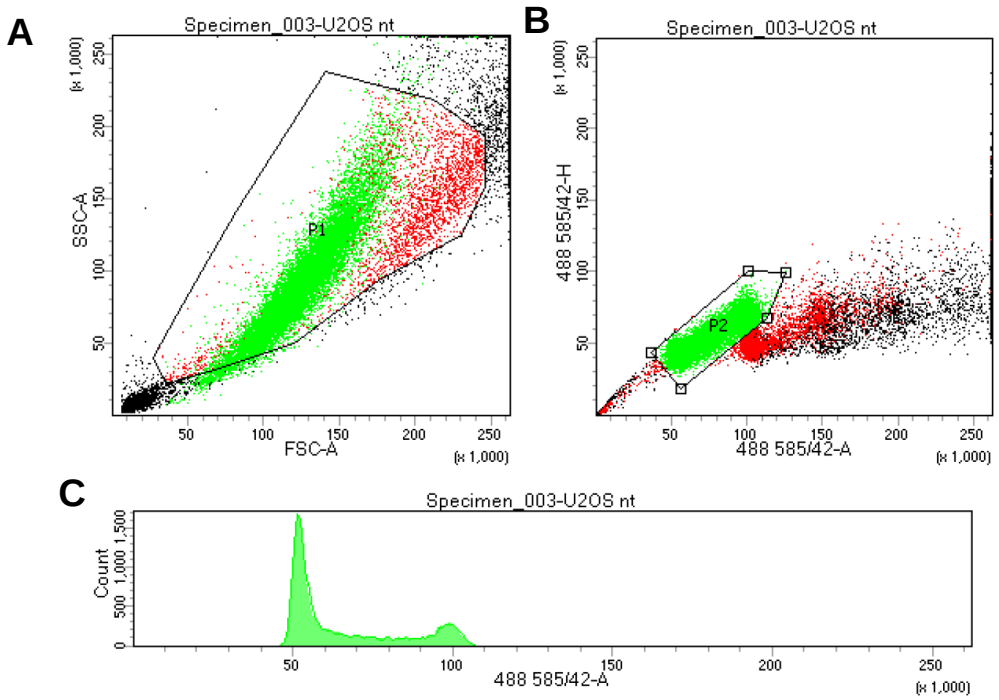

Figure a18 Cell cycle analysis with propidium iodide of U2OS cells incubate with NT-siRNA.

Forward (FSC-A) and side (SSC-A) scatter **(A)** were used to identify the cells (area P1), while pulse shape analysis **(B)** was used to identify clumps and doublets. Single cells were circled in the area P2. The percentage of cells in each phase of the cell cycle were quantified by the program **(C)**. 488 585/42 indicates the wavelength and the filter used.

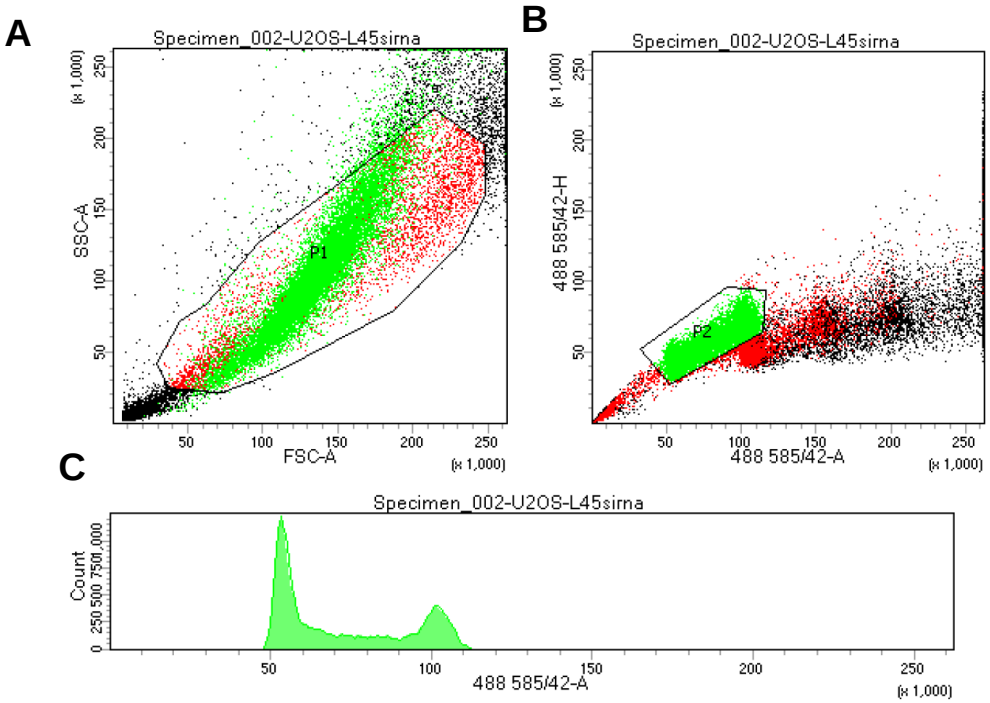

Figure a19 Cell cycle analysis with propidium iodide of U2OS cells incubate with MRPL45-siRNA.

Forward (FSC-A) and side (SSC-A) scatter **(A)** were used to identify the cells (area P1), while pulse shape analysis **(B)** was used to identify clumps and doublets. Single cells were circled in the area P2. The percentage of cells in each phase of the cell cycle were quantified by the program **(C)**. 488 585/42 indicates the wavelength and the filter used.

Appendix 8: MRPL45WT clone sequencing

The following figures represent the sequences obtained for the forward (CMV) and reverse (BGH) primers used to confirm the identity of the cloned sequence. The output was analysed with *SeqScanner*.

CMV

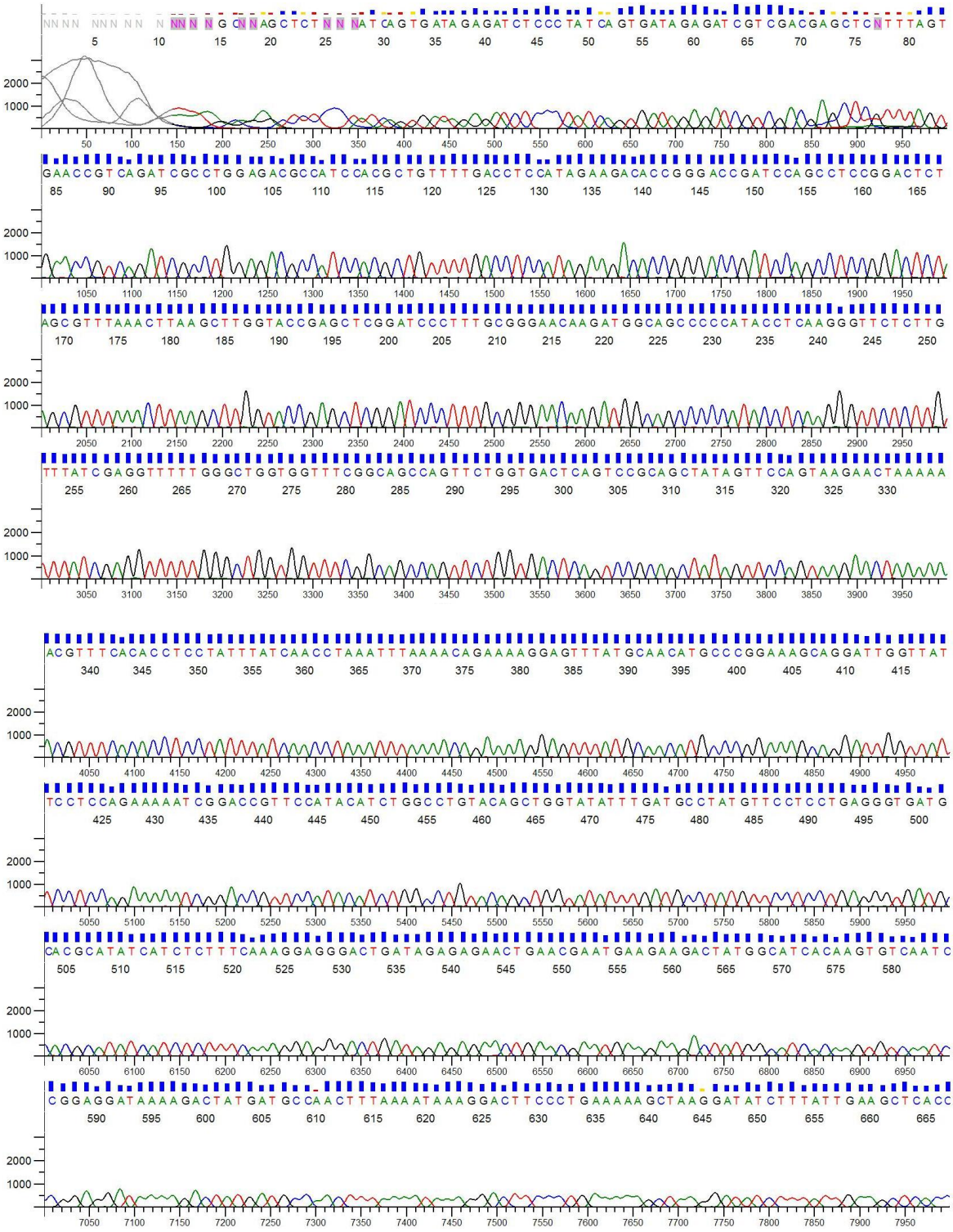

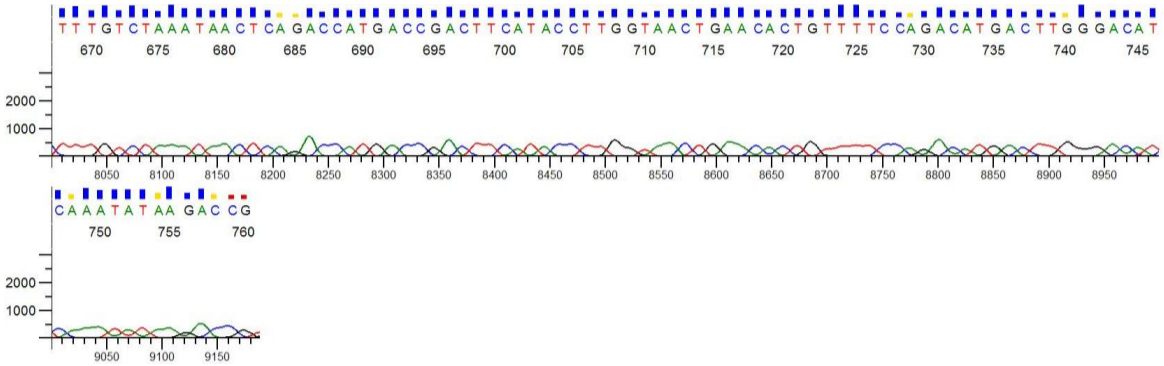

BGH

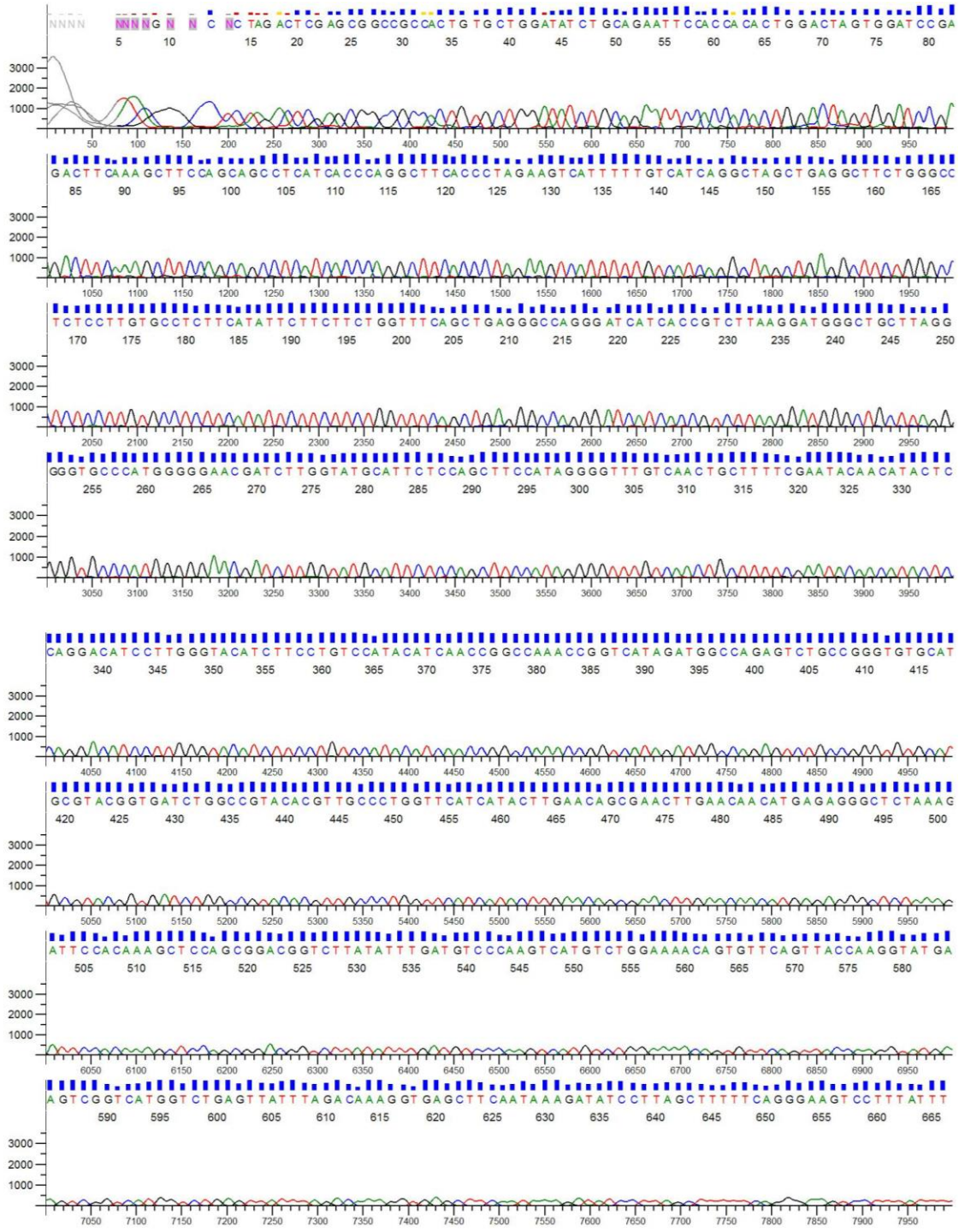

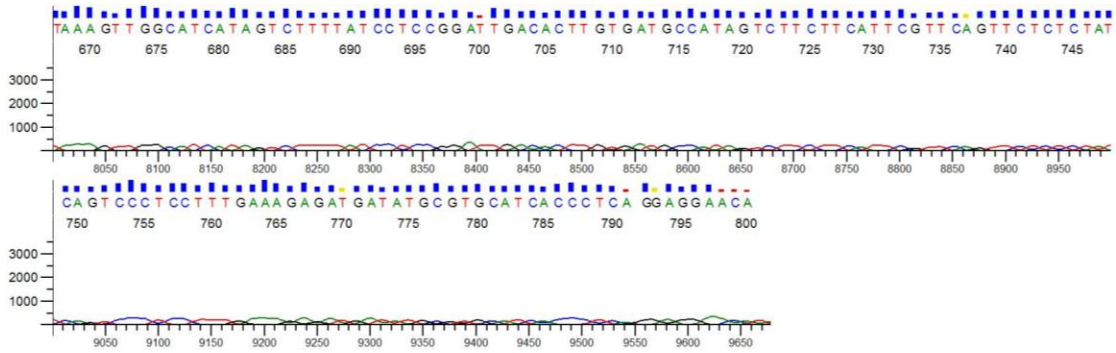
TAAAGTTGGCATCATAGTCTTTTATCCTCCGGATTGACACTTGTGATGCCATAGTCTTCTTCATTCGTTCAGTTCTCTCTAT
670 675 680 685 690 695 700 705 710 715 720 725 730 735 740 745
3000
2000
1000
8050 8100 8150 8200 8250 8300 8350 8400 8450 8500 8550 8600 8650 8700 8750 8800 8850 8900 8950
CAGTCCCTCCTTTGAAAGAGATGATATGCGTGCATCACCCTCA GGAGGAACA
750 755 760 765 770 775 780 785 790 795 800
3000
2000
1000
9050 9100 9150 9200 9250 9300 9350 9400 9450 9500 9550 9600 9650

Appendix 9: MRPL45FLAG clone sequencing

The following figures represent the sequences obtained for the forward (CMV) and reverse (BGH) primers used to confirm the identity of the cloned sequence. The output was analysed with *SeqScanner*.

CMV

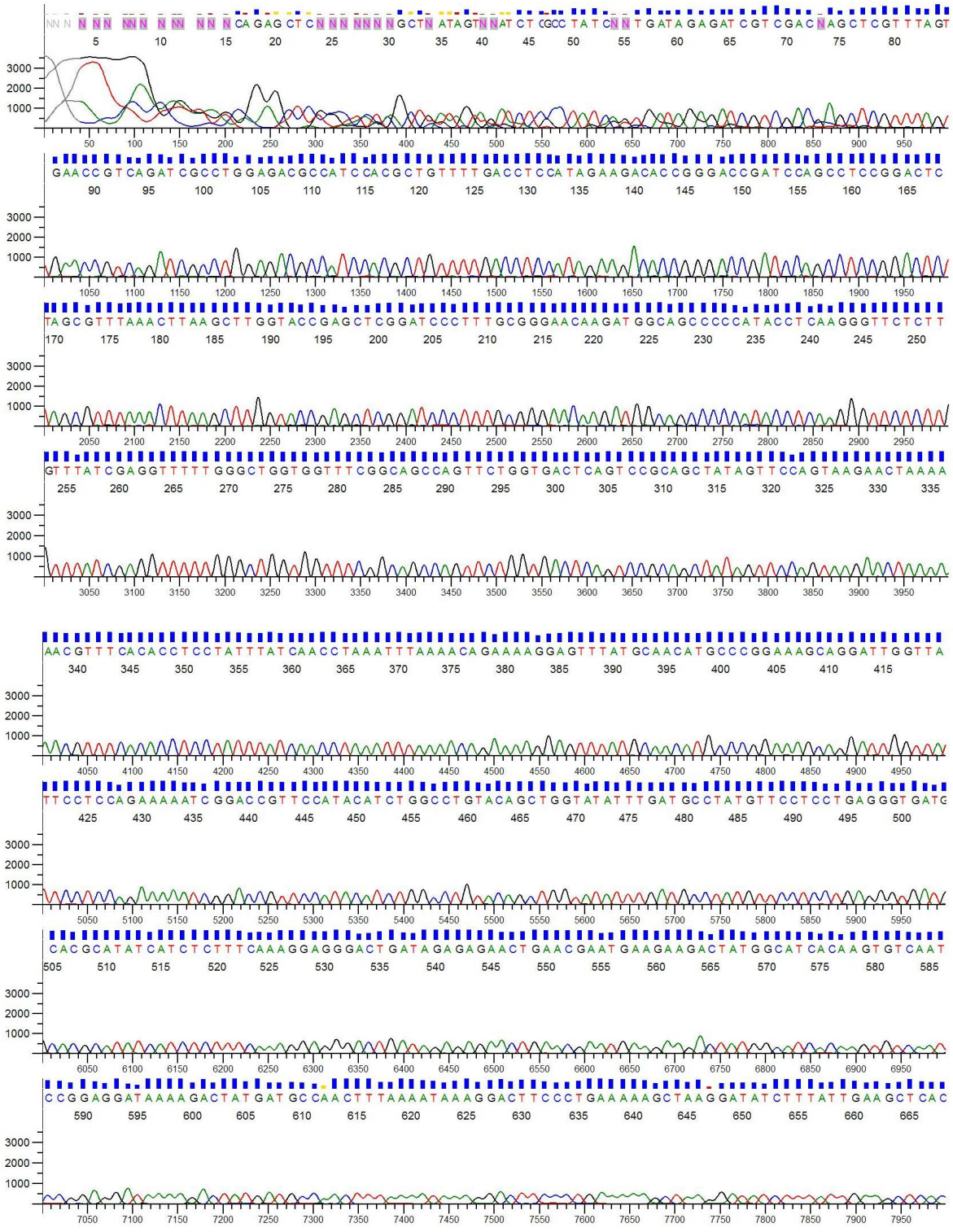

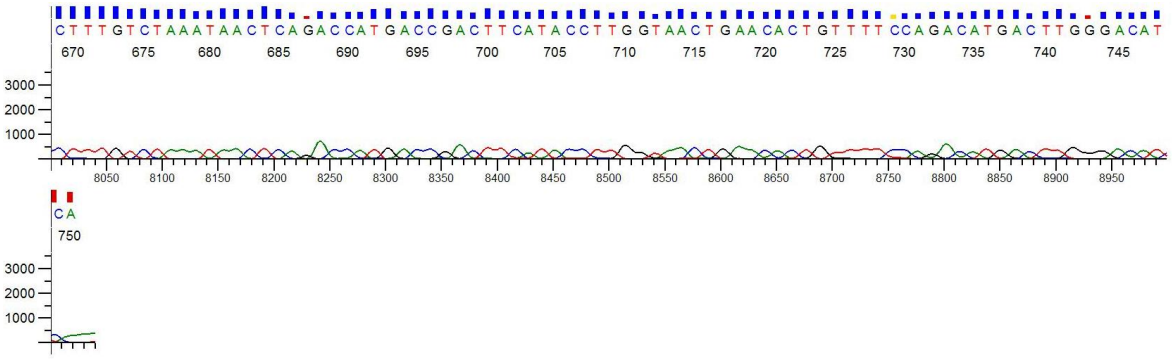

BGH

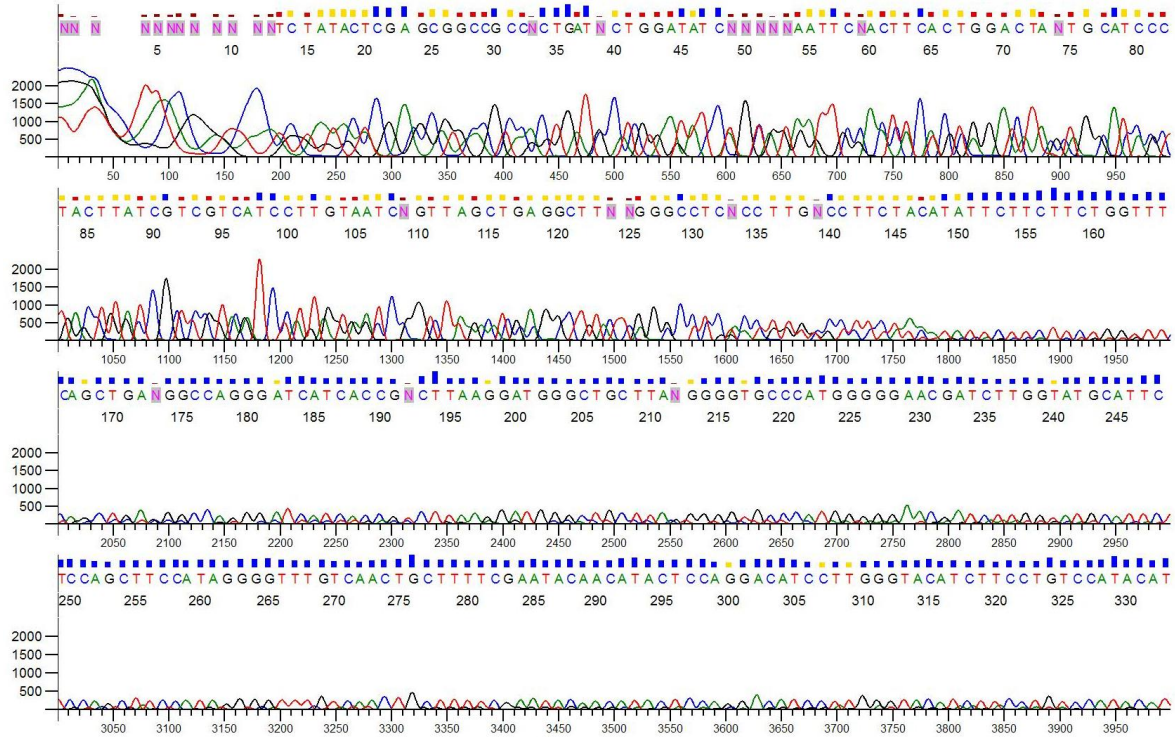

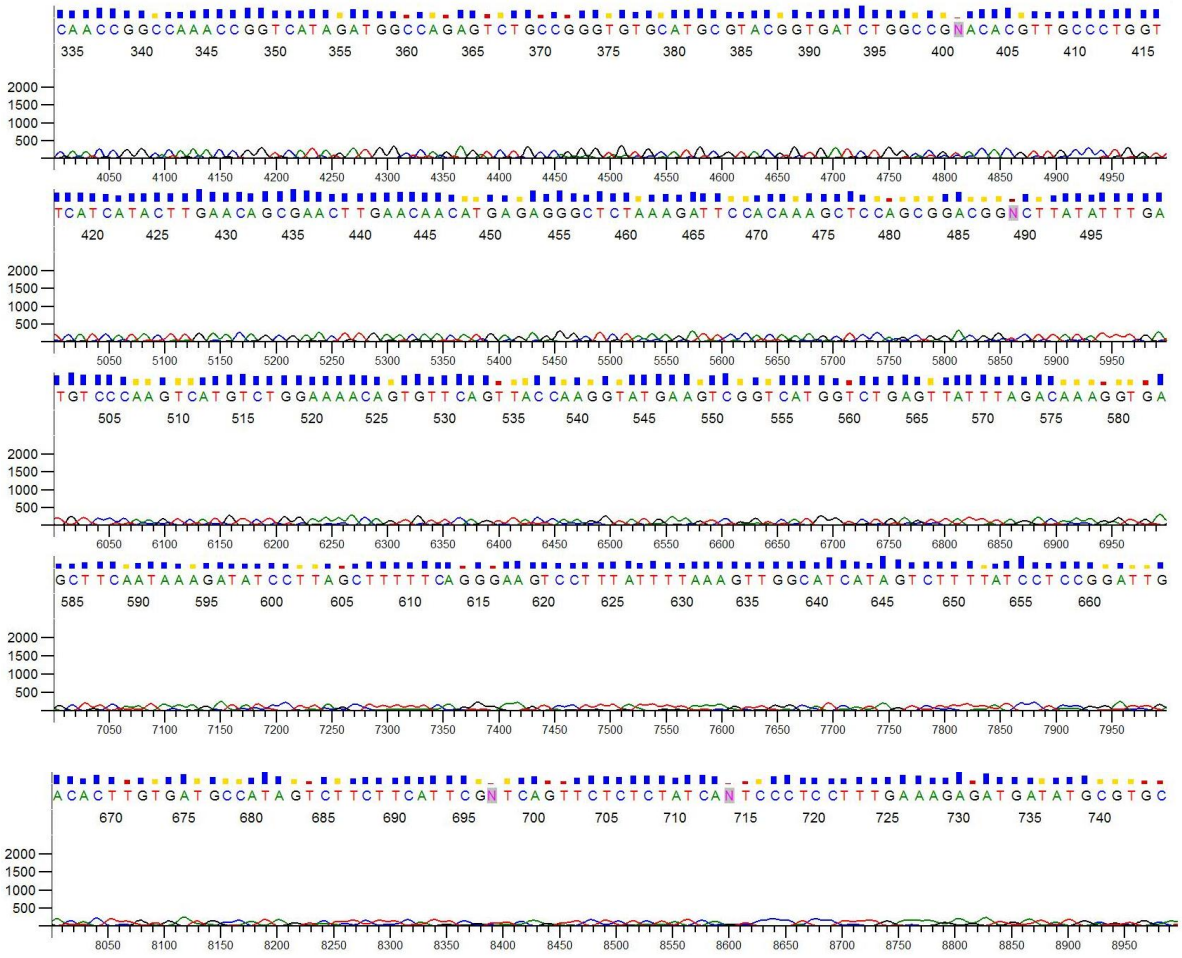
CAACCGGCCAAACCGGTCATAGATGGCCAGAGTCTGCCGGGTGTGCATGCGTACGGTGATCTGGCCGNACACGTTGCCCTGGT
335 340 345 350 355 360 365 370 375 380 385 390 395 400 405 410 415
2000 1500 1000 500
4050 4100 4150 4200 4250 4300 4350 4400 4450 4500 4550 4600 4650 4700 4750 4800 4850 4900 4950
TCATCATACTTGAACAGCGAACTTGAACAACATGAGAGGGCTCTAAAGATTCCACAAAGCTCCAGCGGACGGNCTTATATTTGA
420 425 430 435 440 445 450 455 460 465 470 475 480 485 490 495
2000 1500 1000 500
5050 5100 5150 5200 5250 5300 5350 5400 5450 5500 5550 5600 5650 5700 5750 5800 5850 5900 5950
TGTCCCAAGTCATGTCTGGAAAACAGTGTTCAGTTACCAAGGTATGAAGTCGGTCATGGTCTGAGTTATTTAGACAAAGGTGA
505 510 515 520 525 530 535 540 545 550 555 560 565 570 575 580
2000 1500 1000 500
6050 6100 6150 6200 6250 6300 6350 6400 6450 6500 6550 6600 6650 6700 6750 6800 6850 6900 6950
GCTTCAATAAAGATATCCTTAGCTTTTTTCAGGGAAGTCCTTTATTTTAAAGTTGGCATCATAGTCTTTTTATCCTCCGGATTG
585 590 595 600 605 610 615 620 625 630 635 640 645 650 655 660
2000 1500 1000 500
7050 7100 7150 7200 7250 7300 7350 7400 7450 7500 7550 7600 7650 7700 7750 7800 7850 7900 7950
ACACTTGTGATGCCATAGTCTTCTTCATTCGNTCAGTTCTCTCTATCANTCCCTCCTTTGAAAGAGATGATATGCGTGC
670 675 680 685 690 695 700 705 710 715 720 725 730 735 740
2000 1500 1000 500
8050 8100 8150 8200 8250 8300 8350 8400 8450 8500 8550 8600 8650 8700 8750 8800 8850 8900 8950

Appendix 10: MRPL45FLala clone sequencing

The following figures represent the sequences obtained for the forward (CMV) and reverse (BGH) primers used to confirm the identity of the cloned sequence. The output was analysed with *SeqScanner*.

CMV

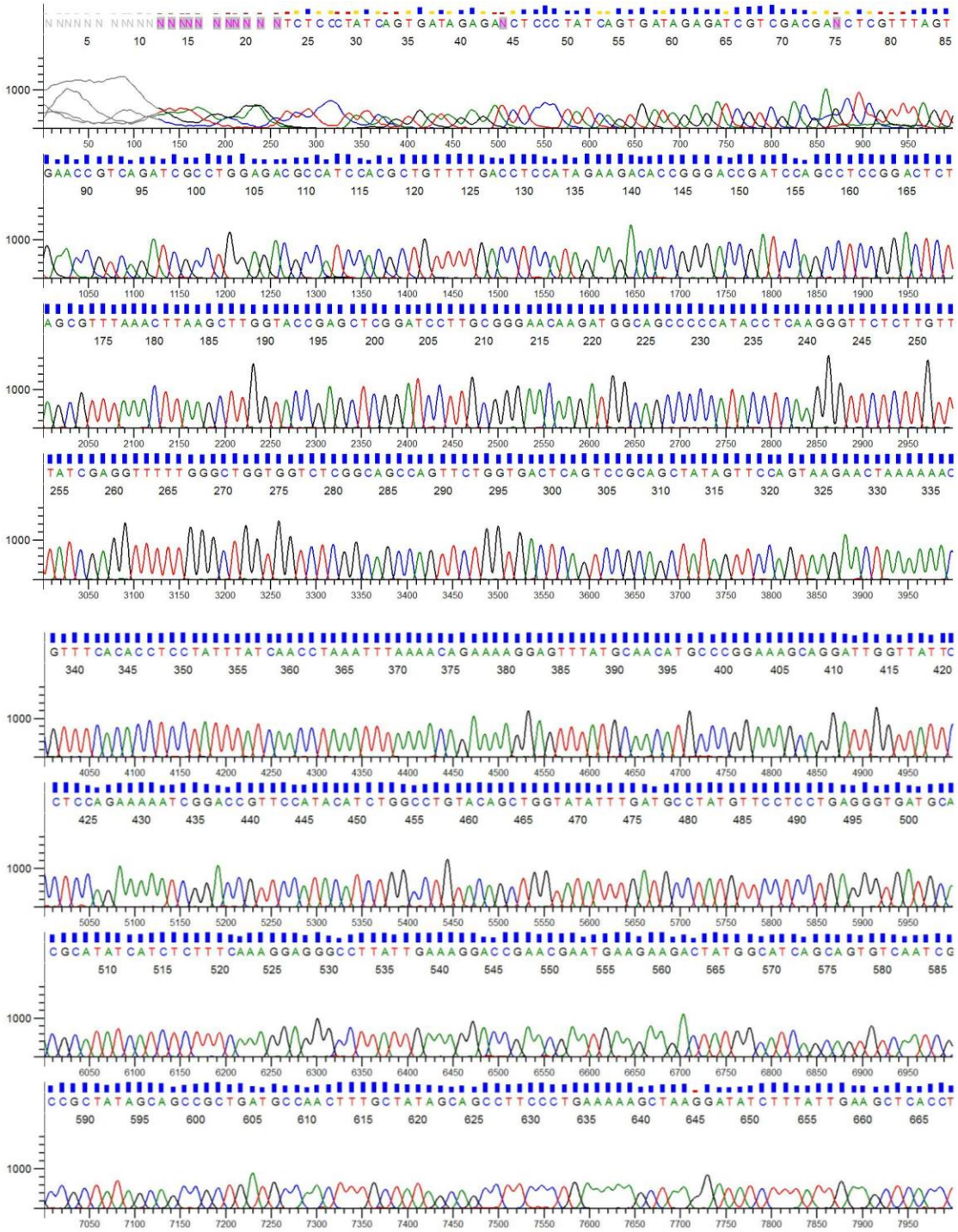

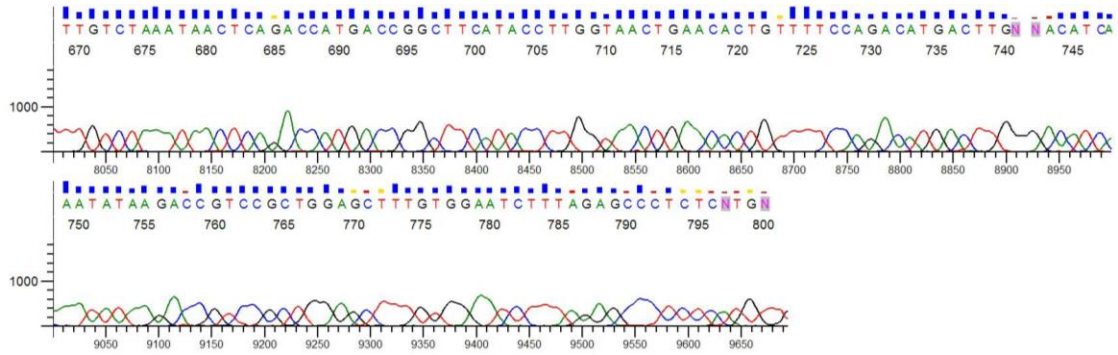

BGH

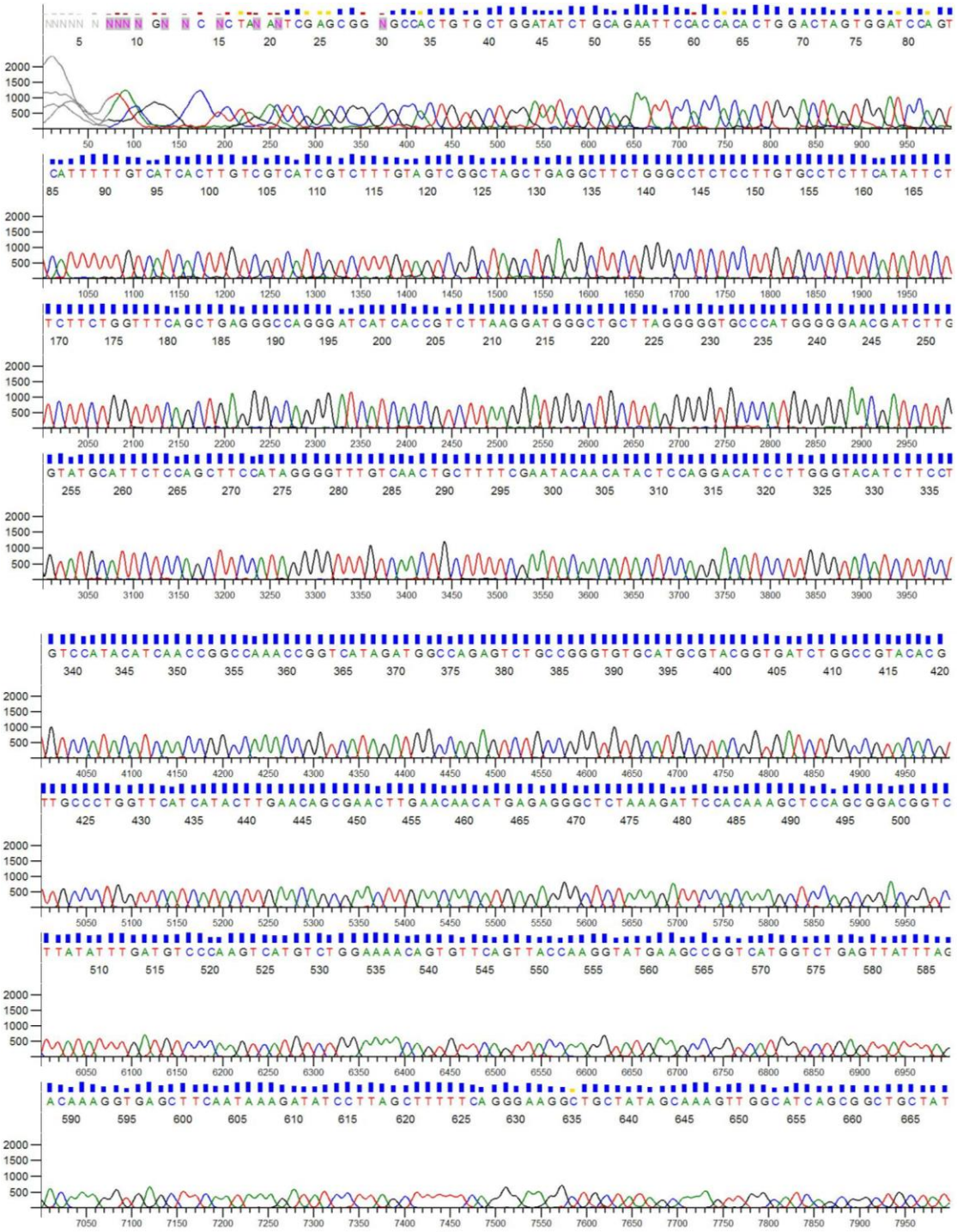

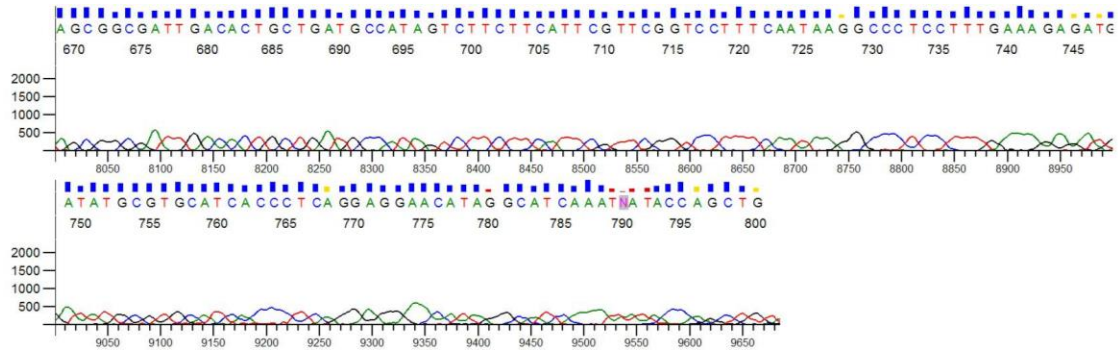
AGCGGGCGATTGACACTGCTGATGCCATAGTCTTCTTCATTCGTTCGGTCCTTTCAATAAGGCCCTCCTTTGAAAGAGATC
670 675 680 685 690 695 700 705 710 715 720 725 730 735 740 745
2000
1500
1000
500
8050 8100 8150 8200 8250 8300 8350 8400 8450 8500 8550 8600 8650 8700 8750 8800 8850 8900 8950

ATATGCGTGCATCACCCTCAGGAGGAACATAGGCATCAAATNATACCAGCTG
750 755 760 765 770 775 780 785 790 795 800
2000
1500
1000
500
9050 9100 9150 9200 9250 9300 9350 9400 9450 9500 9550 9600 9650

Appendix 11: MRPL45FLAGsil clone sequencing

The following figures represent the sequences obtained for the forward (CMV) and reverse (BGH) primers used to confirm the identity of the cloned sequence. The output was analysed with *SeqScanner*.

CMV

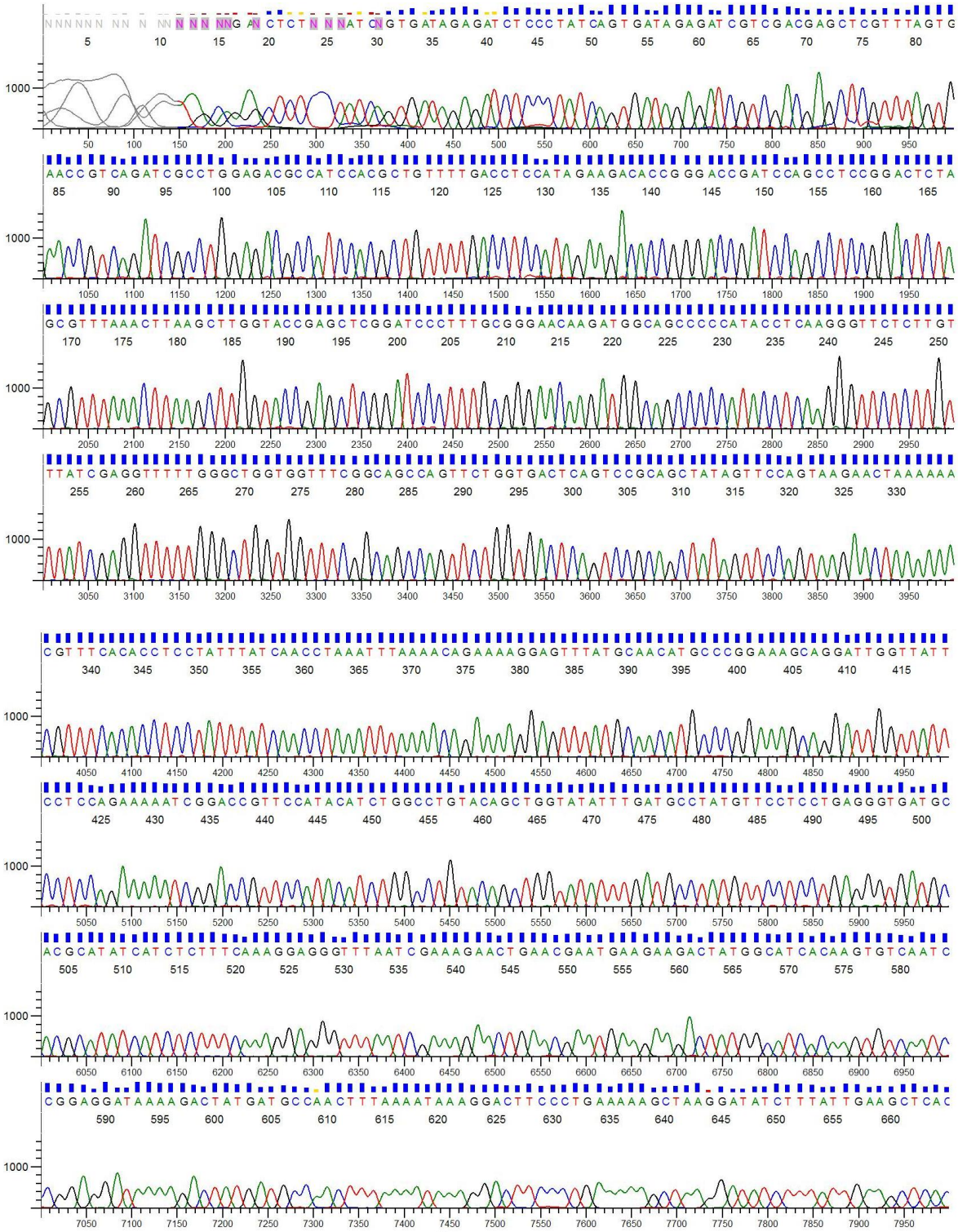

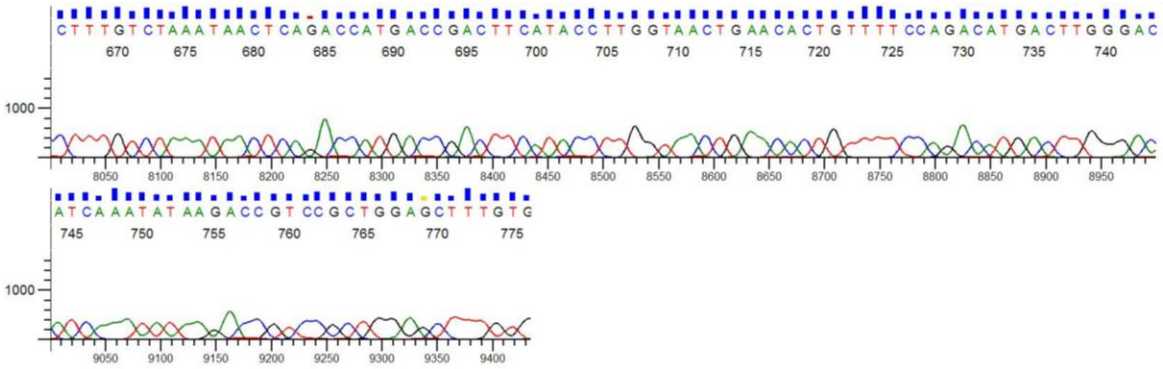

BGH

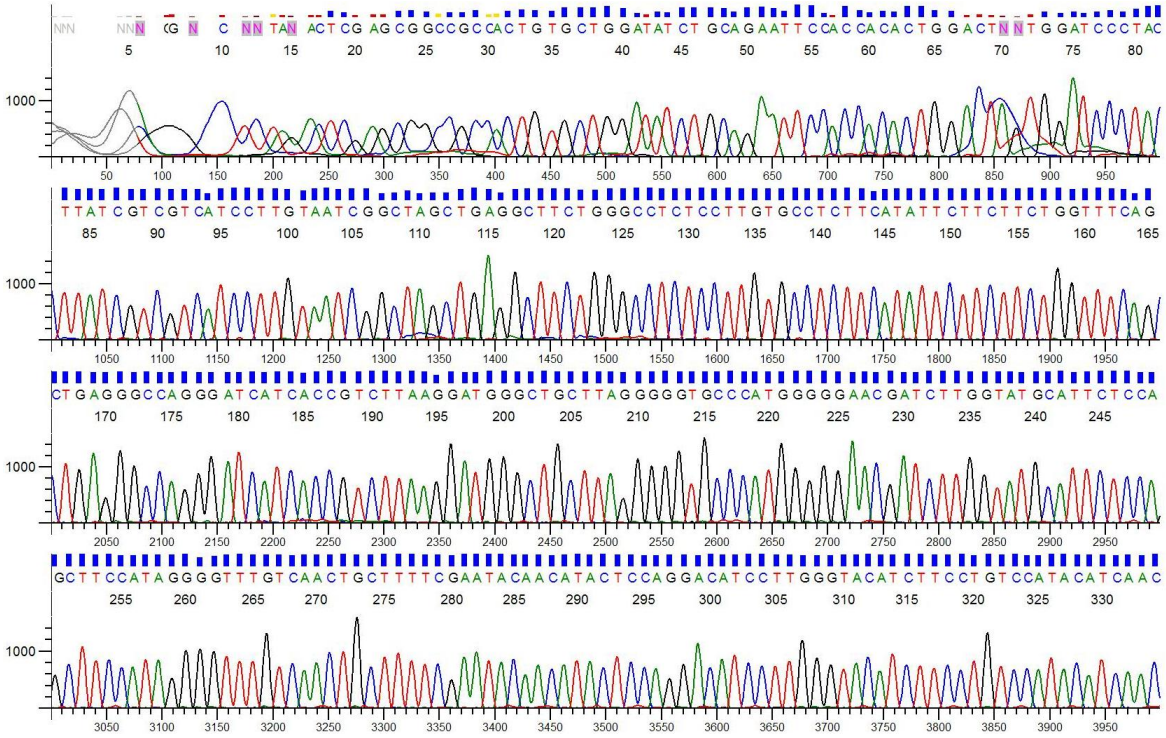

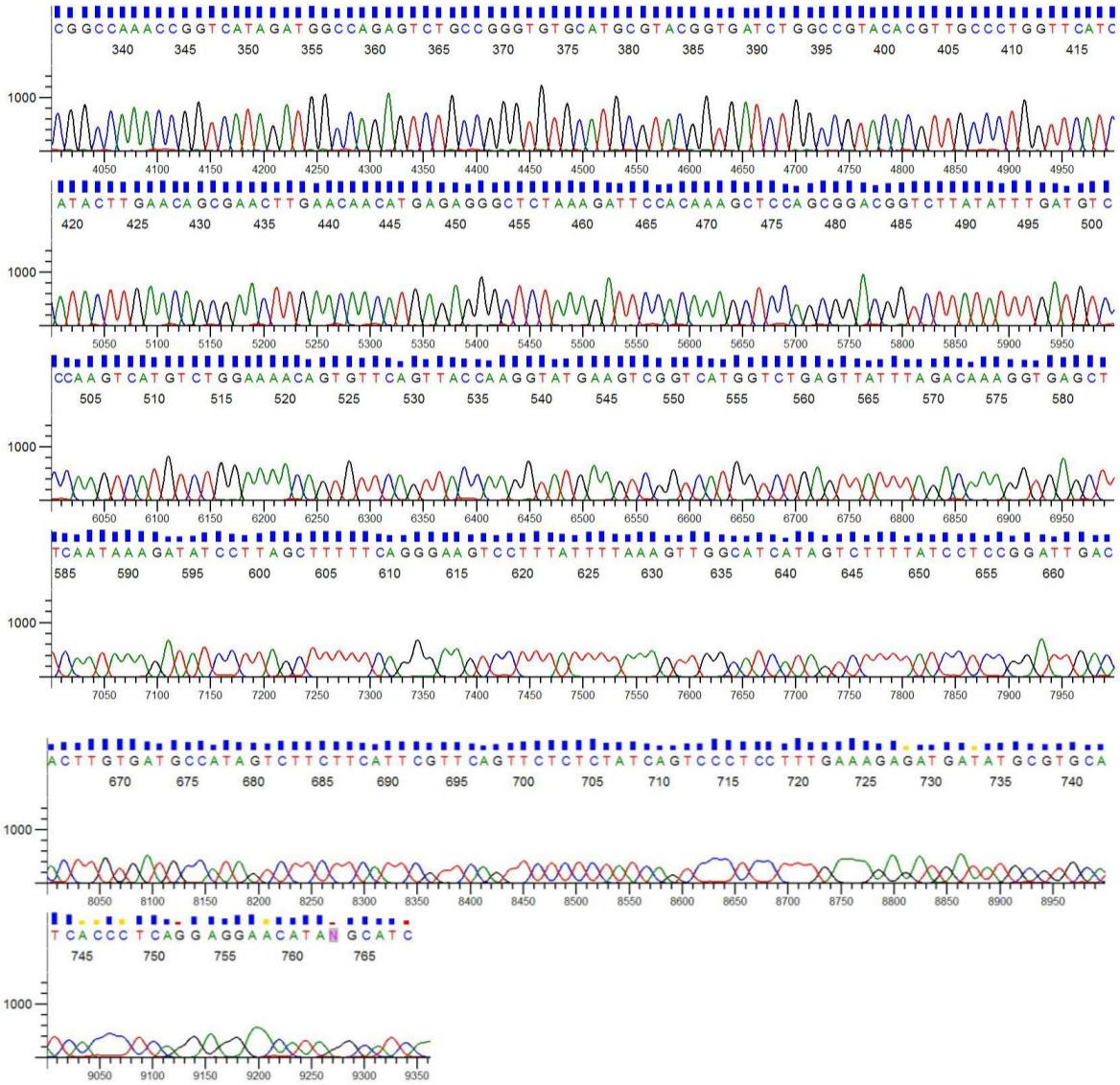
CGGCCAAACCGGTCATAGATGGCCAGAGTCTGCCGGGTGTGCATGCGTACGGTGATCTGGCCGTACACGTTGCCCTGGTTCATC
340 345 350 355 360 365 370 375 380 385 390 395 400 405 410 415
1000
4050 4100 4150 4200 4250 4300 4350 4400 4450 4500 4550 4600 4650 4700 4750 4800 4850 4900 4950
ATACTTGAACAGCGAACTTGAACAACATGAGAGGGCTCTAAAGATTCCACAAAGCTCCAGCGGACGGTCTTATATTTGATGTC
420 425 430 435 440 445 450 455 460 465 470 475 480 485 490 495 500
1000
5050 5100 5150 5200 5250 5300 5350 5400 5450 5500 5550 5600 5650 5700 5750 5800 5850 5900 5950
CCAAGTCATGTCTGGAAAACAGTGTTCAGTTACCAAGGTATGAAGTCGGTCATGGTCTGAGTTATTTAGACAAAGGTGAGCT
505 510 515 520 525 530 535 540 545 550 555 560 565 570 575 580
1000
6050 6100 6150 6200 6250 6300 6350 6400 6450 6500 6550 6600 6650 6700 6750 6800 6850 6900 6950
TCAATAAAGATATCCTTAGCTTTTTCAGGGAAGTCCTTTATTTTAAAGTTGGCATCATAGTCTTTTATCCTCCGGATTGAC
585 590 595 600 605 610 615 620 625 630 635 640 645 650 655 660
1000
7050 7100 7150 7200 7250 7300 7350 7400 7450 7500 7550 7600 7650 7700 7750 7800 7850 7900 7950
ACTTGTGATGCCATAGTCTTCTTCATTCGTTCAGTTCTCTCTATCAGTCCCTCCTTTGAAAGAGATGATATGCGTGCA
670 675 680 685 690 695 700 705 710 715 720 725 730 735 740
1000
8050 8100 8150 8200 8250 8300 8350 8400 8450 8500 8550 8600 8650 8700 8750 8800 8850 8900 8950
TCACCCTCAGGAGGAACATANGCATC
745 750 755 760 765
1000
9050 9100 9150 9200 9250 9300 9350

Appendix 12: MRPL45FLΔ clone sequencing

The following figures represent the sequences obtained for the forward (CMV) and reverse (BGH) primers used to confirm the identity of the cloned sequence. The output was analysed with *SeqScanner*.

CMV

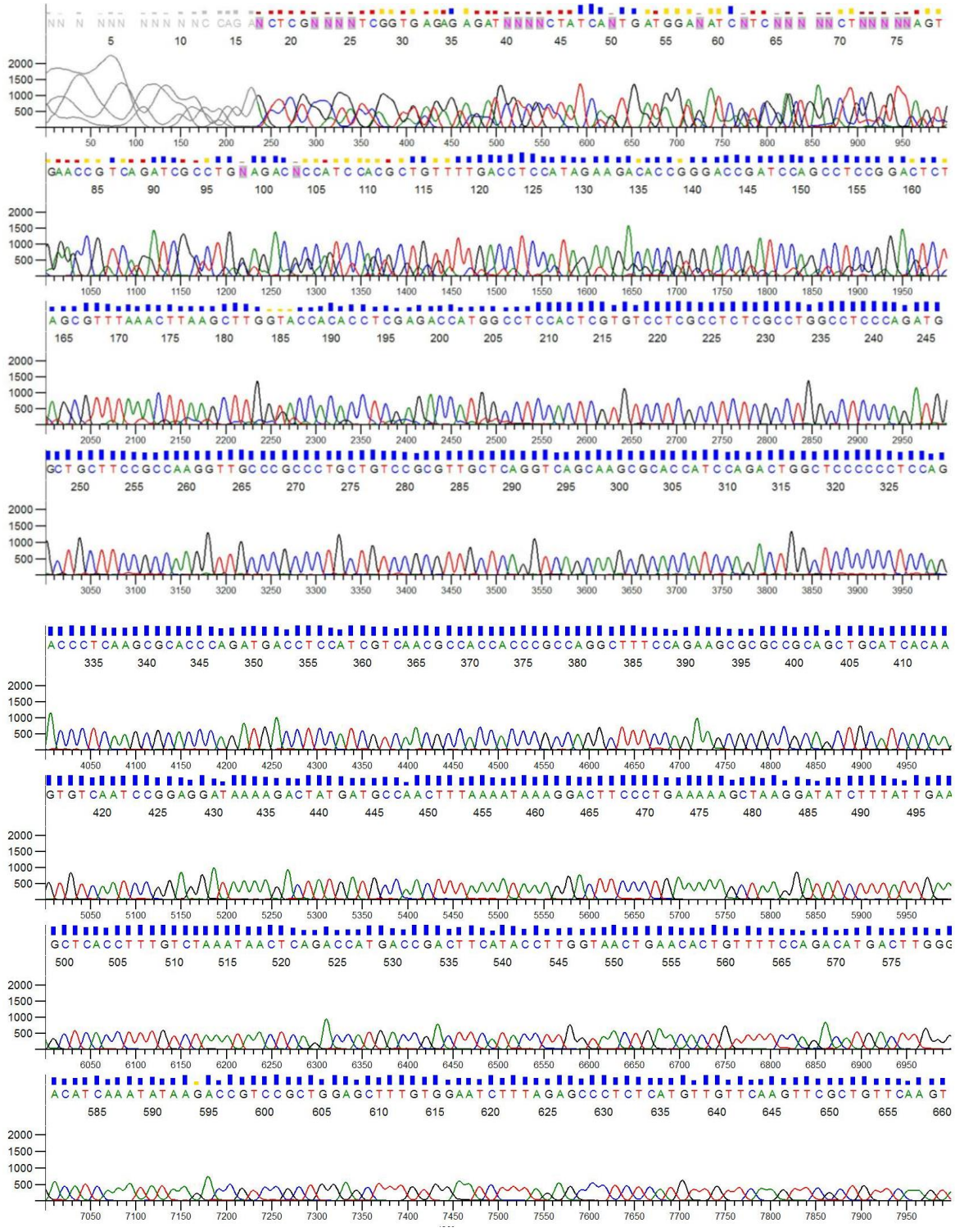

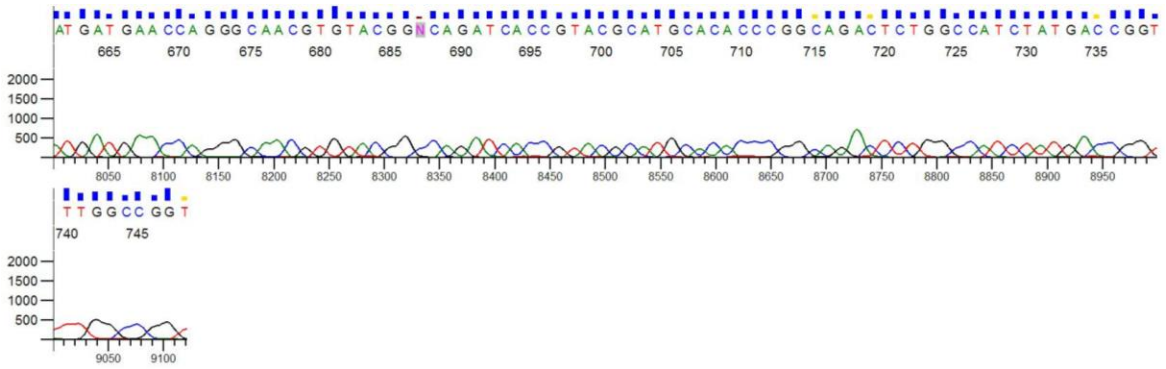

BGH

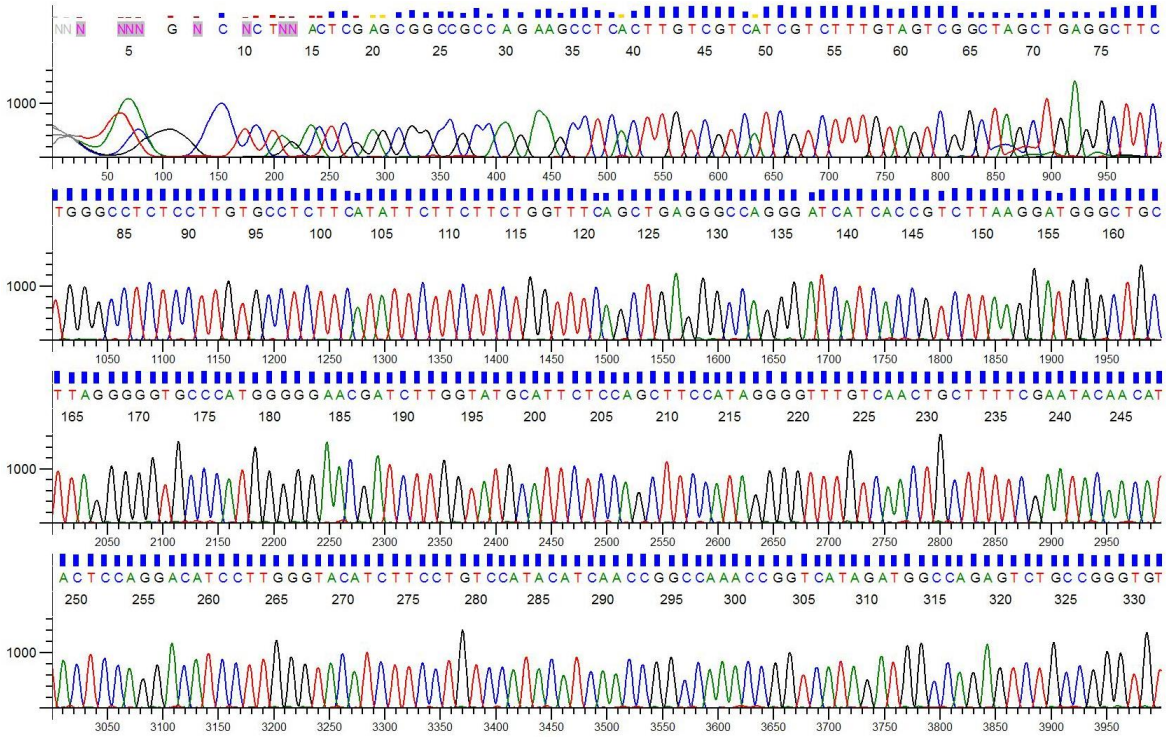

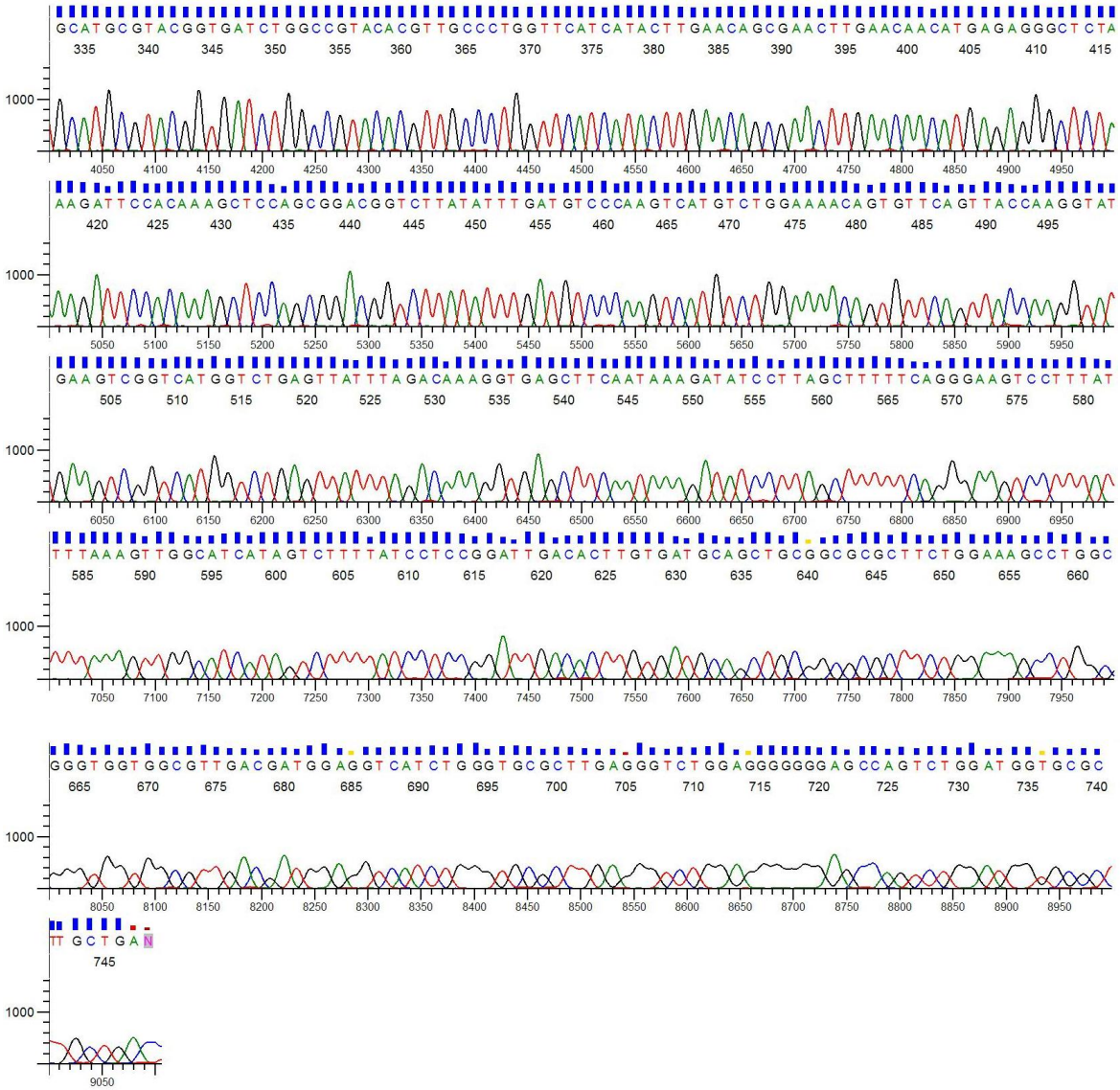
GCATGCGTACGGTGATCTGGCCGTACACGTTGCCCTGGTTCATCATACTTGAACAGCGAACTTGAACAACATGAGAGGGCTCTA
335 340 345 350 355 360 365 370 375 380 385 390 395 400 405 410 415
1000
4050 4100 4150 4200 4250 4300 4350 4400 4450 4500 4550 4600 4650 4700 4750 4800 4850 4900 4950
AAGATTCCACAAAGCTCCAGCGGACGGTCTTATATTTGATGTCCCAAGTCATGTCTGGAAAACAGTGTTCAGTTACCAAGGTAT
420 425 430 435 440 445 450 455 460 465 470 475 480 485 490 495
1000
5050 5100 5150 5200 5250 5300 5350 5400 5450 5500 5550 5600 5650 5700 5750 5800 5850 5900 5950
GAAGTCGGTCATGGTCTGAGTTATTTAGACAAAGGTGAGCTTCAATAAAGATATCCTTAGCTTTTTTCAGGGAAGTCCTTTAT
505 510 515 520 525 530 535 540 545 550 555 560 565 570 575 580
1000
6050 6100 6150 6200 6250 6300 6350 6400 6450 6500 6550 6600 6650 6700 6750 6800 6850 6900 6950
TTTAAAGTTGGCATCATAGTCTTTTTATCCTCCGGATTGACACTTGTGATGCAGCTGCGGCGCGCTTCTGGAAAGCCTGGC
585 590 595 600 605 610 615 620 625 630 635 640 645 650 655 660
1000
7050 7100 7150 7200 7250 7300 7350 7400 7450 7500 7550 7600 7650 7700 7750 7800 7850 7900 7950
GGGTGGTGGCGTTGACGATGGAGGTCATCTGGGTGCGCTTGAGGGTCTGGAGGGGGGGAGCCAGTCTGGATGGTGCGC
665 670 675 680 685 690 695 700 705 710 715 720 725 730 735 740
1000
8050 8100 8150 8200 8250 8300 8350 8400 8450 8500 8550 8600 8650 8700 8750 8800 8850 8900 8950
TTGCTGAN
745
1000
9050

Appendix 13: FLAG immunoprecipitation on induced HEK293-MRPL45FLAG cells in presence of ethidium bromide

Only the mitochondrial protein identified in the samples are listed. The following data obtained from the mass spectrometry analysis are reported:

- log(I) = Sum of raw spectra
- rI = Number of peptides found
- log(e) = Expectation of finding the protein stochastically. A cut-off of −2 was chosen for this score, which corresponds to a 1 in 100 chance of a stochastic protein assignment.

Biological repeat n. 1

Samples

MRPL45FLAG: FLAG-immunoprecipitation from mitochondria of ethidium bromide treated and induced HEK293-MRPL45FLAG cells

Control: FLAG-immunoprecipitation from mitochondria of ethidium bromide treated HEK293 cells

Sample	Identifier	Protein	log(I)	rI	log(e)
MRPL45FLAG	ENSP00000308901	MRPL45	8.24	170	-426.0
MRPL45FLAG	ENSP00000297185	mt-HSP70	7.83	106	-360.0
MRPL45FLAG	ENSP00000373620	HSP60	7.38	42	-253.0
MRPL45FLAG	ENSP00000381736	ATP5α	7.35	27	-213.0
MRPL45FLAG	ENSP00000262030	ATP5β	7.28	27	-187.0
MRPL45FLAG	ENSP00000360671	ADP/ATP translocase 2	7.15	19	-130.0
MRPL45FLAG	ENSP00000300408	Prohibitin	7.21	13	-96.0
MRPL45FLAG	ENSP00000441875	Prohibitin2	7.01	14	-87.9
MRPL45FLAG	ENSP00000370808	ADP/ATP translocase 3	6.84	13	-86.8
MRPL45FLAG	ENSP00000265333	VDAC1	6.68	10	-69.5
MRPL45FLAG	ENSP00000322439	mt-EF-Tu	6.72	8	-63.0
MRPL45FLAG	ENSP00000246957	HSP75	6.52	6	-59.7
MRPL45FLAG	ENSP00000265838	Acetyl-CoA acetyltransferase	6.73	9	-56.6
MRPL45FLAG	ENSP00000368031	ATPase family AAA domain-containing protein 3A	6.52	7	-51.3
MRPL45FLAG	ENSP00000298468	VDAC2	6.75	8	-49.2
MRPL45FLAG	ENSP00000280346	Pyruvate dehydrogenase complex component E2	6.49	6	-36.9
MRPL45FLAG	ENSP00000307241	Pyruvate dehydrogenase E1 component subunit β	6.24	6	-36.6
MRPL45FLAG	ENSP00000298510	Thioredoxin-dependent peroxide reductase	6.50	5	-36.5
MRPL45FLAG	ENSP00000349142	ATP5γ	6.50	5	-35.2
MRPL45FLAG	ENSP00000290299	ATP5O	6.38	5	-34.9
MRPL45FLAG	ENSP00000263774	Complex I-30kD	6.23	4	-34.3

MRPL45FLAG	ENSP00000356290	Formyltetrahydrofolate synthetase	6.39	4	-32.8
MRPL45FLAG	ENSP00000277865	GDH 1	6.21	4	-32.3
MRPL45FLAG	ENSP00000265631	Mitochondrial aspartate glutamate carrier 2	6.16	5	-31.6
MRPL45FLAG	ENSP00000394382	Pyruvate dehydrogenase, subunit α	6.17	3	-28.2
MRPL45FLAG	ENSP00000315122	Apoptosis-inducing factor 1	6.05	3	-27.9
MRPL45FLAG	ENSP00000225665	Mitochondrial 2-oxoglutarate/malate carrier protein	6.05	3	-27.2
MRPL45FLAG	ENSP00000317159	Cytochrome c1	6.16	3	-24.7
MRPL45FLAG	ENSP00000428845	VDAC3	6.26	4	-23.1
MRPL45FLAG	ENSP00000383898	Phosphate carrier protein	6.37	6	-22.6
MRPL45FLAG	ENSP00000360268	Gamma-glutamyl kinase	6.10	3	-21.7
MRPL45FLAG	ENSP00000261413	MRPS27	6.01	3	-21.0
MRPL45FLAG	ENSP00000420961	Sideroflexin-1	5.98	2	-12.6
MRPL45FLAG	ENSP00000294053	CLPB	5.82	2	-12.4
MRPL45FLAG	ENSP00000359151	Dihydrolipoamide branched chain transacylase	5.97	2	-12.3
MRPL45FLAG	ENSP00000284967	MRPL39	5.80	2	-11.3
MRPL45FLAG	ENSP00000387262	Mitofilin	6.14	3	-11.3
MRPL45FLAG	ENSP00000262570	CHCHD3	5.74	2	-11.0
MRPL45FLAG	ENSP00000370023	Trifunctional enzyme subunit α	5.81	2	-10.7
MRPL45FLAG	ENSP00000216121	NipSnap1	5.84	2	-10.4
MRPL45FLAG	ENSP00000318115	TIM50	6.08	3	-9.9
MRPL45FLAG	ENSP00000357838	Ornithine aminotransferase	5.55	1	-9.6
MRPL45FLAG	ENSP00000358737	ATP5b	5.82	2	-9.2
MRPL45FLAG	ENSP00000378812	CHCHD2	6.02	4	-9.2
MRPL45FLAG	ENSP00000333667	Serine hydroxymethyltransferase	5.62	1	-8.6
MRPL45FLAG	ENSP00000249269	Mitochondrial-processing peptidase, subunit β	5.85	2	-8.5
MRPL45FLAG	ENSP00000354525	MRPL24	5.63	1	-7.0
MRPL45FLAG	ENSP00000457733	Mitochondrial ATP-Mg/Pi carrier protein 1	5.67	1	-6.0
MRPL45FLAG	ENSP00000348886	Stomatin-like protein 2	5.50	1	-4.9
MRPL45FLAG	ENSP00000317379	L-glutamine amidohydrolase	5.30	1	-4.0
MRPL45FLAG	ENSP00000327070	Malate dehydrogenase	5.64	1	-3.9
MRPL45FLAG	ENSP00000437996	ATP5d	5.23	1	-3.9
MRPL45FLAG	ENSP00000321070	Malic enzyme 2	5.34	1	-3.7
MRPL45FLAG	ENSP00000168216	Mitochondrial RNase P protein 2	5.80	2	-3.5
MRPL45FLAG	ENSP00000260665	LRPPRC	5.66	1	-3.5

MRPL45FLAG	ENSP00000245206	Aspartate aminotransferase	5.46	1	-3.1
MRPL45FLAG	ENSP00000400646	PNPase 1	5.54	1	-3.1
MRPL45FLAG	ENSP00000269143	Paraplegin-like protein	5.40	1	-3.0
MRPL45FLAG	ENSP00000446779	Citrate synthase	5.45	1	-2.8
MRPL45FLAG	ENSP00000264954	GrpE protein homolog 1	5.84	1	-2.4
MRPL45FLAG	ENSP00000253577	ATP-binding cassette transporter 7	5.27	1	-2.2
MRPL45FLAG	ENSP00000439565	MRPL12	5.44	1	-1.3
MRPL45FLAG	ENSP00000321971	MIRO-2	5.53	1	-1.2
MRPL45FLAG	ENSP00000215882	Citrate transport protein	5.75	1	-1.1
MRPL45FLAG	ENSP00000270538	TIM44	5.73	1	-1.1
MRPL45FLAG	ENSP00000350191	Succinate-semialdehyde dehydrogenase	5.98	1	-1.1
Control	ENSP00000381736	ATP5α	7.10	14	-130.0
Control	ENSP00000262030	ATP5β	6.70	12	-79.4
Control	ENSP00000360671	ADP/ATP translocase 2	6.70	10	-75.0
Control	ENSP00000265838	Acetyl-CoA acetyltransferase	6.68	9	-65.6
Control	ENSP00000297185	mt-HSP70	6.60	9	-56.1
Control	ENSP00000300408	Prohibitin	6.87	7	-54.1
Control	ENSP00000322439	mtEF-Tu	6.38	5	-47.7
Control	ENSP00000370808	ADP/ATP translocase 3	6.48	7	-39.6
Control	ENSP00000298468	VDAC2	6.33	4	-36.0
Control	ENSP00000373620	HSP60	6.32	5	-30.9
Control	ENSP00000298510	Peroxiredoxin-3	6.22	3	-21.7
Control	ENSP00000349142	ATP5γ	6.09	3	-21.7
Control	ENSP00000393496	ATP5O	5.96	3	-21.0
Control	ENSP00000265333	VDAC1	6.19	3	-20.6
Control	ENSP00000317159	Cytochrome C1	5.84	2	-12.4
Control	ENSP00000356290	Formyltetrahydrofolate synthetase	6.11	2	-11.4
Control	ENSP00000261413	MRPS27	5.92	2	-9.4
Control	ENSP00000457733	Mitochondrial ATP-Mg/Pi carrier protein 1	5.29	1	-5.2
Control	ENSP00000348886	Stomatin-like protein 2	5.35	1	-4.5
Control	ENSP00000383898	Phosphate carrier protein	5.64	2	-3.2
Control	ENSP00000388658	Mitochondrial aspartate glutamate carrier 1	5.40	1	-3.1
Control	ENSP00000168216	Mitochondrial RNase P protein 2	5.19	1	-2.8
Control	ENSP00000215882	Citrate transport protein	5.70	1	-1.7

Biological repeat n. 2

Samples

MRPL45FLAG: FLAG-immunoprecipitation from mitochondria of ethidium bromide treated and induced HEK293-MRPL45FLAG cells

Control: FLAG-immunoprecipitation from mitochondria of ethidium bromide treated and induced HEK293-MRPS27FLAG cells

Sample	Identifier	Protein	log(I)	rI	log(e)
MRPL45FLAG	ENSP00000308901	MRPL45	3.17	23	-89.9
MRPL45FLAG	ENSP00000297185	mt-HSP70	2.6	16	-89.8
MRPL45FLAG	ENSP00000262030	ATP5β	2.36	12	-56.9
MRPL45FLAG	ENSP00000300408	Prohibitin	1.66	6	-28.5
MRPL45FLAG	ENSP00000373620	HSP60	1.86	4	-18.3
MRPL45FLAG	ENSP00000370023	Trifunctional enzyme subunit α	1.24	2	-10.5
MRPL45FLAG	ENSP00000356290	Formyltetrahydrofolate synthetase	0.82	2	-10.2
MRPL45FLAG	ENSP00000419038	mtEF-G1	1.21	2	-9.9
MRPL45FLAG	ENSP00000260665	LRPPRC	1.41	2	-9.3
MRPL45FLAG	ENSP00000360268	Gamma-glutamyl kinase	0.99	2	-8.8
MRPL45FLAG	ENSP00000381736	ATP5α	1.69	2	-7.4
MRPL45FLAG	ENSP00000311766	ATPase family AAA domain-containing protein 3B	1.41	2	-4.3
MRPL45FLAG	ENSP00000360671	ADP/ATP translocase 2	1.23	1	-4.2
MRPL45FLAG	ENSP00000392451	tRNA pseudouridine synthase A	0.45	1	-2.5
MRPL45FLAG	ENSP00000431040	MRPL22	0.49	1	-1.9
MRPL45FLAG	ENSP00000265333	VDAC1	1.06	1	-1.9
MRPL45FLAG	ENSP00000287025	mTERF3	0.82	1	-1.4
MRPL45FLAG	ENSP00000451320	Bcl-2-like protein 2	0.53	1	-1.3
MRPL45FLAG	ENSP00000281456	ADP/ATP translocase 1	0.83	1	-1.3
MRPL45FLAG	ENSP00000244571	Alanine-tRNA ligase	0.57	1	-1.1
MRPL45FLAG	ENSP00000402535	Apoptosis-inducing factor 1	0.79	1	-1.1
Control	ENSP00000261413	MRPS27	3.75	91	-316
Control	ENSP00000297185	mt-HSP70	2.42	17	-70.6
Control	ENSP00000262030	ATP5β	2.37	14	-60.2
Control	ENSP00000418008	MRPS22	2.04	8	-48.7
Control	ENSP00000373620	mt-HSP60	2	6	-37.7
Control	ENSP00000300408	Prohibitin	1.97	7	-31
Control	ENSP00000260665	LRPPRC	1.53	4	-23.6
Control	ENSP00000322439	mtEF-Tu	1.76	4	-22
Control	ENSP00000356290	Formyltetrahydrofolate synthetase	1.03	3	-17.8
Control	ENSP00000360671	ADP/ATP translocase 2	2.27	5	-16.9

Control	ENSP00000369682	MRPS26	1.67	6	-13
Control	ENSP00000259873	MRPS18b	1.7	6	-11.9
Control	ENSP00000370023	Trifunctional enzyme subunit α	1.04	2	-10.1
Control	ENSP00000402535	Apoptosis-inducing factor 1	1.04	2	-8.8
Control	ENSP00000281456	ADP/ATP translocase 1	2.13	2	-8.4
Control	ENSP00000177742	MRPS34	1.85	3	-8.2
Control	ENSP00000225665	Mitochondrial 2-oxoglutarate/malate carrier protein	0.74	2	-7.9
Control	ENSP00000311766	ATPase family AAA domain-containing protein 3B	1.34	2	-4.3
Control	ENSP00000265838	Acetyl-CoA acetyltransferase	1.25	2	-3.8
Control	ENSP00000452762	Electron transfer flavoprotein subunit α	0.44	1	-2.7
Control	ENSP00000246957	HSP75	1.41	2	-2
Control	ENSP00000244571	Alanine-tRNA ligase	0.48	1	-1.9
Control	ENSP00000254636	Mitofilin	1.05	2	-1.4
Control	ENSP00000249269	Mitochondrial-processing peptidase. subunit β	0.93	1	-1.4
Control	ENSP00000355741	Chaperone-ABC1-like	0.78	1	-1.1

Appendix 14: MRPL45 immunoprecipitation on induced HEK293-MRPL45 cells in presence of ethidium bromide

Only the mitochondrial protein identified in the samples are listed. The following data obtained from the mass spectrometry analysis are reported:

- log(I) = Sum of raw spectra
- rI = Number of peptides found
- log(e) = Expectation of finding the protein stochastically. A cut-off of −2 was chosen for this score, which corresponds to a 1 in 100 chance of a stochastic protein assignment.

Samples

MRPL45: MRPL45-immunoprecipitation from mitochondria of ethidium bromide treated and induced HEK293-MRPL45FLAG cells.
Control: MNKI-immunoprecipitation from mitochondria of ethidium bromide treated HEK293 cells.

Biological repeat n. 1

Sample	Identifier	Protein	log(I)	rI	log(e)
MRPL45	ENSP00000308901	MRPL45	2.79	23	-45.3
MRPL45	ENSP00000297185	mt-HSP70	2.04	6	-24.3
MRPL45	ENSP00000373620	HSP60	1.10	1	-1.5
MRPL45	ENSP00000281456	ADP/ATP translocase 1	1.16	1	-1.5
Control	ENSP00000281456	ADP/ATP translocase 1	1,04	1	-1,1

Biological repeat n. 2

Sample	Identifier	Protein	log(I)	rI	log(e)
MRPL45	ENSP00000308901	MRPL45	2,7	17	-55
MRPL45	ENSP00000297185	mt-HSP70	1,03	4	-22,1
MRPL45	ENSP00000262030	ATP5β	0,67	1	-2,2
MRPL45	ENSP00000440846	Monoamine oxidase type A	0,53	1	-1,5
Control	ENSP00000262030	ATP5β	1,48	3	-10,6
Control	ENSP00000381736	ATP5α	1,06	1	-1,8

Appendix 15: Resolved structure of human MRPL45 to date

The following figure represent the resolved structure of human MRPL45 to date (Brown A et al., 2014). The DSSP legend is found at the bottom of the figure.

Appendix 16: Alignment of human MRPL45, yeast TIM44 and human TIM44

The alignment was performed using ClustalOmega.

```
MRPL45          -------------------------MAAPIPQGFSCLSRFLGWWFRQPVLVTQSAAI---
TIM44yeast      ----MHRSTFIRTS----GTSSRTL-------TARYRSQYT-GLLVARVLFSTSTTRAQG
TIM44human      MAAAALRSGWCRCPRRCLGSGIQFLSSHNLPHGSTYQMRRPGGELPL-------SKSYSS
                                                :    :         :

MRPL45          ------------------------------------------------------------
TIM44yeast      GNPRSPLQIFRDTFKKEWEKSQELQENIKTLQDASGKLGESEAYKKAREAYLKAQRGST-
TIM44human      GNRKGFLSGLLDNVKQELAKNKEMKESIKKFRDEARRLEESDVLQEARRKYKTIESETVR


MRPL45          ------------------------------------------------------VPVRT-
TIM44yeast      ---IVGKTLKKTGETMEHIATKAWESELGKNTRKAAAATAKKLDESF-------EPVRQT
TIM44human      TSEVLRKKLGELTGTVKESLHEVSKSDLGRKIKEGVEEAAKTAKQSAESVSKGGEKLGRT
                                                                       :

MRPL45          ---------------------KKRFTPPIY--QPKFKTEKEFMQHARKAGLVIPPEKSDR
TIM44yeast      KIYKEV-------SEVIDDGESSRYGGFITKEQRRLKRERDLASGKR--HRAVKSNEDAG
TIM44human      AAFRALSQGVESVKKEIDDSVLGQTGPYRR--PQRLRKRTEFAGDKFKEEKVFEPNEEA-
                              :          ::: . ::         ..  ::.

MRPL45          SIHLACTA-----------------GIFDAYVP------PEGDARIS----------SLS
TIM44yeast      TAVVATNIESKESFGKKVEDFKEKTVVGRSIQSLKNKLWDESENPLIVVM----RKITNK
TIM44human      ---LGVVLHKDSKWYQQWKDFKENNVVFNRFFEMK-MKYDESDNAFIRASRALTDKVTDL
                   :.                     :            *.:  :           :

MRPL45          KEGLIERTERMKKTMASQVSIRRIKDYDANFKIKDFPEKAKDIFIEAHL-CLNNSDHDRL
TIM44yeast      VGGFFAETES-------SRVYSQFKLMDPTFSNESFTRHLREYIVPEILEAYVKGDVKVL
TIM44human      LGGLFSKTEM-------SEVLTEILRVDPAFDKDRFLKQCENDIIPNVLEAMISGELDIL
                  *:: .**        .    .:   *  *. . * .: .: ::   * .  ..: . *

MRPL45          HTLVTEHCFPDMTWDIK-YKTVRWSFVESLEPSHVVQVRCSSMMNQGNVYGQITVRMHTR
TIM44yeast      KKWFSEAPFNVYAAQQKIFKEQDVYADGRILDIRGVEIVSAKLLAPQDIPVLVVGCRAQE
TIM44human      KDWCYEATYSQLAHPIQQAKALGLQFHSRILDIDNVDLAMGKMMEQG--PVLIITFQAQL
                :    *  :   :   :  *         :     *::  ..::        :

MRPL45          QTLAIYDRFGRLMYGQEDVPKDVLEYVVF----EKQLTNPYGSWRMHTKIVPPWAPPKQP
TIM44yeast      INLYRKKKTGEIAAGDEANILMSSYAMVFTRDPEQIDDDETEGWKILEFVRGGS----RQ
TIM44human      VM-VVRNPKGEVVEGDPDKVLRMLYVWALCRDQDEL--NPYAAWRLLDISASST----EQ
                      .  *.:  *:           .:    ::   :   .*::            .

MRPL45          ILKTVMIPGPQLKPEEEYEEAQGEAQKPQLA
TIM44yeast      FT-----------------------------
TIM44human      IL-----------------------------
                :
```

Appendix 17: mRNA sequences targeted by OXA1L siRNA

The sequences of OXAsi02, OXAsi03 and OXAsi04 were analysed to identify targets using BLAST (http://blast.ncbi.nlm.nih.gov/). The targets and the percentage of their query cover and identity are reported in the following table.

siRNA	Target	Query cover	Identity
OXAsi01	OXA1L	100%	100%
	MIP, Major intrinsic protein of lens fiber	78%	100%
	DDX46, DEAD-box helicase 46	73%	100%
	FBXO38, F-box protein 38	73%	100%
	RHOU, Ras homolog family member U	73%	100%
OXAsi02	OXA1L	100%	100%
	HLF, Hepatic leukemia factor	73%	100%
	MYL12A, Myosin regulatory light chain 12A	68%	100%
	SPG7, Paraplegin	68%	100%
	REG3G, Regenerating islet-derived protein 3-gamma	68%	100%
	CELSR3, Epidermal growth factor-like protein 1	68%	100%
	KRT4, Cytokeratin-4	68%	100%
	PLEKHF1, Pleckstrin homology domain-containing family F member 1	68%	100%
	SFXN5, Sideroflexin-5	68%	100%
OXAsi03	OXA1L	100%	100%
	PANK1, Pantothenate kinase 1	73%	100%
	DIS3, Exosome complex exonuclease RRP44	68%	100%
	SIX4, SIX homeobox 4	68%	100%
	GLANT4, Polypeptide N-acetylgalactosaminyltransferase 4	68%	100%
	GNRH1, Progonadoliberin-1	68%	100%
	ZNF711, Zinc finger protein 711	68%	100%
OXAsi04	OXA1L	100%	100%
	C5orf63, Glutaredoxin-like protein C5orf63	73%	100%
	MEIG1, Meiosis/spermiogenesis associated 1	73%	100%
	DMRTA1, Doublesex- and mab-3-related transcription factor A1	73%	100%
	CDHR4, Cadherin-related family member 4	68%	100%
	DNAH11, Dynein heavy chain 11, axonemal	68%	100%
	SLC22A16, Solute carrier family 22 member 16	68%	100%
	RNF165,	68%	100%

Appendix 18: The role of LetM1 in the interaction between mitoribosome and IMM

Introduction

As previously stated throughout this work, mitochondrial translation is likely to be localised in close proximity to the IMM in order to allow the rapid insertion of the highly hydrophobic OXPHOS components synthesised within the organelle itself. In yeast, together with Oxa1, another IMM protein has been suggested to mediate this interaction. This protein, named Mdm38, is conserved amongst eukaryotes and its homologue in human is named LetM1 (leucine zipper EF-hand-containing transmembrane protein 1).

Mdm38 (RefSeq. NP_014615.1) was found to interact with the large mitoribosomal subunit via a ribosome binding domain (RBD, between residues 182 and 404) located on the matrix side (Frazier AE et al., 2006). This domain has been confirmed to bind the mitoribosome *in vitro*, and structural studies assigned a 14-3-3-like structure to this domain (Lupo D et al., 2011). This structure is canonically consists of 9 antiparallel α-helices arranged in a U-like conformation and creates a cavity that allows the interaction with other proteins (Aitken A, 2006). The cavity allows the interaction with phosphorylated proteins via a conserved triad arginine-arginine-tyrosine (Rittinger K et al., 1999), but also with hydrophobic proteins via the side chain of a conserved leucine (Ottmann C et al., 2007). A large hydrophobic cavity was observed for the RBD of Mdm38. This cavity presented 2 leucine residues (387 and 390, Fig. a3 in red) that correspond to the conserved leucine residues found in other 14-3-3-like proteins. These observations suggested that this cavity might mediate the interaction of Mdm38 with the mitoribosome.

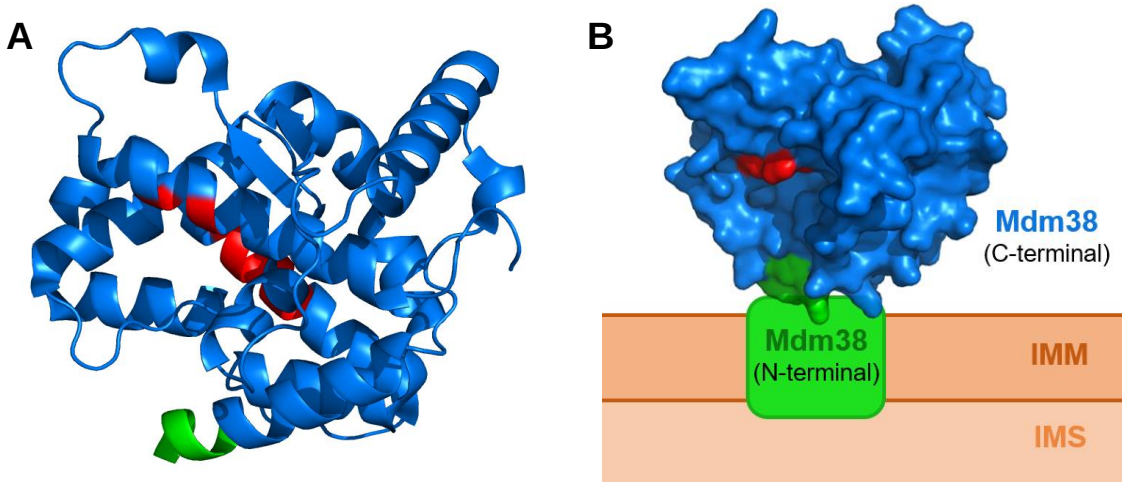

Figure a3 Structure of Mdm38 C-terminal domain.

The structure of the C-terminal of Mdm38 was visualised as cartoon (A) and as surface (B) using Pymol, from the available PDB file 3SKQ (Lupo D et al., 2011). This domain corresponds to the soluble domain of the protein, and the first 5 amino acids resolved were depicted in green and docked on the transmembrane domain, represented by a green box. The leucine residues present in the hydrophobic cavity are depicted in red.

The role of Mdm38 in yeast was further investigated upon deletion of *Mdm38*. A growth defect, impairment in the transport of proteins from the matrix and an altered morphology of mitochondria were observed upon *Mdm38* deletion.

This protein was also suggested to play a role in the assembly of some OXPHOS complexes, although its effects on mitochondrial protein synthesis are still under debate. According to Frazier et al, deletion of *Mdm38* caused an impairment of mitochondrial translation and defects in the insertion of Atp6 and cytochrome *b* (Frazier AE et al., 2006). A different effect on mitochondrial translation was observed by Bauerschmitt et al and by Nowikovsky et al, whose deletion experiments in yeast showed that this process was not severely affected by the absence of Mdm38 (Bauerschmitt H et al., 2010; Nowikovsky K et al., 2007). An effect on mitochondrial translation was observed by Bauerschmitt et al for Mdm38 and Mba1 double mutants, particularly for *COXI and CYTB* mRNA (Bauerschmitt H et al., 2010).

The growth defect observed for *mdm38*-deleted mutants was efficiently recovered by overexpression of LetM1, suggesting a similar function to the yeast protein for the mammalian homologue (Nowikovsky K et al., 2004). LetM1 is an IMM protein that was found to be present in high molecular weight complexes of approximately 300 kDa and 500-600 kDa (Dimmer KS et al., 2008; Tamai S et al., 2008). This protein is important for mitochondrial morphology, with its depletion causing swelling and loss of cristae structure (Tamai S et al., 2008). In the absence of LetM1, the assembly of complexes I, III and IV was compromised, although the steady state levels of the tested subunits did not seem to be affected. The authors suggested the possibility that the effects observed might be related to the loss of cristae and not directly to a role of LetM1 in the assembly of the OXPHOS complexes (Tamai S et al., 2008). The importance of this protein was further confirmed by the lethality in the early stages of embryogenesis of *LetM1* knockout in mice (Jiang D et al., 2013).

In addition to its role in mitochondrial gene expression, Mdm38 has been suggested to play a role in H^+/K^+ exchange (Nowikovsky K et al., 2004; Nowikovsky K et al., 2007). Swelling of mitochondria was observed upon deletion of Mdm38, and this effect can be explained by osmosis due to the increase of K^+ concentration after impairment of ion exchange. The role of LetM1 in cation transport is under investigation. The swelling of mitochondria observed for LetM1 depletion was reversed by nigericin, which catalyses the electroneutral change of H^+ with K^+, and was phenocopied by addition of valinomycin, a ionophore that catalyses the electrophoretic flux of K^+. Because of these pieces of data, it was suggested that the increase in the mitochondrial volume might be due to K^+ accumulation. On the other hand, a genome-wide siRNA screen in *Drosophila* identified a reduction of Ca2+ influx in the absence of LetM1 (Jiang D et al., 2013), suggesting a role for this protein as a Ca^{2+}/H^+ antiporter. The same effect was observed for LetM1 knockdown in HEK293 cells (Jiang D et al., 2013). Whether LetM1 has a role in the transport of K^+ or Ca^{2+} is still under debate in the field (Nowikovsky K et al., 2014).

As previously mentioned, Mdm38 was shown to interact with the mitoribosomal large subunit. In absence of the mitoribosome, it was demonstrated an interaction of this protein with Mba1 (homologue of MRPL45 in yeast) (Bauerschmitt H et al., 2010). Because of the conservations of these 2 proteins in eukaryotes, it is possible that their interaction is still retained in mammals. The only study on LetM1 and its interaction with the mitoribosome is based on immunoprecipitation experiments on cell line overexpressing either LetM1, MRPL36 or both the proteins. These experiments suggested a direct interaction of these 2 proteins (Piao L et al., 2009).

LetM1 was also demonstrated to directly interact with BCS1L (Tamai S et al., 2008), a chaperone necessary for the assemble of complex III (de Lonlay P et al., 2001) and for the formation of LetM1 complexes.

Mutations in LetM1 have also been linked to pathologies. The gene encoding this protein is one of the genes deleted in the Wolf-Hirschhorn syndrome (Endele S et al., 1999), where the severity of the disease is related to the size of the deletion. The main symptoms are mental retardation, seizures, hypertonia and characteristic facial features (Bergemann AD et al., 2005). It is thought that LetM1 might play a role in the onset of seizures, due to its possible role in regulating the levels of calcium and potassium (Rauch A et al., 2001; South ST et al., 2007). An altered level of LetM1 has also been found in cancerous tissue, which appear to contain a higher amount of this protein (Hwang SK et al., 2010; Li N et al., 2015; Piao L et al., 2009).

Since only one study attempted to confirm the interaction of LetM1 with the mitoribosome, I decided to further confirm it. In addition, the collaboration of Prof Taylor with Dr Carrozzo in Rome, allowed me to study the phenotype of a patient carrying mutations on LetM1, which will be discussed in this chapter.

Prediction of the LetM1 structure

A crystal structure for LetM1 (RefSeq NP_036450.1) was still not available, therefore inferences on its structure were made from information available on its domains (Fig. a3) and from a structural prediction obtained using Phyre2 (Fig. a4).

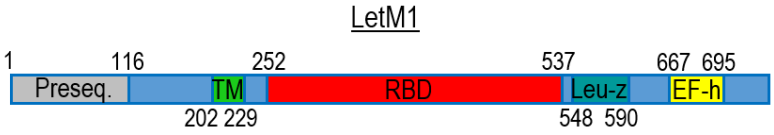

Figure a4 Domains predicted for LetM1.

Summary of the domain information available for LetM1 (RefSeq NP_036450.1). The presequence (gray) was predicted by TargetP 1.1 to be between residues 1 and 116 . The transmembrane domain (TM, green) was assigned by TM pred to lie between residues 202 and 229, whereas the ribosome binding domain (RBD, red) was predicted to be between residues 252 and 537. After this domain, a leucine-zipper domain (Leu-z, turquois) was identified between residues 548 and 590. Finally, the EF-hand domain (EF-h, yellow) was assigned between residues 667 and 695.

As a nuclear-encoded mitochondrial protein, LetM1 possesses a presequence that targets the protein to mitochondria. TargetP 1.1 (Emanuelsson O et al., 2000) predicted this transit peptide to target the protein to mitochondria and to be cleaved between the residues 115 and 116. LetM1 is an IMM protein and its analysis with TM pred (Hofmann K et al., 1993) identified residues 202 and 228 as a possible transmembrane domain from the inside (IMS) to the outside (matrix) (Fig. a4, in green). The presence of a transmembrane domain in the same part of the sequence was also confirmed by the analysis of the hydrophobicity of the protein obtained with the Kyte-Doolittle method (Fig. a5). Uniprot suggested that a ribosome binding domain (RBD, Fig. a4, in red) is present between residues 252 and 537, followed by a leucine-zipper domain (residues 548-590, Fig. a4, in turquoise). Finally, despite 2 EF-hand domains having been identified in LetM1 (Endele S et al., 1999), the first, located in the leucine-zipper motif, is likely to have lost its function due to alteration of its structure from the canonical EF-hand structure (Kawasaki H et al., 1994). On the other hand, the second identified between residues 667 and 695 may still retain the ability to bind Ca^{2+} (Fig. a4, in yellow).

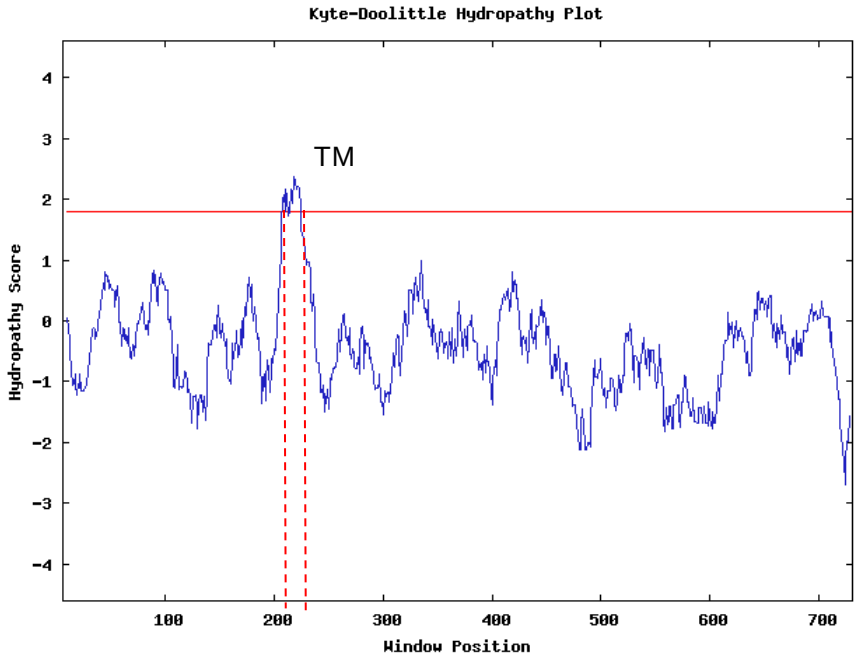

Figure a5 Prediction of a transmembrane domain within LetM1 using the Kyte-Doolittle plot.
Kyte-Doolittle hydropathy analysis was performed on LetM1. The window was set at 19 and the result is shown in a plot with the hydropathy score in function of the window position. A score higher than 1.8 (red horizontal line) indicates the presence of possible transmembrane (TM) domains.

The same colour code used for the analysis of the domains present on LetM1 was also used to colour the Phyre2 prediction of the protein. The full prediction obtained is shown in Fig. a6.

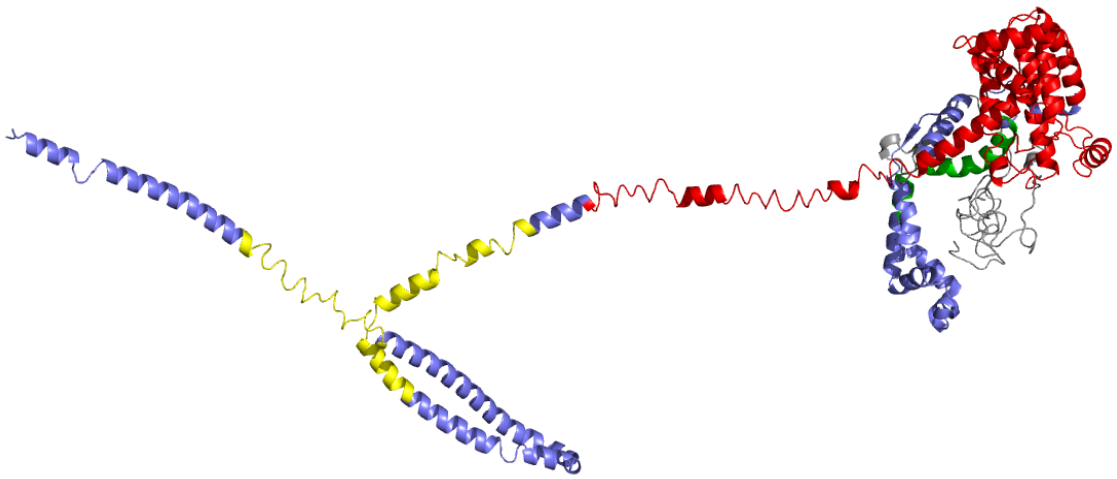

Figure a6 Prediction of LetM1 structure.

LetM1 structure was predicted using Phyre2. The result is shown as a cartoon and coloured according to different domains reported to be present in LetM1 (Presequence=gray, Transmembrane domain=green, Ribosome binding domain=red, Leucine-zipper=turquoise, EF-hand=yellow). The ribosome binding domain was aligned with high confidence (99.9%) and identity (37%) to Mdm38.

The prediction aligned residues 252-444 with the structure available of Mdm38 (PDB 3SKQ), with a confidence of 99.9%, and a sequence identity of 37% and corresponds to the ribosome binding domain (Fig. a6, red). This result suggests that LetM1 might have conserved the function observed for Mdm38. The remaining structure was not aligned with high confidence or sequence identity with any other known structure.

Interaction of LetM1 with the mitoribosome

The LetM1 yeast homologue, Mdm38, has been reported to interact with the mitoribosome. Because the analysis of LetM1 structure suggested a high homology with the yeast counterpart, the possibility of LetM1 to interact with the IMM was explored.

In case of any interaction with the mt-LSU, LetM1 might co-localise with mt-LSU in an isokinetic sucrose gradient analysis. To test this, a cell lysate (800 µg) from HEK293 cells was loaded on a 10-30% isokinetic sucrose gradient and its components were separated within the gradient upon centrifugation (qv 2.8.). The 11 fractions obtained were TCA-precipitated (qv 2.5.3.) and then analysed by western blot (Fig. a7).

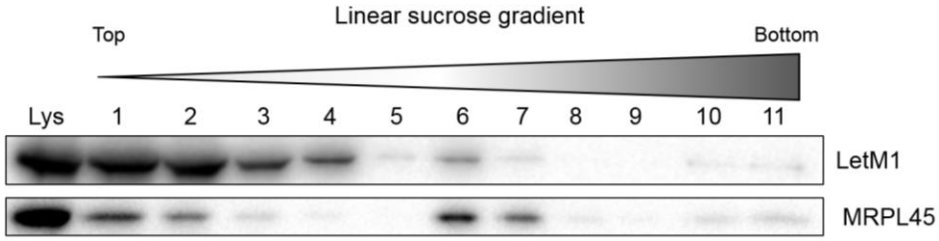

Figure a7 Distribution of LetM1 on isokinetic sucrose gradients.

HEK293 cells were lysed and ≈800 µg of protein were loaded at the top of a 10-30% sucrose gradient (qv 2.8.). After centrifugation, 11 fractions were obtained, TCA-precipitated (qv 2.5.3.) and analysed via western blotting. An aliquot of the cell lysate 'load' (Lys; ≈40 µg) was also loaded on the gel. Antibodies against MRPL11 localised the position of the mt-LSU, and antibodies targeting LetM1 identified its distribution. The figure is representative of 2 biological repeats.

The sucrose gradient analysis showed that the majority of LetM1 was present in the first fractions, while a weaker signal was obtained in the fractions corresponding to the mt-LSU.

Since the sucrose gradient analysis could not confirm the ability of LetM1 to interact with the mitoribosome, this hypothesis was investigated via immunoprecipitation of LetM1 from mitochondria extracted from HEK293 cells. Magnetic beads were coated with 5 µg of LetM1 antibody and the experiment was carried out as in 2.9. The 8 µL of eluted sample (25 µL total) were analysed via western blotting to determine the presence of mitoribosomal proteins (Fig. a8).

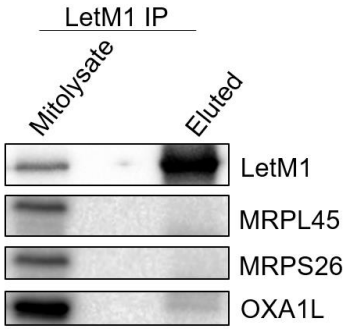

Figure a8 Immunoprecipitation of LetM1.

Western blot analysis was performed on mitolysate (15 µL) and eluted sample (1/3 of the volume) from immunoprecipitation of LetM1 in HEK293 cells. The efficiency of the immunoprecipitation was detected with antibodies targeting LetM1. The presence of mitoribosomal proteins MRPL45 and MRPS26, as well as the IMM protein OXA1L, were also detected. The experiment was not repeated.

The immunoprecipitation was very efficient, as shown by the presence of large amounts of LetM1 present in the eluted fraction (Fig. a8). Despite this, cross reacting material was obtained in the western blot analysis for the mitoribosomal proteins tested (MRPL45, MRPL26), of which a distinct signal could not be detected. LetM1 immunoprecipitation also showed the presence of a weak signal for OXA1L.

Phenotype of a patient with mutations in LetM1

As mentioned in the introduction, deletions of *LETM1* gene have been widely associated with the Wolf-Hirschhorn syndrome. After starting to work on LetM1, I discovered the existence of a patient with mutation in this gene. This is the first case of missense mutations in *LetM1*. Thanks to the help of Prof Taylor, I got in touch with Dr Carrozzo who was studying the phenotype of the patient, that kindly agreed to send me primary fibroblast to investigate the potential effect of this mutation on the ability of LetM1 to bind the mitoribosome.

Dr Carrozzo reported that the patient presented with encephalopathy, hypertrophic cardiomyopathy and cataract. Increased lactate, α-ketoacids and Krebs intermediate products were also observed. Muscle hystochemistry showed the reduction or the absence of COX in several fibres. Muscle also showed a reduction of the activity of complex I and IV of the 40% each. The search for a mutation identified a homozygous mutation for *LETM1*. The mutation (c.898C>T) caused the proline at position 300 to be translated as serine. Due to the presence of a nitrogen-containing ring, proline is constrained in its folding as compared to the majority of the other residues. As a consequence, proline often introduces tight turns in protein structures or kinks into α-helices. Serine is also able to fold in a conformation that allows tight turns. The hydroxyl oxygen on the side chain of this small amino acid is able to form a hydrogen bond with the protein backbone, mimicking proline. As a consequence, it is possible that this mutation will not severely damage the stability of the function of the protein. Despite this, PolyPhen (Adzhubei IA et al., 2010) scored the mutation as probably damaging, assigning it the highest score of 1. This program predicts the effects of the mutation taking into consideration not only the change of the volume of the side chain or of the accessibility to the solvent, but also the contacts that the residue might do with other amino acids. It is therefore possible that, despite serine can mock proline, this mutation within the sequence of LetM1 is causing a deleterious effect on its structure or function.

The fibroblast of the LetM1 patient were cultured and the steady state level of OXPHOS components and mitoribosomal proteins was analysed via western blot (Fig. a9).

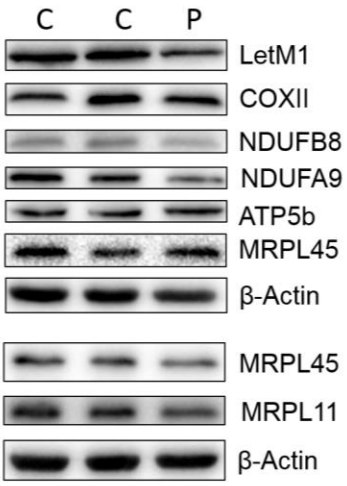

Figure a9 Steady state levels of mitochondrial proteins in a patient with mutation in LetM1 gene.

Cell lysate (≈50 µg) from primary fibroblasts of 2 controls (C) and a LetM1 patient (P) were separated by 12% SDS-PAGE, and analysed via western blot. The steady state level of LetM1 was assessed, as well as the level of OXPHOS components (COXII, NDUFB8, NDUFA9, ATP5β). A second western blot was used to detect the levels of the mitoribosomal proteins MRPL11 and MRPL45. The equality of the loading was verified using antibodies against β-Actin. The figure is representative of 3 biological repeats.

The phenotype observed for LetM1 patient fibroblast was not very strong. The mutations affected the steady state level of LetM1, which was reduced by approximately 30% when compared to the control, and might indicate a mild effect of the mutation on the protein's stability. While the level of complex IV did not seem affected, a reduction of the nuclear encoded components of complex I NDUFA9 and NDUFB8 was observed. No effect on the F1 component of complex V was observed. Regarding the mitoribosomal proteins, a marginal effect on the steady state levels of both MRPL45 and MRPL11 was found using western blot analysis.

The phenotype observed in the fibroblast was very mild when compared to the information obtained in muscle by Dr Carrozzo. Therefore, no further analyses were possible on the phenotype of the patient using this cell line.

Conclusions

Despite several studies on yeast Mdm38 that support its importance for mitochondria and cell homeostasis, the mammalian homologue is still not well understood. While its role in ion transport is still contradictory, its role in mitochondrial translation has not been widely explored to date.

LetM1 depletion has been reported to compromise the assembly of complexes I, III and IV, without affecting the steady state levels of the tested subunits (Tamai S et al., 2008). It is important to notice that all the subunits tested by the authors were nuclear encoded and, therefore, this result gave no information on the effects of the depletion on mitochondrial translation. Because of the effects on complex assembly, it is however tempting to infer that the effects observed on complex assembly might be caused by the lack of availability of mt-encoded subunits due to defects in

mitochondrial protein synthesis. The authors also suggested that this effect could be linked to the loss of cristae observed in LetM1 depletion. I believe that this hypothesis is unlikely as, in these circumstances an effect on complexes II and V (unaffected according to the authors) should be detected.

Ideally I would repeat the depletion experiment and investigate the effects of the depletion on mitochondrial translation. However, due to the limited time frame of my project, I decided to focus on the possibility of an interaction between LetM1 and the mitoribosome. As stated in the introduction of this chapter, yeast Mdm38 has been reported to interact with the mitoribosome and, in particular, with Mba1 (MRPL45 homologue in yeast). LetM1 has been reported to interact with MRPL36 (Piao L et al., 2009). The authors studied the interaction of these 2 proteins in HeLa cells based on the data published by Ott et al on the interaction with Mdm38 with the yeast mitoribosome (Bauerschmitt H et al., 2010). This was a misinterpretation of the work by Ott et al, where MRPL36 antibody was used as a marker to detect the presence of the mitoribosome as a whole and was, therefore, not indicating a direct interaction of Mdm38 with this mitoribosomal protein.

The sucrose gradient analysis performed on HEK293 cells in this chapter failed to demonstrate colocalisation of the IMM protein with the mitoribosome. The immunoprecipitation of LetM1 from the same cell line did not lead to the co-precipitation of the mitoribosome. Altogether these data suggested that LetM1 does not interact with the mitoribosome.

Deletion of LetM1 has been widely connected to Wolf-Hirschhorn syndrome. For the first time, a patient with a mutation in this gene has been identified and studied by Dr. Carrozzo, I was kindly given access to the primary fibroblast cell line from this patient to test the effects of the mutation on the stability of the mitoribosome. The mutation mildly affected the steady state level of LetM1, which caused a mild reduction of the levels of component of complexes I and IV. This effect could be due to a minor defect of mitochondrial translation, as well as to a defect in membrane insertion. The steady state levels of the mitoribosomal proteins detected appeared to be mildly reduced. Unfortunately, because the phenotype shown by the fibroblasts was not very pronounced, it was not possible to clearly assess the effects of this mutation on the mitoribosome or on mitochondrial translation. The muscle sample analysed by Dr. Carrozzo showed a more marked phenotype (Carozzo, personal communication). The difference in severity between fibroblasts, a low requiring energy tissue, and muscle, a high requiring tissue, is very frequently observed and it is problematic for investigating the role of mutated mitochondrial proteins in diseases.

Due to the lack of more convincing data on the role of LetM1 and to its involvement in diseases, I believe it is important to further study this protein to understand its role both in the Wolf-Hirschhorn syndrome and in the patient studied by Dr. Carrozzo.

References

Abe Y, Shodai T, Muto T, Mihara K, Torii H, Nishikawa S, Endo T, & Kohda D. (2000). Structural basis of presequence recognition by the mitochondrial protein import receptor Tom20. *Cell, 100*, 551-560.

Adzhubei IA, Schmidt S, Peshkin L, Ramensky VE, Gerasimova A, Bork P, Kondrashov AS, & Sunyaev SR. (2010). A method and server for predicting damaging missense mutations. *Nat Methods, 7*, 248-249.

Aitken A. (2006). 14-3-3 proteins: a historic overview. *Semin Cancer Biol, 16*, 162-172.

Akabane S, Ueda T, Nierhaus KH, & Takeuchi N. (2014). Ribosome rescue and translation termination at non-standard stop codons by ICT1 in mammalian mitochondria. *PLoS Genet, 10*, e1004616.

Al Rawi S, Louvet-Vallee S, Djeddi A, Sachse M, Culetto E, Hajjar C, Boyd L, Legouis R, & Galy V. (2011). Postfertilization autophagy of sperm organelles prevents paternal mitochondrial DNA transmission. *Science, 334*(6059), 1144-1147.

Allen JF, & Raven JA. (1996). Free-radical-induced mutation vs redox regulation: costs and benefits of genes in organelles. *J Mol Evol, 42*, 482-492.

Altamura N, Capitanio N, Bonnefoy N, Papa S, & Dujardin G. (1996). The Saccharomyces cerevisiae OXA1 gene is required for the correct assembly of cytochrome c oxidase and oligomycin-sensitive ATP synthase. *FEBS Lett, 382*, 111-115.

Amunts A, Brown A, Toots J, Scheres SH, & Ramakrishnan V. (2015). Ribosome. The structure of the human mitochondrial mitoribosome. *Science, 348*(6230), 95-98.

Anderson EM, Birmingham A, Baskerville S, Reynolds A, Maksimova E, Leake D, Fedorov Y, Karpilow J, & Khvorova A. (2008). Experimental validation of the importance of seed complement frequency to siRNA specificity. *RNA, 14*, 853-861.

Anderson P, & Kedersha N. (2006). RNA granules. *J Cell Biol, 172*, 803-808.

Anderson S, Bankier AT, Barrell BG, De Bruijn MHL, Coulson AR, Drouin J, Eperon IC, Nierlich DP, Roe BA, Sanger F, Schreier PH, Smith AJH, Staden R, & Young IG. (1981). Sequence and organization of the human mitochondrial genome. *Nature, 290*, 457-465.

Antonicka H, Sasarman F, Nishimura T, Paupe V, & Shoubridge EA. (2013). The mitochondrial RNA-binding protein GRSF1 localizes to RNA granules and is required for posttranscriptional mitochondrial gene expression. *Cell Metab, 17*(3), 386-398.

Antonicka H, & Shoubridge EA. (2015). Mitochondrial RNA granules are centers for posttranscriptional RNA processing and ribosome biogenesis. *Cell Rep*.

Appleby RD, Porteous WK, Hughes G, James AM, Shannon D, Wei YH, & Murphy MP. (1999). Quantitation and origin of the mitochondrial membrane potential in human cells lacking mitochondrial DNA. *Eur J Biochem., 262*, 108-116.

Arnold JJ, Smidansky, E., Moustafa IM, & Cameron CE. (2012). Human mitochondrial RNA polymerase: structure-function, mechanism and inhibition. *Biochim Biophys Acta, 1819*(9-10), 948-960.

Arnould T, Mercy L, Houbion A, Vankoningsloo S, Renard P, Pascal T, Ninane N, Demazy C, & Raes M. (2003). mtCLIC is up-regulated and maintains a mitochondrial membrane potential in mtDNA-depleted L929 cells. *FASEB J, 17*, 2145-2147.

Asin-Cayuela J, Schwend T, Farge G, & Gustafsson CM. (2005). The human mitochondrial transcription termination factor (mTERF) is fully active in vitro in the nonphosphorylated form. *J Biol Chem, 280*, 25499-25505.

Ban N, Beckmann R, Cate JH, Dinman JD, Dragon F, Ellis SR, Lafontaine DL, Lindahl L, Liljas A, Lipton JM, McAlear, M., Moore PB, Noller HF, Ortega J, Panse VG, Ramakrishnan V, Spahn CM, Steitz TA, Tchorzewski M, Tollervey D, Warren AJ, Williamson JR, Wilson D, Yonath A, & Yusupov M. (2014). A new system for naming ribosomal proteins. *Curr Opin Struct Biol, 24*, 165-169. doi: 10.1016/j.sbi.2014.01.002

Ban N, Nissen P, Hansen J, Moore PB, & Steitz TA. (2000). The complete atomic structure of the large ribosomal subunit at 2.4 A resolution. *Science, 289*, 905-920.

Banci L, Bertini I, Cefaro C, Cenacchi L, Ciofi-Baffoni S, Felli IC, Gallo A, Gonnelli L, Luchinat E, Sideris D, & Tokatlidis K. (2010). Molecular chaperone function of Mia40 triggers consecutive induced

folding steps of the substrate in mitochondrial protein import. *Proc Natl Acad Sci USA, 107*, 20190-20195.

Banci L, Bertini I, Cefaro C, Ciofi-Baffoni S, Gallo A, Martinelli M, Sideris DP, Katrakili N, & Tokatlidis K. (2009). MIA40 is an oxidoreductase that catalyzes oxidative protein folding in mitochondria. *Nat Struct Mol Biol, 16*, 198-206.

Bauerschmitt H, Mick DU, Deckers M, Vollmer C, Funes S, Kehrein K, Ott M, Rehling P, & Herrmann JM. (2010). Ribosome-binding proteins Mdm38 and Mba1 display overlapping functions for regulation of mitochondrial translation. *Mol Biol Cell, 21*(12), 1937-1944.

Benz R. (1994). Permeation of hydrophilic solutes through mitochondrial outer membranes: review on mitochondrial porins. *Biochim Biophys Acta, 1197*, 167-196.

Berg JM, Tymoczko JL, & Stryer L. (2002). Biochemistry. 5th edition. *New York: W H Freeman*.

Bergemann AD, Cole F, & Hirschhorn K. (2005). The etiology of Wolf-Hirschhorn syndrome. *Trends Genet, 21*, 188-195.

Bernstein P, & Ross J. (1989). Poly(A), poly(A) binding protein and the regulation of mRNA stability. *Trends Biochem Sci, 14* 373-377.

Birmingham A, Anderson EM, Reynolds A, Ilsley-Tyree D, Leake D, Fedorov Y, Baskerville S, Maksimova E, Robinson K, Karpilow J, Marshall WS, & Khvorova A. (2006). 3' UTR seed matches, but not overall identity, are associated with RNAi off-targets. *Nat Methods, 3*, 199-204.

Bogenhagen D, & Clayton DA. (1977). Mouse L cell mitochondrial DNA molecules are selected randomly for replication throughout the cell cycle. *Cell, 11*(4), 719-727.

Bogenhagen DF. (2012). Mitochondrial DNA nucleoid structure. *Biochim Biophys Acta, 1819*(9-10), 914-920.

Bogenhagen DF, Martin DW, & Koller A. (2014). Initial steps in RNA processing and ribosome assembly occur at mitochondrial DNA nucleoids. *Cell Metab, 19*, 618-629.

Bonnefoy N, Chalvet F, Hamel P, Slominski PP, & Dujardin G. (1994). OXA1, a Saccharomyces cerevisiae nuclear gene whose sequence is conserved from prokaryotes to eukaryotes controls cytochrome oxidase biogenesis. *J Mol Biol, 239*, 201 - 212.

Bonora M, Bononi A, De Marchi E, Giorgi C, Lebiedzinska M, Marchi S, Patergnani S, Rimessi A, Suski JM, Wojtala A, Wieckowski MR, Kroemer G, Galluzzi L, & Pinton P. (2013). Role of the c subunit of the FO ATP synthase in mitochondrial permeability transition. *Cell Cycle, 12*, 674-683.

Borowski LS, Dziembowski A, Hejnowicz MS, Stepien PP, & Szczesny RJ. (2013). Human mitochondrial RNA decay mediated by PNPase-hSuv3 complex takes place in distinct foci. *Nucleic Acids Res, 41*, 1223-1240.

Borowski LS, Szczesny RJ, Brzezniak LK, & Stepien PP. (2010). RNA turnover in human mitochondria: more questions than answers? *Biochim Biophys Acta, 1797*, 1066-1070.

Bowmaker M, Yang MY, Yasukawa T, Reyes A, Jacobs HT, Huberman JA, & Holt IJ. (2003). Mammalian mitochondrial DNA replicates bidirectionally from an initiation zone. *J Biol Chem, 278*, 50961-50969.

Bratic A, Clemente P, Calvo-Garrido J, Maffezzini C, Felser A, Wibom R, Wedell A, Freyer C, & Wredenberg A. (2016). Mitochondrial polyadenylation is a one-step process required for mRNA integrity and tRNA maturation. *PLoS Genet, 12*, e1006028.

Brix J, Dietmeier K, & Pfanner N. (1997). Differential recognition of preproteins by the purified cytosolic domains of the mitochondrial import receptors Tom20, Tom22, and Tom70. *J Biol Chem, 272*, 20730-20735.

Brocks JJ, Logan GA, Buick R, & Summons RE. (1999). Archean molecular fossils and the early rise of eukaryotes. *Science, 285*, 1033-1036.

Brown A, Amunts A, Bai XC, Sugimoto Y, Edwards PC, Murshudov G, Scheres SH, & Ramakrishnan V. (2014). Structure of the large ribosomal subunit from human mitochondria. *Science, 346*, 718-722.

Bruni F, Gramegna P, Oliveira JM, Lightowlers RN, & Chrzanowska-Lightowlers ZM. (2013). REXO2 is an oligoribonuclease active in human mitochondria. *PLoS One, 8*, e64670.

Brzezniak LK, Bijata M, Szczesny RJ, & Stepien PP. (2011). Involvement of human ELAC2 gene product in 3' end processing of mitochondrial tRNAs. *RNA Biol, 8*(4), 616-626.

Buchet K, & Godinot C. (1998). Functional F1-ATPase essential in maintaining growth and membrane potential of human mitochondrial DNA-depleted rho degrees cells. *J Biol Chem, 273*, 22983-22989.

Bukau B, & Horwich AL. (1998). The Hsp70 and Hsp60 chaperone machines. *Cell, 92*, 351-366.

Caffrey DR, Zhao J, Song Z, Schaffer ME, Haney SA, Subramanian RR, Seymour AB, & Hughes JD. (2011). siRNA off-target effects can be reduced at concentrations that match their individual potency. *PLoS One, 6*, e21503.

Cai YC, Bullard JM, Thompson NL, & Spremulli LL. (2000). Interaction of mitochondrial elongation factor Tu with aminoacyl-tRNA and elongation factor Ts. *J Biol Chem, 275*, 20308–20314.

Cámara Y, Asin-Cayuela J, Park CB, Metodiev MD, Shi Y, Ruzzenente B, Kukat C, Habermann B, Wibom R, Hultenby K, Franz T, Erdjument-Bromage H, Tempst P, Hallberg BM, Gustafsson CM, & Larsson NG. (2011). MTERF4 regulates translation by targeting the methyltransferase NSUN4 to the mammalian mitochondrial ribosome. *Cell Metab, 13*, 527-539.

Camasamudram V, Fang JK, & Avadhani NG. (2003). Transcription termination at the mouse mitochondrial H-strand promoter distal site requires an A/T rich sequence motif and sequence specific DNA binding proteins. *Eur J Biochem, 270*, 1128-1140.

Carrozzo R, Wittig I, Santorelli FM, Bertini E, Hofmann S, Brandt U, & Schägger H. (2006). Subcomplexes of human ATP synthase mark mitochondrial biosynthesis disorders. *Ann Neurol, 59*, 265-275.

Chan DC. (2006). Mitochondrial fusion and fission in mammals. *Annu Rev Cell Dev Biol, 22*, 79-99.

Christian BE, & Spremulli LL. (2010). Preferential selection of the 5'-terminal start codon on leaderless mRNAs by mammalian mitochondrial ribosomes. *J Biol Chem, 285*, 28379-28386.

Christian BE, & Spremulli LL. (2012). Mechanism of protein biosynthesis in mammalian mitochondria. *Biochim Biophys Acta, 1819*, 1035-1054.

Christie DA, Lemke CD, Elias IM, Chau LA, Kirchhof MG, Li B, Ball EH, Dunn SD, Hatch GM, & Madrenas J. (2011). Stomatin-like protein 2 binds cardiolipin and regulates mitochondrial biogenesis and function. *Mol Cell Biol, 31*(18), 3845-3856.

Chrzanowska-Lightowlers ZM, Pajak A, & Lightowlers RN. (2011). Termination of protein synthesis in mammalian mitochondria. *J Biol Chem, 286*(40), 34479-34485.

Chujo T, Ohira T, Sakaguchi Y, Goshima N, Nomura N, Nagao A, & Suzuki T. (2012). LRPPRC/SLIRP suppresses PNPase-mediated mRNA decay and promotes polyadenylation in human mitochondria. *Nucleic Acids Res, 40*, 8033-8047.

Claros MG, & Vincens P. (1996). Computational method to predict mitochondrially imported proteins and their targeting sequences. *Eur J Biochem, 241*, 779-786.

Clayton DA. (1982). Replication of animal mitochondrial DNA. *Cell, 28*(4), 693–705.

Colbeau A, Nachbaur J, & Vignais PM. (1971). Enzymic characterization and lipid composition of rat liver subcellular membranes. *Biochim Biophys Acta, 249*, 462-492.

Comte J, Maïsterrena B, & Gautheron DC. (1976). Lipid composition and protein profiles of outer and inner membranes from pig heart mitochondria. Comparison with microsomes. *Biochim Biophys Acta, 419*, 271-284.

Cory S, & Adams JM. (2002). The Bcl2 family: regulators of the cellular life-or-death switch. *Nat Rev Cancer, 2*, 647-656.

Czech B, & Hannon GJ. (2011). Small RNA sorting: matchmaking for argonautes. *Nat Rev Genet, 12*, 19-31.

D'Silva P, Liu Q, Walter W, & Craig EA. (2004). Regulated interactions of mtHsp70 with Tim44 at the translocon in the mitochondrial inner membrane. *Nat Struct Mol Biol, 11*, 1084-1091.

Dalla Rosa I, Durigon R, Pearce SF, Rorbach J, Hirst EM, Vidoni S, Reyes A, Brea-Calvo G, Minczuk M, Woellhaf MW, Herrmann JM, Huynen MA, Holt IJ, & Spinazzola A. (2014). MPV17L2 is required for ribosome assembly in mitochondria. *Nucleic Acids Res, 42*(13), 8500-8515.

Davidzon G, Mancuso M, Ferraris S, Quinzii C, Hirano M, Peters HL, Kirby D, Thorburn DR, & DiMauro S. (2005). POLG mutations and Alpers syndrome. *Ann Neurol, 57*, 921-924.

Davies SM, Lopez Sanchez MI, Narsai R, Shearwood AM, Razif MF, Small ID, Whelan J, Rackham O, & Filipovska A. (2012). MRPS27 is a pentatricopeptide repeat domain protein required for the translation of mitochondrially encoded proteins. *FEBS Lett, 586*(20), 3555-3561.

De Bary A. (1878). Über Symbiose. *Versammlung deutscher Naturforscher und Aerzte in Cassel, 51*, 121-126.

de Lonlay P, Valnot I, Barrientos A, Gorbatyuk M, Tzagoloff A, Taanman JW, Benayoun E, Chrétien D, Kadhom N, Lombès A, de Baulny HO, Niaudet P, Munnich A, Rustin P, & Rötig A. (2001). A mutant mitochondrial respiratory chain assembly protein causes complex III deficiency in patients with tubulopathy, encephalopathy and liver failure. *Nat Genet, 29*, 57-60.

De Silva D, Tu YT, Amunts A, Fontanesi F, & Barrientos A. (2015). Mitochondrial ribosome assembly in health and disease. *Cell Cycle, 14*, 2226-2250.

Dennerlein S, Rozanska A, Wydro M, Chrzanowska-Lightowlers ZM, & Lightowlers RN. (2010). Human ERAL1 is a mitochondrial RNA chaperone involved in the assembly of the 28S small mitochondrial ribosomal subunit. *Biochem J, 430*(3), 551-558.

Des Marais DJ. (1998). Earth's early biosphere. *Gravit Space Biol Bull, 11*, 23-30.

Dianov GL, Souza-Pinto N, Nyaga SG, Thybo T, Stevnsner T, & Bohr VA. (2001). Base excision repair in nuclear and mitochondrial DNA. *Prog Nucleic Acid Res Mol Biol, 68*, 285-297.

Dimmer KS, Navoni F, Casarin A, Trevisson E, Endele S, Winterpacht A, Salviati L, & Scorrano L. (2008). LETM1, deleted in Wolf-Hirschhorn syndrome is required for normal mitochondrial morphology and cellular viability. *Hum Mol Genet, 17*(2), 201-214.

Diodato D, Ghezzi D, & Tiranti V. (2014). The mitochondrial aminoacyl tRNA synthetases: genes and syndromes. *Int J Cell Biol, 2014*, ID 787956.

Dodson RF, Patten BM, Hyman BM, & Chu LW. (1976). Mitochondrial abnormalities in progressive ophthalmoplegia. *Cytobios, 15*, 57-60.

Doersen CJ, Guerrier-Takada C, Altman S, & Attardi F. (1985). Characterization of an RNase P activity from HeLa cell mitochondria. Comparison with the cytosol RNase P activity. *J Biol Chem, 260*(10), 5942-5949.

Drozdetskiy A, Cole C, Procter J, & Barton GJ. (2015). JPred4: a protein secondary structure prediction server. *Nucl Acids Res*.

du Plessis DJF, Nouwen N, & Driessen AJM. (2006). Subunit a of cytochrome o oxidase requires both YidC and SecYEG for membrane insertion. *J Biol Chem, 281*, 12248-12252.

Dubin DT, & Taylor RH. (1978). Modification of mitochondrial ribosomal RNA from hamster cells: The presence of GmG and late-methylated UmGmU in the large subunit (17S) RNA. *J Mol Biol, 121*, 523-540.

Dudek J, Rehling P, & van der Laan M. (2013). Mitochondrial protein import: Common principles and physiological networks. *BIochem Biophys Acta, 1833*, 274-285.

Efremov RG, Baradaran R, & Sazanov LA. (2010). The architecture of respiratory complex I. *Nature, 465*(7297), 441-445.

Emanuelsson O, Nielsen H, S, B., & von Heijne G. (2000). Predicting subcellular localization of proteins based on their N-terminal amino acid sequence. *J Mol Biol, 300*, 1005-1016.

Embley TM, van der Giezen M, Horner DS, Dyal PL, Bell S, & Foster PG. (2003). Hydrogenosomes, mitochondria and early eukaryotic evolution. *IUBMB Life, 55*, 387-395.

Endele S, Fuhry M, Pak SJ, Zabel BU, & Winterpacht A. (1999). LETM1, a novel gene encoding a putative EF-hand Ca(2+)-binding protein, flanks the Wolf-Hirschhorn syndrome (WHS) critical region and is deleted in most WHS patients. *Genomics, 60*, 218-225.

Falkenberg M, Larsson NG, & Gustafsson CM. (2007). DNA replication and transcription in mammalian mitochondria. *Annu Rev Biochem, 76*, 679-699.

Feaga HA, Quickel MD, Hankey-Giblin PA, & Keiler KC. (2016). Human cells require non-stop ribosome rescue activity in mitochondria. *PLoS Genet, 12*, e1005964.

Fernandez-Silva P, Martinez-Azorin F, Micol V, & Attardi G. (1997). The human mitochondrial transcription termination factor (mTERF) is a multizipper protein but binds to DNA as a monomer, with evidence pointing to intramolecular leucine zipper interactions. *EMBOJ, 16*(5), 1066-1079.

Filipovska A, & Rackham O. (2013). Modular blocks for building RNA-binding proteins. *RNA Biol, 10*, 1426–1432.

Foury F, Roganti T, Lecrenier N, & Purnelle B. (1998). The complete sequence of the mitochondrial genome of Saccharomyces cerevisiae. *FEBS Lett, 440*, 325-331.

Frazier AE, Taylor RD, Mick DU, Warscheid B, Stoepel N, Meyer HE, Ryan MT, Guiard B, & Rehling P. (2006). Mdm38 interacts with ribosomes and is a component of the mitochondrial protein export machinery. *J Cell Biol, 172*, 553-564.

Frohman MA. (2015). Role of mitochondrial lipids in guiding fission and fusion. *J Mol Med, 93*, 263-269.

Frolova LY, Tsivkovskii RY, Sivolobova GF, Oparina NY, Serpinsky OI, Blinov VM, Tatkov SI, & Kisselev LL. (1999). Mutations in the highly conserved GGQ motif of class 1 polypeptide release factors abolish ability of human eRF1 to trigger peptidyl-tRNA hydrolysis. *RNA, 5*, 1014–1020.

Fung S, Nishimura T, Sasarman F, & Shoubridge EA. (2013). The conserved interaction of C7orf30 with MRPL14 promotes biogenesis of the mitochondrial large ribosomal subunit and mitochondrial translation. *Mol Biol Cell, 24*, 184-193.

Gagnon MG, Seetharaman SV, Bulkley D, & Steitz TA. (2012). Structural basis for the rescue of stalled ribosomes: structure of YaeJ bound to the ribosome. *Science, 335*, 1370-1372.

Galtier N. (2011). The intriguing evolutionary dynamics of plant mitochondrial DNA. *BMC Biol, 9*, 61.

García JJ, Ogilvie I, Robinson BH, & Capaldi RA. (2000). Structure, functioning, and assembly of the ATP synthase in cells from patients with the T8993G mitochondrial DNA mutation. Comparison with the enzyme in Rho(0) cells completely lacking mtDNA. *J Biol Chem, 275*, 11075-11081.

Gelfand R, & Attardi G. (1981). Synthesis and turnover of mitochondrial ribonucleic acid in HeLa cells: the mature ribosomal and messenger ribonucleic acid species are metabolically unstable. *Mol Cell Biol, 1*, 497-511.

Glick BS, Brandt A, Cunningham K, Müller S, Hallberg RL, & Schatz G. (1992). Cytochromes c1 and b2 are sorted to the intermembrane space of yeast mitochondria by a stop-transfer mechanism. *Cell, 69*, 809-822.

Glick BS, & Von Heijne G. (1996). Saccharomyces cerevisiae mitochondria lack a bacterial-type sec machinery. *Protein Sci, 5*, 2651-2652.

Gogvadze V, Orrenius S, & Zhivotovsky B. (2006). Multiple pathways of cytochrome c release from mitochondria in apoptosis. *Biochim Biophys Acta, 1757*, 639-647.

Gohil VM, & Greenberg ML. (2009). Mitochondrial membrane biogenesis: phospholipids and proteins go hand in hand. *J Cell Biol, 184*, 469-472.

Gray MW. (1999). Mitochondrial Evolution. *Science, 283*(5407), 1476-1481.

Greber BJ, & Ban N. (2016). Structure and function of the mitochondrial ribosome. *Annu Rev Biochem, 85*, 103-132.

Greber BJ, Bieri P, Leibundgut M, Leitner A, Aebersold R, Boehringer D, & Ban N. (2015). The complete structure of the 55S mammalian mitochondrial ribosome. *Science, 348*, 303-308.

Greber BJ, Boehringer D, Leibundgut M, Bieri P, Leitner A, Schmitz N, Aebersold R, & Ban N. (2014). The complete structure of the large subunit of the mammalian mitochondrial ribosome. *Nature, 515*(7526), 283-286.

Greber BJ, Boehringer D, Leitner A, Bieri P, Voigts-Hoffmann F, Erzberger JP, Leibundgut M, Aebersold R, & Ban N. (2014). Architecture of the large subunit of the mammalian mitochondrial ribosome. *Nature, 505*(7484), 515-519.

Greggains GD, Lister LM, Tuppen HA, Zhang Q, Needham LH, Prathalingam N, Hyslop LA, Craven L, Polanski Z, Murdoch AP, Turnbull DM, & Herbert M. (2014). Therapeutic potential of somatic cell nuclear transfer for degenerative disease caused by mitochondrial DNA mutations. *Sci Rep, 4*, 3844.

Gruschke S, Gröne K, Heublein M, Hölz S, Israel L, Imhof A, Herrmann JM, & Ott M. (2010). Proteins at the polypeptide tunnel exit of the yeast mitochondrial ribosome. *J Biol Chem, 18*, 19022-19028.

Gustafsson CM, Falkenberg M, & Larsson NG. (2016). Maintenance and expression of mammalian mitochondrial DNA. *Ann Rev Biochem, 85*, 133-160.

Hage AE, & Tollervey D. (2004). A surfeit of factors: why is ribosome assembly so much more complicated in eukaryotes than bacteria? *RNA Biol, 1*, 10-15.

Handa N, Kishishita S, Morita S, Akasaka R, Jin Z, Chrzas J, Chen L, Liu ZJ, Wang BC, Sugano S, Tanaka A, Terada T, Shirouzu M, & Yokoyama S. (2007). Structure of the human Tim44 C-terminal domain in complex with pentaethylene glycol: ligand-bound form. *Acta Crystallogr D Biol Crystallogr, 63*, 1225-1234.

Haque ME, Elmore KB, Tripathy A, Koc H, Koc EC, & Spremulli LL. (2010). Properties of the C-terminal tail of human mitochondrial inner membrane protein Oxa1L and its interactions with mammalian mitochondrial ribosomes. *J Biol Chem, 285*(36), 28353-28362.

Hartl FU, & Hayer-Hartl M. (2002). Molecular chaperones in the cytosol: from nascent chain to folded protein. *Science, 295*, 1852-1858.

He J, Cooper HM, Reyes A, Di Re M, Kazak L, Wood SR, Mao CC, Fearnley IM, Walker JE, & Holt IJ. (2012). Human C4orf14 interacts with the mitochondrial nucleoid and is involved in the biogenesis of the small mitochondrial ribosomal subunit. *Nucleic Acids Res, 40*, 6097-6108.

He J, Cooper HM, Reyes A, Di Re M, Sembongi H, Litwin TR, Gao J, Neuman KC, Fearnley IM, Spinazzola A, Walker JE, & Holt IJ. (2012). Mitochondrial nucleoid interacting proteins support mitochondrial protein synthesis. *Nucleic Acids Res, 40*, 6109-6121.

Hell K, Herrmann JM, Pratje E, Neupert W, & Stuart RA. (1998). Oxa1p, an essential component of the N-tail protein export machinery in mitochondria. *Proc Natl Acad Sci U S A, 95*, 2250-2255.

Hennon SW, Soman R, Zhu L, & Dalbey RE. (2015). YidC/Alb3/Oxa1 family of insertases. *J Biol Chem, 290*(24), 14866-14874.

Hensen F, Cansiz S, Gerhold JM, & Spelbrink JN. (2014). To be or not to be a nucleoid protein: a comparison of mass-spectrometry based approaches in the identification of potential mtDNA-nucleoid associated proteins. *Biochimie*, 219-226.

Herrmann JM, Woellhaf MW, & Bonnefoy N. (2013). Control of protein synthesis in yeast mitochondria: the concept of translational activators. *Biochim Biophys Acta, 1833*, 286-294.

Hildenbeutel M, Theis M, Geier M, Haferkamp I, Neuhaus HE, Herrmann JM, & Ott M. (2012). The membrane insertase Oxa1 is required for efficient import of carrier proteins into mitochondria. *J Mol Biol, 423*, 590-599.

Hockenbery D, Nuñez G, Milliman C, Schreiber RD, & Korsmeyer SJ. (1990). Bcl-2 is an inner mitochondrial membrane protein that blocks programmed cell death. *Nature, 348*, 334-336.

Hofmann K, & Stoffel W. (1993). TMbase - A database of membrane spanning proteins segments. *Biol Chem Hoppe-Seyler, 374*, 166.

Hofmann S, Rothbauer U, Muehlenbein N, Baiker K, Hell K, & Bauer MF. (2005). Functional and mutational characterization of human MIA40 acting during import into the mitochondrial intermembrane space. *J Mol Biol, 353*, 517-528.

Holt IJ, Lorimer HE, & Jacobs HT. (2000). Coupled leading- and lagging-strand synthesis of mammalian mitochondrial DNA. *Cell, 100*(5), 515-524.

Holt IJ, & Reyes A. (2012). Human mitochondrial DNA replication. *Cold Spring Harb Perspect Biol, 4*(12).

Horvath SE, & Daum G. (2013). Lipids of mitochondria. *Prog Lipid Res, 52*, 590-614.

Hwang SK, Piao L, Lim HT, Minai-Tehrani A, Yu KN, Ha YC, Chae CH, Lee KH, Beck GR, Park J, & Cho MH. (2010). Suppression of lung tumorigenesis by leucine zipper/EF hand-containing transmembrane-1. *PLoS One, 5*, e12535.

Jackson AL, Burchard J, Leake D, Reynolds A, Schelter J, Guo J, Johnson JM, Lim L, Karpilow J, Nichols K, Marshall W, Khvorova A, & Linsley PS. (2006). Position-specific chemical modification of siRNAs reduces "off-target" transcript silencing. *RNA, 12*, 1197-1205.

Jackson AL, & Linsley PS. (2010). Recognizing and avoiding siRNA off-target effects for target identification and therapeutic application. *Nat Rev Drug Discov, 9*, 57-67.

Jia L, Dienhart M, Schramp M, McCauley M, Hell K, & Stuart RA. (2003). Yeast Oxa1 interacts with mitochondrial ribosomes: the importance of the C-terminal region of Oxa1. *EMBO J, 22*, 6438-6447.

Jia L, Dienhart MK, & Stuart RA. (2007). Oxa1 directly interacts with Atp9 and mediates its assembly into the mitochondrial F1Fo-ATP synthase complex. *Mol Biol Cell, 18*, 1897-1908.

Jia L, Kaur J, & Stuart RA. (2009). Mapping of the Saccharomyces cerevisiae Oxa1-mitochondrial ribosome interface and identification of MrpL40, a ribosomal protein in close proximity to

Oxa1 and critical for oxidative phosphorylation complex assembly. *Eukaryot Cell, 8*(11), 1792-1802.

Jiang D, Zhao L, Clish CB, & Clapham DE. (2013). Letm1, the mitochondrial Ca2+/H+ antiporter, is essential for normal glucose metabolism and alters brain function in Wolf-Hirschhorn syndrome. *Proc Natl Acad Sci USA, 110*(24), 2249-2254.

Jiang X, & Wang X. (2004). Cytochrome C-mediated apoptosis. *Annu Rev Biochem, 73*, 87-106.

Jonckheere AI, Smeitink JA, & Rodenburg RJ. (2012). Mitochondrial ATP synthase: architecture, function and pathology. *J Inherit Metab Dis, 35*(2), 211-225.

Jones ME. (1980). Pyrimidine nucleotide biosynthesis in animals: genes, enzymes, and regulation of UMP biosynthesis. *Ann Rev Biochem, 49*, 253-279.

Josyula R, & Sha B. (2006). Crystal structure of yeast mitochondrial peripheral membrane protein Tim44p C-terminal domain. *J Mol Biol, 359* 798-804.

Jourdain AA, Boehm E, Maundrell K, & Martinou JC. (2016). Mitochondrial RNA granules: Compartmentalizing mitochondrial gene expression. *J Cell Biol, 212*, 611-614.

Jourdain AA, Koppen M, Rodley CD, Maundrell K, Gueguen N, Reynier P, Guaras AM, Enriquez JA, Anderson P, Simarro M, & Martinou JC. (2015). A mitochondria-specific isoform of FASTK is present in mitochondrial RNA granules and regulates gene expression and function. *Cell Rep, 10*, 1110-1121.

Jourdain AA, Koppen M, Wydro M, Rodley CD, Lightowlers RN, Chrzanowska-Lightowlers ZM, & Martinou JC. (2013). GRSF1 regulates RNA processing in mitochondrial RNA granules. *Cell Metab, 17*, 399-410.

Karlberg O, Canbäck B, Kurland CG, & Andersson SG. (2000). The dual origin of the yeast mitochondrial proteome. *Yeast, 30*, 170-187.

Kawasaki H, & Kretsinger RH. (1994). Calcium-binding proteins. 1: EF-hands. *Protein Profile, 1*, 343-517.

Kedrov A, Sustarsic M, de Keyzer J, Caumanns JJ, Wu ZC, & Driessen AJ. (2013). Elucidating the native architecture of the YidC: ribosome complex. *J Mol Biol, 425*, 4112-4124.

Keenan RJ, Freymann DM, Stroud RM, & Walter P. (2001). The signal recognition particle. *Annu Rev Biochem, 70*, 755-775.

Keil M, Bareth B, Woellhaf MW, Peleh V, Prestele M, Rehling P, & Herrmann JM. (2012). Oxa1-ribosome complexes coordinate the assembly of cytochrome C oxidase in mitochondria. *J Biol Chem, 287*(41), 34484-34493.

Kelley LA, Mezulis S, Yates CM, Wass MN, & Sternberg MJ. (2015). The Phyre2 web portal for protein modeling, prediction and analysis. *Nat Protoc, 10*, 845-858.

Kissil JL, Cohen O, Raveh T, & Kimchi A. (1999). Structure-function analysis of an evolutionary conserved protein, DAP3, which mediates TNF-alpha- and Fas-induced cell death. *EMBO J, 18*(2), 353-362.

Koc EC, Burkhart W, Blackburn K, Moseley A, & Spremulli LL. (2001). The small subunit of the mammalian mitochondrial ribosome. Identification of the full complement of ribosomal proteins present. *J Biol Chem, 276*(22), 19363-19374.

Koc EC, Burkhart W, Blackburn K, Moyer MB, Schlatzer DM, Moseley A, & Spremulli LL. (2001). The large subunit of the mammalian mitochondrial ribosome. Analysis of the complement of ribosomal proteins present. *J Biol Chem, 276*(47), 43958-43969.

Kohler R, Boehringer D, Greber B, Bingel-Erlenmeyer R, Collinson I, Schaffitzel C, & Ban N. (2009). YidC and Oxa1 form dimeric insertion pores on the translating ribosome. *Mol Cell, 34*(3), 344-353.

Kol S, Majczak W, Heerlien R, van der Berg JP, Nouwen N, & Driessen AJM. (2009). Subunit a of the F1F0 ATP synthase requires YidC and SecYEG for membrane insertion. *J Mol Biol, 390*, 893-901.

Korhonen JA, Pham XH, Pellegrini M, & Falkenberg M. (2004). Reconstitution of a minimal mtDNA replisome in vitro. *EMBO J, 23*, 2423-2429.

Kotani T, Akabane S, Takeyasu K, Ueda T, & Takeuchi N. (2013). Human G-proteins, ObgH1 and Mtg1, associate with the large mitochondrial ribosome subunit and are involved in translation and assembly of respiratory complexes. *Nucleic Acids Res, 41*, 3713-3722.

Kozjak-Pavlovic V. (2016). The MICOS complex of human mitochondria. *Cell Tissue Res*.

Krüger V, Deckers M, Hildenbeutel M, van der Laan M, Hellmers M, Dreker C, Preuss M, Herrmann JM, Rehling P, Wagner R, & Meinecke M. (2012). The mitochondrial oxidase assembly protein1 (Oxa1) insertase forms a membrane pore in lipid bilayers. *J Biol Chem, 287*, 33314-33326.

Kukat C, Davies KM, Wurm CA, Spåhr H, Bonekamp NA, Kühl I, Joos F, Polosa PL, Park CB, Posse V, Falkenberg M, Jakobs S, Kühlbrandt W, & Larsson NG. (2015). Cross-strand binding of TFAM to a single mtDNA molecule forms the mitochondrial nucleoid. *Proc Natl Acad Sci USA, 112*, 11288-11293.

Kumazaki K, Chiba S, Takemoto M, Furukawa A, Nishiyama K, Sugano Y, Mori T, Dohmae N, Hirata K, Nakada-Nakura Y, Maturana AD, Tanaka Y, Mori H, Sugita Y, Arisaka F, Ito K, Ishitani R, Tsukazaki T, & Nureki O. (2014). Structural basis of Sec-independent membrane protein insertion by YidC. *Nature Reviews Genetics, 509*, 516-520.

Kumazaki K, Kishimoto T, Furukawa A, Mori H, Tanaka Y, Dohmae N, Ishitani R, Tsukazaki T, & Nureki O. (2014). Crystal structure of Escherichia coli YidC, a membrane protein chaperone and insertase. *Sci Rep, 4*, 7299.

Kunau WH, Dommes V, & Schulz H. (1995). Beta-oxidation of fatty acids in mitochondria, peroxisomes, and bacteria: a century of continued progress. *Prog Lipid Res, 34*, 267-342.

Kurland CG, & Andersson SG. (2000). Origin and evolution of the mitochondrial proteome. *Microbiol Mol Biol Rev, 64*, 786-820.

Kyte J, & Doolittle RF. (1982). A simple method for displaying the hydropathic character of a protein. *J Mol Biol, 157*, 105-132.

Labrousse AM, Zappaterra MD, Rube DA, & van der Bliek AM. (1999). C. elegans dynamin-related protein DRP-1 controls severing of the mitochondrial outer membrane. *Mol Cell, 4*, 815-826.

Lee KW, & Bogenhagen DF. (2014). Assignment of 2'-O-methyltransferases to modification sites on the mammalian mitochondrial large subunit 16 S ribosomal RNA (rRNA). *J Biol Chem, 289*, 24936-24942.

Levshenkova EV, Ukraintsev KE, Orlova VV, Alibaeva RA, Kovriga IE, Zhugdernamzhilyn O, & Frolova EI. (2004). The structure and specific features of the cDNA expression of the human gene MRPL37. *Bioorg Khim, 30*, 499-506.

Levy S, Allerston CK, Liveanu V, Habib MR, Gileadi O, & Schuster G. (2016). Identification of LACTB2, a metallo-β-lactamase protein, as a human mitochondrial endoribonuclease. *Nucleic Acids Res, 44*, 1813-1832.

Li LY, Luo X, & Wang X. (2001). Endonuclease G is an apoptotic DNase when released from mitochondria. *Nature Reviews Genetics, 412*, 95-99.

Li N, Zheng Y, Xuan C, Lin Z, Piao L, & Liu S. (2015). LETM1 overexpression is correlated with the clinical features and survival outcome of breast cancer. *Int J Clin Exp Pathol, 8*, 12893-12900.

Lightowlers RN, & Chrzanowska-Lightowlers ZM. (2013). Human pentatricopeptide proteins: only a few and what do they do? *RNA Biol, 10*, 1433-1438.

Lightowlers RN, Rozanska A, & Chrzanowska-Lightowlers ZM. (2014). Mitochondrial protein synthesis: figuring the fundamentals, complexities and complications, of mammalian mitochondrial translation. *FEBS Lett, 588*(15), 2496-2503.

Lightowlers RN, Taylor RW, & Turnbull DM. (2015). Mutations causing mitochondrial disease: What is new and what challenges remain? *Science, 25*, 1494-1499.

Lill R, & Mühlenhoff U. (2005). Iron-sulfur-protein biogenesis in eukaryotes. *Trends in biochemical sciences, 30*, 133-141.

Linder P, & Jankowsky E. (2011). From unwinding to clamping - the DEAD box RNA helicase family. *Nat Rev Mol Cell Biol, 12*, 505-516.

Liu M, & Spremulli LL. (2000). Interaction of mammalian mitochondrial ribosomes with the inner membrane. *J Biol Chem, 275*(38), 29400-29406.

Liu Q, & Fredrick K. (2016). Intersubunit bridges of the bacterial ribosome. *J Mol Biol*.

Liu X, Weaver D, Shirihai O, & Hajnóczky G. (2009). Mitochondrial 'kiss-and-run': interplay between mitochondrial motility and fusion-fission dynamics. *EMBO J, 28*, 3074-3089.

Lorenzi I, Oeljeklaus S, Ronsör C, Bareth B, Warscheid B, Rehling P, & Dennerlein S. (2016). The ribosome-associated Mba1 escorts Cox2 from insertion machinery to maturing assembly intermediates. *Mol Cell Biol*.

Lotz C, Lin AJ, Black CM, Zhang J, Lau E, Deng N, Wang Y, Zong NC, Choi JH, Xu T, Liem DA, Korge P, Weiss JN, Hermjakob H, Yates JR 3rd, Apweiler R, & Ping P. (2014). The characterization, design, and function of the mitochondrial proteome: from organs to organisms. *J Proteome Res, 13*, 433-446.

Lupo D, Vollmer C, Deckers M, Mick DU, Tews I, Sinning I, & Rehling P. (2011). Mdm38 is a 14-3-3-like receptor and associates with the protein synthesis machinery at the inner mitochondrial membrane. *Traffic, 12*(10), 1457-1466.

Mai N, Chrzanowska-Lightowlers ZM, & Lightowlers RN. (2016). The process of mammalian mitochondrial protein synthesis. *Cell Tissue Res*.

Mannella CA. (1992). The 'ins' and 'outs' of mitochondrial membrane channels. *Trends Biochem Sci, 17*, 315-320.

Marom M, Safonov R, Amram S, Avneon Y, Nachliel E, Gutman M, Zohary K, Azem A, & Tsfadia Y. (2009). Interaction of the Tim44 C-terminal domain with negatively charged phospholipids. *Biochemistry, 48*(47), 11185-11195.

Martin J, Mahlke K, & Pfanner N. (1991). Role of an energized inner membrane in mitochondrial protein import. Delta psi drives the movement of presequences. *J Biol Chem, 266*, 18051-18057.

Martin M, Cho J, Cesare AJ, Griffith JD, & Attardi G. (2005). Termination factor-mediated DNA loop between termination and initiation sites drives mitochondrial rRNA synthesis. *Cell, 123*, 1227-1240.

Matthews PM, Brown RM, Morten K, Marchington D, Poulton J, & Brown G. (1995). Intracellular heteroplasmy for disease-associated point mutations in mtDNA: implications for disease expression and evidence for mitotic segregation of heteroplasmic units of mtDNA. *Hum Genet, 96*, 261-268.

McLean J, Cohn GL, Brandt IK, & Simpson MV. (1958). Incorporation of labeled amino acids into the protein of muscle and liver mitochondria. *J Biol Chem, 233*, 657-663.

Mercer TR, Neph S, Dinger ME, Crawford J, Smith MA, Shearwood AM, Haugen E, Bracken CP, Rackham O, Stamatoyannopoulos JA, Filipovska A, & Mattick JS. (2011). The human mitochondrial transcriptome. *Cell, 146*, 645-658.

Metodiev MD, Lesko N, Park CB, Cámara Y, Shi Y, Wibom R, Hultenby K, Gustafsson CM, & Larsson NG. (2009). Methylation of 12S rRNA is necessary for in vivo stability of the small subunit of the mammalian mitochondrial ribosome. *Cell Metab, 9*, 386-397.

Metodiev MD, Spåhr H, Loguercio Polosa P, Meharg C, Becker C, Altmueller J, Habermann B, Larsson NG, & Ruzzenente B. (2014). NSUN4 is a dual function mitochondrial protein required for both methylation of 12S rRNA and coordination of mitoribosomal assembly. *PLoS Genet, 10*, e1004110.

Miller JL, Cimen H, & Koc EC. (2009). Phosphorylated proteins of the mammalian mitochondrial ribosome: implications in protein synthesis. *J Proteome Res, 8*, 4789-4798.

Miller JL, Koc H, & Koc EC. (2008). Identification of phosphorylation sites in mammalian mitochondrial ribosomal protein DAP3. *Protein Sci, 17*, 251-260.

Minczuk M, He J, Duch AM, Ettema TJ, Chlebowski A, Dzionek K, Nijtmans LG, Huynen MA, & Holt IJ. (2011). TEFM (c17orf42) is necessary for transcription of human mtDNA. *Nucleic Acids Res, 39*, 4284-4299.

Minczuk M, Piwowarski J, Papworth MA, Awiszus K, Schalinski S, Dziembowski A, Dmochowska A, Bartnik E, Tokatlidis K, Stepien PP, & Borowski P. (2002). Localisation of the human hSuv3p helicase in the mitochondrial matrix and its preferential unwinding of dsDNA. *Nucleic Acids Res, 30*, 5074-5086.

Mokranjac D, & Neupert W. (2005). Protein import into mitochondria. *Biochem Soc Trans, 33*, 1019-1023.

Montoya J, Christianson T, Levens D, Rabinowitz M, & Attardi G. (1982). Identification of initiation sites for heavy-strand and light-strand transcription in human mitochondrial DNA. *Proc Natl Acad Sci USA, 79*, 7195-7199.

Montoya J, Ojala D, & G, A. (1981). Distinctive features of the 5'-terminal sequences of the human mitochondrial mRNAs. *Nature, 290*(5806), 465-470.

Morris RL, & Hollenbeck PJ. (1995). Axonal transport of mitochondria along microtubules and F-actin in living vertebrate neurons. *J Cell Biol, 131*, 1315-1326.

Nagaike T, Suzuki T, Katoh T, & Ueda T. (2005). Human mitochondrial mRNAs are stabilized with polyadenylation regulated by mitochondria-specific poly(A) polymerase and polynucleotide phosphorylase. *J Biol Chem, 280*(20), 19721-19727.

Nagaike T, Suzuki T, Tomari Y, Takemoto-Hori C, Negayama F, Watanabe K, & Ueda T. (2001). Identification and characterization of mammalian mitochondrial tRNA nucleotidyltransferases. *J Biol Chem, 276*(43), 40041-40049.

Nass MK, & Nass S. (1963). Intramitochondrial fibers with DNA characteristics: I. Fixation and electron staining reactions. *J Cell Biol, 19*, 593–611.

Nijtmans LG, Artal SM, Grivell LA, & Coates PJ. (2002). The mitochondrial PHB complex: roles in mitochondrial respiratory complex assembly, ageing and degenerative disease. *Cell Mol Life Sci, 59*, 143-155.

Noeske J, Wasserman MR, Terry DS, Altman RB, Blanchard SC, & Cate JH. (2015). High-resolution structure of the Escherichia coli ribosome. *Nat Struct Mol Biol, 22*, 336-341.

Nolden M, Ehses S, Koppen M, Bernacchia A, Rugarli EI, & Langer T. (2005). The m-AAA protease defective in hereditary spastic paraplegia controls ribosome assembly in mitochondria. *Cell, 123*, 277-289.

Nouws J, Goswami AV, Bestwick M, McCann BJ, Surovtseva YV, & Shadel GS. (2016). Mitochondrial ribosomal protein L12 is required for POLRMT stability and exists as two forms generated by alternative proteolysis during import. *J Biol Chem, 291*(2), 989-997.

Nowikovsky K, & Bernardi P. (2014). LETM1 in mitochondrial cation transport. *Front Physiol, 5*. doi: doi: 10.3389/fphys.2014.00083

Nowikovsky K, Froschauer EM, Zsurka G, Samaj J, Reipert S, Kolisek M, Wiesenberger G, & Schweyen RJ. (2004). The LETM1/YOL027 gene family encodes a factor of the mitochondrial K+ homeostasis with a potential role in the Wolf-Hirschhorn syndrome. *J Biol Chem, 279*, 30307-30315.

Nowikovsky K, Reipert S, Devenish RJ, & Schweyen RJ. (2007). Mdm38 protein depletion causes loss of mitochondrial K+/H+ exchange activity, osmotic swelling and mitophagy. *Cell Death Differ, 14*, 1647-1656.

O'Brien TW, & Kalf GF. (1967). Ribosomes from rat liver mitochondria. *J Biol Chem, 242*(9), 2172-2179.

Ofengand J, & Bakin A. (1997). Mapping to nucleotide resolution of pseudouridine residues in large subunit ribosomal RNAs from representative eukaryotes, prokaryotes, archaebacteria, mitochondria and chloroplasts. *J Mol Biol, 266*, 246-268.

Ojala D, Montoya J, & Attardi G. (1981). tRNA punctuation model of RNA processing in human mitochondria. *Nature, 290*, 470-474.

Ortiz A, Killian JA, Verkleij AJ, & Wilschut J. (1999). Membrane fusion and the lamellar-to-inverted-hexagonal phase transition in cardiolipin vesicle systems induced by divalent cations. *Biophys J, 77*, 2003-2014.

Ott M, Amunts A, & Brown A. (2016). Organization and regulation of mitochondrial protein synthesis. *Annu Rev Biochem, 85*, 77-101.

Ott M, Prestele M, Bauerschmitt H, Funes S, Bonnefoy N, & Herrmann JM. (2006). Mba1, a membrane-associated ribosome receptor. *EMBO J, 25*, 1603-1610.

Ottmann C, Yasmin L, Weyand M, Veesenmeyer JL, Diaz MH, Palmer RH, Francis MS, Hauser AR, Wittinghofer A, & Hallberg B. (2007). Phosphorylation-independent interaction between 14-3-3 and exoenzyme S: from structure to pathogenesis. *EMBO J, 26*, 902-913.

Paradies G, Paradies V, De Benedictis V, Ruggiero FM, & Petrosillo G. (2014). Functional role of cardiolipin in mitochondrial bioenergetics. *Biochim Biophys Acta, 1837*, 408-417.

Pavlakis SG, Phillips PC, DiMauro S, De Vivo DC, & Rowland LP. (1984). Mitochondrial myopathy, encephalopathy, lactic acidosis, and strokelike episodes: a distinctive clinical syndrome. *Ann Neurol, 16*, 481-488.

Péquignot MO, Dey R, Zeviani M, Tiranti V, Godinot C, Poyau A, Sue C, Di Mauro S, Abitbol M, & Marsac C. (2001). Mutations in the SURF1 gene associated with Leigh syndrome and cytochrome C oxidase deficiency. *Hum Mutat, 17*, 374-381.

Pfeffer S, Woellhaf MW, Herrmann JM, & Forster F. (2015). Organization of the mitochondrial translation machinery studied in situ by cryoelectron tomography. *Nat Commun, 6*. doi: doi: 10.1038/ncomms7019

Piao L, Li Y, Kim SJ, Byun HS, Huang SM, Hwang SK, Yang KJ, Park KA, Won M, Hong J, Hur GM, Seok JH, Shong M, Cho MH, Brazil DP, Hemmings BA, & Park J. (2009). Association of LETM1 and MRPL36 contributes to the regulation of mitochondrial ATP production and necrotic cell death. *Cancer Res, 69*(8), 3397-3404.

Ponka P. (1999). Cell biology of heme. *Am J Med Sci, 318*(4), 241-256.

Popow J, Alleaume AM, Curk T, Schwarzl T, Sauer S, & Hentze MW. (2015). FASTKD2 is an RNA-binding protein required for mitochondrial RNA processing and translation. *RNA, 21*, 1873-1884.

Preuss M, Leonhard K, Hell K, Stuart RA, Neupert W, & Herrmann JM. (2001). Mba1, a novel component of the mitochondrial protein export machinery of the yeast Saccharomyces cerevisiae. *J Cell Biol, 153*(5), 1085-1096.

Quirós PM, Langer T, & López-Otín C. (2015). New roles for mitochondrial proteases in health, ageing and disease. *Nat Rev Mol Cell Biol, 16*, 345-359.

Rackham O, Busch JD, Matic S, Siira SJ, Kuznetsova I, Atanassov I, Ermer JA, Shearwood AM, Richman TR, Stewart JB, Mourier A, Milenkovic D, Larsson NG, & Filipovska A. (2016). Hierarchical RNA processing is required for mitochondrial ribosome assembly. *Cell Rep, 16*, 1874-1890.

Rajas F, Gire V, & Rousset B. (1996). Involvement of a membrane-bound form of glutamate dehydrogenase in the association of lysosomes to microtubules. *J Biol Chem, 271*, 29882-29890.

Rapoport TA. (2007). Protein translocation across the eukaryotic endoplasmic reticulum and bacterial plasma membranes. *Nature, 450*, 663-669.

Rauch A, Schellmoser S, Kraus C, Dörr HG, Trautmann U, Altherr MR, Pfeiffer RA, & Reis A. (2001). First known microdeletion within the Wolf-Hirschhorn syndrome critical region refines genotype-phenotype correlation. *Am J Med Genet, 99*, 338-342.

Rawat S, & Stemmler TL. (2011). Key players and their role during mitochondrial iron-sulfur cluster biosynthesis. *Chemistry, 17*, 746-753.

Ray PD, Huang BW, & Tsuji Y. (2012). Reactive oxygen species (ROS) homeostasis and redox regulation in cellular signaling. *Cell Signal., 24*(5), 981-990.

Rehm M, Düssmann H, & Prehn JH. (2003). Real-time single cell analysis of Smac/DIABLO release during apoptosis. *J Cell Biol, 162*, 1031-1043.

Richter-Dennerlein R, Oeljeklaus S, Lorenzi I, Ronsör C, Bareth B, Schendzielorz AB, Wang C, Warscheid B, Rehling P, & Dennerlein S. (2016). Mitochondrial protein synthesis adapts to influx of nuclear-encoded protein. *Cell, 167*, 471-483.

Richter R, Rorbach J, Pajak A, Smith PM, Wessels HJ, Huynen MA, Smeitink JA, Lightowlers RN, & Chrzanowska-Lightowlers ZM. (2010). A functional peptidyl-tRNA hydrolase, ICT1, has been recruited into the human mitochondrial ribosome. *EMBO J, 29*, 1116-1125.

Ricquier D, & Bouillaud F. (2000). Mitochondrial uncoupling proteins: from mitochondria to the regulation of energy balance. *J Physiol, 529*, 3-10.

Rittinger K, Budman J, Xu J, Volinia S, Cantley LC, Smerdon SJ, Gamblin SJ, & Yaffe MB. (1999). Structural analysis of 14-3-3 phosphopeptide complexes identifies a dual role for the nuclear export signal of 14-3-3 in ligand binding. *Mol Cell, 4*, 153-166.

Rizzuto R, De Stefani D, Raffaello A, & Mammucari C. (2012). Mitochondria as sensors and regulators of calcium signalling. *Nat Rev Mol Cell Biol, 13*(9), 566-578.

Rorbach J, Boesch P, Gammage PA, Nicholls TJ, Pearce SF, Patel D, Hauser A, Perocchi F, & Min czuk M. (2014). MRM2 and MRM3 are involved in biogenesis of the large subunit of the mitochondrial ribosome. *Mol Biol Cell, 25*, 2542-2555.

Rorbach J, Gammage PA, & Minczuk M. (2012). C7orf30 is necessary for biogenesis of the large subunit of the mitochondrial ribosome. *Nucleic Acids Res, 40*(9), 4097-4109.

Rorbach J, Richter R, Wessels HJ, Wydro M, Pekalski M, Farhoud M, Kuhl I, Gaisne M, Bonnefoy N, Smeitink JA, Lightowlers RN, & Chrzanowska-Lightowlers ZM. (2008). The human mitochondrial ribosome recycling factor is essential for cell viability. *Nucleic Acids Res, 36*(18), 5787-5799.

Rossignol R, Faustin B, Rocher C, Malgat M, Mazat JP, & Letellier T. (2003). Mitochondrial threshold effects. *Biochem J, 370*, 751-762.

Rouault TA. (2012). Biogenesis of iron-sulfur clusters in mammalian cells: new insights and relevance to human disease. *Dis Model Mech, 5*, 155-164.

Saada A, Shaag A, Mandel H, Nevo Y, Eriksson S, & Elpeleg O. (2001). Mutant mitochondrial thymidine kinase in mitochondrial DNA depletion myopathy. *Nat Genet, 29*, 342-344.

Sacconi S, Trevisson E, Pistollato F, Baldoin MC, Rezzonico R, Bourget I, Desnuelle C, Tenconi R, Basso G, DiMauro S, & Salviati L. (2005). hCOX18 and hCOX19: two human genes involved in cytochrome c oxidase assembly. *Biochem Biophys Res Commun, 337*, 832-839.

Salinas-Giege T, Giege R, & Giege P. (2015). tRNA biology in mitochondria. *Int J Mol Sci, 16*, 4518-4559.

Samuelson JC, Chen M, Jiang F, Möller I, Wiedmann M, Kuhn A, Phillips GJ, & Dalbey RE. (2000). YidC mediates membrane protein insertion in bacteria. *Nature Reviews Genetics, 406*, 637-641.

Saracco SA, & Fox TD. (2002). Cox18p is required for export of the mitochondrially encoded Saccharomyces cerevisiae Cox2p C-tail and interacts with Pnt1p and Mss2p in the inner membrane. *Mol Biol Cell, 13*, 1122-1131.

Sasarman F, Brunel-Guitton C, Antonicka H, Wai T, & Shoubridge EA. (2010). LRPPRC and SLIRP interact in a ribonucleoprotein complex that regulates posttranscriptional gene expression in mitochondria. *Mol Biol Cell, 21*, 1315-1323.

Schapira AH, Cooper JM, Dexter D, Jenner P, Clark JB, & Marsden CD. (1989). Mitochondrial complex I deficiency in Parkinson's disease. *Lancet, 1*, 1269.

Schiller D, Cheng YC, Liu Q, Walter W, & EA., C. (2008). Residues of Tim44 involved in both association with the translocon of the inner mitochondrial membrane and regulation of mitochondrial Hsp70 tethering. *Mol Cell Biol, 28*, 4424-3443.

Schmeing TM, Huang KS, Strobel SA, & Steit TA. (2005). An induced-fit mechanism to promote peptide bond formation and exclude hydrolysis of peptidyl-tRNA. *Nature, 438*, 520-524.

Schmidt O, Harbauer AB, Rao S, Eyrich B, Zahedi RP, Stojanovski D, Schönfisch B, Guiard B, Sickmann A, Pfanner N, & Meisinger C. (2011). Regulation of mitochondrial protein import by cytosolic kinases. *Cell, 144* 227-239.

Schneider S, & Excoffier L. (1999). Estimation of past demographic parameters from the distribution of pairwise differences when the mutation rates vary among sites: application to human mitochondrial DNA. *Genetics, 152*, 1079-1089.

Schuwirth BS, Borovinskaya MA, Hau CW, Zhang W, Vila-Sanjurjo A, Holton JM, & Cate JH. (2005). Structures of the bacterial ribosome at 3.5 A resolution. *Science, 310*, 827-834.

Schwartz M, & Vissing J. (2002). Paternal inheritance of mitochondrial DNA. *N Engl J Med, 347*, 576-580.

Schwendener S. (1867). Über die wahre Natur der Flechten. *Verhandlungen der Schweizerischen Naturforschenden Gesellschaft in Rheinfelden, 51*, 88-90.

Scorrano L, Ashiya M, Buttle K, Weiler S, Oakes SA, Mannella CA, & Korsmeyer SJ. (2002). A distinct pathway remodels mitochondrial cristae and mobilizes cytochrome c during apoptosis. *Dev Cell, 2*, 55-67.

Scotti PA, Urbanus ML, Brunner J, de Gier JWL, von Heijne G, van der Does C, Driessen AJM, Oudega B, & Luirink J. (2000). YidC, the Escherichia coli homologue of mitochondrial Oxa1p, is a component of the Sec translocase. *EMBO J, 19*, 542-549.

Seidel-Rogol BL, McCulloch V, & Shadel GS. (2002). Human mitochondrial transcription factor B1 methylates ribosomal RNA at a conserved stem-loop. *Nat Genet, 33*, 23-24.

Sharma MR, Koc EC, Datta PP, Booth TM, Spremulli LL, & Agrawal RK. (2003). Structure of the mammalian mitochondrial ribosome reveals an expanded functional role for its component proteins. *Cell, 115*, 97-108.

Shin HW, Shinotsuka C, Torii S, Murakami K, & Nakayama K. (1997). Identification and subcellular localization of a novel mammalian dynamin-related protein homologous to yeast Vps1p and Dnm1p. *J Biochem, 122*, 525-530.

Slomovic S, Laufer D, Geiger D, & Schuster G. (2005). Polyadenylation and degradation of human mitochondrial RNA: the prokaryotic past leaves its mark. *Mol Cell Biol, 25*, 6427-6435.

Smeitink J, van den Heuvel L, & DiMauro S. (2001). The genetics and pathology of oxidative phosphorylation. *Nature Reviews Genetics, 2*, 342-352.

Smirnova E, Griparic L, Shurland DL, & van Der Bliek AM. (2001). Dynamin-related protein drp1 is required for mitochondrial division in mammalian cells. *Mol Biol Cell, 12*, 2245-2256.

Soleimanpour-Lichaei HR, Kuhl I, Gaisne M, Passos JF, Wydro M, Rorbach J, Temperley R, Bonnefoy N, Tate W, Lightowlers RN, & Chrzanowska-Lightowlers ZM. (2007). mtRF1a is a human mitochondrial translation release factor decoding the major termination codons UAA and UAG. *Mol Cell, 27*(5), 745-757.

South ST, Bleyl SB, & Carey JC. (2007). Two unique patients with novel microdeletions in 4p16.3 that exclude the WHS critical regions: implications for critical region designation. *Am J Med Genet A, 143A*, 2137-2142.

Souza-Pinto N, Mason PA, Hashiguchi K, Weissman L, Tian J, Guay D, Lebel M, Stevnsner TV, Rasmussen LJ, & Bohr VA. (2009). Novel DNA mismatch-repair activity involving YB-1 in human mitochondria. *DNA Repair, 8*, 704–719.

Spelbrink JN, Li FY, Tiranti V, Nikali K, Yuan QP, Tariq M, Wanrooij S, Garrido N, Comi G, Morandi L, Santoro L, Toscano A, Fabrizi GM, Somer H, Croxen R, Beeson D, Poulton J, Suomalainen A, Jacobs HT, Zeviani M, & Larsson C. (2001). Human mitochondrial DNA deletions associated with mutations in the gene encoding Twinkle, a phage T7 gene 4-like protein localized in mitochondria

Nat Genet, 28, 223-231.

Srinivasula SM, Datta P, Fan XJ, Fernandes-Alnemri T, Huang Z, & Alnemri ES. (2000). Molecular determinants of the caspase-promoting activity of Smac/DIABLO and its role in the death receptor pathway. *J Biol Chem, 275*, 36152-36157.

Stiburek L, Fornuskova D, Wenchich L, Pejznochova M, Hansikova H, & Zeman J. (2007). Knockdown of human Oxa1l impairs the biogenesis of F1Fo-ATP synthase and NADH:ubiquinone oxidoreductase. *J Mol Biol, 374*(2), 506-516.

Stiller SB, Höpker J, Oeljeklaus S, Schütze C, Schrempp SG, Vent-Schmidt J, Horvath SE, Frazier AE, Gebert N, van der Laan M, Bohnert M, Warscheid B, Pfanner N, & Wiedemann N. (2016). Mitochondrial OXA translocase plays a major role in biogenesis of inner-membrane proteins. *Cell Metab, 23*, 901-908.

Sun L, Liu Y, Frémont M, Schwarz S, Siegmann M, Matthies R, & Jost JP. (1998). A novel 52 kDa protein induces apoptosis and concurrently activates c-Jun N-terminal kinase 1 (JNK1) in mouse C3H10T1/2 fibroblasts. *Gene, 208*, 157-166.

Surovtseva YV, Shutta TE, Cotneya J, Cimenb H, Chena SY, Koc EC, & Shadela GS. (2011). Mitochondrial Ribosomal Protein L12 selectively associates with human mitochondrial RNA polymerase to activate transcription. *PNAS, 108*, 17921-17926.

Susin SA, Zamzami N, Castedo M, Hirsch T, Marchetti P, Macho A, Daugas E, Geuskens M, & Kroemer G. (1996). Bcl-2 inhibits the mitochondrial release of an apoptogenic protease. *J Exp Med, 184*, 1331-1341.

Suzuki T. (2014). A complete landscape of post-transcriptional modifications in mammalian mitochondrial tRNAs. *Nucleic Acids Res, 42*, 7346-7357.

Suzuki T, Nagao A, & Suzuki T. (2011). Human mitochondrial tRNAs: biogenesis, function, structural aspects, and diseases. *Annu Rev Genet, 45*, 299-329.

Suzuki Y, Imai Y, Nakayama H, Takahashi K, Takio K, & Takahashi R. (2001). A serine protease, HtrA2, is released from the mitochondria and interacts with XIAP, inducing cell death. *Mol Cell, 8*, 613-621.

Swerdlow RH, Burns JM, & Khan SM. (2010). The Alzheimer's disease mitochondrial cascade hypothesis. *J Alzheimers Dis, 20*, S 265-279.

Szczepanowska K, Maiti P, Kukat A, Hofsetz E, Nolte H, Senft K, Becker C, Ruzzenente B, Hornig-Do HT, Wibom R, Wiesner R, Kruger M, & Trifunovic A. (2016). CLPP coordinates mitoribosoal assemby through the regulation of ERAL1 levels. *EMBO J, 35*, 2566-2583.

Szklarczyk R, Wanschers BF, Cuypers TD, Esseling JJ, Riemersma M, van den Brand MA, Gloerich J, Lasonder E, van den Heuvel LP, Nijtmans LG, & Huynen MA. (2012). Iterative orthology prediction uncovers new mitochondrial proteins and identifies C12orf62 as the human ortholog of COX14, a protein involved in the assembly of cytochrome c oxidase. *Genome Biol, 13*, R12.

Tamai S, Iida H, Yokota S, Sayano T, Kiguchiya S, Ishihara N, Hayashi J, Mihara K, & Oka T. (2008). Characterization of the mitochondrial protein LETM1, which maintains the mitochondrial tubular shapes and interacts with the AAA-ATPase BCS1L. *J Cell Sci, 121*, 2588-2600.

Taylor AB, Smith BS, Kitada S, Kojima K, Miyaura H, Otwinowski Z, Ito A, & Deisenhofer J. (2001). Crystal structures of mitochondrial processing peptidase reveal the mode for specific cleavage of import signal sequences. *Structure, 9*, 615-625.

Temperley R, Richter R, Dennerlein S, Lightowlers RN, & Chrzanowska-Lightowlers ZM. (2010). Hungry codons promote frameshifting in human mitochondrial ribosomes. *Science, 327*, 301.

Tomecki R, Dmochowska A, Gewartowski K, Dziembowski A, & Stepien PP. (2004). Identification of a novel human nuclear-encoded mitochondrial poly(A) polymerase. *Nucleic Acids Res, 32*, 6001-6014.

Tsuboi M, Morita H, Nozaki Y, Akama K, Ueda T, Ito K, Nierhaus KH, & Takeuchi N. (2009). EF-G2mt is an exclusive recycling factor in mammalian mitochondrial protein synthesis. *Mol Cell, 35*, 502-510.

Tsukihara T, Aoyama H, Yamashita E, Tomizaki T, Yamaguchi H, Shinzawa-Itoh K, Nakashima R, Yaono R, & Yoshikawa S. (1996). The whole structure of the 13-subunit oxidized cytochrome c oxidase at 2.8 A. *Science, 272*, 1136-1144.

Tu YT, & Barrientos A. (2015). The human mitochondrial DEAD-box protein DDX28 resides in RNA granules and functions in mitoribosome assembly. *Cell Rep, .*

Tucker EJ, Hershman SG, Köhrer C, Belcher-Timme CA, Patel J, Goldberger OA, Christodoulou J, Silberstein JM, McKenzie M, Ryan MT, Compton AG, Jaffe JD, Carr SA, Calvo SE, RajBhandary UL, Thorburn DR, & Mootha VK. (2011). Mutations in MTFMT underlie a human disorder of formylation causing impaired mitochondrial translation. *Cell Metab, 14*, 428-434.

Tucker EJ, Wanschers BF, Szklarczyk R, Mountford HS, Wijeyeratne XW, van den Brand MA, Leenders AM, Rodenburg RJ, Reljić B, Compton AG, Frazier AE, Bruno DL, Christodoulou J, Endo H, Ryan MT, Nijtmans LG, Huynen MA, & Thorburn DR. (2013). Mutations in the UQCC1-interacting protein, UQCC2, cause human complex III deficiency associated with perturbed cytochrome b protein expression. *PLoS Genet, 9*, e1004034.

Tuppen HA, Blakely EL, Turnbull DM, & Taylor RW. (2010). Mitochondrial DNA mutations and human disease. *BIochem Biophys Acta, 1797*, 113-128.

Tzagoloff A. (1969). Assembly of the mitochondrial membrane system. II. Synthesis of the mitochondrial adenosine triphosphatase F1. *J Biol Chem, 244*, 5027-5033.

Uchiumi T, Ohgaki K, Yagi M, Aoki Y, Sakai A, Matsumoto S, & Kang D. (2010). ERAL1 is associated with mitochondrial ribosome and elimination of ERAL1 leads to mitochondrial dysfunction and growth retardation. *Nucleic Acids Res, 38*, 5554-5568.

Uniacke J, & Zerges W. (2008). Stress induces the assembly of RNA granules in the chloroplast of Chlamydomonas reinhardtii. *J Cell Biol, 182*, 641-646.

van der Bliek AM, Shen Q, & Kawajiri S. (2013). Mechanisms of mitochondrial fission and fusion. *Cold Spring Harb Perspect Biol, 5*, a011072.

van der Giezen M, & Tovar J. (2005). Degenerate mitochondria. *EMBO Rep, 6*, 525-530.

van der Laan M, Bechtluft P, Kol S, Nouwen N, & Driessen AJM. (2004). F1F0 ATP synthase subunit c is a substrate of the novel YidC pathway for membrane protein biogenesis. *J Cell Biol, 165*, 213-222.

Vial S, Lu H, Allen S, Savory P, Thornton D, Sheehan J, & Tokatlidis K. (2002). Assembly of Tim9 and Tim10 into a functional chaperone. *J Biol Chem, 277*, 36100-36108.

Visapaa I, Fellman V, Vesa J, Dasyarma A, Hutton JL, Kumar V, Payne GS, Makarow M, Van Coster R, Taylor RW, Turnbull DM, Suomalainen A, & Peltonen L. (2002). GRACILE syndrome, a lethal metabolic disorder with iron overload, is caused by a point mutation in BCS1L. *Am J Hum Genet, 71*, 863-876.

Vogel F, Bornhovd C, Neupert W, & Reichert AS. (2006). Dynamic subcompartmentalization of the mitochondrial inner membrane. *J Cell Biol*, 237-247.

von Heijne G. (1986). Why mitochondria need a genome. *FEBS Lett, 198*, 1-4.

Voos W, von Ahsen O, Müller H, Guiard B, Rassow J, & Pfanner N. (1996). Differential requirement for the mitochondrial Hsp70-Tim44 complex in unfolding and translocation of preproteins. *EMBO J, 15*(11), 2668-2677.

Waizenegger T, Schmitt S, Zivkovic J, Neupert W, & Rapaport D. (2005). Mim1, a protein required for the assembly of the TOM complex of mitochondria. *EMBO Rep, 6*, 57-62.

Wang C, & Youle RJ. (2009). The role of mitochondria in apoptosis. *Annu Rev Genet, 43*, 95-118.

Wang G, Chen HW, Oktay Y, Zhang J, Allen EL, Smith GM, Fan KC, Hong JS, French SW, McCaffery JM, Lightowlers RN, Morse HC 3rd, Koehler CM, & Teitell MA. (2010). PNPASE regulates RNA import into mitochondria. *Cell, 142*, 456-467.

Wang Z, Cotney J, & Shadel GS. (2007). Human mitochondrial ribosomal protein MRPL12 interacts directly with mitochondrial RNA polymerase to modulate mitochondrial gene expression. *J Biol Chem, 282*, 12610-12618.

Warburg O. (1956). On respiratory impairment in cancer cells. *Science, 124*, 269-270.

Weraarpachai W, Antonicka H, Sasarman F, Seeger J, Schrank B, Kolesar JE, Lochmüller H, Chevrette M, Kaufman BA, Horvath R, & Shoubridge EA. (2009). Mutation in TACO1, encoding a translational activator of COX I, results in cytochrome c oxidase deficiency and late-onset Leigh syndrome. *Nat Genet, 41*, 833-837.

Weraarpachai W, Sasarman F, Nishimura T, Antonicka H, Auré K, Rötig A, Lombès A, & Shoubridge EA. (2012). Mutations in C12orf62, a factor that couples COX I synthesis with cytochrome c oxidase assembly, cause fatal neonatal lactic acidosis. *Am J Hum Genet, 90*, 142-151.

Wettstein FO, & Noll H. (1965). Binding of transfer ribonucleic acid to ribosomes engaged in protein synthesis: number and properties of ribosomal binding sites. *J Mol Biol, 11*, 35-53.

Wickles S, Singharoy A, Andreani J, Seemayer S, Bischoff L, Berninghausen O, Soeding J, Schulten K, van der Sluis EO, & Beckmann R. (2014). A structural model of the active ribosome-bound membrane protein insertase YidC. *Elife, 3*, e03035.

Wilson WC, Hornig-Do HT, Bruni F, Chang JH, Jourdain AA, Martinou JC, Falkenberg M, Spåhr H, Larsson NG, Lewis RJ, Hewitt L, Baslé A, Cross HE, Tong L, Lebel RR, Crosby AH, Chrzanowska-Lightowlers ZM, & Lightowlers RN. (2014). A human mitochondrial poly(A) polymerase mutation reveals the complexities of post-transcriptional mitochondrial gene expression. *Hum Mol Genet, 23*, 6345-6355.

Winiewski JR, A, Z., Nagaraj N, & Mann M. (2009). Universal sample preparation method for proteome analysis. *Nature Methods, 6*, 359 - 362.

Wolf AR, & Mootha VK. (2014). Functional genomic analysis of human mitochondrial RNA processing. *Cell Rep, 7*, 918-931.

Wredenberg A, Lagouge M, Bratic A, Metodiev MD, Spåhr H, Mourier A, Freyer C, Ruzzenente B, Tain L, Grönke S, Baggio F, Kukat C, Kremmer E, Wibom R, Polosa PL, Habermann B, Partridge L, Park CB, & Larsson NG. (2013). MTERF3 regulates mitochondrial ribosome biogenesis in invertebrates and mammals. *PLoS Genet, 9*, e1003178.

Xu F, & Cohen SN. (1995). RNA degradation in Escherichia coli regulated by 3' adenylation and 5' phosphorylation. *Nature, 374*, 180-183.

Xuesong L, Caryn NK, Jie Y, Jemmerson R, & Wang X. (1996). Induction of apoptotic program in cell-free extracts: requirement for dATP and cytochrome c. *Cell, 86*(1), 147-157.

Yang QH, Church-Hajduk R, Ren J, Newton ML, & Du C. (2003). Omi/HtrA2 catalytic cleavage of inhibitor of apoptosis (IAP) irreversibly inactivates IAPs and facilitates caspase activity in apoptosis. *Genes Dev, 17*, 1487-1496.

Yasukawa T, Reyes A, Cluett TJ, Yang MV, Bowmaker M, Jacobs HT, & Holt IJ. (2006). Replication of vertebrate mitochondrial DNA entails transient ribonucleotide incorporation throughout the lagging strand. *EMBO J, 25*(22), 5358-5371.

Yoo YA, Kim MJ, Park JK, Chung YM, Lee JH, Chi SG, Kim JS, & Yoo YD. (2005). Mitochondrial ribosomal protein L41 suppresses cell growth in association with p53 and p27Kip1. *Mol Cell Biol, 25*, 6603-6616.

Young JC, Hoogenraad NJ, & Hartl FU. (2003). Molecular chaperones Hsp90 and Hsp70 deliver preproteins to the mitochondrial import receptor Tom70. *Cell, 112*, 41-50.

Zhang X, Zuo X, Yang B, Li Z, Xue Y, Zhou Y, Huang J, Zhao X, Zhou J, Yan Y, Zhang H, Guo P, Sun H, Guo L, Zhang Y, & Fu XD. (2014). MicroRNA directly enhances mitochondrial translation during muscle differentiation. *Cell, 158*, 607-619.